

UC San Diego

Research Theses and Dissertations

Title

Peroxidative Halogenation Catalyzed by Vanadium Bromoperoxidase: Mechanism and Reactivity

Permalink

<https://escholarship.org/uc/item/0cv2r947>

Author

Winter, Gretchen E.M.

Publication Date

1996

Peer reviewed

INFORMATION TO USERS

This manuscript has been reproduced from the microfilm master. UMI films the text directly from the original or copy submitted. Thus, some thesis and dissertation copies are in typewriter face, while others may be from any type of computer printer.

The quality of this reproduction is dependent upon the quality of the copy submitted. Broken or indistinct print, colored or poor quality illustrations and photographs, print bleedthrough, substandard margins, and improper alignment can adversely affect reproduction.

In the unlikely event that the author did not send UMI a complete manuscript and there are missing pages, these will be noted. Also, if unauthorized copyright material had to be removed, a note will indicate the deletion.

Oversize materials (e.g., maps, drawings, charts) are reproduced by sectioning the original, beginning at the upper left-hand corner and continuing from left to right in equal sections with small overlaps. Each original is also photographed in one exposure and is included in reduced form at the back of the book.

Photographs included in the original manuscript have been reproduced xerographically in this copy. Higher quality 6" x 9" black and white photographic prints are available for any photographs or illustrations appearing in this copy for an additional charge. Contact UMI directly to order.

UMI

A Bell & Howell Information Company
300 North Zeeb Road, Ann Arbor MI 48106-1346 USA
313/761-4700 800/521-0600

**UNIVERSITY OF CALIFORNIA
Santa Barbara**

**Peroxidative Halogenation Catalyzed by Vanadium
Bromoperoxidase: Mechanism and Reactivity**

**A Dissertation submitted in partial satisfaction of the requirements for the
degree of**

Doctor of Philosophy

in

Chemistry

by

Gretchen Eileen Meister Winter

Committee in charge:

Professor Alison Butler, Chairperson

Professor Hellmut Eckert

Professor William Kaska

Professor Marcello DiMare

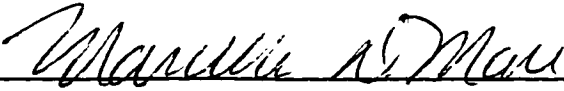
UMI Number: 9717405

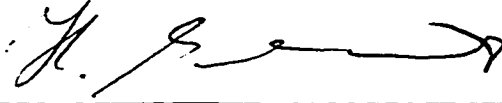
UMI Microform 9717405
Copyright 1997, by UMI Company. All rights reserved.

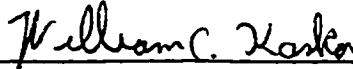
**This microform edition is protected against unauthorized
copying under Title 17, United States Code.**

UMI
300 North Zeeb Road
Ann Arbor, MI 48103

The dissertation of
Gretchen Eileen Meister Winter
is approved.









Committee Chairperson

August, 1996

Curriculum Vitae
Gretchen Eileen Meister Winter

Education

B.S. in Chemistry with Honors in Chemistry. Penn State University, May, 1989.

Experience

Research Assistant. Department of Chemistry, University of California, Santa Barbara, June, 1992-August, 1996.

Teaching Assistant. Department of Chemistry, University of California, Santa Barbara, September, 1990- June, 1992.

Research Assistant. Department of Chemistry, Penn State University, January, 1988- August, 1989.

Teaching Assistant. Department of Chemistry, Penn State University, January, 1988- May, 1988.

Summer Intern. Research and Development, Mobay Chemical Corporation, June, 1987- August, 1987.

Awards

B.R. Baker Memorial Award in bio-organic chemistry. University of California, Santa Barbara, March, 1996.

Doctoral Scholars Fellowship. University of California, Santa Barbara, September, 1990 -September, 1994.

National Science Foundation Graduate Research Fellowships Honorable Mention. January, 1991.

Braddock Scholarship. Penn State Eberly College of Science, August, 1985- May, 1989.

Publications

Winter, G.E.M.; Butler, A. "Inactivation of Vanadium Bromoperoxidase: Formation of 2-oxohistidine." (1996) *Biochemistry*, in press.

Meister, G.E.; Butler, A. "Molybdenum(VI)- and Tungsten(VI)- Mediated Biomimetic Chemistry of Vanadium Bromoperoxidase." (1994) *Inorg. Chem.* 33:3269.

Butler, A.; Clague, M.J.; Meister, G.E. "Vanadium Peroxide Complexes." (1994) *Chem. Rev.* 94: 625.

Holz, R.C.; Meister, G.E.; Horrocks, W.DeW. "Spectroscopic Characterization of a Series of Europium(III) Amino Phosphonate Complexes in Solution." (1990) *Inorg. Chem.* 29:5183.

Acknowledgements

I would like to thank California Sea Grant for a Traineeship as part of projects to Prof. Alison Butler (R/MP-53 and R/MP-69) for partial support of this work. I would also like to thank the University of California for a Doctoral Scholars Fellowship for partial support of this work.

I would like to thank my family and friends for their unfaltering support of me throughout this work, including Dr. and Mrs. Donald G. Meister and family, Mr. and Mrs. Louis E. Winter and family, and Butler group members, past and present. Most of all, I would like to thank my wonderful husband, Gentle Galaxy Emil Winter, for sharing your life and love with me (4 elways!) and giving me the strength to see this through.

Abstract

Peroxidative Halogenation Catalyzed by Vanadium Bromoperoxidase:

Mechanism and Reactivity

by

Gretchen Eileen Meister Winter

Peroxidative halogenation catalyzed by vanadium bromoperoxidase (V-BrPO) from the marine alga *Ascophyllum nodosum* was investigated using a broad range of experimental approaches.

V-BrPO is irreversibly inactivated under turnover conditions at pH 4.0. Inactivation is concurrent with oxidation of histidine to 2-oxohistidine. At low pH, HOBr reacts with N^α-benzoylhistidine to form N^α-benzoyl-2-oxohistidine. V-BrPO no longer coordinates vanadium upon inactivation. Inclusion of a bromoperoxidase substrate, i.e., monochlorodimedone, protects against inactivation. Functional mimics of V-BrPO, i.e. VO₂⁺, oxidize N^α-benzoylhistidine in the presence of hydrogen peroxide and bromide to N^α-benzoyl-2-oxohistidine.

Oxidiperoxomolybdenum(VI) and oxidiperoxotungsten(VI) are effective catalysts for the oxidation of bromide by hydrogen peroxide in acid. The reactions are first order in metal complex and bromide, and independent of hydrogen peroxide. Catalysis mediated by molybdenum(VI) is inhibited by chloride.

The major products of the reaction of luminol, V-BrPO, H₂O₂, and KBr are brominated luminols. Luminol is preferentially brominated by V-BrPO over phenol red. Luminol decreases the rate of dioxygen evolution by V-BrPO. V-BrPO quenches the fluorescence of luminol at pH 6. A binding constant of $2.62 \times 10^5 \text{ M}^{-1}$ for luminol and V-BrPO was calculated from Stern-Volmer analysis. Bromination of luminol by V-BrPO at pH 8.0 results in luminescence with a λ_{max} at 425 nm which shifts over time to 441 nm.

The major product of bromination of 1,3-di-*tert*-butylindole at pH 6.0 catalyzed by V-BrPO is the 2-oxo derivative, while reaction of 1,3-di-*tert*-butylindole with HOBr also results in the formation of other brominated products. V-BrPO prevents bromination on the sterically preferred benzene ring of the indole.

Photoaffinity labeling of V-BrPO with 5-azido-2-phenylindole results in specific crosslinking to the enzyme. Amino acid analysis of photolabeled V-BrPO shows losses of phenylalanine, leucine, and isoleucine relative to native V-BrPO.

Irradiation of dilute (nM) V-BrPO at 308 nm results in vanadium-dependent and time-dependent inactivation. The enzyme loses affinity for vanadium upon irradiation, and no cleavage is observed by SDS-PAGE. Oxygen is not required for inactivation. Amino acid analysis shows losses of glycine, alanine, and proline, and gains in aspartate, glutamate, and threonine in photolyzed V-BrPO relative to native V-BrPO.

Table of Contents

Curriculum vita.	iii
Acknowledgements	v
Abstract.	vi
Table of Contents.	viii
List of Tables.	xiv
List of Figures.	xvi
List of Schemes.	xxiv
Abbreviations.	xxvii
<u>Chapter 1. Introduction.</u>	1
Haloperoxidases and Halometabolites.	1
MCD Assay for Haloperoxidase Activity.	3
Classes of Haloperoxidases.	3
Iron heme haloperoxidases.	3
Bacterial non-heme haloperoxidases.	8
Vanadium haloperoxidases.	10
Isolation and purification of V-BrPO.	11
The vanadium site in V-BrPO.	13
Vanadium chloroperoxidase.	15
Reactivity of V-BrPO.	18
Kinetic studies on V-BrPO.	20
Mechanistic studies on V-BrPO.	21
Functional mimics of V-BrPO.	25
Vanadium Peroxide Complexes: Structural Characterization.	30
References.	42
<u>Chapter 2. Characterization of the Irreversible Inactivation of Vanadium</u> <u>Bromoperoxidase by Hydrogen Peroxide at Low pH.</u>	52
Introduction.	52
Materials and Methods.	57
Bromoperoxidase preparation.	57
Bromoperoxidase activity measurements.	57
H ₂ O ₂ inactivation of V-BrPO.	59

Turnover of V-BrPO with chloride at low pH.	59
Preparation of 2-oxohistidine and N ^α benzoyl-2-oxohistidine.	60
Method A. CuSO ₄ /ascorbate oxidation of	
N ^α benzoylhistidine.	60
Method B. HOBr oxidation of N ^α -benzoylhistidine.	61
Amino acid analyses.	61
HPLC electrochemical detection.	63
Atomic absorption analyses.	64
Trypsin digestion.	65
General reagents and procedures.	67
Results and Interpretation.	68
Electrochemical Detection of 2-oxohistidine in Hydrolyzed	
Samples of the Low-pH Turnover- inactivated V-BrPO.	68
Organic Substrate Protection of V-BrPO Against Turnover	
Inactivation.	70
Reaction of Hypobromite with N ^α - benzoylhistidine.	72
Reactivity of V-BrPO Mimics.	83
Vanadium Binding to Turnover-Inactivated V-BrPO.	86
Quantitation of 2-Oxohistidine in Turnover-Inactivated	
V-BrPO.	88
Reaction of V-BrPO with Bromide and Stoichiometric	
Hydrogen Peroxide at Low pH.	90
The Effect of Peroxidative Chloride Oxidation on Activity	
of V-BrPO.	93
Detection of 2-Oxohistidine in Other Peroxidases.	96
Discussion and Conclusion.	99
References.	107

<u>Chapter 3: Molybdenum (VI)- and Tungsten (VI)-Mediated Biomimetic</u>	
<u>Chemistry of Vanadium Bromoperoxidase.</u>	111
Introduction.	111
Materials and Methods.	119
Bromination reactions.	119
UV/visible and kinetic experiments.	120
GC experiments.	120

Oxygen evolution experiments.	121
General reagents and procedures.	121
Results and Interpretation.	122
Molybdenum(VI) Mediated Peroxidative Bromination Reactions.	122
Dependence of the Peroxidation of Bromide on Acid Concentration.	127
Dependence of the Rate of Bromide Peroxidation on Bromide and 1,3,5-trimethoxybenzene Concentrations.	131
Effect of Alcohols on the Rate of Bromide Peroxidation.	133
Dioxygen Formation.	137
Radical Versus Electrophilic Bromination.	138
Effect of Chloride on Peroxidative Bromide Oxidation Catalyzed by Molybdenum(VI)	139
Tungsten(VI)-Mediated Peroxidative Bromination Reactions	149
Further Reactions with $\text{MoO}(\text{O}_2)_2(\text{ox})^{2-}$ and $\text{WO}(\text{O}_2)_2(\text{ox})^{2-}$	160
Discussion.	168
References	177
Chapter 4. Luminol as a Substrate for Vanadium Bromoperoxidase.	180
Introduction.	180
Materials and Methods.	187
Preparation of luminol products for analysis.	187
Silica chromatography of the luminol products.	187
HPLC analysis of luminol reaction products.	187
Analysis of reaction products.	188
Competition studies with phenol red.	189
Competition studies between substrate attack and oxygen evolution.	189
Fluorescence quenching.	190
Luminescence emission spectrum.	191
Results and Interpretation.	192
Identification of the Products of Luminol in the V-BrPO-Catalyzed Reaction.	192
TLC analyses.	192
Mass spectral analyses.	194

NMR analyses.	200
HPLC analysis of the luminol product mixtures.	202
Reaction of Brominated Luminols with Hypochlorite.	210
Kinetic Competition Experiments.	213
Substrate competition experiments between luminol and phenol red at pH 6.5.	213
Competition between luminol bromination and dioxygen evolution at pH 6.5.	214
pH dependence of the kinetic competition between luminol and phenol red.	217
pH dependence of the kinetic competition between luminol bromination and dioxygen evolution.	227
Calculation of K_{app}	230
Fluorescence Quenching of Luminol by V-BrPO.	232
Luminescence Emission Produced by the V- BrPO/H ₂ O ₂ /NaBr/luminol System	236
Discussion	240
References	245

Chapter 5. Indoles as Preferred Substrates of Vanadium

<u>Bromoperoxidase: Product Analyses and Photoaffinity Labeling.</u>	246
Introduction.	246
Materials and Methods.	251
Synthesis of 1,3-di- <i>tert</i> -butylindole.	251
Reactions with 1,3-di- <i>tert</i> -butylindole.	252
HPLC analysis of 1,3-di- <i>tert</i> -butylindole reaction products.	253
Mass spectral analysis of reaction products	253
NMR analysis of reaction products.	254
Synthesis of 5-azido-2-phenylindole.	254
Synthesis of 5-nitro-2-phenylindole.	254
Synthesis of 5-amino-2-phenylindole.	254
Synthesis of 5-azido-2-phenylindole.	255
Photoaffinity labeling of vanadium bromoperoxidase.	256
Trypsin digestion.	256
Electrospray mass spectral analysis of tryptic fragments.	258
General reagents and procedures.	259

Results and Interpretation.	260
I. Regioselectivity of V-BrPO with 1,3-di- <i>tert</i> -butylindole.	260
HPLC Analysis of the Enzymatic and Chemical Reaction	
Products of 1,3-di- <i>tert</i> -butylindole.	260
Mass Spectrometry of the Reaction Products of 1,3-di- <i>tert</i> -	
butylindole and HOBr.	263
NMR of the Reaction Products of 1,3-di- <i>tert</i> -butylindole	
and HOBr.	267
II. Photoaffinity Labeling of V-BrPO with	
5-azido-2-phenylindole.	268
Photolabeling of V-BrPO and Analysis of Tryptic Digest	
by HPLC.	268
Mass Spectral Analysis of Modified Peptide.	271
Photolabeling of V-BrPO and Analysis by LC-MS.	271
HPLC Analysis of Tryptic Digestion.	276
Mass Spectral Analysis of Collected Peptides.	276
Micro-Amino Acid Analysis.	279
Discussion.	283
Regioselectivity of V-BrPO.	283
Photoaffinity Labeling of V-BrPO.	285
References.	292

Chapter 6. Vanadium Dependent Photomodification of Vanadium

<u>Bromoperoxidase.</u>	293
Introduction.	293
Materials and Methods.	299
Bromoperoxidase preparation.	299
Bromoperoxidase activity measurements.	299
Irradiation of vanadium bromoperoxidase.	299
Preparation of apo-bromoperoxidase and re-incorporation	
of vanadium(V).	300
Anaerobic irradiation of V-BrPO.	300
Atomic absorption analyses.	301
Reduction of irradiated bromoperoxidase.	301
Trypsin digestion.	302
Acid hydrolysis of enzyme samples.	303

HPLC electrochemical detection.303
Amino acid analyses.304
General reagents and procedures.	304
Results and Interpretation.305
Attempted Reactivation of V-BrPO.	311
Anaerobic Irradiation of V-BrPO.315
HPLC-ECD Analysis of Photomodified V-BrPO.317
Amino Acid Analyses.318
Discussion.322
References.327

Appendix I. Optimization of Purification of Vanadium Bromoperoxidase

<u>from <i>Ascophyllum nodosum</i></u>	329
Removal of Phenols from Algal Extracts.	329
Purification of Vanadium Bromoperoxidase by Electroelution330
Preparative Gel Electrophoresis Purification of V-BrPO.	331
References.333

List of Tables

	Page
Table 1-1. Amino acid sequence alignment of regions of high similarity between V-CIPO from <i>Curvularia inaequalis</i> and V-BrPO from <i>Ascophyllum nodosum</i>	17
Table 1-2. Bond lengths of peroxovanadium(V) compounds.	33
Table 1-3. Stretching frequencies of selected peroxovanadium(V) compounds.	38
Table 2-1. Gradient program for amino acid analysis by HPLC.	63
Table 2-2. Gradient program for analysis of tryptic peptides by HPLC.	67
Table 2-3. PITC amino acid analysis of native V-BrPO and turnover-inactivated V-BrPO.	89
Table 2-4. V-BrPO activities as determined by the MCD assay after incubation with varied concentrations of hydrogen peroxide for ten hours.	90
Table 4-1. Binding and dissociation constants for luminol and V-BrPO at different pH values calculated from dioxygen evolution data.	230
Table 5-1. Gradient for separation of tryptic peptides by HPLC.	258
Table 5-2. Gradient for separation and analysis of tryptic peptides by LC-MS.	259
Table 5-3. Amino acid analyses of control V-BrPO and V-BrPO photoaffinity labeled with 5-azido-2-phenylindole.	281
Table 6-1. Vanadium content and bromination activity of native and irradiated V-BrPO samples.	311
Table 6-2. Bromination activity measurements of V-BrPO samples incubated overnight with varied concentrations of borate.	315

Table 6-3. Micro-amino acid analysis data of 50 pmol samples of native V-BrPO and V-BrPO irradiated under conditions of 60 nM enzyme in 0.1 M Tris pH 8.3 for three minutes. 312

List of Figures

	Page
Figure 1-1. Halogenated marine natural products.	2
Figure 1-2. Standard assay for haloperoxidase activity using the substrate MCD.	3
Figure 1-3. Regioselective chlorination of indole catalyzed by the non-heme chloroperoxidase from <i>Pseudomonas pyrrocinia</i>	10
Figure 1-4. Coordination environment of vanadium(V) center in V-BrPO as initially proposed from EXAFS data.	14
Figure 1-5. Potential coordination environment of the vanadium(V) center in V-BrPO as proposed by a bond valence sum analysis.	15
Figure 1-6. Vanadium site in the vanadium chloroperoxidase from <i>Curvularia inaequalis</i>	16
Figure 1-7. Examples of the reactions mediated by vanadium(V) peroxo complexes.	31
Figure 1-8. The coordination geometry of mono- and diperoxo vanadium complexes.	36
Figure 2-1. Structure of the vanadium site in V-CIPO from <i>Curvularia inaequalis</i>	54
Figure 2-2. Silver-stained 12.5 % denaturing SDS-PAGE gel of size-exclusion purified V-BrPO.	58
Figure 2-3. HPLC-electrochemical detection of 2-oxohistidine in turnover-inactivated V-BrPO at low pH.	69
Figure 2-4. Effect of pH on the formation of 2-oxohistidine during turnover of V-BrPO.	71

Figure 2-5. HPLC-ECD of N^α-benzoylhistidine oxidation by HOBr and Cu(II)/ascorbate.	73
Figure 2-6. HPLC-ECD of N^α-benzoyl-2-oxohistidine prepared by the reaction of N^α-benzoylhistidine and HOBr undergoing hydrolysis to form 2-oxohistidine.	75
Figure 2-7. Effect of pH on the formation of N^α-benzoyl-2-oxohistidine in the reaction of HOBr with N^α-benzoylhistidine.	76
Figure 2-8. HPLC-electrochemical detection of N^α-benzoyl-2-oxohistidine from the reaction of HOBr and N^α-benzoylhistidine in acid.	78
Figure 2-9. Effect of the ratio of N^α-benzoylhistidine to HOBr added on the formation of N^α-benzoyl-2-oxohistidine detected by HPLC-ECD.	79
Figure 2-10. HPLC chromatograms at 230 nm of the products of the reaction of N^α-benzoylhistidine with varied equivalents of HOBr.	81
Figure 2-11. HPLC-electrochemical detection of N^α-benzoyl-2-oxohistidine from N^α-benzoylhistidine included in the incubation of 15 nM V-BrPO in 100 mM H₂O₂, 100 mM KBr, 0.1 M citrate pH 4.0.	82
Figure 2-12. HPLC-electrochemical detection of the formation of N^α-benzoyl-2-oxohistidine from the reaction of cis-VO₂⁺, H₂O₂, and KBr plus N^α-benzoyl-2-histidine.	84
Figure 2-13. HPLC electrochemical detection of the formation of N^α-benzoyl-2-oxohistidine from the reaction of MoO(O₂)₂(ox)²⁻, 0.1 M KBr, and 1.5 mM N^α-benzoylhistidine.	85
Figure 2-14. HPLC chromatograms at 230 nm of the products formed by the reaction of two titanium-containing heterogeneous silicate catalysts, H₂O₂, KBr, and N^α-benzoylhistidine.	87
Figure 2-15. Trypsin digestion traces at 280 nm.	92

Figure 2-16. HPLC chromatograms at 230 nm of the products formed by the reaction of N ^α -benzoylhistidine with varied equivalents of HOCl.	95
Figure 2-17. Activity of lactoperoxidase samples after incubation in citrate buffer at pH 4.0 as measured by triiodide formation.	98
Figure 3-1. Gas chromatographic analysis of the peroxidative bromination of TMB in acid solution catalyzed by MoO ₃	123
Figure 3-2. Time course for the disappearance of MoO(O ₂) ₂ (H ₂ O) ₂ in the presence of Br ⁻ and TMB as a function of H ₂ O ₂ concentration at 25.0°C. . .	125
Figure 3-3. Plot of the observed rate constant for the disappearance of MoO(O ₂) ₂ (H ₂ O) ₂ and MoO(O ₂) ₂ (H ₂ O)(OH) ⁻ monitored at 328 nm during the peroxidative bromination of TMB vs. acid concentration.	128
Figure 3-4. Plot of the initial rate of tribromide formation monitored at 266 nm mediated by MoO(O ₂) ₂ (H ₂ O) ₂ oxidation of bromide vs. molybdenum(VI) concentration.	130
Figure 3-5. Plot of the observed rate constant for the disappearance of MoO(O ₂) ₂ (H ₂ O) ₂ monitored at 328 nm during the peroxidative bromination of TMB vs. bromide concentration.	132
Figure 3-6a. Plot of the initial rate of tribromide formation monitored at 266 nm mediated by MoO(O ₂) ₂ (H ₂ O) ₂ oxidation of bromide vs. percent methanol in solution.	134
Figure 3-6b. Plot of the initial rate of tribromide formation monitored at 266 nm mediated by MoO(O ₂) ₂ (H ₂ O) ₂ oxidation of bromide vs. percent ethanol in solution.	135
Figure 3-7. Carbon-13 NMR spectrum of ¹³ C-labeled methanol in acidic aqueous solution.	136
Figure 3-8. Effect of chloride on the time course of the disappearance of MoO(O ₂) ₂ (H ₂ O) ₂ monitored at 328 nm during the peroxidative bromination of TMB.	141

Figure 3-9. Effect of chloride on the uv-vis spectrum of $\text{MoO}(\text{O}_2)_2(\text{H}_2\text{O})(\text{OH})^-$	143
Figure 3-10. Effect of chloride on the uv-vis spectrum of $\text{MoO}(\text{O}_2)_2(\text{ox})^{2-}$	144
Figure 3-11. Effect of fluoride on the uv-vis spectrum of $\text{MoO}(\text{O}_2)_2(\text{H}_2\text{O})_2$	146
Figure 3-12. Effect of fluoride on the uv-vis spectrum of $\text{MoO}(\text{O}_2)_2(\text{H}_2\text{O})(\text{OH})^-$	147
Figure 3-13. Effect of fluoride on the uv-vis spectrum of $\text{MoO}(\text{O}_2)_2(\text{ox})^{2-}$	148
Figure 3-14. Comparison of the rates of molybdenum(VI)-, tungsten(VI)- and vanadium(V)-catalyzed formation of tribromide.	150
Figure 3-15. Gas chromatographic analysis of the peroxidative bromination of TMB in acid solution catalyzed by WO_3	151
Figure 3-16. Plot of the observed rate constant of the peroxidative bromination of TMB monitored at 266 nm mediated by $\text{WO}(\text{O}_2)_2(\text{H}_2\text{O})(\text{OH})^-$ oxidation of bromide vs. acid concentration.	153
Figure 3-17. Plot of the initial rate tribromide formation monitored at 266 nm mediated by $\text{WO}(\text{O}_2)_2(\text{H}_2\text{O})(\text{OH})^-$ oxidation of bromide versus W(VI) concentration.	154
Figure 3-18. Plot of the observed rate constant of the peroxidative bromination of TMB monitored at 266 nm mediated by $\text{WO}(\text{O}_2)_2(\text{H}_2\text{O})(\text{OH})^-$ oxidation of bromide versus bromide concentration.	155
Figure 3-19a. Plot of initial rate of tribromide formation monitored at 266 nm mediated by $\text{WO}(\text{O}_2)_2(\text{H}_2\text{O})(\text{OH})^-$ oxidation of bromide versus percent methanol or ethanol in solution.	157

Figure 3-19b. Plot of initial rate of tribromide formation monitored at 266 nm mediated by $\text{WO}(\text{O}_2)_2(\text{H}_2\text{O})(\text{OH})^-$ oxidation of bromide versus percent methanol or ethanol in solution.	158
Figure 3-20. Carbon-13 nuclear magnetic resonance spectrum of ^{13}C -labeled methanol in acidic aqueous solution.	159
Figure 3-21. Absorbance at 324 nm vs. time for the reaction of $\text{MoO}(\text{O}_2)_2(\text{ox})^{2-}$	161
Figure 3-22. Gas chromatographic analysis of the peroxidative bromination of TMB catalyzed by $\text{MoO}(\text{O}_2)_2(\text{ox})^{2-}$	163
Figure 3-23. Gas chromatographic analysis of the peroxidative bromination of TMB catalyzed by $\text{WO}(\text{O}_2)_2(\text{ox})^{2-}$	164
Figure 3-24. Absorbance at 320 nm versus time for the reaction of $\text{MoO}(\text{O}_2)_2(\text{ox})^{2-}$ and bromide at varied H_2O_2 concentrations.	165
Figure 3-25. Formation of $\text{MoO}(\text{O}_2)_2(\text{ox})^{2-}$ monitored at 324 nm by incubation of $\text{MoO}_2(\text{O}_2)(\text{ox})^{2-}$ with H_2O_2 versus time.	167
Figure 4-1. Positive APCI mass spectrum of the solid products from the reaction of luminol and HOBr.	195
Figure 4-2. Positive APCI mass spectrum of 3-aminophthalic acid.	197
Figure 4-3. Positive APCI mass spectrum of the yellow filtrate from the reaction of luminol and HOBr.	199
Figure 4-4. Proton NMR spectrum in deuterated methanol of the solid products from the reaction of luminol and HOBr.	201
Figure 4-5. HPLC chromatograms at 230 nm of the reaction mixture of luminol, V-BrPO, H_2O_2 , and KBr at pH 5.7.	203
Figure 4-6. UV/vis spectrum of the major product in the chromatogram in Figure 4-5.	205

Figure 4-7. HPLC chromatograms at 230 nm of the products of the reaction of luminol plus HOBr at pH 5.7.	206
Figure 4-8. HPLC chromatograms at 230 nm of the reaction mixture of luminol, V-BrPO, H₂O₂, and KBr at pH 8.0.	207
Figure 4-9. HPLC chromatograms at 230 nm of the products of the reaction of luminol plus HOBr at pH 8.0.	208
Figure 4-10. HPLC chromatogram at 230 nm of 3-aminophthalic acid.	209
Figure 4-11. Positive APCI mass spectrum of the product of the reaction of “bromoluminol”–luminol, monobromoluminol, and dibromoluminol–with excess HOCl.	211
Figure 4-12a. Bromination of phenol red catalyzed by V-BrPO at pH 6.5 at varied luminol concentration.	215
Figure 4-12b. Bromination of phenol red by HOBr at pH 6.5 at varied luminol concentration.	216
Figure 4-13. Dioxygen formation from the disproportionation of hydrogen peroxide at pH 6.5.	218
Figure 4-14a. Bromination of phenol red catalyzed by V-BrPO at pH 5.7 at varied luminol concentration.	220
Figure 4-14b. Bromination of phenol red by HOBr at pH 5.7 at varied luminol concentration.	221
Figure 4-15a. Bromination of phenol red catalyzed by V-BrPO at pH 7.2 at varied luminol concentration.	222
Figure 4-15b. Bromination of phenol red by HOBr at pH 7.2 at varied luminol concentration.	223

Figure 4-16a. Bromination of phenol red catalyzed by V-BrPO at pH 8.1 at varied luminol concentration.	224
Figure 4-16b. Bromination of phenol red by HOBr at pH 8.1 at varied luminol concentration.	225
Figure 4-17. Change in the rate of phenol red bromination in the presence of bromoluminols.	228
Figure 4-18. Formation of dioxygen catalyzed by V-BrPO at varied luminol concentration and varied pH.	229
Figure 4-19. Plots of r_{O_2}/r_{O_2} versus luminol concentration at varied pH.	231
Figure 4-20. Quenching of luminol fluorescence at 425 nm by BSA and V-BrPO at pH 6.5.	233
Figure 4-21. Modified Stern-Volmer plot of the quenching of luminol fluorescence at 425 nm by V-BrPO at pH 6.5.	234
Figure 4-22. Luminescence spectra of the reaction mixture of luminol, V-BrPO, H ₂ O ₂ , and NaBr at pH 8.0.	237
Figure 4-23. Luminescence spectra of the reaction mixture of luminol, V-BrPO, H ₂ O ₂ , and KI at pH 8.0.	239
Figure 5-1. HPLC chromatograms at 280 nm of the bromoperoxidative oxidation of 1,3-di- <i>tert</i> -butylindole catalyzed by V-BrPO.	261
Figure 5-2. HPLC chromatograms at 280 nm of the reaction mixture of 1,3-di- <i>tert</i> -butylindole, 0.1 M KBr, 0.1 M phosphate pH 5.7 and a) No HOBr; b) 1.0 mM HOBr; c) 2.0 mM HOBr.	262
Figure 5-3. Mass spectral data for the reaction of 1,3,-di- <i>tert</i> -butylindole and HOBr.	265
Figure 5-4. Spectrum of 5-azido-2-phenylindole in ethanol/water.	269

Figure 5-5. HPLC chromatograms of 6 hour tryptic peptides.	270
Figure 5-6. Positive electrospray mass spectrum of the peptide collected from the photolabeled sample in Figure 5-5 at 116.5 minutes retention time.272
Figure 5-7. Microbore LC Chromatograms at 214 nm of the tryptic digests of a) native V-BrPO; b) photolabeled V-BrPO.	274
Figure 5-8. Mass spectrum of the peak at 13.03 minutes in the LC chromatogram of native V-BrPO in Figure 5-7a.	275
Figure 5-9. HPLC chromatograms of 12 hour tryptic peptides.	277
Figure 5-10. Positive electrospray mass spectra of peptides separated by HPLC in Figure 5-9.278
Figure 5-11. Micro- amino acid analysis chromatograms of a) native V-BrPO ; b) photolabeled V-BrPO.	280
Figure 6-1. MCD assay profiles of a) native V-BrPO and b) irradiated V-BrPO.	306
Figure 6-2. MCD bromination activity of irradiated V-BrPO versus time of irradiation.	307
Figure 6-3. MCD bromination activity of irradiated V-BrPO versus time after irradiation.308
Figure 6-4. MCD activity profiles for a) apo-BrPO and b) irradiated apo-BrPO after overnight incubation with $(\text{NH}_4)_2(\text{VO}_3)$.310
Figure 6-5. MCD activity profiles for a) irradiated V-BrPO and b) irradiated V-BrPO incubated with 50 mM NaBH_4.	314
Figure 6-6. MCD activity profiles for a) native V-BrPO, b) V-BrPO irradiated in air, and c) V-BrPO irradiated anaerobically.316

List of Schemes

	Page
Scheme 1-1. General reaction mechanism for the halogenation of organic substrates by iron heme haloperoxidases.	6
Scheme 1-2. Proposed mechanism for the peroxidation of halides catalyzed by a bacterial non-heme haloperoxidase.	10
Scheme 1-3. Reaction scheme for the reactivity of V-BrPO with bromide and hydrogen peroxide.	18
Scheme 1-4. Lewis acid mechanism for the peroxidative oxidation of bromide catalyzed by V-BrPO.	22
Scheme 1-5. Proposed revised scheme for the peroxidation of bromide catalyzed by V-BrPO.	24
Scheme 1-6. Reaction mechanism for the oxidation of bromide by $(VO)_2(O_2)_3$	27
Scheme 1-7. Reaction mechanism for the oxidation of bromide by peroxide catalyzed by $(HPS)V(OH)$	28
Scheme 2-1. Proposed mechanism for the bromination of the C-2 position of $R(2,4,5-Br_3ImH)^{2+}$ and subsequent bromide hydrolysis to parabanic acid.	102
Scheme 3-1. Reaction mechanism for the oxidation of bromide by $(VO)_2(O_2)_3$	114
Scheme 3.2. Reaction mechanism for the oxidation of bromide by peroxide catalyzed by $(HPS)V(OH)$	116
Scheme 3-3. Bromination of 2,3-dimethoxytoluene by Br^+ versus $Br\bullet$	139

Scheme 3-4. Proposed mechanism for oxidation of bromide by oxodiperoxomolybdenum(VI)..	169
Scheme 4-1. Illustration of a typical ELISA sandwich assay.	182
Scheme 4-2. Reaction sequence for the unenhanced chemiluminescent oxidation of luminol catalyzed by horse radish peroxidase.	183
Scheme 4-3. Oxidation of luminol to a radical catalyzed by HRP in the presence of an enhancer.	184
Scheme 4-4. Updated reaction scheme for vanadium bromoperoxidase from <i>Ascophyllum nodosum</i> including an enzyme bound intermediate and organic substrate binding.	186
Scheme 4-5. Detailed scheme of luminol oxidation pathways.	244
Scheme 5-1. Basic reaction scheme for the V-BrPO catalyzed bromination/bromoperoxidative oxidation of substrates and halide-assisted disproportionation of hydrogen peroxide.	246
Scheme 5-2. Updated reaction scheme for the V-BrPO catalyzed bromination/bromoperoxidative oxidation of substrates and halide-assisted disproportionation of hydrogen peroxide including the potential substrate binding step.	247
Scheme 5-3. Attack of a bromonium ion equivalent on the double bond of the indole pyrrole ring to form a bromoindolinium cation.	248
Scheme 5-4. Bromination of a sterically hindered 3-<i>tert</i>-butyl substituted indole on the benzene ring of the indole.	248
Scheme 5-5. Formation of 1,3-dihydro-1,3-di-<i>tert</i>-butyl-2H-indol-2-one catalyzed by V-BrPO.	249
Scheme 5-6. Bromination of 1,3-di-<i>tert</i>-butylindole at the 5 or the 6 position.	267

Scheme 5-7. Pathways for the coupling of aryl nitrenes to proteins. 288

**Scheme 6-1. Oxidation of serine in rabbit skeletal myosin to a
“serine aldehyde” and subsequent reduction with [³H]NaBH₄. 296**

Abbreviations

APCI -atmospheric pressure chemical ionization
BCA - bichinchonic acid
BSA - bovine serum albumin
BVS -bond valence sum analysis
BrPO - bromoperoxidase
Br-TMB - 2-bromo-1,3,5-trimethoxybenzene
Bz-his - N^α-benzoylhistidine
Bz-2-oxohis - N^α-benzoyl-2-oxohistidine
CI -chemical ionization
CIPO - chloroperoxidase
DMT - 3,5-dimethoxytoluene
ESI- electrospray ionization
ESR - electron spin resonance
ESEEM - electron spin echo envelope modulation
EXAFS - extended x-ray absorption fine structure
FAB - fast atom bombardment
H₂ada - N-(2-amidomethyl)iminodiacetic acid
H₃eida - N-(2-hydroxyethyl)inimodiacetic acid
H₂HPS - hydroxyphenylsalicylideneimine
H₃nta - nirtilotriacetic acid
H₂ox - oxalic acid
HPLC - high performance liquid chromatography
HPLC-ECD high performance liquid chromatography-electrochemical detection
MCD - monochlorodimedone (5,5-dimethyl-2-chloro-1,3-cyclohexanedione)
MES - 2(*N*-morpholino)-ethane-sulfonic acid
NMR - nuclear magnetic resonance
PAGE - polyacrylamide gel electrophoresis
PITC -phenylisothiocyanate
SDS-PAGE - sodium dodecyl sulfate polyacrylamide gel electrophoresis
TEA - triethylamine
TFA - trifluoroacetic acid
TMB - 1,3,5-trimethoxybenzene
Tris - tris(hydroxymethyl) aminomethane
V-BrPO - vanadium bromoperoxidase
V-CIPO - vanadium chloroperoxidase

Chapter 1. Introduction

Haloperoxidases and Halometabolites

Haloperoxidases are enzymes that catalyze the oxidation of halides by hydrogen peroxide. Typically, the oxidized halogen species halogenate suitable organic substrate as shown in equation 1:



These enzymes are typically named according to the most electronegative halide they can oxidize; i.e., a chloroperoxidase can oxidize chloride, bromide, and iodide while a bromoperoxidase can only oxidize bromide and iodide.

Haloperoxidases have been isolated from a wide variety of species, including mammals, birds, plants, algae, molds, and bacteria, and are presumed to be responsible for the production of the many halometabolites that have been identified in these species (Neidleman & Geigert, 1986). A wide variety of halometabolites have been isolated from marine organisms, particularly sponges and algae (Faulkner, D.G., 1980; Fenical, W., 1980). Haloperoxidases have been found in all classes of marine algae and several other marine organisms (Butler & Walker, 1993).

While the natural functions of haloperoxidases and halometabolites in marine systems are not clearly understood, they are likely involved in defense mechanisms. Many of the halogenated compounds isolated from marine

organisms, in particular, have pharmacological activity, including antifungal, antibacterial, and anti-inflammatory activities. The types of compounds isolated include halogenated C₁₅ enynes such as laurencin from the red alga *Laurencia glandulifera* (Irie et al., 1968), monoterpenes such as violacene from the red alga *Plocameum violaceum* (Van Engen et al., 1978; Mynderse et al., 1975), and chamigrenes such as elatol from *Laurencia elata* (Sims et al., 1974). Many brominated phenolic metabolites such as laurinterol (*Laurencia* sp.) (Irie et al., 1970) exhibit antibacterial activity. Elatone, an oxidation product of elatol, exhibits insecticidal activity, and solenolide E, isolated from a gorgonian, exhibits antiviral and anti-inflammatory activities (Groweiss et al., 1988).

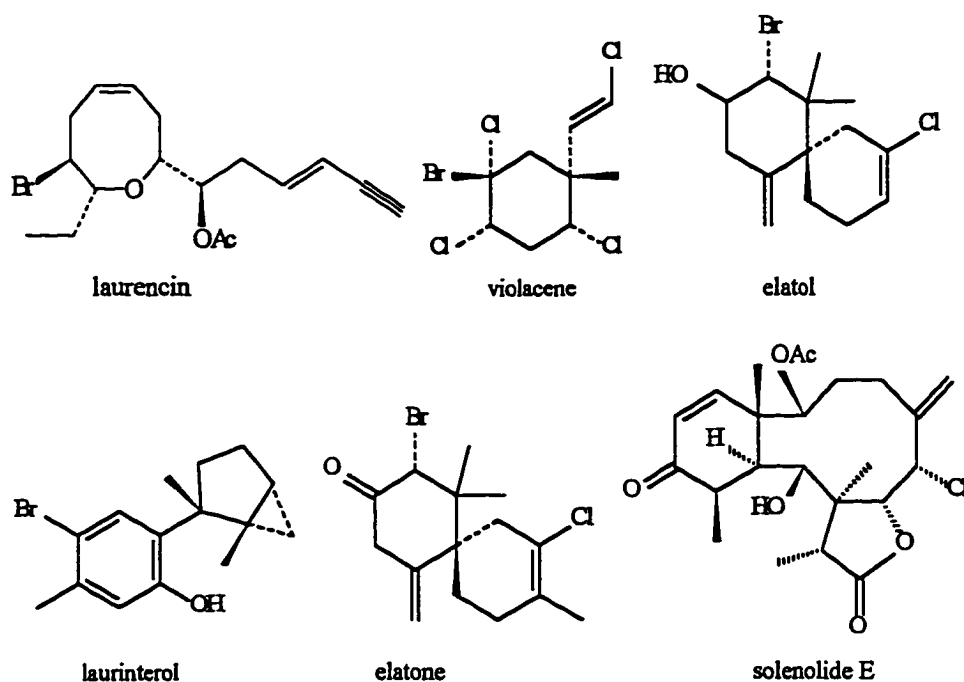


Figure 1-1. Halogenated marine natural products.

MCD Assay for Haloperoxidase Activity.

The standard assay for haloperoxidase activity is the halogenation of MCD, monochlorodimedone (5,5-dimethyl-2-chloro-1,3-cyclohexanedione), using hydrogen peroxide as the oxidant (Hager et al., 1966). In this assay, the halogenation of MCD is monitored spectrophotometrically at 290 nm. At this wavelength, the enolate form of MCD has an extinction coefficient of $19,900 \text{ M}^{-1} \text{ cm}^{-1}$, which drops to approximately $100 \text{ M}^{-1} \text{ cm}^{-1}$ upon halogenation of the 2 position:

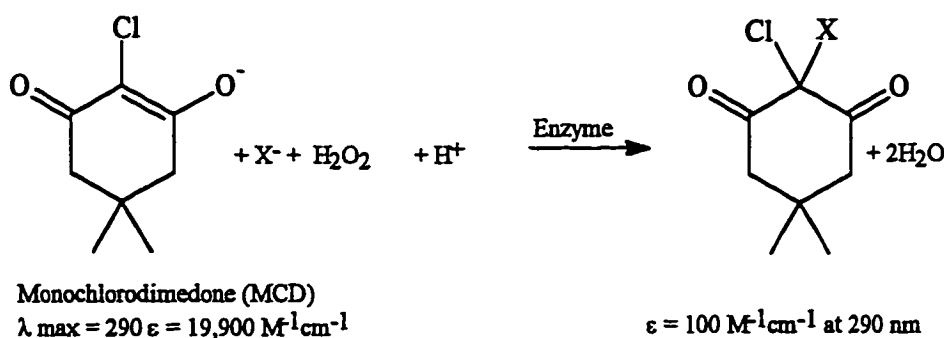


Figure 1-2. Standard assay for haloperoxidase activity using the substrate MCD.

Haloperoxidase activity is measured in terms of micromoles of MCD halogenated per minute per milligram of enzyme (i.e., U/mg; U = μmol MCD halogenated/minute).

Classes of Haloperoxidases

Iron heme haloperoxidases. Three primary categories of haloperoxidases have been identified: iron heme haloperoxidases, bacterial non-heme haloperoxidases and vanadium haloperoxidases. The most thoroughly studied category of haloperoxidases is the iron heme haloperoxidases. Haloperoxidases containing ferriprotoporphyrin IX have been isolated from a wide range of species. Lactoperoxidase, salivary peroxidase (Neidleman & Geigert, 1986), thyroid peroxidase (Hosoya & Morrison, 1967a, 1967b; Danner & Morrison, 1971), myeloperoxidase, and eosinophil peroxidase (Neidleman & Geigert, 1986) are isolated from mammalian sources, and horse radish peroxidase is isolated from horse radish root (Keilin & Hartree, 1951). Chloroperoxidase, which is isolated from the mold *Caldariomyces fumago*, has been the subject of extensive investigation (Hager et al., 1966).

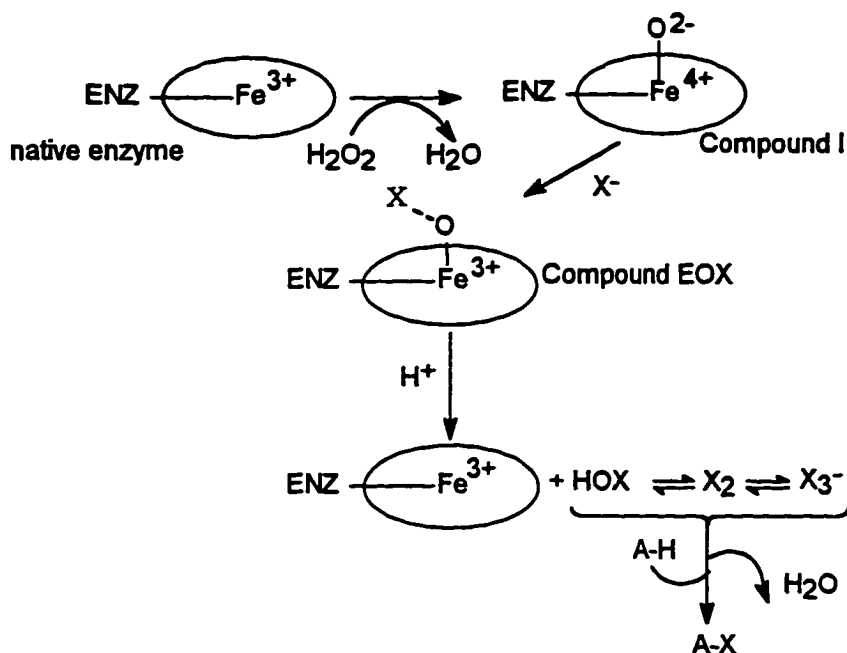
Several iron heme bromoperoxidases have been isolated from marine sources, including Rhodophyta (Pederson, 1986; Ahren et al., 1980), Chlorophyta (Manthey & Hager, 1981; Baden & Corbett, 1980), and marine worms (Ahren et al., 1980; Chen et al., 1991). The bromoperoxidase from the green alga *Penicillus capitatus* has been investigated in detail (Manthey & Hager, 1981; Baden & Corbett, 1980). This enzyme is a dimeric protein of molecular weight ~100,000

Da possessing two identical subunits that each possess a ferriprotoporphyrin IX containing high spin iron(III) in the native state.

The bromoperoxidase from *Penicillium capitatus* has been implicated in biosynthetic pathways. This enzyme has been shown to catalyze the formation of multiply brominated ketones from 3-oxooctanoic acid, hydrogen peroxide, and bromide (Beissner et al., 1981). Halogenated ketones have been isolated from several species of algae, including multiple species of *Asparagopsis* (Fenical, 1975; Burreson et al., 1975; McConnell & Fenical, 1977a; Fenical, 1974) and *Bonnemaisonia* (Siuda et al., 1975; Rinehart et al., 1975; McConnell & Fenical, 1977b; McConnell & Fenical, 1977c). In addition, bromoperoxidase from *P. capitatus* converts α -amino acids and peptides to decarboxylated nitriles and aldehydes in the presence of bromide and hydrogen peroxide (Neider & Hager, 1985). This enzyme catalyzes the conversion of methoxytyrosine to *p*-methoxyacetonitrile, which suggests that bromoperoxidase is involved in the formation of aerophysin-I, a brominated aromatic nitrile found in marine sponges that exhibits antibiotic activity (Fattoruso et al., 1970; Fulmore et al., 1970).

A general reaction mechanism for the oxidation of halides by heme containing haloperoxidases is given in Scheme 1-1. In this mechanism, the iron(III) heme moiety reacts with hydrogen peroxide to generate Compound I, which is iron(IV) with a pi cation radical on the porphyrin ring. Compound I can then react

with a halide ion, X^- , which surrenders two electrons to Compound I to generate a halonium ion equivalent and the ferric resting state of the enzyme.



Scheme 1-1. General reaction mechanism for the halogenation of organic substrates by iron heme haloperoxidases.

The existence of a bound halonium intermediate, represented in Scheme 1-1 as Compound EOX, versus a freely diffusable oxidized halogen species has been an issue of some debate (Libby et al., 1980; Lambier & Dunford, 1983; Griffin & Haddox, 1985; Geigert et al., 1983). Recent substrate competition studies by Libby et al. (1992) on chloroperoxidase from *C. fumago* indicate that an enzyme bound intermediate $EOCl$ is formed upon the oxidation of chloride. They suggest

that suitable organic substrates can then bind to this intermediate and undergo an enzyme-mediated reaction. According to their results, organic substrates that bind to Compound EOCI compete with free chloride ion, which can react with Compound EOCI to generate Cl_2 which is released from the enzymes. Despite the evidence supporting the existence of an enzyme bound intermediate and the large number of chiral halogenated metabolites that have been isolated, to date neither stereo- nor regioselective halogenation has been demonstrated with any iron heme haloperoxidases. However, recent work by Chi-Huey Wong and coworkers demonstrated high stereo- and regioselectivity for the bromohydratation of glycals (Fu et al., 1992; Liu et al., 1992).

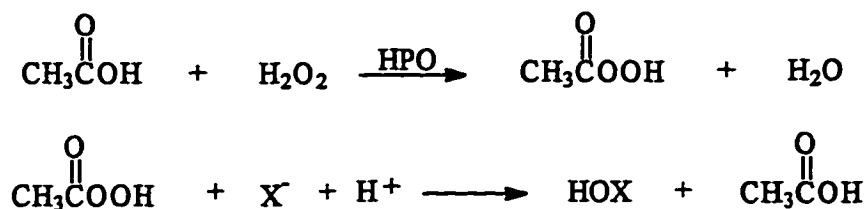
Like "classical" iron heme peroxidases, the iron heme haloperoxidases have been shown to catalyze the oxidation of organic compounds by hydrogen peroxide. Iron heme BrPO from *Penicillium capitatus* has been shown to catalyze the oxidation of compounds such as pyrogallol, *o*-dianisidine (Manthey & Hager, 1981), and monochlorodimedone (Manthey & Hager, 1985). Among the entirety of iron heme haloperoxidases, the terrestrial enzymes horse radish peroxidase and the chloroperoxidase from *C. fumago* are both efficient catalysts of organic peroxidation reactions. Efficiently oxidized substrates include indoles, aniline derivatives, and sulfides. In addition, Geigert, et al. (1983) have shown that chloroperoxidase oxidizes primary alcohols to their corresponding aldehydes.

Evidence is mounting that indicates that iron heme haloperoxidases are capable of regio- and stereoselective oxidations of organic substrates. The chloroperoxidase from *C. fumago* has proven to be a highly selective biocatalyst for organic oxidation reactions. Colonna et al. (1990, 1992) demonstrated that chloroperoxidase oxidizes sulfides to the corresponding (*R*)-sulfoxides with good enantiomeric excesses when either *tert*-butyl hydroperoxide or hydrogen peroxide was used as the peroxide source. In addition, enantioselective epoxidation of *cis*-2-alkenes and matched 2-methylalkenes has been demonstrated by Hager and coworkers (Allain et al., 1993; Dexter et al., 1995). To date, regio- or stereoselective oxidation by the *Penicillus* enzyme has not been demonstrated.

Bacterial non-heme haloperoxidases. More recently, a class of haloperoxidases has been isolated from bacteria that are not dependent upon a cofactor or a prosthetic group for catalytic activity. These enzymes have been isolated from several strains of *Streptomyces* (Pelletier et al., 1994; Pfeifer et al., 1992) and *Pseudomonas* (Wiesner et al., 1988; Pelletier & Altenbuchner, 1995). Several of these enzymes have been sequenced and display regions of high homology (Pelletier et al., 1994; Pfeifer et al., 1992; Wolfframm et al., 1993; Bantleon et al., 1994). The catalytic mechanism(s) and natural function(s) of this group of enzymes are not yet well understood.

Recently, Pelletier & Altenbuchner (1995) determined that an esterase from *Pseudomonas fluorescens* possesses 40 to 50% identical amino acids to the bacterial haloperoxidases and, in fact, is capable of haloperoxidase activity. Furthermore, analysis of the bacterial haloperoxidases revealed some low esterase activity. Both the esterase and the haloperoxidases possess the motif Gly-X₁-Ser-X₂-Gly, which indicates that they belong to the family of serine-hydrolases. In the haloperoxidases and the esterase, the other members of the so-called catalytic triad are aspartic acid and histidine (Pelletier & Altenbuchner, 1995; Pelletier et al., 1995).

In general, serine hydrolases execute hydrolysis by a mechanism involving nucleophilic attack of the serine hydroxyl group on the carbonyl oxygen of the substrate. The imidazole of the histidine and the carboxyl group of aspartic acid act as a charge relay system (Brady, L. et al., 1990; Schrag, J.D. et al., 1991). It has previously been demonstrated that the serine hydrolase enzymes are capable of using hydrogen peroxide; in particular, some serine hydrolases have been shown to peroxidize carboxylic acids to give peracids for industrial applications (Bjorkling, et al. 1990; Cuperus et al., 1990). Accordingly, Pelletier, et al. (1995) have proposed that halogenation in the bacterial haloperoxidases occurs by first a conversion of acetic acid to peracetic acid, which is then capable of oxidizing halides as shown in Scheme 1-2.



Scheme 1-2. Proposed mechanism for the peroxidation of halides catalyzed by a bacterial non-heme haloperoxidase (Pelletier et al., 1995).

The non-heme chloroperoxidase from *Pseudomonas pyrocinia* is the only example of this class of haloperoxidases thus far that has proved capable of regioselective chlorination (Wiesner et al., 1986). This enzyme chlorinates indole at the unfavored 7 position of the aromatic ring:

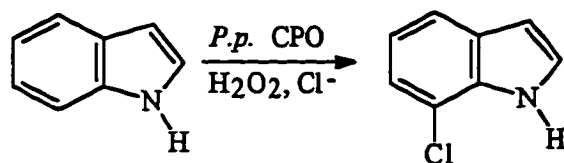


Figure 1-3. Regioselective chlorination of indole catalyzed by the non-heme chloroperoxidase from *Pseudomonas pyrocinia* (Wiesner et al., 1986).

Vanadium haloperoxidases. The third class of haloperoxidases known are the vanadium haloperoxidases. Vanadium-dependent bromoperoxidases have been isolated from several species of marine brown algae, including *Ascophyllum nodosum* (Vilter, 1984; Krenn et al., 1989), *Lamanaria saccharina* (de Boer et al., 1986), *Laminaria digitata* (Jordan & Vilter, 1991), *Fucus distichus* (Soedjak &

Butler, 1990), *Macrocystis pilulifera* (Soedjak & Butler, 1990), species of the marine red algae *Corallina*, species of the marine green algae *Halimeda* (Soedjak, 1991), and a terrestrial lichen, *Xanthoria parietina* (Plat et al., 1987). This class of enzymes are of interest in the present discourse. In addition to the bromoperoxidases, vanadium-dependent chloroperoxidases have recently been isolated from terrestrial fungi, including *Curvularia inaequalis* (van Schijndel et al., 1993) and *Dreschlera biseptata* (Vollenbroek et al., 1995).

The vanadium-dependent bromoperoxidases isolated from marine algae are all acidic glycoproteins (Krenn et al., 1989; de Boer, E. et al., 1986) with pI values between 4 and 5 and similar amino acid compositions (Wever et al., 1988). The subunit molecular weight of vanadium bromoperoxidase (V-BrPO) determined by reducing SDS-PAGE is approximately 68,000 Da. Vanadium can be removed from these bromoperoxidases by dialysis against phosphate at low pH, and vanadium content up to one vanadium atom per subunit can be restored by incubation with vanadate at neutral or slightly basic pH.

Isolation and purification of V-BrPO. The vanadium-dependent bromoperoxidase from the marine brown alga *Ascophyllum nodosum*, the first naturally occurring vanadium-containing enzyme to be isolated (Vilter, 1984), is the most thoroughly studied of the vanadium-dependent bromoperoxidases. Isolation of V-BrPO from *A. nodosum* requires first homogenization of the algae in

an equal volume of 0.1 to 0.2 M Tris-sulfate buffer, pH 8.3 containing 1.5% crosslinked PVP (polyvinylpyrrolidone). The ground mixture is centrifuged and the supernatant collected. The remaining pellet is reextracted until the bromoperoxidase activity as measured by the MCD assay has decreased significantly. The alginic acids present in the supernatant are next precipitated by the addition of 0.1 M calcium chloride and then removed by centrifugation. The resulting supernatant is then washed and concentrated via a hollow fiber filter concentrator and batch loaded onto an anion exchange column. The enzyme is separated by a potassium chloride salt gradient. The resulting enzyme solution can then be subjected to gel filtration columns and, if necessary, preparative gel electrophoresis techniques (see Appendix I). Effective isolation of V-BrPO from species of *Laminaria* has been achieved using a two-phase system involving polyethylene glycol and potassium carbonate (Jordan & Vilter 1991; Vilter, 1990). However, this procedure has not proven effective for the isolation of V-BrPO from *A. nodosum*.

Two different isozymes of V-BrPO that differ in carbohydrate content have been isolated from *A. nodosum*. The more abundant of these isozymes is present in the thallus of the alga while the other is found on the thallus surface (Krenn et al., 1989, Vilter & Glombitza, 1983). The roles of these two enzymes have not been elucidated; however, it has been proposed that the surface enzyme is part of a host

defense mechanism (Wever et al., 1991). Vanadium-dependent bromoperoxidase activity has been also detected in the cortical and surface protoplasts of *Macrocystis pyrifera* (Butler et al., 1990), *Lamanaria saccharina*, and *Laminaria digitata* (Jordan et al., 1991). In addition, the synthesis of V-BrPO in the protoplasts of *L. saccharina* has been demonstrated with ³⁵S-labeled methionine.

The vanadium site in V-BrPO. The vanadium center in V-BrPO is in the +5 oxidation state (d^0). The oxidation state was established by EPR experiments that showed that no EPR signal is observed for the enzyme alone or under turnover conditions. A vanadium(IV) EPR signal can be detected when the vanadium center is reduced by dithionite (de Boer et al., 1988a). In addition, ⁵¹V NMR of the native V-BrPO from *A. nodosum* shows a broad signal at -1250 ppm (relative to VOCl_3), which is indicative of vanadium(V) (Vilter & Rehder, 1987).

To date the coordination environment of the vanadium center in V-BrPO has not been characterized. Early EXAFS data (Arber et al., 1989) indicated that the vanadium(V) ion was in a distorted octahedral environment, with a terminal oxide at 1.61 Å, three oxygen or nitrogen donor ligands at 1.72 Å, and two nitrogen donor ligands, probably histidines, at 2.11 Å as shown in Figure 1-4.

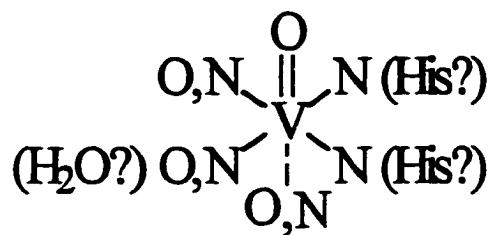


Figure 1-4. Coordination environment of the vanadium(V) center in V-BrPO as initially proposed from EXAFS data (Arber et al., 1989).

EXAFS data of V-BrPO reduced with dithionite (Arber et al., 1989) was consistent with coordination environment of a terminal oxide at 1.63 Å and five oxygen or nitrogen donor ligands comprised of three at 1.91 Å and two at 2.11 Å. The EPR data of the reduced enzyme suggest that the vanadium is coordinated to terminal oxo, several oxygen and/or nitrogen donor ligands, and a water molecule (de Boer et al., 1988a). ESEEM (Electron Spin Envelope Echo Modulation) data of reduced V-BrPO further confirmed that a nitrogen ligand is present in the equatorial plane and that exchangeable protons are present near the vanadium(IV) ion (de Boer et al., 1988b).

A bond valence sum analysis (Thorp, 1992) of the vanadium center in active vanadium bromoperoxidase using the bond lengths obtained by EXAFS was most consistent with a five-coordinate structure (Carrano et al., 1994; Butler & Clague, 1995). A bond valence of 5.08 was obtained for active V-BrPO when a five coordinate structure with one oxide ligand at 1.61 Å, two short V-O bonds at

1.72 Å, and two long V-N bonds at 2.11 Å was assumed. Substitution of the long V-N bonds for V-O bonds gives a calculated valence of 4.83 (Butler & Clague, 1995). For the reduced enzyme, a bond valence close to 4 was obtained using one V=O bond at 1.63 Å, two V-N bonds at 2.11 Å, and two V-O bonds at 1.91 Å (Carrano et al., 1994).

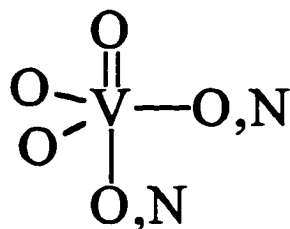


Figure 1-5. Potential coordination environment of the vanadium(V) center in V-BrPO as proposed by a bond valence sum analysis (Carrano et al., 1994; Butler & Clague, 1995).

Vanadium chloroperoxidase. In 1992, a vanadium-dependent chloroperoxidase (V-CIPO) was isolated from the fungus *Curvularia inaequalis*. This enzyme gives an axially symmetric EPR signal very similar to that of V-BrPO from *Ascophyllum nodosum*, suggesting that the vanadium sites in these enzymes are very similar. The kinetic behavior and stability (van Schijndel et al., 1993) of the two enzymes are also comparable. The recently solved crystal structure of the fungal chloroperoxidase (Messerschmidt & Wever, 1996) reveals that the vanadium center, which is located at the end of a four helix tunnel, is bound

essentially as vanadate with three oxygens in the equatorial plane, a hydroxy (or oxo) ligand in one apical position and a single bound histidine residue at the other apical position. The vanadate oxygens are stabilized in the active site by hydrogen bonding to positively charged amino acid side chains and the amide nitrogen of glycine 403. The vanadium binding site in the chloroperoxidase is depicted below:

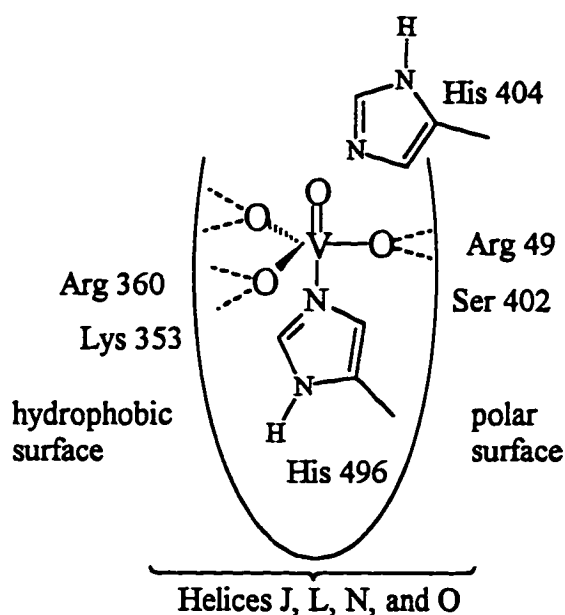


Figure 1-6. Vanadium binding site in vanadium chloroperoxidase from *C. inaequalis*.

Comparison of the sequence of V-CIPO (Simons, B.H. et al., 1995) and the partial sequence of V-BrPO from *A. nodosum* (Vilter, 1995; Messerschmidt & Wever, 1996) reveals areas of high similarity, albeit not true ‘homology’ (Messerschmidt & Wever, 1996). Sections of similarity were found in the region

of the bound histidine residue, the residues that hydrogen bond to the vanadium, and the histidine determined in chloroperoxidase to be critical to catalysis (see below and Chapter 2) (van Schijndel et al., 1994). Thus the vanadium centers, in particular, of the two enzymes are expected to be quite comparable. The bond valence sum analysis of the vanadium center in V-BrPO (Carrano et al., 1994) fits well to a trigonal planar coordination environment with three oxygens in the plane, an oxo ligand in one apical position, and a histidine ligand in the opposite apical position.

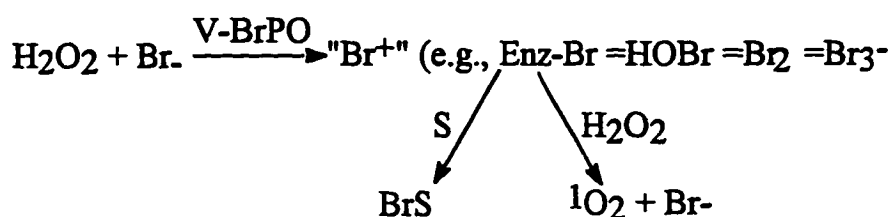
Table 1-1. Amino acid sequence alignment of regions of high similarity between V-CIPO from *Curvularia inaequalis* and V-BrPO from *Ascophyllum nodosum* (Simons et al., 1995; Vilter, 1995)

CIPO	343	T	D	A	G	I	F	S	W	K	E	K	W	E	F	-	E	F	W	R	P	L	S	-	G	V
BrPO	14	E	L	A	Q	R	S	S	W	Y	Q	N	W	Q	V	H	R	F	A	R	P	E	A	L	G	G
Match				A				S	W			W					F		R	P				G		
CIPO	393	F	K	P	P	F	P	A	Y	P	S	G	H	A	T	F	G	G	A	V	F	Q	M	V	R	R
BrPO	90	G	T	P	T	H	P	S	Y	P	S	G	H	A	T	X	N	G	A	F	A	T	V	L	K	A
Match				P			P		Y	P	S	G	H	A	T		G	A								
CIPO	480	W	E	L	M	F	E	N	A	I	S	R	I	F	L	G	V	H	W	R	F	D	A	A	A	
BrPO	152	K	K	L	A	V	N	V	A	F	G	R	Q	M	L	G	I	H	Y	R	F	D	G	I	Q	
Match				L	A			V	A			R			L			H		R	F	D		Q		

The amino acid sequence of the vanadium chloroperoxidase has 609 residues and a resultant molecular mass of 67,488 Da, which is consistent with the SDS-PAGE result of 67 kDa (Simons et al., 1995). Furthermore, this molecular mass agrees

with the SDS-PAGE result for the bromoperoxidase from *A. nodosum*, which further suggests that these enzymes are very similar¹.

Reactivity of V-BrPO. V-BrPO catalyzes both the peroxidative halogenation of suitable organic substrates and the halide assisted disproportionation of hydrogen peroxide. A reaction mechanism for V-BrPO catalyzing the oxidation of bromide is given in Scheme 1-3. In this reaction scheme, V-BrPO first catalyzes the oxidation of a halide by hydrogen peroxide, forming a two-electron oxidized halogen species, i.e., in the case of bromide, a ‘bromonium ion equivalent’. The nature of this species has been pursued by several researchers (see below). Regardless, the oxidized halogen species can then halogenate or ‘bromoperoxidatively oxidize’ a suitable organic substrate or, alternatively, react with a second equivalent of hydrogen peroxide to form dioxygen as shown in Scheme 1-3. Unlike the iron heme haloperoxidases, this enzyme does not exhibit activity in the absence of halides.



Scheme 1-3. Reaction scheme for the reactivity of V-BrPO with bromide and hydrogen peroxide.

¹ Atomic absorption data suggests that the molecular weight of V-BrPO may be higher than 67kDa. See Table 6-1, footnote “a”.

In the absence of a suitable organic substrate, the bromide assisted disproportionation of hydrogen peroxide is stoichiometric with regard to peroxide added; one equivalent of dioxygen is produced for every two equivalents of hydrogen peroxide consumed (Soedjak et al., 1995). In the case of bromide, the dioxygen formed by the halide-assisted disproportionation of hydrogen peroxide was shown to be in the singlet excited state, as was identified by a peak at 1268 nm in the near infrared absorbance spectrum (Everett & Butler, 1989). Unlike the iron heme haloperoxidases, vanadium bromoperoxidase has been shown to be very stable in the presence of singlet oxygen (Everett et al., 1990b). Consistent with the formation of singlet oxygen, oxygen -18 labeling experiments showed that only $^{16}\text{O}_2$ and $^{18}\text{O}_2$ are formed from a mixture of $\text{H}_2^{16}\text{O}_2$ and $\text{H}_2^{18}\text{O}_2$; no mixed isotope products were formed in the disproportionation reaction, which demonstrated that both atoms in the dioxygen come from the same molecule of hydrogen peroxide (Soedjak, 1991; Soedjak et al., 1995).

The rate of formation of dioxygen in the absence of a suitable organic substrate such as MCD is equivalent to the bromination of MCD at high MCD and low H_2O_2 , which suggests that these pathways are competitive and proceed through a common intermediate ("Br⁺" in the case of bromide) formed in the rate limiting step (Everett & Butler, 1989). Furthermore, Everett, et al. demonstrated that the rate of dioxygen formation in the absence of organic substrate (MCD) is

equivalent to the sum of the rates of MCD bromination and dioxygen production in the presence of MCD (Everett et al., 1990a). At higher pH values, dioxygen production competes more effectively with MCD bromination since a much lower concentration of H_2O_2 is necessary to direct the reaction to the disproportionation pathway. The pH of optimum reactivity of V-BrPO as measured by the bromide-assisted production of dioxygen is approximately 5.0, but this value is dependent on the concentrations of bromide and hydrogen peroxide. (Everett et al., 1990a.)

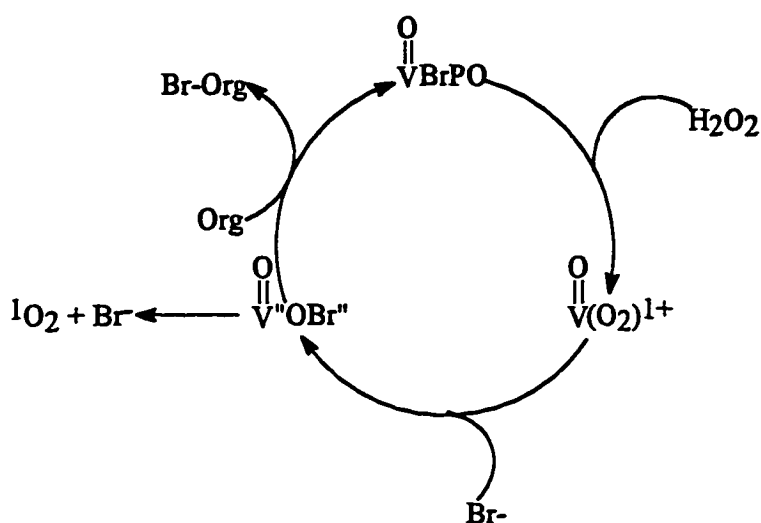
Kinetic studies on V-BrPO. Steady state kinetic analyses of both MCD bromination (Everett et al., 1990a; de Boer & Wever, 1988) and bromide-assisted dioxygen formation (Everett et al., 1990a; Soedjak & Butler, 1991) catalyzed by V-BrPO are consistent with a substrate-inhibited bi-bi ping-pong kinetic mechanism. Kinetic parameters agreed within a factor of two for both pathways. In the case of V-BrPO, the substrates bromide and hydrogen peroxide can each act as noncompetitive inhibitors at certain pH values. Noncompetitive (albeit weak) inhibition by bromide is strongest at pH 4.5 to 5.5 ($K_{ii} = 316 \text{ mM}$, $K_{is} = 262 \text{ mM}$ at pH 5.25 for dioxygen production). Bromide inhibition is essentially non-existent above pH 6.0 (Everett et al., 1990a). Noncompetitive inhibition by hydrogen peroxide increases with pH and is strongest at pH 7-8 ($K_{ii} = 63 \text{ mM}$, $K_{is} = 67 \text{ mM}$ at pH 7.0) (Soedjak, 1991; Soedjak et al., 1995). The K_m for H_2O_2 and accordingly the affinity of the enzyme for this substrate increases dramatically from

pH 4.55 to 6.52; at pH 4.55, the K_m is 662 mM while at pH 6.52, the K_m is 113 for MCD bromination (Everett et al., 1990a). Conversely, the affinity of the enzyme for bromide decreases with increasing pH: at pH 4.55, the K_m for bromide is 4.0 mM while at pH 6.52, the K_m is 25.8 mM for MCD bromination (Everett et al., 1990a).

Mechanistic studies on V-BrPO. Evidence suggests that the V-BrPO-mediated catalysis of bromide oxidation by hydrogen peroxide requires coordination of peroxide to the metal center. A small absorbance decrease between 300 and 340 nm has been reported upon the addition of hydrogen peroxide to V-BrPO (Tromp et al., 1990), which disappears upon addition of bromide. Furthermore, Soedjak (1991) showed that stoichiometric bromination of MCD did not occur when excess bromide was added to high (micromolar) concentrations of V-BrPO, demonstrating that V-BrPO does not oxidize bromide in the absence of peroxide. Thus, the mechanism of catalysis likely involves coordination of peroxide to the metal followed by oxidation of bromide.

The experiments discussed in the previous paragraph suggest that the vanadium center in V-BrPO likely functions as a Lewis acid catalyst that coordinates and activates hydrogen peroxide toward halide oxidation and does not itself undergo any changes in oxidation. A Lewis acid catalytic mechanism is illustrated in Scheme 1-4. If the vanadium(V) ion were to function by an electron

transfer mechanism, it would be reduced to vanadium(III) or vanadium(IV) and a protein anion radical upon halide oxidation and would be subsequently reoxidized by peroxide to vanadium(V). However, in this mechanism, bromide oxidation and accordingly MCD bromination would be expected to occur. As described above, a peroxide source is required for bromination (Soedjak, 1991). In addition, because V-BrPO does not exhibit an ESR signal during turnover (de Boer et al., 1988a) and does not exhibit bromination activity in the one electron-reduced state, vanadium(IV) most likely does not play a role in the catalytic mechanism.

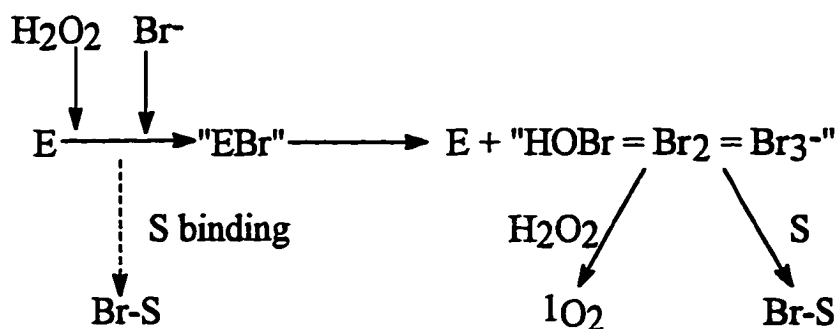


Scheme 1-4. Lewis acid mechanism for the peroxidative oxidation of bromide catalyzed by V-BrPO.

As discussed above and further in Chapter 5, the nature of the ‘bromonium ion equivalent’ intermediate species remains of some debate and has been investigated by several researchers. De Boer and Wever attempted to characterize

the oxidized bromine intermediate by examining the dependence of bromination or bromoperoxidative oxidation of organic substrates on the concentration of these substrates under conditions of high bromide concentration, high enzyme concentration, and low pH (pH 5) (conditions under which tribromide formation is favored) (de Boer & Wever, 1988). The lack of a dependence on organic substrate concentration suggested that the enzyme was simply generating tribromide and HOBr. However, the abundance of chiral halogenated natural products found in marine algae containing V-BrPO enzymes suggests otherwise.

More recently, kinetic studies on the bromination and bromoperoxidative oxidation of several 2 - and 3-substituted indoles demonstrated that the reactions of these substrates catalyzed by V-BrPO differed from those of freely diffusable aqueous bromine species. Furthermore, strong evidence for binding of these indoles to V-BrPO was obtained from Stern-Volmer fluorescence quenching studies (Tschirret-Guth & Butler, 1994); V-BrPO was able to effectively quench the fluorescence of 2-phenylindole. A binding constant of $1.1 \times 10^5 \text{ M}^{-1}$ for V-BrPO and 2-phenylindole at pH 8.0 was calculated from these experiments. These results suggested a revised scheme for the enzymatic reaction (Scheme 1-5):



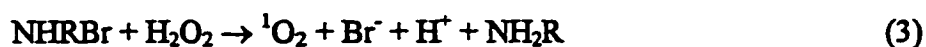
Scheme 1-5. Proposed revised scheme for the peroxidation of bromide catalyzed by V-BrPO.

Thus, current evidence suggests that the nature of the brominating intermediate as free or enzyme-bound depends on the nature of the substrate. In the absence of an appropriate organic substrate, the enzyme releases freely diffusable oxidized bromine species.

Bromamines, "Br⁺NHR", have previously been proposed as intermediates in haloperoxidase reactions, specifically with regard to the generation of singlet oxygen (Kanofsky, 1989), and present an attractive option for an enzyme-bound "bromonium ion equivalent" depicted in Scheme 1-4. These compounds can be formed by the reaction of an amine, bromide, and a peroxide source:



Bromamine formation can not be detected if it occurs from the turnover of V-BrPO with bromide and hydrogen peroxide because bromamines rapidly react with hydrogen peroxide to generate singlet oxygen:

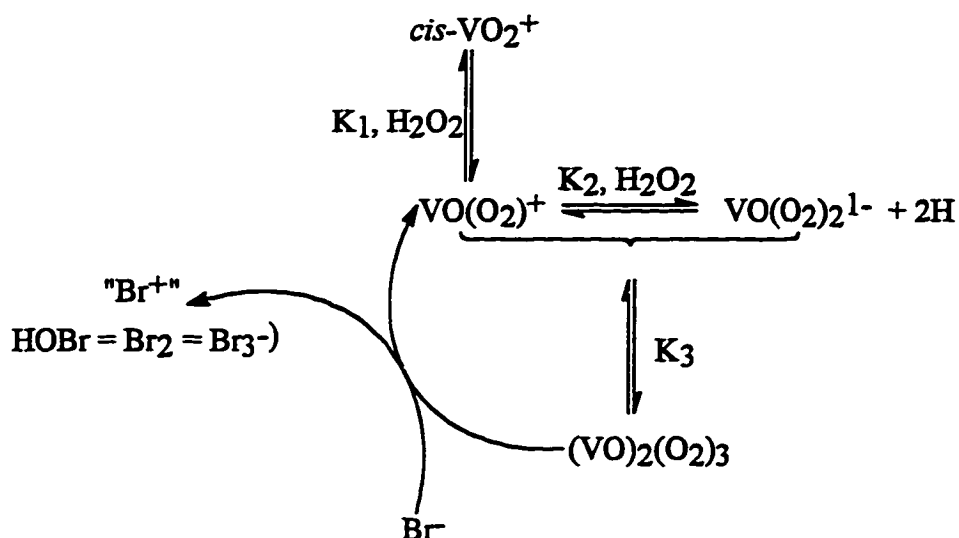


However, bromination of exogenous amines by V-BrPO has been observed when peracetic acid is used as the peroxide source (Soedjak & Butler, 1990), because peracetic acid is not capable of reducing the bromamine. Thus, it is quite feasible that bromamines are formed during the turnover of bromide and hydrogen peroxide by V-BrPO; accordingly, an enzyme bound bromamine could provide a means for selective bromination of preferred organic substrates (e.g., indoles).

Functional biomimics of V-BrPO. In the absence of a spectroscopic "handle" by which to monitor the mechanism of catalysis of V-BrPO, functional inorganic model complexes have been investigated in which the vanadium (V) center can be observed (de la Rosa, et al, 1992; Clague & Butler, 1995; Colpas, et al, 1994; Colpas et al., 1996)). The first functional mimic of V-BrPO to be reported in the literature was *cis*-dioxovanadium(V), VO_2^+ (de la Rosa et al., 1992). VO_2^+ functions in acidic solution as a biomimic of V-BrPO by catalyzing the bromination of organic substrates and the bromide-assisted disproportionation of hydrogen peroxide to form dioxygen (de la Rosa et al., 1992; Clague & Butler, 1995).

In acidic solution, VO_2^+ coordinates one or two equivalents of hydrogen peroxide to form $\text{VO}(\text{O}_2)^+$ or $\text{VO}(\text{O}_2)_2^-$, respectively, depending on the concentrations of acid and H_2O_2 . The first formation constant, K_1 , is 3.5×10^4 and

the second formation constant, K_2 , is about 1, depending on ionic strength (Secco, 1980; Orhanovic & Wilkins, 1967). Thus, in acid, even in the presence of excess H_2O_2 both the monoperoxo and diperoxo species are present. Recently, Clague and Butler (1995) demonstrated that the initial rate of oxidation of bromide by micromolar concentrations of VO_2^+ in the presence of 25- to 200-fold excess H_2O_2 over vanadium and 200-fold excess NH_4Br over peroxide in acidic solution exhibits a second order dependence on vanadium concentration (Clague & Butler, 1995). ^{51}V NMR experiments by Harrison and Howarth (1985) have indicated that the monoperoxo and diperoxo complexes of vanadium(V) can dimerize to form a triperoxo dimer. In fact, the maximal rate of bromide oxidation in the study by Clague and Butler (1995) was achieved when the concentrations of the mono- and diperoxo complexes were determined to be equal, suggesting that in fact the triperoxo dimer is the active oxidizing species in this mimic. Clague and Butler (1995) determined a formation constant of $32 M^{-1}$ for the dimer:

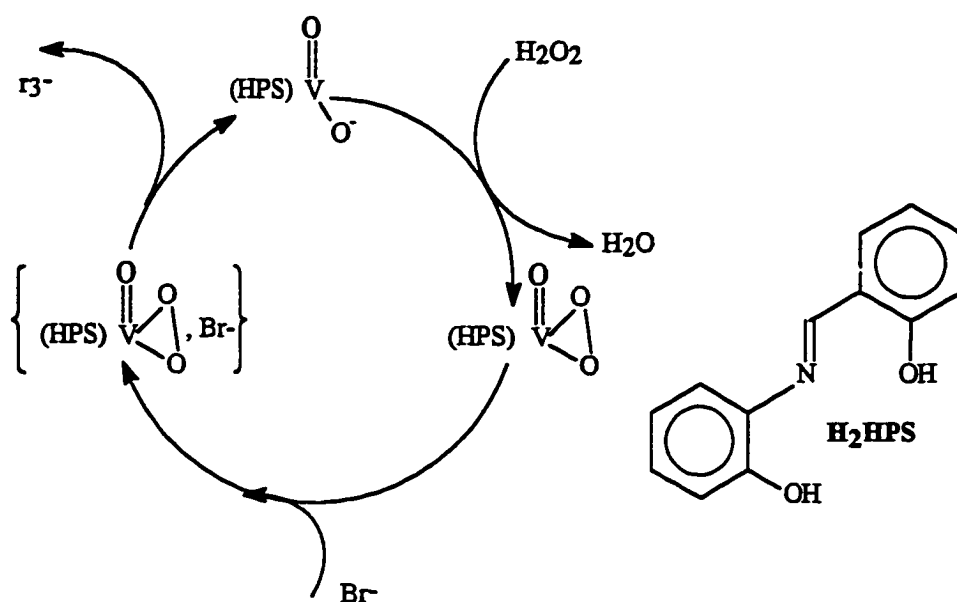


Scheme 1-6. Reaction mechanism for the oxidation of bromide by $(\text{VO})_2(\text{O}_2)_3$.

The bimolecular rate constant for bromide oxidation by $(\text{VO})_2(\text{O}_2)_3$ was calculated to be $4.1 \text{ M}^{-1} \text{ s}^{-1}$. This value is 10^3 to 10^5 times slower than that for the enzyme. In addition, because formation of the dimer requires both $\text{VO(O}_2\text{)}^+$ and $\text{VO(O}_2\text{)}_2^-$, this mimic functions only in acidic conditions, while the enzyme functions optimally at near neutral pH. Neither $\text{VO(O}_2\text{)}^+$ nor $\text{VO(O}_2\text{)}_2^-$ can oxidize bromide.

$(\text{HPS})\text{VO(OH)}$, where H_2HPS is the Schiff base ligand hydroxyphenylsalicylideneimine, is also a catalyst of bromide oxidation by hydrogen peroxide in aqueous DMF solution (Clague & Butler, 1993). ^{51}V NMR results establish that $(\text{HPS})\text{VO(OH)}$ coordinates one equivalent of H_2O_2 forming the monoperoxo, $(\text{HPS})\text{VO(O}_2\text{)}^-$ species and releasing one equivalent of H_3O^+ .

The monoperoxo complex $(\text{HPS})\text{VO}(\text{O}_2)^-$ then oxidizes bromide forming the dioxo species $(\text{HPS})\text{VO}_2^-$, which can then coordinate another equivalent of H_2O_2 and start through the cycle again as shown in Scheme 1-7. In the absence of added acid only one turnover is observed; however, upon the addition of stoichiometric acid with respect to H_2O_2 consumed, the reaction becomes catalytic. Thus this model system requires relatively mild acidic conditions for catalytic bromination compared to *cis*-dioxovanadium(V).



Scheme 1-7. Reaction mechanism for the oxidation of bromide by peroxide catalyzed by $(\text{HPS})\text{V}(\text{OH})$.

Similar systems were developed by Pecoraro and coworkers (Colpas et al., 1994, 1996). They prepared several functional complexes with derivatized tripodal amine chelating ligands, including $\text{VO}(\text{O}_2)(\text{Heida})^-$, where H_3eida is *N*-(2-

hydroxyethyl)iminodiacetic acid, $\text{VO}(\text{O}_2)(\text{ada})^-$, where H_2ada is *N*-(2-amidomethyl)iminodiacetic acid, and $\text{VO}(\text{O}_2)(\text{Hnta})^-$, where H_3nta is nitrilotriacetic acid. Like the peroxo complex of HPS, each of these compounds requires one equivalent of acid to oxidize one equivalent of bromide or iodide in acetonitrile. In addition, these complexes also recoordinate peroxide and proceed through catalytic oxidations provided that the necessary equivalents of acid are present.

Vanadium Peroxo Complexes: Structural Characterization

While studies on vanadium peroxo complexes that catalyze halide oxidation have only recently been initiated, the scope of the reactivity of these complexes is actually remarkably broad. Peroxovanadium(V) complexes perform a variety of net two-electron oxidation reactions. For example, alkenes and allylic alcohols can be epoxidized and hydroxylated (Talsi et al., 1991, 1993; Sharpless & Michaelson, 1973; Michaelson et al., 1977; Sharpless & Verhoeven, 1979; Mimoun et al., 1983a, 1983b, 1986; Bortolini et al., 1980), and primary and secondary alcohols can be oxidized to aldehydes and ketones (Bortolini et al., 1985; Conte et al., 1988). Benzene and other arenes and alkanes can also be hydroxylated (Mimoun et al., 1983a, 1983b; Shul'pin et al., 1983; Attansio et al., 1992; Bonchio et al., 1989; Bianchi, et al., 1993). In addition, sulfides can be oxidized to sulfoxides and sulfones (Bortolini et al., 1980; Nakajima et al., 1989; Ballisteri et al., 1991;

Bortolini et al., 1982; Bonchio et al., 1989). Examples of these reactions are given in Figure 1-7.

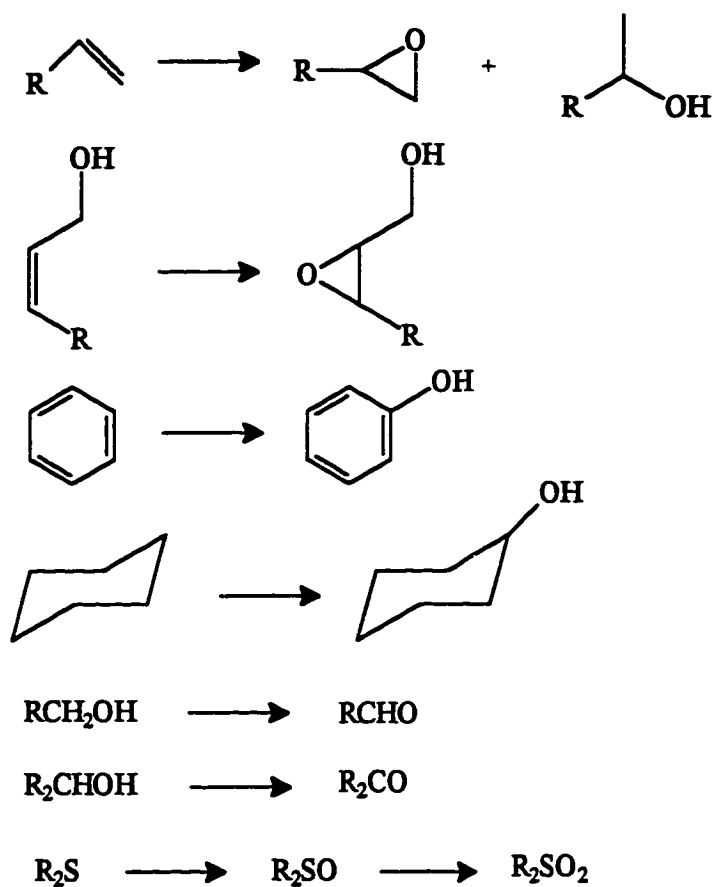


Figure 1-7. Examples of the reactions mediated by vanadium(V) peroxo complexes.

Some of these transformations have even been modified to be enantioselective. For instance, chiral hydroxamic acids serve as ligands to vanadium(V) in the catalytic, asymmetric epoxidation of allylic alcohols by *t*-BuOOH (Michaelson et al., 1977). In addition, H₂sal-L-ala forms a complex with

vanadium(V), which is catalytically active in the asymmetric oxidation of methyl phenyl sulfide by *t*-BuOOH (Nakajima et al., 1989).

In order to gain insight into the reactivity of these complexes with both organic and inorganic substrates (e.g., halides) numerous oxoperoxovanadium(V) and oxodiperoxovanadium(V) complexes have been characterized at the crystallographic level (Table 1-2). Peroxide is side-on bound in all of the cases shown (Figure 1-8). The monomeric oxoperoxo complexes all have one or two peroxides bound in the equatorial plane relative to the oxo ligand. In the majority of the structures the geometry is pentagonal bipyramidal. In a few cases a pentagonal pyramidal is considered; however, the oxo ligand of another molecule may well serve as the seventh ligand as a long axial bond.

The key differences in peroxide coordination between mono- and diperoxo complexes can be seen in Table 1-2. In general, the O-O peroxy bond is longer in diperoxo complexes than in monoperoxo complexes. In the monoperoxo complexes, the peroxide is symmetrically coordinated, while in the diperoxo complexes, the V-O_{trans} bond is slightly longer than the V-O_{cis} bonds, where V-O_{trans} and V-O_{cis} are defined in Figure 1-8.

Table 1-2. Bond lengths of peroxovanadium(V) compounds^d

	O-O	V-Operoxo-cis	V-Operoxo-trans	V=O	Reference ^a
			Oxoperoxo complexes		
[VO(O ₂)(pic)(bipy)]·H ₂ O	1.424(7)	1.862(5), 1.887(5)		1.604(5)	Szentivanyi & Stomberg, 1983a
K ₃ [VO(O ₂)(ox) ₂]-1/2H ₂ O	1.430(10)	1.871(6), 1.882(6)		1.625(6)	Stomberg, 1986
NH ₄ [VO(O ₂)(H ₂ O)(dipic)]·1.3H ₂ O	1.441(3)	1.870(2), 1.872(2)		1.579(2)	Drew & Einstein, 1973
NH ₄ [VO(O ₂)(DA)]	1.435(5)	1.876(3), 1.886(3)		1.587(3)	Djordjevic et al., 1985
[VO(O ₂)(bipy) ₂]ClO ₄	1.24c	1.81, 1.86		1.625	Sergienko et al., 1988
[VO(O ₂)(phen) ₂]ClO ₄	1.3c	1.83, 1.86		1.679	Sergienko et al., 1988
VO(O ₂)(PAN)(pyr)	1.440(7)	1.859(5), 1.847(5)		1.608(5)	Mimoun et al., 1983a
			Oxidiperoxo complexes		
(NH ₄) ₂ [VO(O ₂)(bipy)] ₂ ·4H ₂ O	1.467(3) ^a	1.875(2) ^a	1.912(2) ^a	1.612(2)	Miecheng et al., 1988
NH ₄ [VO(O ₂)(bipy)]·4H ₂ O	1.465(4), 1.471(4)	1.883(3), 1.880(3)	1.911(3), 1.909(3)	1.619(3)	Campbell et al., 1983
K ₃ [VO(O ₂)(CO ₃)]	1.467(3) ^a	1.873(2) ^a	1.945(2) ^a	1.617(3)	Szentivanyi & Stomberg, 1983b
K ₃ [VO(O ₂)(ox)]·H ₂ O	1.466(4) ^a	1.876(3) ^a	1.923(3) ^a	1.620(3)	Miecheng et al., 1988
K ₃ [VO(O ₂)(ox)]·H ₂ O	1.460(6), 1.451(6)	1.868(4), 1.856(4)	1.934(4), 1.911(4)	1.622(4)	Stomberg, 1985
K ₂ [VO(O ₂)(pic) ₂ ·2H ₂ O	1.464(5), 1.458(6)	1.881(4), 1.895(4)	1.899(4), 1.917(4)	1.599(4)	Begin et al., 1975
K ₂ [VO(O ₂)(OHpic) ₂ ·3H ₂ O	1.463(2), 1.461(2)	1.902(2), 1.877(2)	1.924(2), 1.908(2)	1.608(2)	Begin et al., 1975
(NH ₄) ₃ [VF ₂ O(O ₂)]	1.466(2), 1.462(2)	1.890(2), 1.887(2)	1.921(2), 1.927(2)	1.609(2)	Stomberg, 1984a
Cs ₂ [VFO(O ₂)] ₂	1.44(3), 1.46(2)	1.85(2), 1.90(2)	1.90(2), 1.90(2)	1.62(2), 1.62(3) ^b	Stomberg & Olson, 1984

K ₂ [VO(O ₂) ₂]	1.48(3), 1.52(4) ^b 1.468(7), 1.505(6)	1.96(2), 1.86(3) ^b 1.882(5), 1.880(4) 1.930(5), 1.882(7)	1.91(2), 1.92(3) ^b 1.906(6), 1.901(4) 1.888(6), 1.858(7)	1.620(5), 1.605(7)	Stromberg, 1984b
NH ₄ [VO(O ₂) ₂ (NH ₃)	1.472(4) ^a	1.882(3) ^a	1.883(3) ^a	1.606(3)	Drew & Einfeld, 1972
(Hbipy)[VO(O ₂) ₂ (bipy)(3+x)H ₂ O 2-(2-x)H ₂ O	1.473(4), 1.474(4)	1.862(3), 1.914(3)	1.942(3), 1.938(3)	1.619(3)	Stromberg & Szerthavnyl, 1984
Oxoperoxo dimers					
K ₂ [VO(O ₂)(cit)] ₂ · H ₂ O	1.427(7) ^a	1.873(1), 1.868(1) ^a		1.661(1) ^a	Djordjevic et al., 1989
K ₃ [F(O ₂)[VO(O ₂)F] ₂	1.441(5), 1.447(5), 1.467(5) (bridge)	1.856(5), 1.872(5), 2.038(4) (bridge)	1.873(4), 1.871(5), 1.974(4) (bridge)		Lapshin et al., 1990a
Oxodiperoxo dimers					
Λ ₃ (NH ₄) ₃ [HO(VO(O ₂) ₂) ₂] · H ₂ O (NH ₄) ₄ [O(VO(O ₂) ₂) ₂]	1.449(26), 1.44(24) 1.447(24), 1.436(24)	1.879(4), 1.864(3), 1.876(4), 1.879(3)	1.893(4), 1.915(3), 1.881(3), 1.912(3)	1.597(4) ^a 1.578(18) ^a	Campbell et al., 1985 Sverinsson & Stromberg, 1971
(NH ₄) ₄ [O(VO(O ₂) ₂) ₂]	1.469(4), 1.465(3), 1.474(4), 1.463(4)	1.884(3), 1.875(3), 1.882(3), 1.878(3)	1.896(3), 1.914(3), 1.895(3), 1.912(2)	1.601(3), 1.613(3)	Stromberg et al., 1984
(Hbipy)[H(VO(O ₂) ₂ (bipy))] ₂ · xH ₂ O · 6H ₂ O	1.461(3), 1.471(3) ^a	1.892(2), 1.869(2) ^a	1.995(2), 1.903(2) ^a	1.612(2) ^a	Szerthavnyl & Stromberg, 1984
[N(CH ₃) ₄] ₂ [V ₂ P ₂ (O ₂) ₄ (H ₂ O)] · 2 H ₂ O	1.466(5), 1.460(4) 1.458(5), 1.468(5)	1.868(3), 1.883(4) 1.868(3), 1.919(4)	1.880(4), 1.863(4) 1.865(3), 1.878(3)	1.601(4), 1.591(4)	Lapshin et al., 1989
K ₂ [V ₂ O ₂ (O ₂) ₄ (H ₂ O)] · 3H ₂ O	1.465(4), 1.469(3), 1.470(5), 1.457(5)	1.869(4), 1.891(4), 1.947(4), 1.878(3)	1.869(4), 1.914(4), 1.894(4), 1.881(3)	1.604(5), 1.586(3)	Lapshin et al., 1990b

Triperoxo Complex		Westermann et al., 1988
(NH ₄) ₂ V(O ₂) ₃ F	1.47(3) ^a	
	1.84(4), 1.95(3), 2.07(3) ^a	
Alkylperoxo Complex		Mimoun et al., 1983b
(dipic)V(O)(OOtBu)·H ₂ O	1.503(6)	
	1.872(3), 1.999(3)	1.574(3)

^a Averages reported. ^b Duplicate structures analyzed. ^c The authors attribute these short bonds to the transfer of electron density from the peroxide ligand to the aromatic ligands. Since such an effect is not observed (or observed to an even lesser degree) in other peroxo or diperoxo complexes containing aromatic ligands, the short bonds may arise from disorder in the crystals. ^d Abbreviations: bipy: 2,2'-bipyridine; OHpic: 3-hydroxypyridine-2-carboxylate; cit: citraoxx:oxalato; dpic:pyridine-2,6-dicarboxylate; PAN: 1-(2-pyridylazo)-2-naphthol; GlyH:glycine; pic:picolinato; pyridine-2-carboxylate; Hbipy:2,2'-bipyridiumphen:1,10-phenanthroline; IDA:iminodiacetato. ^e References for the table are listed at the end of the chapter.

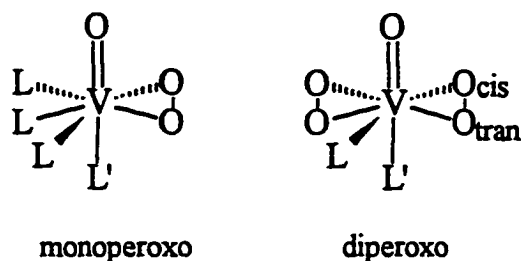


Figure 1-8. The coordination geometry of mono- and diperoxo vanadium complexes.

Infrared and Raman spectroscopy have also provided much information on the structure of vanadium(V) peroxo complexes (Griffith & Wickins, 1968). The mode of peroxide coordination can be established by these methods. Bidentate peroxide creates a local C_{2v} environment that has three IR and Raman active modes: the symmetric O-O stretch, the symmetric metal-peroxo stretch and the asymmetric metal peroxo stretch (Griffith & Wickins, 1968). These vibrations occur at approximately 880, 600, and 500 cm^{-1} respectively, although the metal peroxo stretches are not always clearly distinguishable (Griffith & Wickins, 1968). In fact, bidentate peroxide is the norm and representative vibrational bands are shown in Table 1-3. In the case of an end-on bound hydroperoxide, only one metal-peroxo oxygen stretch would be seen and an OOH deformation should be seen above 1100 cm^{-1} . Bridging peroxide has only a weak dipole and should be

very weak in the IR, and, likewise, peroxide of crystallization should be invisible in the IR (Griffith & Wickins, 1968).

Table 1-3. Stretching Frequencies of Selected Peroxovanadium(V) Compounds^a

	V=O	O-O	V-Opc	Ref ^b
Oxoperoxo complexes				
VO(O ₂)(pic)(py) ₂	945	935	575,560	Mimoun et al., 1983a
VO(O ₂)(pic)(bipy)(H ₂ O)	945	935	575,560	Mimoun et al., 1983a
VO(O ₂)(pic)(MeOH)(H ₂ O)	975	940	580,550	Mimoun et al., 1983a
(NH ₄)[VO(O ₂)(OH)F ₂]	970s	895vs	590s,550s	Chakrovorti & Sarkar, 1976
Pentagonal Bipyramidal Oxodiperoxo Complexes				
K[VO(O ₂) ₂ (bipy)]_5H ₂ O	930 vs	875s,856vs	621m,582s	Vuletic & Djordjevic, 1973
K[VO(O ₂) ₂ (phen)]_3H ₂ O	925 vs	870s,854vs	635m,590m	Vuetic & Djordejevic, 1973
K ₃ [VO(O ₂) ₂ (ox)]_2H ₂ O	930vs	877s,852w	631s,5845s	Vuletic & Djordjevic, 1973
[VO(O ₂) ₂ (ox)] ³⁻ solution	949vs	894s	636w,592m	Schwendt & Pliscarcik, 1990
K ₃ [VO(O ₂) ₂ CO ₃]	936s	877m	626m,586m	Schwendt et al., 1980

Pentagonal Pyramidal Oxodiperoxo Complexes

$[\text{VO}(\text{O}_2)_2\text{GlyH}]^+$	960	850	605,510	Bhattacharjee et al., 1990
$[\text{VO}(\text{O}_2)_2\text{F}]^+$	952s	875s	618s,526m	Nour et al., 1989
$(\text{NH}_4)[\text{VO}(\text{O}_2)_2\text{NH}_3]$	1000m,957s	884S	623m,533vs	Schwendt & Písarčík, 1982
$[\text{VO}(\text{O}_2)_2\text{NH}_3]^+$ solution	984s	888s	627m,537vs	Schwendt & Písarčík, 1982

Triperoxo Complexes

$\text{Na}[\text{V}(\text{O}_2)_3]$	850	600,530	Chaudhuri et al., 1985
$\text{K}_2[\text{V}(\text{O}_2)_3\text{Cl}]$	855	620	Chaudhuri & Ghosh, 1984

38

Tetraperoxo Complexes

$\text{K}_3[\text{V}(\text{O}_2)_4]$	854s	620s567vs	Campbell et al., 1989
--------------------------------------	------	-----------	-----------------------

^a The vibrational modes of peroxovanadium complexes have been recently reassigned by Schwendt, et al. (1988) from normal coordinate analysis. The older analysis as described by Griffith has been used in this table (Griffith & Wickins, 1968). This analysis assumes a C_{2v} symmetry for the vanadium-peroxo triangle which has $2A_1 + B_2$ modes: $\nu_1 = A_1 = \text{O-O stretch}$, $\nu_2 = A_1 = \text{symmetric V-O}_{\text{peroxide}} \text{ stretch}$, and $\nu_3 = B_2 = \text{asymmetric V-O}_{\text{peroxide}} \text{ stretch}$. ^b References for the table are listed at the end of the chapter.

In the absence of interfering ligand vibrations, important structural distinctions can be determined from the frequencies of the symmetric and asymmetric metal-peroxo vibrations. In monoperoxo complexes, these vibrations essentially overlap at about 560 cm^{-1} or are only slightly separated. A monodentate ligand on a diperoxo complex results in a splitting of roughly 100 cm^{-1} , with the two bands occurring at approximately 630 and 520 cm^{-1} , and a bidentate ligand results in a splitting of roughly 40 cm^{-1} , with the two bands occurring at approximately 625 and 585 cm^{-1} (Schwendt, 1983). Representative examples of the vibrational frequencies detected for these different types of complexes are shown in Table 1-3.

Chaudhuri and coworkers have reported the preparation of complexes of the form $A[V(O_2)_3]$ where A^+ is Na^+ or K^+ (Chaudhuri et al., 1985) and $A_2[V(O_2)_3L]$ where $L = F^-$ or Cl^- (Chaudhuri & Ghosh, 1982, 1984) and A^+ is NH_4^+ , Na^+ or K^+ . The IR spectra of these complexes do not have $V=O$ bands, and the O-O bands are shifted to lower frequencies than the mono- and diperoxo complexes, possibly due to a reduction in bond order (see Table 1-3). More recently the structure of $(NH_4)_2[V(O_2)_3F] \cdot H_2O$ was reported to be a trigonal prism with bidentate peroxide ligands. Like the pentagonal bipyramidal diperoxo complexes, two of the three peroxides are asymmetrically coordinated. The peroxo ligand trans to fluoride has much longer bonds as shown in Table 1-2 (Westermann et al., 1988). Triperoxo

complexes containing bidentate heteroligands, $A_3[V(O_2)_3L]$ where $L = \text{bipy, phen,}$ or ox^{2-} have also been reported (Guerchais & Sala-Pala, 1971). However, later IR analyses by Vuletic and Djordjevic suggested that diperoxo complexes were formed in these preparations (Vuletic & Djordjevic, 1973). In addition, the crystal structure of " $K_3[V(O_2)_3(\text{ox})] \cdot H_2O$ " was more recently reported and found to actually be $K_3[VO(O_2)_2(\text{ox})] \cdot H_2O_2$ (Campbell et al., 1983).

To date, no structures of tetraperoxo complexes have been reported. The complex $K_3[V(O_2)_4]$ has been analyzed by infrared (Schwendt, 1983; Offner & Dehand, 1971; Campbell et al., 1989) and Raman spectroscopy (Campbell et al., 1989). Like the triperoxo complexes, the O-O stretch is shifted to a lower frequency, which may be indicative of longer O-O bonds. In addition, modes at 620 and 565 cm^{-1} indicate bidentate peroxide coordination (Schwendt, 1983; Offner & Dehand, 1971; Campbell et al., 1989).

While many peroxovanadium(V) complexes have been characterized in the solid state, the solution conformations of these complexes are less clear. Vibrational data show that side-on bound peroxide is still the norm in aqueous solution. Raman data recorded on the complexes $K_2[VO(O_2)_2(\text{ox})] \cdot H_2O$ (Schwendt & Pisarcik, 1990) and $NH_4[VO(O_2)_2NH_3]$ (Schwendt & Pisarcik, 1982) in water suggest that these species have essentially the same bonding configurations in solution and the solid state.

Circular dichroism (CD) was used in a series of clever experiments to provide evidence for side-on bound peroxide in organic solvents as well (Bortolini et al., 1981; DiFuria & Modena, 1985). Addition of excess H_2O_2 to the vanadate complex of the chiral ligand (-)-menthol, $\text{VO}(\text{OMent})_3$ should give either $\text{VO}(\text{OMent})(\text{OOH})(\text{OO}^-)$ if peroxide is end-on bound or $\text{VO}(\text{O}_2)_2^-$ if peroxide is side-on bound. The latter no longer has a chiral ligand and thus should not have a CD spectrum. Furia and Modena showed that addition of H_2O_2 to $\text{VO}(\text{OMent})_3$ in DMF (where only the diperoxo species is observed) caused the $\text{VO}(\text{OMent})_3$ CD band to disappear and no new bands appeared, thus suggesting that peroxide coordination is bidentate in solution.

References

- Allain, E.J., Hager, L.P., Deng, L., Jacobsen, E.N. (1993) *J. Am. Chem. Soc.* **115**, 4415-4416.
- Ahren, T.J., Allain, G.G., Medcalf, D.G. (1980) *Biochim. Biophys. Acta* **616**, 329.
- Arber, J.M., de Boer, E., Garner, C.D., Hasnain, S.S., Wever, R. (1989) *Biochemistry*, **28**, 7968-7973.
- Attanasio, D., Suber, L., Shul'pin, G. B. (1992) *Bull. Russ. Acad. Sci.,-Div.Chem. Sci.* **41**, 1502-1504.
- Baden, D.G. & Corbett, M. D.(1980) *Biochem. J.* **187**, 205-211.
- Ballistreri, F.P., Tomaselli, G.A., Toscano, R.M., Conte, V., Di Furia, F. (1991) *J. Am. Chem. Soc.* **113**, 6209-12.
- Bantleon, R., Altenbuchner, J., van Pee, K.-H. (1994) *J. Bacteriol.* **176**, 2339-2347.
- Begin, D., Einstein, F.W.B., Field, J. (1975) *Inorg. Chem.* **14**, 1785-1790.
- Beissner, R.S., Guilford, W.J., Coates, R.M., Hager, L.P. (1981) *Biochemistry* **20**, 3724-3731.
- Bhattacharjee, M., Chaudhury, M.K., Islam, N.S., Paul, P.C. (1990) *Inorg. Chim. Acta* **169**, 97-100.
- Bianchi, M., Bonchio, M., Conte, V., Coppa, V., DiFuria, F., Modena, G., Moro, S., Standen, S. (1993) *J. Mol. Catal.* **83**, 107-116.
- Bjorkling, F., Godtfredsen, S.E., Kirk, O. (1990) *J. Chem. Soc. Chem. Commun.* 1301-1303.
- Bonchio, M., Conte, V., Di Furia, F., Modena, G. (1989a) *J. Org. Chem.* **54**, 4368-71.
- Bonchio, M., Conte, V., Di Furia, F., Modena, G., Padovani, C., Sivak, M. (1989b) *Res. Chem. Intermed.* **12**, 111-24.

- Bortolini, O., Di Furia, F., Scrimin, P., Modena, G. (1980) *J. Mol. Catal.* 7, 59-74.
- Bortolini, O., Di Furia, F., Modena, G., Scattolin, E. (1981) *Nouv. J. Chim.* 5, 537-540.
- Bortolini, O., Di Furia, F., Modena, G. (1982) *J. Mol. Catal.* 16, 61-8.
- Bortolini, O., Conte, V., Di Furia, F., Modena, G. (1985) *Nouv. J. Chim.* 9, 147-50.
- Brady, L., Brzozowski, A., Derewenda, Z.S., Dodson, E., Dodson, G., Tolley, S., Turkenburg, J.P., Christiansen, L., Huge-Jensen, B., Norskov, L., Thim, L., Menge, U. (1990) *Nature* 343, 767-770.
- Burreson, B.J., Moore, R.E., Roller, P. (1975) *Tetrahedron Lett.*, 473-476.
- Butler, A. & Clague, M.J. (1995) in 'Mechanistic Bioinorganic Chemistry', Advances in Chemistry Series Vol 246, Thorp, H.H. & Pecoraro, V.L., eds., Washington, D.C.: American Chemical Society, pp 330-349.
- Butler, A. & Walker, J.V. (1993) *Chem. Rev.* 93, 1937-1944.
- Butler, A., Soedjak, H.S., Polne-Fuller, M., Gibor, A., Boyen, C., Kloareg, B. (1990) *J. Phycol.* 26, 589-592.
- Campbell, N.J., Dengel, A.C., Griffith, W.P. (1989) *Polyhedron* 8, 1379-1386.
- Campbell, N.J., Capparelli, M.V., Griffith, W.P., Skapski, A.C. (1983) *Inorg. Chim. Acta* 77, L215-L216.
- Campbell, N.J., Flanagan, J., Griffith, W.P., Shapski, A.C. (1985) *Transition Met. Chem.* 10, 353-354.
- Carrano, C.J., Mohan, M., Holmes, S.M., de la Rosa, R., Butler, A., Charnock, J.M., Garner, C.D. (1994) *Inorg. Chem.* 33, 646-655.
- Chakrovorti, M.C., Sarkar, A.R., (1976) *J. Fluorine Chem.* 8, 255-262.
- Chaudhuri, M.K., Ghosh, S.K., Islam, N.S. (1985) *Inorg. Chem.* 24, 2706-7.
- Chaudhuri, M.K., Ghosh, S.K. (1984) *Inorg. Chem.* 23, 534-537.

- Chaudhuri, M.K., Ghosh, S.K. (1982) *Inorg. Chem.* 21, 4020-4022.
- Chen, Y.P., Lincoln, D.E., Woodin, S.A., Lovell, C.R. (1991) *J. Biol. Chem.* 266, 23909-23915.
- Clague, M.J. & Butler, A., (1995) *J. Am. Chem. Soc.* 117, 3475-84.
- Clague, M.J. & Butler, A. (1993) *Inorg. Chem.* 32, 4754-4761.
- Colonna, S. Gaggero, N., Manfredi, A., Casella, L., Gullotti, M., Crrea, G., Pasta, P. (1990) *Biochemistry* 29, 10465.
- Colonna, S. Gaggero, N., Manfredi, A., Casella, L., Gullotti, M. (1988) *J. Chem. Soc. Chem. Commun.*, 1451.
- Colpas, G.J.; Hamstra, B.J.; Kampf, J.W.; Pecoraro, V.L. (1996) *J. Am. Chem. Soc.* 118, 3469-3478.
- Colpas, G.J.; Hamstra, B.J.; Kampf, J.W.; Pecoraro, V.L. (1994) *J. Am. Chem. Soc.* 116, 3627-3628.
- Conte, V.; Di Furia, F.; Modena, G. (1988) *J. Org. Chem.* 53, 1665-9.
- Cuperus, F.P., Bouwer, S.T., Kramer, G.F.H., Derksen, J.T.P. (1994) *Biocatalysis* 9, 89-96.
- Danner, D.J. & Morrison, M. (1971) *Biochim. Biophys. Acta* 235, 44.
- de Boer, E., Boon, E., Wever, R. (1988a) *Biochemistry* 27, 1629-1635.
- deBoer, E., Klaassen, A.A.K., Keijzers, C.P., Reijerse, E.J., Collison, D., Garner, C.D., Wever, R. (1988b) *FEBS Lett.* 235, 93-97.
- deBoer, E. & Wever, R. (1988) *J. Biol. Chem.* 263, 12326-32.
- de Boer, E., Tromp, M.G.M., Plat, H., Krenn, B.E., Wever, R. (1986) *Biochim. Biophys. Acta.* 872, 104-115.
- de la Rosa, R. I.; Clague, M. J.; Butler, A. (1992) *J. Am. Chem. Soc.* 114, 760

- Dexter, A.F., Lakner, F.J., Campbell, R.A., Hager, L.P. (1995) *J. Am. Chem. Soc.* **117**, 6412-6413.
- Di Furia, F., Modena, G. (1985) *Rev. Chem. Intermed.* **6**, 51-76.
- Djordjevic, C., Craig, S.A., Sinn, E. (1985) *Inorg. Chem.* **24**, 1283-1285.
- Djordjevic, C., Lee, M., Sinn, E. (1989) *Inorg. Chem.* **28**, 719-723.
- Drew, R.E., Einstein, F.W.B. (1973) *Inorg. Chem.* **12**, 629-635.
- Drew, R.E., Einstein, F.W.B. (1972) *Inorg. Chem.* **11**, 1079-1083.
- Everett, R.R., Soedjak, H.S., Butler, A. (1990a) *J. Biol. Chem.* **265**, 15671-15679.
- Everett, R.R., Kanofsky, J.R., Butler, A. (1990b) *J. Biol. Chem.* **265**, 4908-4914.
- Everett, R.R., Butler, A. (1989) *Inorg. Chem.* **28**, 393-395.
- Fattoruso, E., Minale, L., Sodaro, G. (1970) *Chem. Commun.*, 751-752.
- Faulkner, D.J. (1988) in 'Bromine Compounds: Chemistry and Applications', Price, D., Iddon, B., & Wakefield, B.J. eds., Amsterdam: Elsevier, pp. 121-144.
- Faulkner, D.J. (1980) in 'The Handbook of Environmental Chemistry, Vol. 1., The Natural Environment and Biogeochemical Cycles', Hutsinger, O., ed. Berlin: Springer-Verlag, pp. 229-254.
- Fenical, W. (1980) in 'Organic Chemistry of Seawater', Dawson, R., Duursma, E.K., eds., Amsterdam: Elsevier, pp. 375-394.
- Fenical, W. (1974) *Tetrahedron Lett.*, 4463-4466.
- Fu, H., Kondo, H., Ichikawa, Y., Look, G.C., Wong, C.-H. (1992) *J. Org. Chem.* **57**, 7265-7270.
- Fulmor, W. Lear, G.E., Morton, G.O., Mills, R.D. (1970) *Tetrahedron Lett.*, 4551-4552.
- Geigert, J., Dalietos, D.J., Neidleman, S.L., Lee, T.D., Wadsworth, J. (1983) *Biochem. Biophys. Res. Commun.* **114**, 1104.

- Griffin, B.W. & Haddox, R. (1985) *Arch. Biochem. Biophys* 239, 305-309.
- Griffith, W.P., Wickins, T.D. (1968) *J. Chem.Soc. A*, 397-400.
- Groweiss, A., Look, S., Fenical, W. (1988) *J. Org. Chem.* 53, 2401.
- Guerchais, J.E.; Sala-Pala, J. (1971) *J. Chem. Soc. A*, 1132-1136.
- Hager, L.P., Morris, D.R., Brown, F.S., Eberwein, H. (1966) *J. Biol. Chem.* 241, 1769-1777.
- Hosoya, T. & Morrison, M. (1967) *Biochemistry* 6, 1021.
- Hosoya, T. & Morrison, M. (1967) *J. Biol. Chem.* 242, 2828.
- Irie, T., Suzuki, M., Kurosawa, E., Masamune. (1970) *Tetrahedron* 26, 3271-3277.
- Irie, T., Suzuki, M., Masamune, T. (1968) *Tetrahedron* 24, 4193-4205.
- Jordan, P. & Vilter, H. (1991) *Biochim. Biophys. Acta.* 1073, 98-106.
- Jordan, P., Kloareg, B., Vilter, H. (1991) *J. Plant Physiol.* 137, 520-524.
- Kanofsky, J.R. (1989) *Arch. Biochem. Biophys.* 274, 229-234.
- Keilin, D. & Hartreem E.F. (1951) *Biochem. J.* 49, 88.
- Kobayashi, S., Nakano, M., Kimura, T., Schaap, A.P. (1987) *Biochemistry* 26, 5019
- Krenn, B.E., Tromp, M.G.M., Wever, R. (1989) *J. Biol. Chem.* 264, 19287-19292.
- Lambier, A.- M. & Dunford, H.B. (1983) *J. Biol. Chem.* 258, 13558-13563.
- Lapshin, A.E., Smolin, Y.I., Shepelev, Y.F., Schwendt, P., Gwepesova, D. (1990a) *Acta Crystallogr. C*46, 1753-1755.

- Lapshin, A.E., Smolin, Y.I., Shepelev, Y.F., Schwendt, P., Gwepesova, D. (1990b) *Acta Crystallogr. C46*, 738-741.
- Lapshin, A.E., Smolin, Y.I., Shepelev, Y.F., Gwepesova, D. Schwendt, P. (1989) *Acta Crystallogr. C45*, 1477-1479.
- Libby, R.D., Shedd, A.L., Phipps, A.K., Beachy, T.M., Gerstberger, S.M. (1992) *J.Biol. Chem.* 267, 1769-1775.
- Libby, R.D., Thomas, J.A., Kaiser, L.W., and Hager, L.P. (1980) *J. Biol. Chem.* 255, 5030-5037.
- Liu, K.K.-C. & Wong, C.-H. (1992) *J. Org. Chem.* 57, 3748.
- Manthey, J.A. & Hager, L.P. (1981) *J. Biol. Chem.* 256, 11232-11238.
- Manthey, J.A. & Hager, L.P. (1985) *J. Biol. Chem.* 260, 9654-9659.
- McConnell, O. & Fenical, W. (1980) *Phytochemistry* 19, 233-247.
- McConnell, O. & Fenical, W. (1977a) *Phytochemistry* 16, 367-374.
- McConnell, O. & Fenical, W. (1977b) *Tetrahedron Lett.*, 4159-4162.
- McConnell, O. & Fenical, W. (1977c) *Tetrahedron Lett.*, 1851-1854.
- Messerschmidt & Wever (1996) *Proc. Natl. Acad. Sci. USA* 93, 392-396.
- Michaelson, R.C., Palermo, R.E., Sharpless, K.B. (1977) *J. Am. Chem. Soc.* 99, 1991-1992.
- Miecheng, S., Xun, D., Youqi, T. (1988) *Sci. Sin., Ser. B (engl ed.) XXXI*, 789-799.
- Mimoun, H., Mignard, M., Brechot, P., Saussine, L. (1986) *J. Am. Chem. Soc.* 108, 3711-18.
- Mimoun, H., Saussine, L., Daire, E., Postel, M., Fischer, J., Weiss, R. (1983a) *J. Am. Chem. Soc.* 105, 3101-10.

- Mimoun, H., Chaumette, P., Mignard, M., Saussine, L., Fischer, J., Weiss, R. (1983b) *Nouv. J. Chim.* 7, 467-75.
- Mynderse, J.S., Faulkner, D.J., Finer, J., Clardy, J. (1975) *Tetrahedron Lett.*, 2175-2178.
- Nakajima, K., Kojima, M., Toriumi, K., Saito, K., Fujita, J. (1989) *Bull. Chem. Soc. Jpn.* 62, 760-7.
- Neidleman, S.L. & Geigert, J. (1986) "Biohalogenation: Principles, Basic Roles, and Applications", Chichester: Ellis Horwood.
- Neider, M. & Hager, L. (1985) *Arch. Biochem. Biophys.* 240, 121-1276
- Nour, E.M., El-sayed, A.B., Sadeek, S.A. (1989) *Bull. Chem. Soc. Jpn.* 62, 317-320.
- Offner, F., Dehand, J. (1971) *C. R. Acad. Sci., Ser. C* 273, 50-53.
- Orhanovic, M., Wilkins, R.G. (1967) *J. Am. Chem. Soc.* 89, 278-282
- Pederson, M. (1976) *Physiol. Plant* 37, 6.
- Pelletier, I. & Altenbuchner, J. (1995) *Microbiology* 141, 459-468.
- Pelletier, I., Altenbuchner, J., Mattes, R. (1995) *Biochim. Biophys. Acta* 1250, 149-157.
- Pelletier, I., Pfeifer, O., Altenbuchner, J., van Pee, K.-H. (1994) *Microbiology* 140, 509-516.
- Pfeifer, O., Pelletier, I., Altenbuchner, J., van Pee, K.-H. (1992) *J. Gen. Microbiology* 138, 1123-1131.
- Plat, H., Krenn, B.E., Wever, R. (1987) *Biochim. Biophys. Acta.* 912, 287-291.
- Rinehart, K.L., Jr., Johnson, R.D., Siuda, J.F., Krejcarek, G.E., Shaw, P.D., McMillan, J.A. Paul, I.C. (1975) in "The Nature of Seawater", Golliderg, ed., Berlin:Abakon Verlagsgesellschaft, pp. 623-632.
- Schrag, J.D., Li, Y., Wu, S., Cygler, M. (1991) *Nature* 351, 761-764

- Schwendt, P., Pisarcik, M. (1990) *Spectrochim. Acta* 46A, 397-399.
- Schwendt, P., Volka, K., Suchanek, M. (1988) *Spectrochim. Acta* 44A, 839-844.
- Schwendt, P. (1983) *Collect. Czech. Chem. Commun.* 48, 248-253.
- Schwendt, P., Pisarcik, M. (1982) *Collect. Czech. Chem. Comm.* 47, 1549-1555
- Schwendt, P., Petrovic, P., Uskert, D.Z. (1980) *Anorg. Allg. Chem.* 466, 232-236.
- Secco, F. (1980) *Inorg. Chem.* 19, 2722.
- Sergienko, V.S., Borzunov, V.K., Porai-Koshits, M.A., Loginov, S.V. (1988) *Zh. Neorg. Khim.* 33, 1609-1610.
- Sharpless, K.P., Verhoeven, T.R. (1979) *Aldrich. Acta.* 12, 63-74.
- Sharpless, K.B., Michaelson, R.C. (1973) *J. Am. Chem. Soc.* 95, 6136-6137.
- Shul'pin, G.B., Attanasio, D., Suber, L. (1993) *J. Cat.* 142, 147-152.
- Simons, B.H., Barnett, P., Vollenbroek, E.G.M., Dekker, H.L., Muijers, A.O., Wever, R. (1995) *Eur. J. Biochem.* 229, 566-574.
- Sims, J.J., Lin, G.H.Y., Wing, R.M. (1974) *Tetrahedron Lett.*, 3487-3490.
- Soedjak, H.S., Walker, J.W., Butler, A. (1995) *J. Biol. Chem.*
- Soedjak, H.S. (1991) Ph.D. Dissertation, University of California, Santa Barbara.
- Soedjak, H.S. & Butler, A. (1990) *Biochemistry* 29, 7974-7981.
- Soedjak, H.S. & Butler, A. (1991) *Biochim. Biophys. Acta* 1079, 1-7.
- Stomberg, R. (1986) *Acta Chem. Scand.* A40, 168-176.
- Stomberg, R. (1985) *Acta Chem. Scand.* A39, 725-731.

- Stomberg, R., Olson, S. Svensson., I.B. (1984a) *Acta Chem. Scand. A38*, 653-656.
- Stomberg, R. (1984a) *Acta Chem. Scand. A38*, 541-545.
- Stomberg, R., Olson, S. (1984b) *Acta Chem. Scand. A38*, 821-823.
- Stomberg, R. (1984b) *Acta Chem Scand. A38*, 223-228.
- Stomberg, R., Szentivanyi, H. (1984) *Acta Chem. Scand. A38*, 121-128.
- Suida, J., VanBlaricom, G., Shaw, P., Johson, R., White, R., Hager, L., Rinehart, K. (1975) *J. Am. Chem. Soc.* 97, 937-938.
- Svensson, I.B., Stomberg, R. (1971) *Acta Chem. Scand.* 25, 898-910.
- Szentivanyi, H., Stomberg, R. (1984) *Acta Chem. Scand. A38*, 101-107.
- Szentivanyi, H., Stomberg, R. (1983a) *Acta Chem. Scand.*, A37, 709-14
- Szentivanyi, H., Stomberg, R. (1983b) *Acta Chem. Scand. A37*, 553-559.
- Talsi, E.P., Chinakov, V.P., Babenko, V.P., Zamaraev, K.I. (1993) *J. Molec. Cat* 81, 235-254.
- Talsi, E. P., Chinakov, V. D., Babenko, V. P., Zamaraev, K. I. (1991) *React. Kinet. Catal. Lett* 44, 257-63.
- Thorp, H.H. (1992) *Inorg. Chem.* 31, 1585.
- Tromp, M.G.M., Olafsson, G., Krenn, B.E., Wever, R. (1990) *Biochim. Biophys. Acta* 1040, 192-198.
- Tschirret-Guth, R.A. & Butler, A. (1994) *J. Am. Chem. Soc.* 116, 411-412.
- Van Engen, D., Clardy, J., Kho-Wiseman, E., Crews, P. Higgs, M.D., Faulkner, D.J. (1978) *Tetrahedron Lett.*, 29-32.
- van Schijndel, J.W.P.M., Vollenbroek, E.G.M., Wever, R. (1993) *Biochim. Biophys. Acta.* 1161, 249-256.

Vilter, H. (1995) in "Metal Ions in Biological Systems", Sigel, H. & Sigel, A., eds. Vol 31, New York: Dekker, pp. 326-362.

Vilter, H. (1990) *Bioseparation* 1, 283-292.

Vilter, H. & Rehder, D. (1987) *Inorg. Chim. Acta* 136, L7.

Vilter, H. (1984) *Phytochem.* 12, 1387-1390.

Vollenbroek, E.G.M., Simons, L.H., van Schijndel, J.W.P.M., Barnett, P., Balzar, M., Dekker, H., van der Linden, C., Wever, R. (1995) *Biochem. Soc. Trans.* 23, 267-271.

Vuletic, N., Djordjevic, C. (1973) *J. Chem. Soc., Dalton Trans.* 1137-1141

Wever, R., Krenn, B.E., De Boer, E., Offenberg, H., Plat, H. (1988) *Prog. Clin. Biol. Res. (Oxidases Relat. Redox. Syst.)* 274, 477-493.

Wever, R., Tromp, M.G.M., Krenn, B.E., Marjani, A., Van Tol, M. (1991) *Environ. Sci. Technol.* 25, 446-449.

Westermann, K., Leimkuehler, M., Mattes, R.J. (1988) *J. Less-Common Met.* 137, 181-186.

Wiesner, W., van Pee, K. -H., Lingens, F. (1988) *J. Biol. Chem.* 263, 13725-13732.

Wolframm, C., Lingens, F., Mutzel, R. van Pee, K. -H. (1993) *Gene* 130, 131-135.

Chapter 2. Characterization of the Irreversible Inactivation of Vanadium

Bromoperoxidase by Hydrogen Peroxide at Low pH.

Introduction

Recent studies by Soedjak, et al. (1995) have demonstrated that the substrate hydrogen peroxide can act as a noncompetitive inhibitor or as an inactivator of vanadium bromoperoxidase. These processes are inversely related by pH. At pH values 5.5 to 8, initial-rate measurements of turnover show inhibition by higher concentrations of peroxide, particularly at the higher pH values. Longer reaction times result in inactivation of the enzyme. This inactivation can be completely reversed by the addition of vanadate at high pH. It has been suggested that the inhibition and *reversible* inactivation at high pH is due to the high formation constants of diperoxovanadate complexes under these conditions. At pH values below 5.5, inhibition is negligible. In reactions at pH values between 4 and 5 and at high hydrogen peroxide concentrations (100 mM), vanadium bromoperoxidase is rapidly and *irreversibly* inactivated. Plots of the inhibition constants from the kinetics experiments versus pH suggest that a moiety with a pK_a of 6.5 to 7 plays an important role in the inhibition processes and the inverse relationship between the reversible and irreversible inactivation phenomena. Likely candidates for such a moiety include vanadium-bound water and a histidine residue.

Histidine has been shown to be an essential residue in iron heme peroxidases. Essential histidine residues have been identified for chlorination in the iron heme chloroperoxidase from *Caldariomyces fumago* (Blanke & Hager, 1990) and for both iodination and aromatic oxidation in horseradish peroxidase (Battacharyya, D.K. et al., 1992, 1993) using diethyl pyrocarbonate (DEPC) modification procedures. Several of the iron heme peroxidases, including horseradish peroxidase and cytochrome c peroxidase, have highly conserved sequences in the distal pocket of the heme (Tien & Tu, 1987), which include invariant histidine and arginine residues. Poulos and Kraut (1990) have proposed that the arginine (Arg 48) and the histidine (His 52) work in concert in cytochrome c peroxidase. In their scheme, the Arg 48 assists in heterolytic cleavage of the O-O bond by stabilizing the charge on the RO- group being produced, and His 52 residue acts in an acid-base capacity by assisting proton transfer to the RO- group.

Like the results for V-BrPO, steady state kinetic results of the vanadium chloroperoxidase (V-ClPO) from *Curvularia inaequalis* (van Schijndel, et al, 1994) indicate that H₂O₂ binding is inhibited when a residue with a pK_a > 5 is protonated. Histidine is a likely candidate for this catalytic residue. The recently solved crystal structure of V-ClPO, as described previously, shows that vanadate is coordinated to the protein by a single histidine residue, His 496, in a pentagonal bipyramidal geometry about vanadium(V) (Messerschmidt & Wever, 1996). Histidine 404,

present in the active site channel in close proximity to the vanadate ion, is thought to be the acid-base moiety required for catalysis.

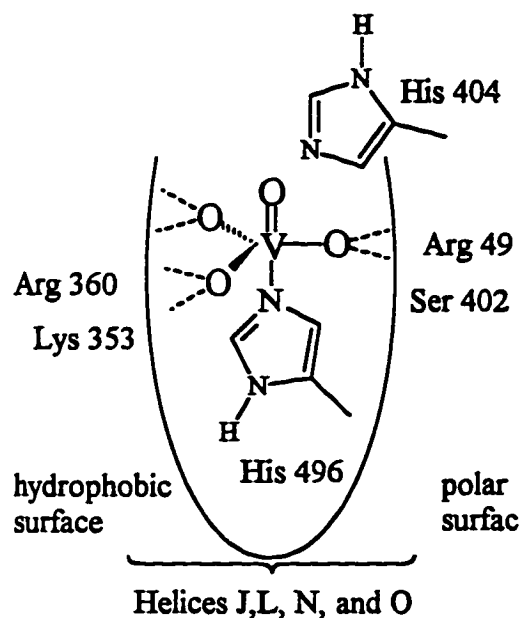


Figure 2-1. Structure of the vanadium site in V-CIPO from *Curvularia inaequalis* (taken from Messerschmidt & Wever, 1996)

Although the full sequence of V-BrPO has not been solved to date, sequence similarity has been demonstrated between this enzyme and the vanadium chloroperoxidase, particularly in the regions of the coordinating histidine 496, four of the five amino acids hydrogen bonded to the vanadate ion, and histidine 404, the proposed acid-base histidine (Messerschmidt & Wever, 1996; Vilter, 1995). Thus, it appears likely that a histidine would also play an acid-base role in V-BrPO as well as in V-CIPO.

Cu,Zn-superoxide dismutase (Cu,Zn-SOD), an enzyme that catalyzes the disproportionation of superoxide ion to dioxygen and hydrogen peroxide, is irreversibly inactivated by its own reaction product, hydrogen peroxide (Hodgson & Fridovich, 1975). The inactivation results from the oxidation of an active-site histidine to 2-oxohistidine, as well as the fragmentation of the enzyme (Uchida & Kawakishi, 1994). The use of HPLC with electrochemical detection enabled the identification of 2-oxohistidine (Uchida & Kawakishi, 1994). 2-Oxohistidine has also been detected in bovine serum albumin during the autooxidation of ascorbic acid by Cu^{2+} (Uchida & Kawakishi, 1993, 1986). The mechanism of oxidation in Cu,Zn-SOD is thought to be a free radical process resulting from reduction of Cu(II) to Cu(I) by H_2O_2 and then subsequent reduction of H_2O_2 by Cu(I) producing the active oxidant. Several other radical generating systems (e.g., metal/ H_2O_2 and metal/ascorbate) also effect oxidation of histidine to 2-oxohistidine (Uchida & Kawakishi, 1994).

The identification of 2-oxohistidine in inactivated Cu,Zn-SOD prompted an investigation into whether the irreversible inactivation of V-BrPO that occurs at low pH under turnover is due to the oxidation of histidine to 2-oxohistidine. 2-Oxohistidine was observed in turnover inactivated V-BrPO; however the mechanism of histidine oxidation likely differs substantially from that in Cu,Zn-SOD. The oxidation of bromide by V-BrPO is a two-electron process, as

established by studies with the substrate 1,3-dimethoxytoluene (Soedjak et al., 1995) while SOD has a radical mechanism (Uchida & Kawakishi, 1994).

Materials and Methods

Bromoperoxidase preparation: Vanadium bromoperoxidase was isolated from *Ascophyllum nodosum* collected at Kornwerderzand, Holland in 1990. The isolation procedure described previously (Everett et al., 1990b) was modified as follows: Crosslinked polyvinylpyrrolidone (1.5%) was included in the initial extraction of V-BrPO in 0.2 M Tris buffer, pH 8.3. In some preparations Sephadex G-100 was used in place of Sephacryl S-200. An SDS-PAGE gel of G-100-purified V-BrPO used in this investigation is shown in Figure 2-2. The ammonium sulfate and ethanolic precipitation steps and the Concanavalin A column were omitted. For some experiments (e.g., amino acid analyses), V-BrPO was purified by electroelution (see Appendix I). Here V-BrPO samples were run on a native 8% BioRad MiniProtean II polyacrylamide gel using 50 mM Tris-HCl pH 8.3 as the running buffer. The edges of the gel were stained for peroxidase activity with *o*-dianisidine (Vilter & Glombitza, 1983) and the remaining unstained gel bands corresponding to V-BrPO were excised. The enzyme was eluted on a BioRad Model 422 Electroeluter with 50 mM Tris, pH 8.3 using a 60 mA current for 3 to 5 hours. The enzyme stock solution was stored in 0.1 M Tris buffer, pH 8.3 or water at 0 or 4 °C.

Bromoperoxidase activity measurements: The standard assay for determining the specific bromoperoxidase activity of V-BrPO from *A. nodosum* is

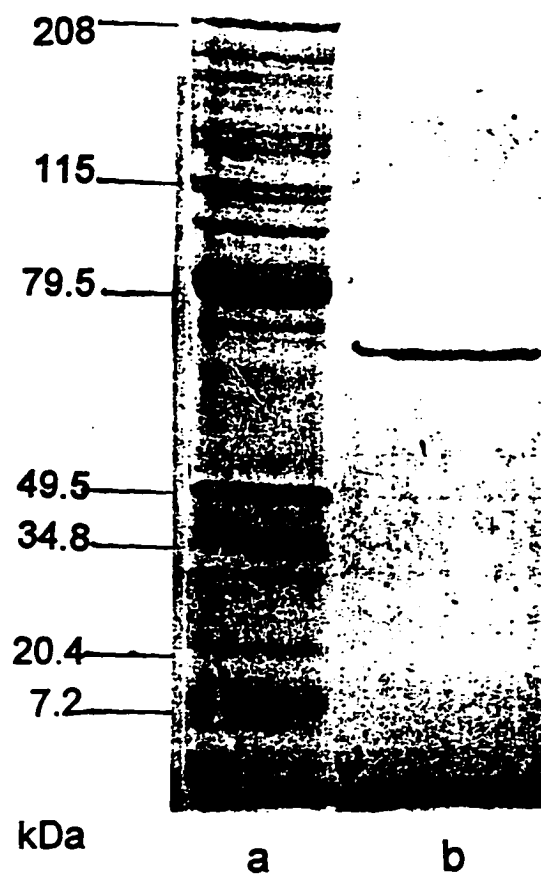


Figure 2-2. Silver-stained 12.5% denaturing SDS-PAGE gel of size-exclusion purified V-BrPO used in this investigation. Lane a: SDS-PAGE broad range protein standards (Bio Rad, Inc.) 1:100 dilution; Lane b: 150 nM V-BrPO.

the bromination of 50 μM monochlorodimedone (MCD), which is monitored spectrophotometrically at 290 nm under conditions of 0.1 M KBr, 2 mM H_2O_2 , in 0.1 M phosphate, pH 6.0. The change in extinction coefficient between MCD and Br-MCD is $19,900 \text{ cm}^{-1}\text{M}^{-1}$ above pH 5. The specific activity of the V-BrPO was 115-125 mmol brominated per minute per milligram V-BrPO (U/mg), varying between different isolations.

H_2O_2 inactivation of V-BrPO. V-BrPO was inactivated by a modified version of a procedure initially described by Soedjak (1991). Typically, 15 nM V-BrPO was incubated with 100 mM H_2O_2 and 100 mM KBr in 50 or 100 mM citrate buffer at pH 4.0 for six minutes, at which time the turnover was quenched by the addition of an AODISK. In some experiments, only 15 nM H_2O_2 was used; these reactions were not quenched. In control reactions either the H_2O_2 or the KBr was excluded from the incubation solution. Some reactions were also done at pH 5.7 and 7.2 using 0.1 M phosphate buffer. In all cases, the reacted solutions were then washed with doubly distilled H_2O by ultrafiltration (i.e., a stirred cell with a YM30 membrane Centriprep 10 or 30 or Centricon 30 to remove remaining hydrogen peroxide and salts.) Washed enzyme solutions were then evaporated to dryness in A Speed Vac concentrator (SVC-100H, Savant, Inc.).

Turnover of V-BrPO with chloride at low pH. V-BrPO (15 nM) was incubated with 100 mM H_2O_2 and 100 mM or 1.0 M KCl in 0.1 M citrate buffer pH

4.0 for 30 minutes to overnight (~18 hours). Controls were performed by eliminating either chloride or peroxide from the reaction mixture. The extent of turnover was estimated by washing the samples through Centricon 30 filters and measuring the remaining peroxide in the filtrate. These samples were then washed and concentrated as described above.

Preparation of 2-oxohistidine and N^αbenzoyl-2-oxohistidine

Method A. CuSO₄/ascorbate oxidation of N^αbenzoylhistidine. N^α-benzoylhistidine (e.g., 0.5 to 5.0 mM) was oxidized by reaction with *ca.* 50 μM copper sulfate and *ca.* 5 mM ascorbate in 0.1 M phosphate buffer, pH 7 overnight at 37 °C (Uchida & Kawakishi, 1986). The reaction mixture was evaporated to dryness and the solid was extracted with *ca.* 1 mL methanol. The methanolic solution was then concentrated, giving N^α- benzoyl-2-oxohistidine. Hydrolysis of N^α-benzoyl-2-oxohistidine, to remove the benzoyl derivatization, was achieved by dissolving the solid (e.g., 0.5 - 1.0 mg) in 300 μL 6 M HCl. The hydrolysis solution was placed in an ampule, deaerated with argon, flame sealed, and placed in an oven at 110 °C overnight as described below. The hydrolyzed sample was then concentrated giving 2-oxohistidine, which was used as a standard for HPLC electrochemical detection (HPLC-ECD; see below). Unhydrolyzed N^α- benzoyl-2-

oxohistidine could also be detected electrochemically using the same electrochemical conditions used to detect 2-oxohistidine.

Method B. HOBr oxidation of N^α-benzoylhistidine. N^α-benzoyl-2-oxohistidine was also prepared by reaction of 0.5 to 5.0 mM N^α-benzoylhistidine with 0.25 to 5 equivalents of HOBr. Reactions were carried out in the presence of 0.1 M KBr and in either 0.05 or 0.1 M HClO₄, 0.1 M HCl, 0.1 M citrate buffer pH 4.0, 0.1 M phosphate buffer pH 5.7, or 0.1 M phosphate buffer pH 7.2. N^α-benzoyl-2-oxohistidine was detected by HPLC-ECD as described above. When collection of the product was necessary, the reaction mixture was lyophilized (Freezone lyophilizer, Labconco, Inc.). N^α-benzoyl-2-oxohistidine was then extracted into methanol and concentrated by rotary evaporation.

Amino acid analyses. Hydrolysis of the enzyme samples (i.e., turnover-inactivated V-BrPO or native V-BrPO) was achieved by dissolving *ca.* 200 μg in *ca.* 300 μL 6.0 M HCl in sealable ampoules and deaerating with argon for approximately two minutes. The deaerated ampoules were then flame sealed and placed in an oven at 110 °C overnight. On completion of hydrolysis, the ampoules were broken open and the contents evaporated to dryness.

The procedure for quantitative amino acid analysis was carried out by a modification of Edman's method as originally described by Ebert (1986). The hydrolyzed protein samples were concentrated then redissolved twice in H₂O and

redried to remove residual HCl. The samples were then dissolved in 5 μ L of 50% ethanol. To this solution was added 10 μ L of phenyl isothiocyanate (PITC) derivatization buffer. The derivatization buffer is composed of a 90% mixture of 7:1:2 ethanol : PITC : triethanolamine (TEA), respectively in H₂O. Derivatization was allowed to proceed for at least ten minutes, at which time the samples were dried in the SpeedVac.

The derivatized amino acids were separated by HPLC using a stepwise gradient modified from that described by Ebert (1986) and listed in Table 2-1. Solvent A was 2.75 mL TEA in 1 L 50 mM sodium acetate set to pH 6.4 with phosphoric acid, and Solvent B was 50 % Solvent A, 40 % acetonitrile, and 10 % methanol. The samples were run on a Waters HPLC system with UV monitoring at 254 nm (the absorbance maximum for PITC derivatives). Amino acids were separated using a Spherisorb ODS-2 column or a YMC ODS-AQ C-18 column; both columns were heated to 37 °C with a water jacket. Samples were dissolved in 150 μ L Solvent A and filtered with 0.2 μ centrifuge filters prior to injection.

Table 2-1. Gradient program for amino acid analysis by HPLC.

Time (min.)	Flow (mL/min.)	Percent A	Percent B
0.0	1.0	95	5
6.0	1.0	80	20
9.0	1.0	80	20
14.0	1.0	50	50
21.0	1.0	50	50
22.0	1.0	0	100
24.0	1.0	0	100
24.5	1.5	0	100
29.0	1.5	0	100
30.0	1.5	95	5
35.0	1.5	95	5
35.5	1.0	95	5
45.0	1.0	95	5
50.0	0.1	95	5

HPLC electrochemical detection. 2-Oxohistidine was analyzed by HPLC electrochemical detection (HPLC-ECD) using a Waters 464 electrochemical detector equipped with a glassy carbon electrode. Detection was run in the DC mode at a potential of 850 mV (Uchida & Kawakishi, 1993). Underivatized protein hydrolysis samples were run on either a Spherisorb ODS-2 column (Phase Separations, LTD) or a YMC ODS-AQ C-18 column (YMC, Inc.). An isocrat of 50 mM NaCl, 0.1% TFA, and 20% methanol at 0.7 mL/min. for the Spherisorb column and 1.0 mL/min. for the YMC column was used to separate the amino acids. The protein hydrolysate samples were dissolved in the elution solvent or water and filtered through 0.2 μ m filters prior to injection. Injections were typically 100-200 μ L. The presence of 2-oxohistidine in the enzyme was identified by

comparison of retention time to a standard of 2-oxohistidine. N^{α} -benzoylhistidine samples (e.g., N^{α} -benzoylhistidine, 2-oxo- N^{α} -benzoylhistidine and 2-oxohistidine) were also monitored spectrophotometrically (typically 230 nm). Under our protein hydrolysate conditions, 2-oxohistidine could not be detected spectrophotometrically because it was not present in high enough concentration.

Most ECD chromatograms were scanned with a Logitech Scan Man 256 scanner using PhotoTouch Color scanning software (Silk, Inc.). Scanned chromatograms were digitized manually using UN-SCAN-IT digitizing software for Windows (Silk, Inc.).

Atomic absorption analyses. The ability of H_2O_2 -inactivated V-BrPO to bind vanadium(V) was examined by atomic absorption spectrometry (AAS). 40 μ g samples of V-BrPO which had been inactivated under the low pH turnover conditions and 75 μ g samples of stoichiometrically inactivated V-BrPO each with relevant controls were washed with 0.1 M Tris buffer, pH 8.3, by ultrafiltration (Centricon 30; Amicon, Inc.). Approximately 50 μ M ammonium vanadate was then added to the washed and concentrated V-BrPO samples and allowed to incubate overnight. The incubated solution was washed thoroughly by further ultrafiltration and tested for vanadium content by AAS. AAS was performed on a Perkin Elmer SpectrAA furnace atomic absorption spectrometer with a 250 ppb vanadium standard. For the excess peroxide inactivation, 10 μ L samples were

tested using a standard additions procedure. For the stoichiometric experiments, 20 μL samples were tested by a basic absorbance analysis. In both cases, samples were auto injected for analysis.

Trypsin digestion: Trypsin digestion was initially performed on control and inactivated samples using procedures described by Stone et al. (1990). In this procedure, ~ 100 μL of a washed enzyme sample was concentrated in the SpeedVac and redissolved in 100 μL 8 M urea in 0.4 M NH_4CO_3 at pH 8.0 to which was added 10 μL 50 mM dithiothreitol. This solution was incubated at 50 $^\circ\text{C}$ for 15 to 30 minutes. Upon cooling, 100 μL 100 mM iodoacetamide was added and the sample was incubated for 15 minutes. H_2O (280 μL) was then added, followed by 5 μL of a 2 mg/mL trypsin solution. The sample was then digested at 37 $^\circ\text{C}$ overnight and then frozen.

Later digests were based on a procedure described by Uchida and Kawakishi (1994). In this procedure, typically 200 μg V-BrPO was first demetallated by incubation in 0.1 M citrate-phosphate buffer, pH 4.0 containing 1.2 mM EDTA. The enzyme sample was typically then concentrated to 400 μL to which was added 50 μL 10 M urea, 20 μL 2-mercaptoethanol, and 10 μL concentrated NH_4OH . This mixture was flushed with pre-purified Argon, sealed, and incubated at 37 $^\circ\text{C}$ for 2 to 3 hours. The protein was then precipitated by the

addition of ~1 mL ethanol containing 2% HCl (v/v). The protein pellet was collected by centrifugation in an Eppendorf 5415C microcentrifuge at 10,000 rpm for 10 min. The pellet was dissolved in 100 μ L 8 M urea; 20 μ L of 20 mg/mL iodacetamide and 10 μ L concentrated NH_4OH were then added and the solution incubated for 20 minutes at 37 °C. The incubated solution was then treated with 20 μ L 2-mercaptoethanol and 10 μ L NH_4OH . The carboxyamidomethylated protein was precipitated twice by the addition of ~ 1 mL ethanol; the pellet was collected each time by centrifugation at 10,000 rpm for a minimum of 10 minutes. The pellet was redissolved in 500 μ L 0.1 M Tris pH 8.3 and 20 μ L of a 1 mg/mL trypsin solution was added. The sample was digested for 2 to 3 hours at 37 °C. The digestion was quenched by the addition of 10 μ L glacial acetic acid.

The digested fragments were in all cases separated by HPLC using a two-step gradient of 0.1 %TFA in H_2O to 80% acetonitrile, 0.1% TFA in H_2O at a flow rate of 0.7 mL/min. The gradient procedure is listed in Table 2-2. The fragments were separated on a YMC ODS-AQ C-18 column. The separation was monitored with a Waters 996 photodiode array detector at a resolution of 1.2 or 2.4 nm and a data acquisition rate of 1 or 2 spectra/second; chromatograms were extracted at 210 nm, 230 nm, 254 nm, and 280 nm for comparison.

Table 2-2. Gradient program for analysis of tryptic peptides by HPLC.

Time (minutes)	FLOW (mL/min.)	Percent A	Percent B
0	0.7 or 1.0	100	0
5	0.7 or 1.0	100	0
80	0.7 or 1.0	50	50
120	0.7 or 1.0	0	100
125	0.7 or 1.0	0	100
135	0.7 or 1.0	100	0
150	0.7 or 1.0	100	0
160	0.7 or 1.0	100	0

General reagents and procedures: HOBr was prepared by bubbling excess bromine vapor through a solution of 0.1 M NaOH. The concentrations of HOBr, HOCl, and H₂O₂ used were determined spectrophotometrically by the formation of triiodide (I₃⁻) (Cotton & Dunford, 1973). Protein concentrations were determined by the bicinchoninic acid assay (BCA) (Smith et al., 1985), with reagents purchased from Pierce Chemical Co. Phenyl isothiocyanate (PITC) and Amino Acid Standard H were also purchased from Pierce Chemical Co. MCD, N^α- benzoylhistidine, and sequencing grade trypsin were purchased from Sigma. Crosslinked polyvinylpyrrolidone was purchased from Aldrich. Atomic absorption vanadium standard was purchased from Johnson Matthey. HPLC grade acetonitrile was purchased from Fisher. All other chemicals were reagent grade.

Results and Interpretation

Electrochemical detection of 2-oxohistidine in hydrolyzed samples of the low-pH-turnover- inactivated V-BrPO

Samples of V-BrPO that were inactivated under turnover conditions at pH 4 (0.1 M citrate with 0.1 M KBr, 0.1 M H₂O₂ for *ca.* 5 min.; see Materials and Methods; Soedjak, 1991) and hydrolyzed *in vacuo* overnight in 6 M HCl (See Materials and Methods) were analyzed by electrochemical detection on HPLC (HPLC-ECD) for the presence of 2-oxohistidine. HPLC-ECD analysis demonstrated that 2-oxohistidine is formed during the low pH inactivation of V-BrPO by comparison of the retention time to an authentic sample of 2-oxohistidine; the peak indicated by the arrow is 2-oxohistidine in Figure 2-3a for the 2-oxohistidine standard and Figure 2-3b for hydrolyzed, turnover-inactivated V-BrPO. When V-BrPO is incubated under identical conditions except in the absence of KBr (i.e., 0.1 M H₂O₂ in 0.1 M citrate, pH 4 for *ca.* 5 min.), then hydrolyzed and analyzed by HPLC-ECD, a small signal due to 2-oxohistidine is evident (Figure 2-3c). The oxidation of a small amount of histidine in this sample is most likely due to bromide contamination in the enzyme sample (Vilter, 1995) and not a direct oxidation of histidine by hydrogen peroxide such as that seen in Cu,Zn-SOD (Uchida and Kawakishi, 1994). On the other hand, when V-BrPO was incubated with 0.1 M KBr under the same conditions, but in the absence of hydrogen

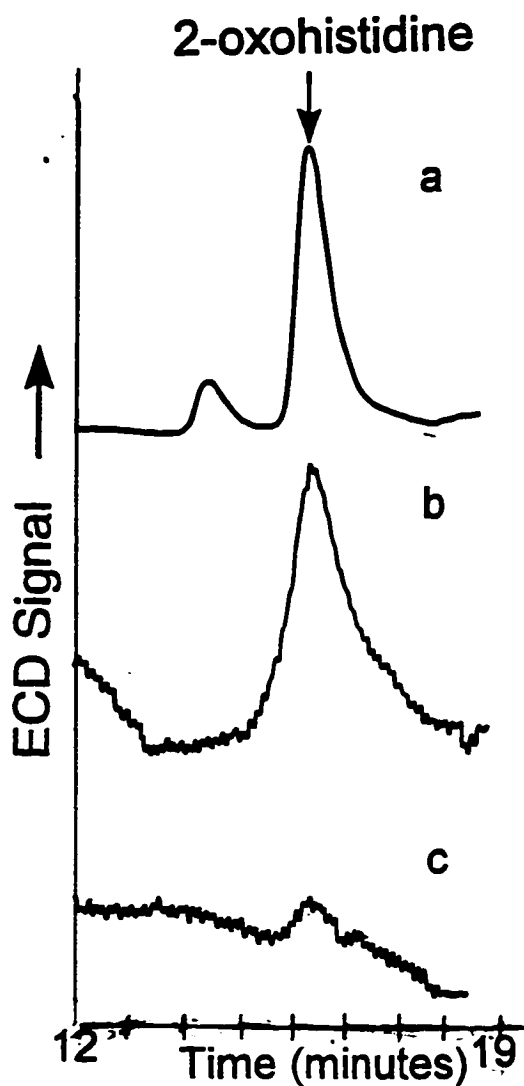


Figure 2-3. HPLC-electrochemical detection of 2-oxohistidine in turnover inactivated V-BrPO at low pH. a) standard of 2-oxohistidine; b) hydrolyzed, turnover-inactivated V-BrPO (see Materials and Methods for inactivation conditions); c) hydrolyzed, native V-BrPO after incubation in 0.1 M H₂O₂, 0.1 M citrate, pH 4 for *ca.* 5 min. The arrow indicates the peak for 2-oxohistidine. The conditions for the HPLC-ECD are described in the Materials and Methods section; the Spherisorb ODS-2 column (Phase Separations, Ltd.) was used.

peroxide, no 2-oxohistidine was formed (data not shown), showing that 2-oxohistidine is not present in native V-BrPO. Thus the formation of 2-oxohistidine requires the presence of both hydrogen peroxide and bromide.

Investigation of the effect of pH on the formation of 2-oxohistidine (Figure 2-4) shows that 2-oxohistidine is formed at pH 4 (Figure 2-4b), but little, if any is formed at pH 5.7 (Figure 2-4c) and pH 7.2 (Figure 2-4d). Figure 2-4a is a standard of 2-oxohistidine prepared by mixed function copper-ascorbate oxidation of N^α-benzoylhistidine and subsequent acid hydrolysis to remove the protecting benzoyl group. The results of these ECD experiments follow the trend for irreversible inactivation that is only observed at pH 4 and 5 (Soedjak, et al, 1995). Thus in addition to the requirement of bromide and hydrogen peroxide, a low pH is required for the formation of significant 2-oxohistidine.

Organic Substrate Protection of V-BrPO Against Turnover Inactivation.

Turnover of V-BrPO at pH 4 in the presence of an organic substrate (i.e., monochlorodimedone; MCD) was found to protect V-BrPO against inactivation as well as 2-oxohistidine formation. These experiments were carried out by comparison of the specific activity of V-BrPO after incubation of 15 nM V-BrPO in a reaction solution of 0.1 M H₂O₂, 0.1 M KBr, 0.5 mM MCD in 0.1 M citrate pH 4 for five minutes. 2-oxohistidine was not observed by HPLC-ECD in the hydrolysate of V-BrPO from this reaction (data not shown). The specific

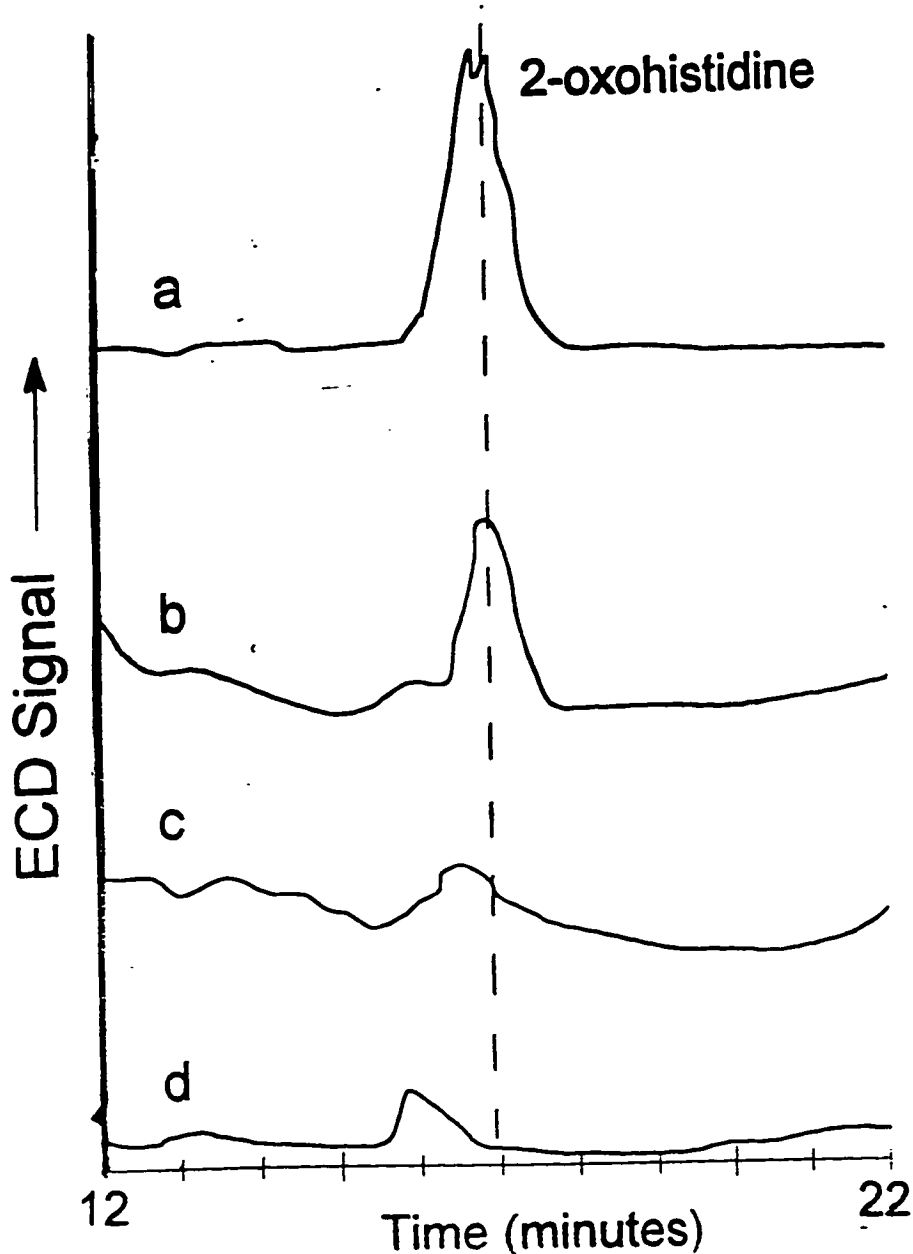


Figure 2-4. Effect of pH on the formation of 2-oxohistidine during turnover of V-BrPO. The turnover conditions were 15 nM V-BrPO, 100 mM H₂O₂, 100 mM KBr in b) 0.1 M citrate pH 4.0; c) 0.1 M phosphate pH 5.7; d) 0.1 M phosphate pH 7.2 for six minutes. Trace "a" is a standard of 2-oxohistidine, which is indicated by the dashed line. The Spherisorb ODS-2 HPLC column (Phase Separations, Ltd.) was used. Data were digitized as described in Materials and Methods.

bromoperoxidase activity of V-BrPO in the presence of MCD was 90 U/mg compared to a specific activity of 115 U/mg for native V-BrPO. Under the same conditions but in the absence of MCD, V-BrPO was completely inactivated. After incubation for 20 minutes in the MCD-containing reaction solution, at which time all the of MCD has been brominated, V-BrPO was similarly completely inactivated. Thus in the presence of MCD, V-BrPO catalyzes the bromination of MCD without significant inactivation of V-BrPO, however, once MCD is consumed, V-BrPO is inactivated at low pH.

Reaction of Hypobromite with N^α- benzoylhistidine.

The possible role of oxidized bromine species in the oxidation of histidine was investigated by reaction of hypobromite with N^α- benzoylhistidine. Hypobromite (i.e., 1 μmole from a stock solution of 10-20 mM OBr⁻ in 0.1 M NaOH) was added to 1 μmole N^α- benzoylhistidine in 0.1 M citrate buffer, pH 4. When hypobromite is diluted into citrate buffer, pH 4, a rapid equilibration occurs producing primarily Br₂ and Br₃⁻. HPLC-ECD analysis shows that the retention time of the product of the HOBr reaction with N^α-benzoylhistidine (Figure 2-5) is the same as that prepared by the method of Uchida and Kawakishi (1986), indicating that HOBr oxidation forms N^α-benzoyl-2-oxohistidine. FAB-MS of the HOBr oxidation product gave a molecular weight of 276 g/mol (M + 1), which is

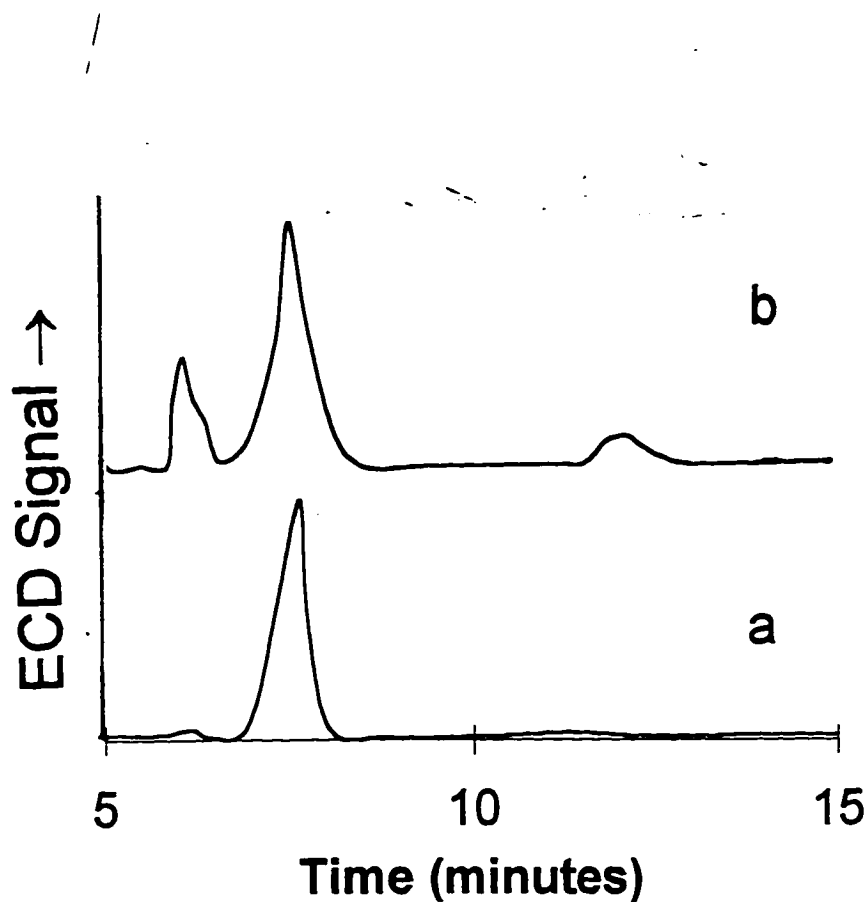


Figure 2-5. HPLC-ECD of N^α -benzoylhistidine oxidation by HOBr and Cu(II)-ascorbate. (a) HOBr oxidation product of N^α -benzoylhistidine; b) authentic N^α -benzoyl-2-oxo-histidine prepared by Cu(II)-ascorbate oxidation of N^α -benzoylhistidine. The YMC ODS-AQ C-18 HPLC column (YMC, Inc.) was used. Data were digitized as described in Materials and Methods.

consistent with the formation of N^α-benzoyl-2-oxohistidine. Furthermore, ¹H NMR data were also indicative of the formation of N^α-benzoyl-2-oxohistidine. (¹H NMR: 3.2 ppm (2H, d) (CH₂); 4.95 ppm (1H, m) (CH); 5.6 ppm (1H, s) (CH=C<); 7 to 8 ppm (5H) (PhCO); 8.6 ppm (1H, s) (CONH).

The stability of the 2-oxohistidine moiety was demonstrated by stepwise hydrolysis of N^α-benzoyl-2-oxohistidine produced by HOBr oxidation (Figure 2-6). N^α-benzoyl-2-oxohistidine formed by the reaction of 1.0 mM N^α-benzoylhistidine and 1.0 mM HOBr in 50 mM HCl was monitored by HPLC-ECD upon completion of the oxidation reaction (Figure 2-6a), after one hour of acid hydrolysis of the lyophilized product in 6 M HCl at 110 °C (Figure 2-6b) and after 18 hours of acid hydrolysis in 6M HCl at 110 °C. The ECD signal at 8.6 minutes of N^α-benzoyl-2-oxohistidine separated on a YMC ODS-AQ C-18 column (Figure 2-6a) decreases in intensity after one hour of hydrolysis and a new signal that matches the retention time of underivatized 2-oxohistidine grows in at 10 minutes (Figure 2-6b). After 18 hours of hydrolysis (Figure 2-6c), the signal from the benzoyl derivative has essentially disappeared and only the 2-oxohistidine signal remains in its place.

Investigation of the pH dependence of the HOBr oxidation of N^α-benzoylhistidine shows that N^α-benzoyl-2-oxohistidine is formed when the reaction was carried out at pH 4 and 5.7 (Figures 2-7a and 2-7b). However, when

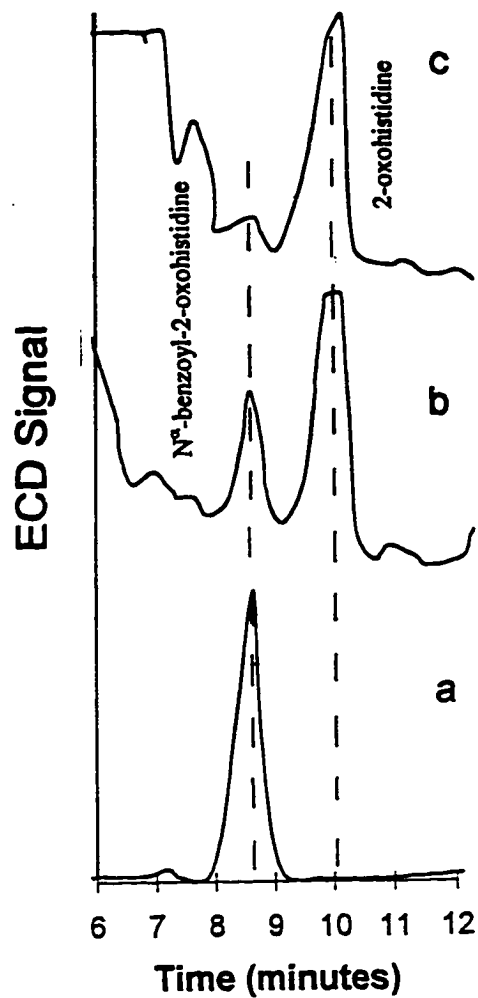


Figure 2-6. HPLC-ECD of N^α -benzoyl-2-oxohistidine prepared by reaction of N^α -benzoylhistidine and HOBr undergoing hydrolysis to form 2-oxohistidine. a) no hydrolysis; b) 1 hour hydrolysis; c) 10 hours hydrolysis. The YMC ODS-AQ C-18 HPLC column (YMC, Inc.) was used.

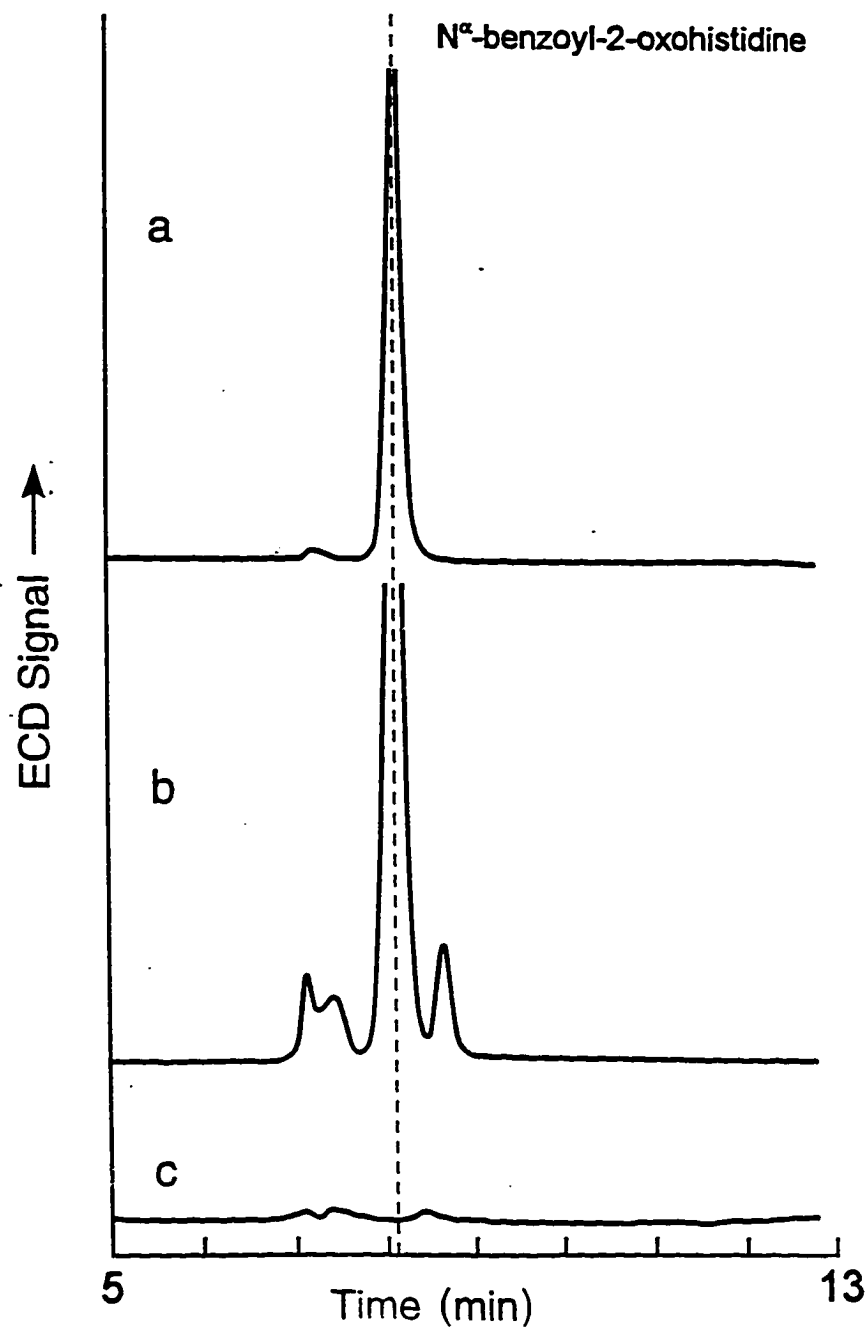


Figure 2-7. Effect of pH on the formation of N^{α} -benzoyl-2-oxohistidine in the reaction of HOBr with N^{α} -benzoylhistidine. Reaction conditions: 1 mM OBr^- was added to 1.0 mM N^{α} -benzoylhistidine in a) 0.1 M citrate pH 4.0; b) 0.1 M phosphate pH 5.7; c) 0.1 M phosphate pH 7.2. The dotted vertical line indicates the peak for N^{α} -benzoyl-2-oxohistidine. The YMC ODS-AQ C-18 HPLC column (YMC, Inc.) was used.

the pH was increased to 7.2 (Figure 2-7c) no 2-oxohistidine derivative was detected. At higher pH, the oxidized bromine species is primarily in the form of hypobromous acid. In addition, under conditions of 50 mM HClO₄ and 0.1 M KBr, where added HOBr rapidly equilibrates primarily to Br₃⁻, addition of 1.0 mM HOBr to N^α-benzoylhistidine also resulted in the formation of the 2-oxo derivative as shown in Figure 2-8. By contrast, N^α-benzoyl-2-oxohistidine was not observed when the oxidized bromine species were reacted with N^α-benzoylhistidine above pH 6 (i.e., pH 7.2 phosphate buffer as shown in Figure 2-7c or pH 6.5 Hepes buffer and pH 8.0 phosphate buffer). At these higher pH values, HOBr becomes an important species in solution. In addition, the reaction of 2.6 mM N^α-benzoylhistidine in 0.1 M phosphate buffer, pH 7.2 containing 8 mM H₂O₂ with 2.6 mM OBr⁻, i.e., conditions in which singlet oxygen would be produced by the oxidation of H₂O₂ by HOBr (Everett et al., 1990a) did not produce 2-oxohistidine (data not shown).

The stoichiometry of the reaction of HOBr with N^α-benzoylhistidine was also examined. Under conditions of 1.0 mM N^α-benzoylhistidine in 0.1 M citrate pH 4.0, appreciable amounts of N^α-benzoyl-2-oxohistidine are formed when 0.25, 0.5, or 1 equivalents of HOBr are added as determined by ECD. However, at higher concentrations of HOBr, the amount of the 2-oxo derivative formed is

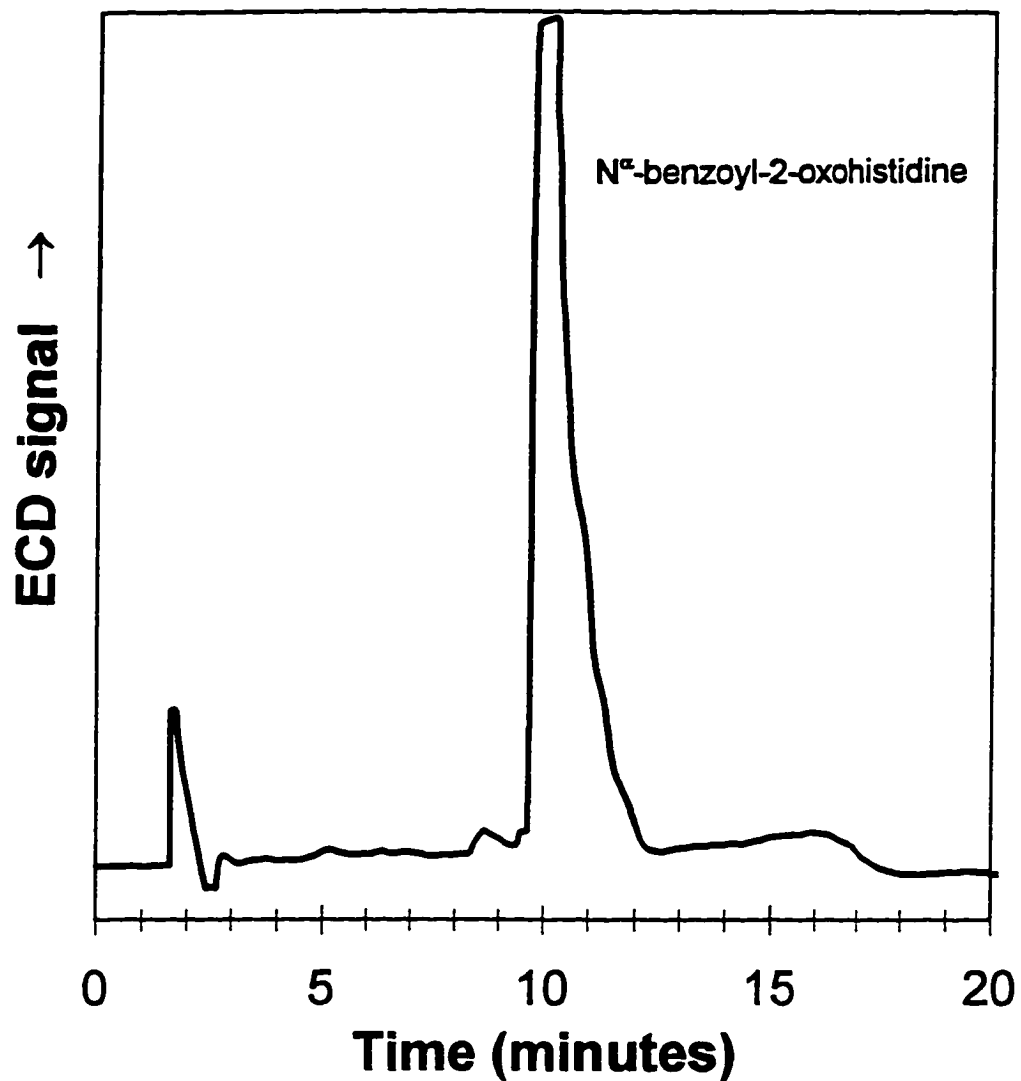


Figure 2-8. HPLC-electrochemical detection of N^α-benzoyl-2-oxohistidine from the reaction of HOBr and N^α-benzoylhistidine in acid. Conditions: 1.0 mM Na-benzoylhistidine, 1.0 mM HOBr in 50 mM HClO₄. The YMC ODS-AQ C-18 HPLC column (YMC, Inc.) was used.

decreased (Figure 2-9). Chromatograms of the products recorded at 230 nm show a corresponding decrease in the 2-oxo-histidine derivative and the appearance of new secondary products which are not detectable by ECD under the conditions used (Figure 2-10).

When the derivative N^α-benzoylhistidine was included in the turnover inactivation of V-BrPO under otherwise standard inactivation conditions, protection from inactivation similar to that observed for MCD was observed. Under conditions of 5 nM V-BrPO, 0.1 M H₂O₂, 0.1 M KBr, in 0.1 M citrate pH 4.0, inclusion of 0.2 mM N^α-benzoylhistidine in the reaction mixture partially protected the enzyme from inactivation. After several minutes the specific activity of the enzyme, which was originally 115 U/mg, had been reduced to 19 U/mg in the absence of the added histidine derivative while that of the enzyme treated with N^α-benzoylhistidine still had a specific activity of 76 U/mg. As expected, incubation of 1.0 mM N^α-benzoylhistidine with 15 nM V-BrPO, 0.1 M H₂O₂, 0.1 M KBr, in 0.1 M citrate pH 4.0 resulted in the formation of N^α-benzoyl-2-oxohistidine as determined by HPLC-ECD (Figure 2-11). Minimal evidence for 2-oxohistidine was found in the hydrolysate of the enzyme protected with N^α-benzoylhistidine by HPLC ECD; however, the associated peak was not clearly distinguishable from the baseline noise (data not shown).

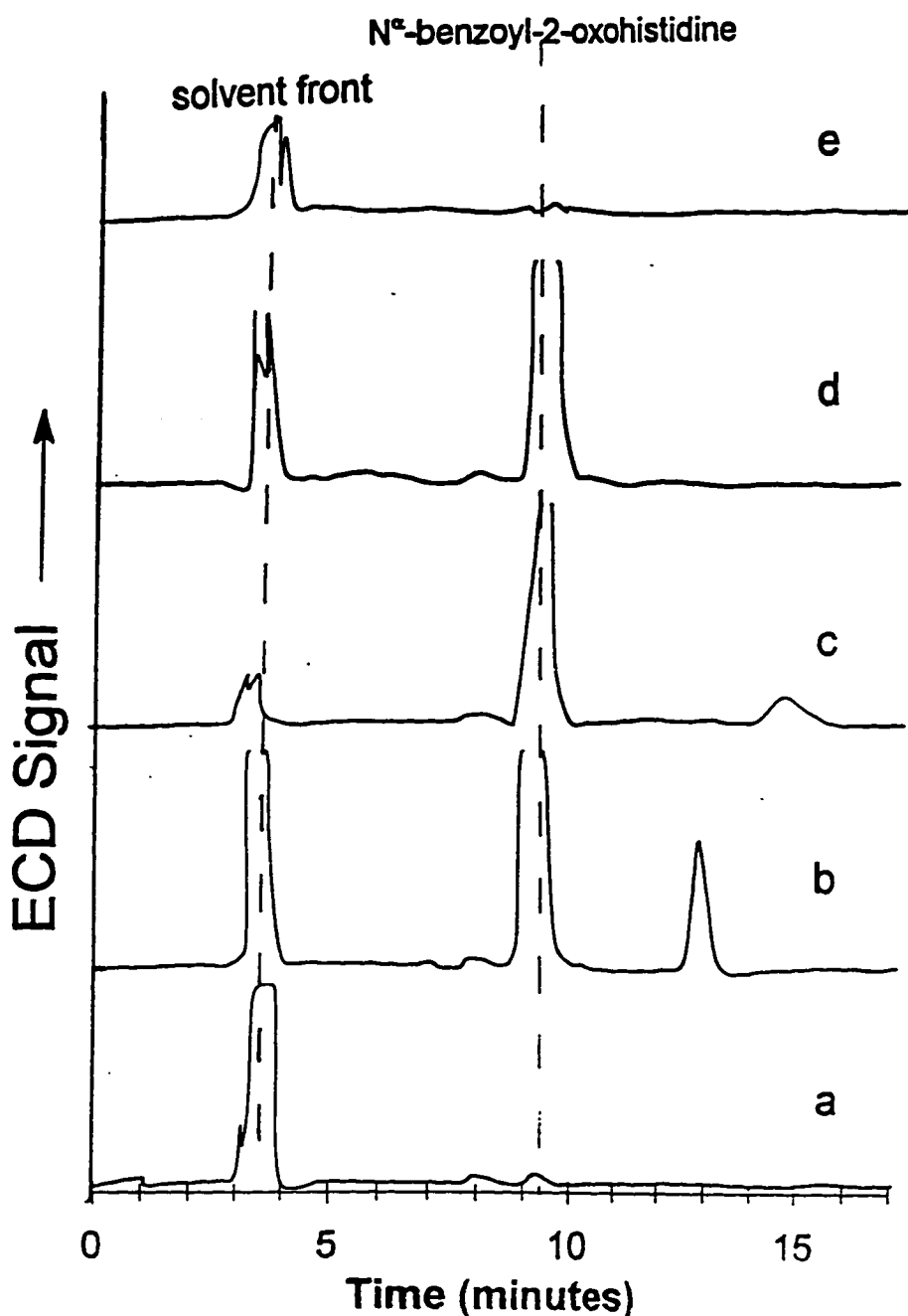


Figure 2-9. Effect of the ratio of N^α -benzoylhistidine to HOBBr added on the formation of N^α -benzoyl-2-oxohistidine detected by HPLC-ECD. Conditions: 1 mM N^α -benzoylhistidine, 0.1 M citrate pH 4.0 a) 0 equivalents of HOBBr; b) 0.25 equivalents of HOBBr; c) 0.5 equivalents of HOBBr; d) 1 equivalent of HOBBr; e) 2.5 equivalents of HOBBr. The dashed line indicates the void volume peak. The YMC ODS-AQ C-18 HPLC column (YMC, Inc.) was used.

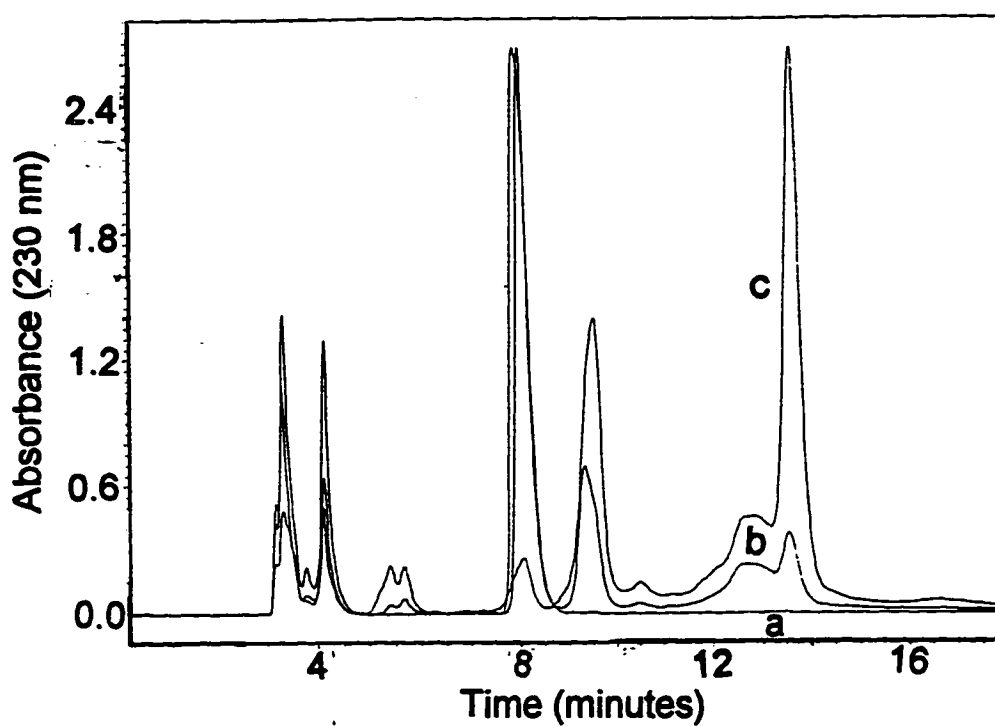


Figure 2-10. HPLC chromatograms at 230 nm of the products of the reaction of N^{α} -benzoylhistidine with varied equivalents of HOBr. Conditions: 1 mM N^{α} -benzoylhistidine, 0.1 M citrate pH 4.0, a) 0 equivalents of HOBr; b) 1 equivalent of HOBr; c) 2.5 equivalents of HOBr.

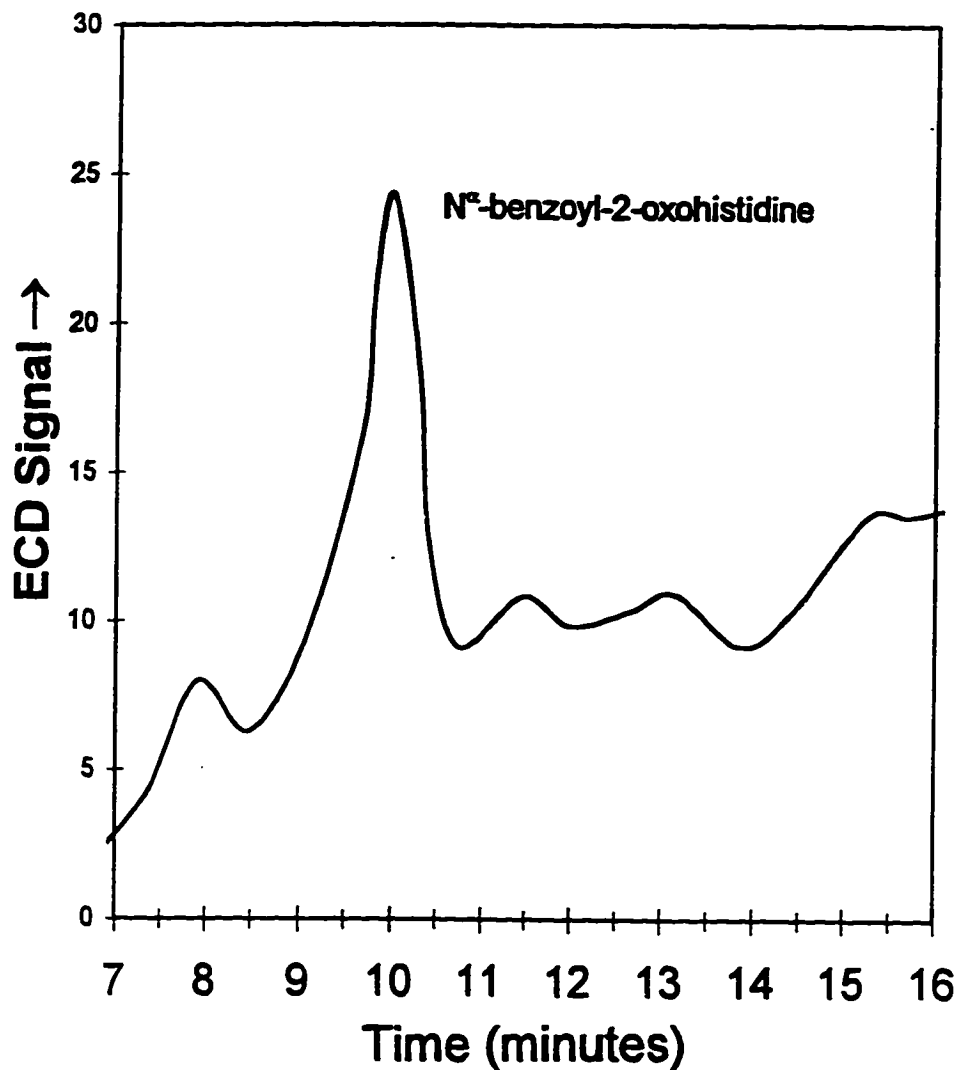


Figure 2-11. HPLC-electrochemical detection of N^{α} -benzoyl-2-oxohistidine from N^{α} -benzoylhistidine included in the incubation of 15 nM V-BrPO in 100 mM H_2O_2 , 100 mM KBr, 0.1 M citrate pH 4.0. The YMC ODS-AQ C-18 HPLC column was used. Data were digitized as described in Materials and Methods.

Reactivity of V-BrPO Mimics

The ability of *cis*-dioxovanadium(V) (VO_2^+), a well-established functional mimic of V-BrPO in strong acid solution (de la Rosa et al., 1992; Clague & Butler, 1995), to catalyze the oxidation of N^α -benzoylhistidine was also investigated. N^α -benzoylhistidine (1.0 or 5.0 mM) was reacted with 5.0 mM H_2O_2 , 0.2 M KBr, 0.4 mM NH_4VO_3 in 0.05 M HClO_4 for 1 hour. Under these conditions, *cis*- VO_2^+ catalyzes the formation of oxidized bromine species (i.e., Br_3^- , Br_2 , HOBr ; Clague & Butler, 1995). HPLC-ECD results indicated the formation of N^α -benzoyl-2-oxohistidine (Figure 2-12). *cis*- VO_2^+ only functions in strongly acidic media; any vanadate (HVO_4^{2-} / H_2VO_4^-) released from inactivated V-BrPO (see below) will not catalyze the oxidation of bromide by hydrogen peroxide (Clague & Butler, 1995). In addition $\text{MoO}(\text{O}_2)_2(\text{ox})^{2-}$ (ox^{2-} = oxalate) another functional mimic of V-BrPO (Meister, *vide infra*, Chapter 3; Meister & Butler, 1994; Reynolds et al., 1994), also catalyzes the bromoperoxidative oxidation of N^α -benzoylhistidine, under conditions of 1.5 mM N^α -benzoylhistidine, 5.0 mM H_2O_2 , 0.1 M KBr, 1.5 mM $\text{MoO}(\text{O}_2)_2(\text{ox})^{2-}$ in 90 mM oxalate buffer, pH 5, for 3 hr. (Figure 2-13). The reproducibly poor shape of this signal is not understood.

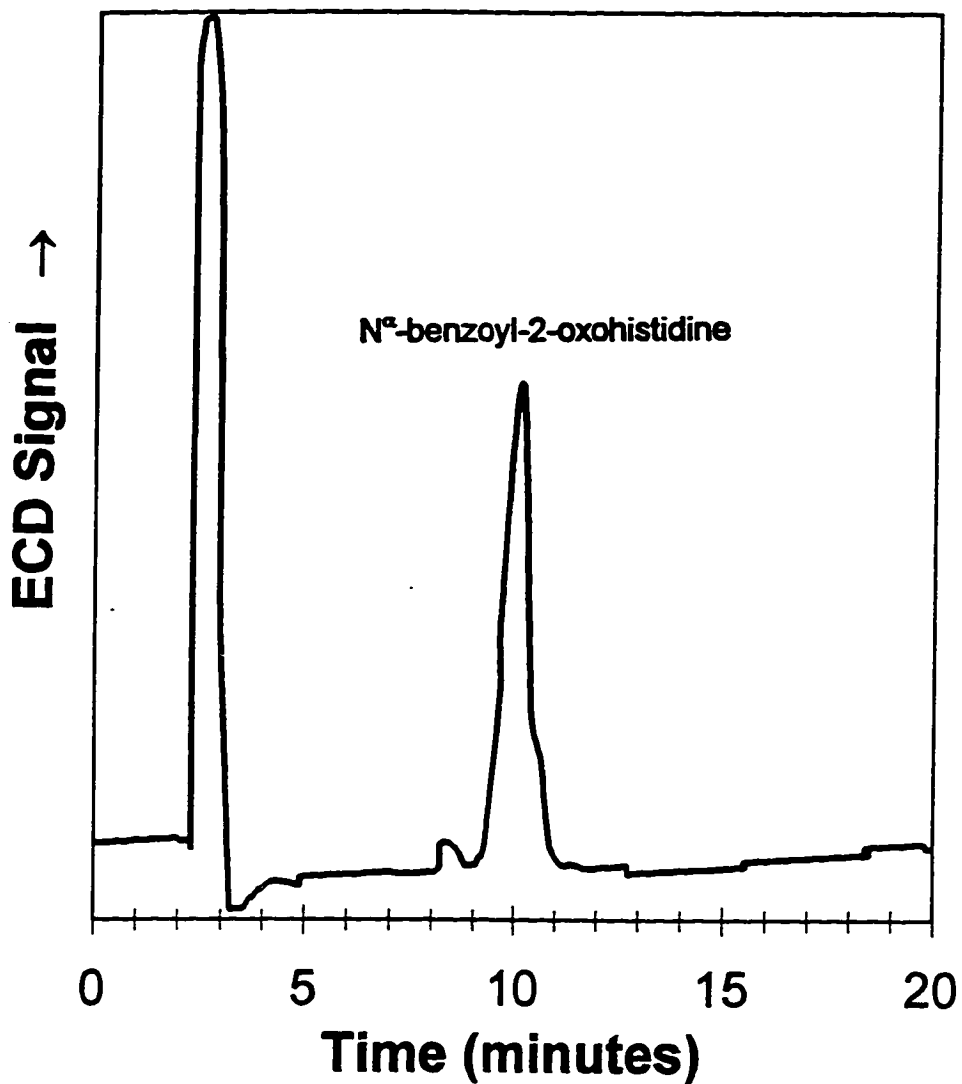


Figure 2-12. HPLC-electrochemical detection of the formation of N^α -benzoyl-2-oxohistidine from the reaction of $cis\text{-VO}_2^+$, H_2O_2 , and KBr plus N^α -benzoylhistidine. Conditions: 0.4 mM NH_4VO_3 , 5.0 mM H_2O_2 , 0.2 M KBr , and 1.0 mM N^α -benzoylhistidine in 50 mM HClO_4 . 1 hour. reaction time prior to injection. The YMC ODS-AQ C-18 HPLC column (YMC, Inc.) was used. Data were digitized as described in Materials and Methods.

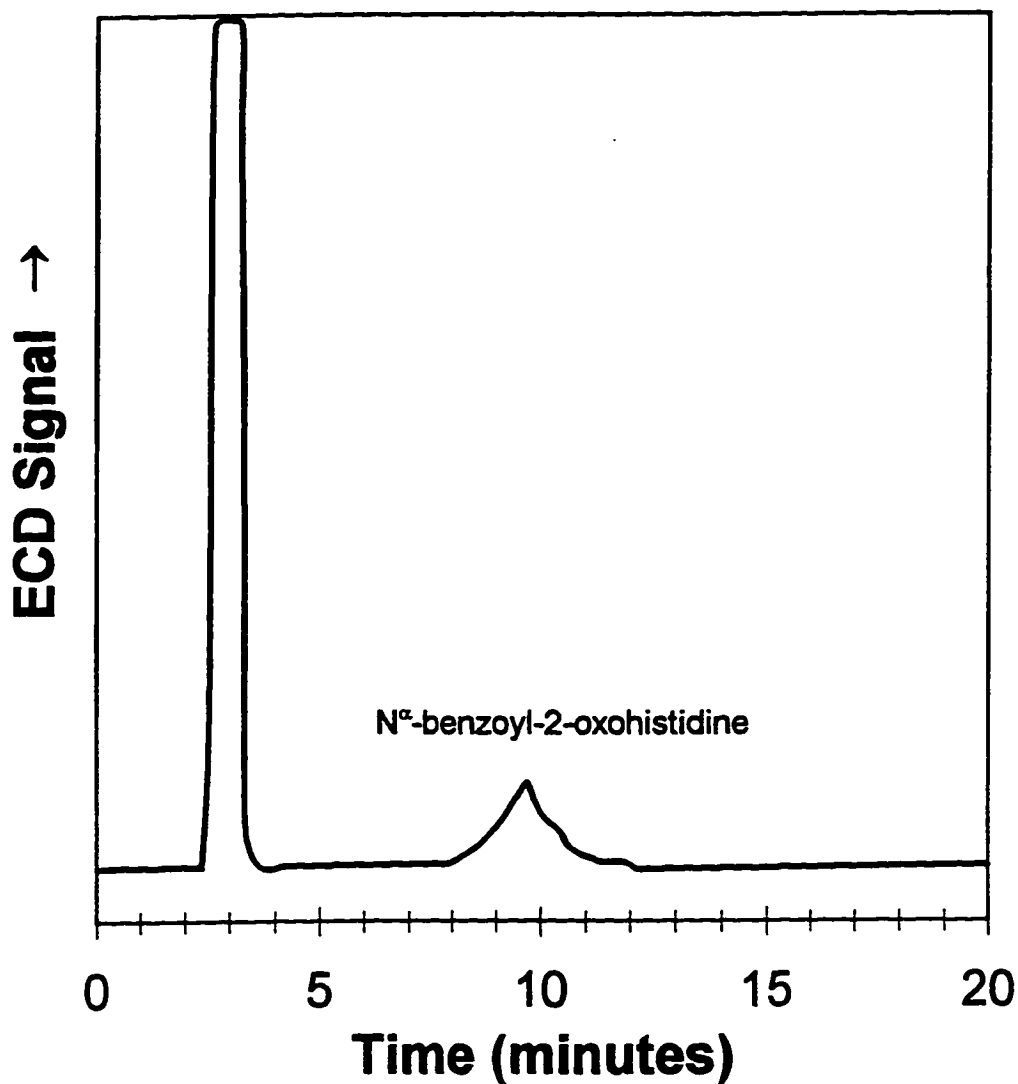


Figure 2-13. HPLC electrochemical detection of the formation of N^α -benzoyl-2-oxohistidine from the reaction of $\text{MoO}(\text{O}_2)_2(\text{ox})^{2-}$, KBr, and N^α -benzoylhistidine. Conditions: 1.5 mM $\text{K}_2\text{MoO}(\text{O}_2)_2(\text{ox})$, 5.0 mM H_2O_2 , 0.1 M KBr, and 1.5 mM N^α -benzoylhistidine in 90 mM oxalate buffer pH 5.1. 3 hour reaction time prior to injection. The YMC ODS-AQ C-18 HPLC column (YMC, Inc.) was used. Data were digitized as described in Materials and Methods.

Titanium-containing silicate-based heterogeneous catalysts that have been shown to oxidize bromide at neutral pH were also examined (Walker et al., manuscript in preparation). Millimolar N^α-benzoylhistidine was mixed with 0.1 M H₂O₂, 0.1 M KBr, and 4 mg of either a 5% vanadium-doped catalyst or a 5% molybdenum doped-catalyst in pH 4.0 citrate buffer for 24 hours. Analysis of the products separated by HPLC equipped with electrochemical detection and UV detection showed that a wide variety of oxidation products, including N^α-benzoyl-2-oxohistidine, were formed overnight in the presence of these catalysts. The UV/vis chromatograms are shown in Figure 2-14.

Vanadium Binding to Turnover-Inactivated V-BrPO.

Upon inactivation of V-BrPO under turnover conditions, the inactivated samples and controls (i.e., V-BrPO incubated in 0.1 M citrate pH 4.0 and 0.1 M KBr without H₂O₂) were washed with 0.1 M Tris buffer, pH 8.3. Ammonium vanadate (50 μM) was added to each sample and allowed to incubate overnight. The samples were then washed by ultrafiltration (i.e., five cycles of washing with water to remove excess vanadium), concentrated and then redissolved in 250 μL H₂O. Atomic absorption analyses of 10 μL samples demonstrated that after reincubation with vanadate, the inactivated sample contained 57% less vanadium than the control. Thus oxidation of histidine in V-BrPO affects vanadate coordination. The basis of the reduced vanadium binding capacity is somewhat

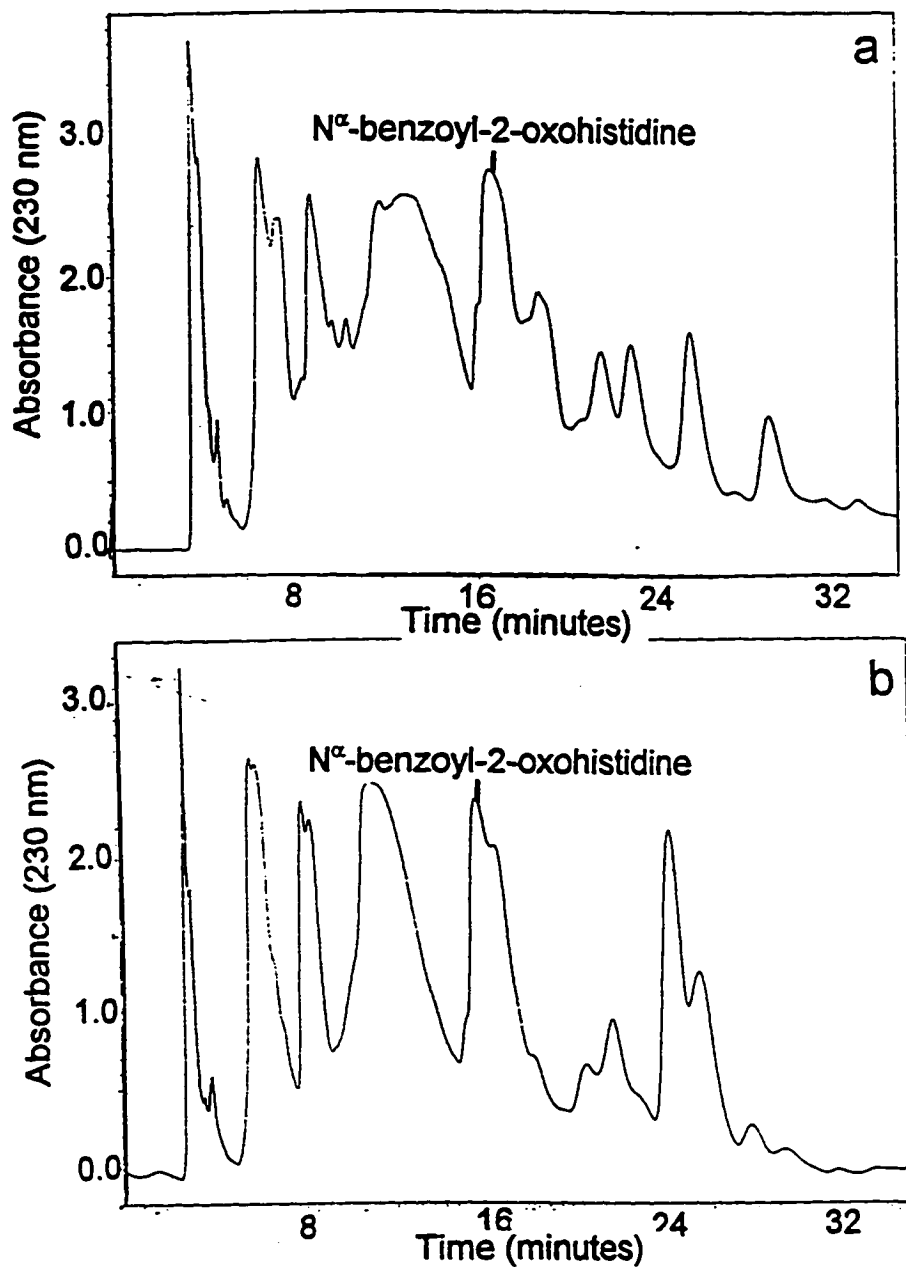


Figure 2-14. HPLC chromatograms at 230 nm of the products formed by the reaction of two titanium-containing heterogeneous silicate catalyst, H_2O_2 , KBr, and N^{α} -benzoylhistidine, Conditions: 100 mM H_2O_2 , 0.1 M KBr, ~ 5 mM N^{α} -benzoylhistidine in 0.1 M citrate buffer pH 4.0. a) 4 mg 5 % vanadium-doped catalyst; b) 4 mg 5 % molybdenum-doped catalyst. 24 hr. reaction time prior to injection.

surprising considering that oxidized imidazoles, including those oxidized at the 2-position, are known to coordinate to transition metals (e.g., $(\text{NH}_3)_5\text{Co}(\text{imidazolidine-2,4,5-trione})^{2+}$; Blackman et al., 1991a,b). On the other hand, histidine oxidation could lead to conformational changes in the protein that could drastically affect vanadate coordination.

Quantitation of 2-Oxohistidine in Turnover-Inactivated V-BrPO

Standard Edman's amino acid analysis was also applied to three separate samples of irreversibly inactivated V-BrPO, which was inactivated under turnover conditions of 15 nM V-BrPO, 100 mM H_2O_2 , 100 mM KBr, and 0.1 M citrate buffer at pH 4. In all cases, loss of 70 to 80% of the histidine residues was detected. The data from one set of analyses is shown in Table 2-3. In this case, approximately 70-74% of the histidine in the pH 4 turnover-inactivated enzyme sample was lost compared to the control (i.e., 15 nM V-BrPO, 100 mM KBr, in 0.1 M citrate pH 4 without H_2O_2). Tyrosine (70 to 100%) may also be consumed during the inactivation of V-BrPO. In the data shown in Table 2-3, no tyrosine was detected in the turnover-inactivated sample. Formation of monobromo- and dibromotyrosine has been demonstrated with both chloroperoxidase and lactoperoxidase using ^{82}Br (Taurog & Dorris, 1991; Knight & Welch, 1978). No new peaks in the amino acid analysis (i.e., with PITC derivatization) of turnover inactivated V-BrPO were detected. Attempts to form derivatized 2-oxohistidine

were not successful, most likely because this species is not stable under the basic conditions necessary for derivatization.

Table 2-3. PITC Amino Acid Analysis of Native V-BrPO and Turnover-inactivated V-BrPO.^a

Amino Acid	Control BrPO moLe%	Inactivated BrPO moLe%
Asx	3.88	2.77
Glx	6.50	5.43
Ser	7.97	6.14
Gly	0.00	0.00
His	2.28	0.60
Arg	10.90	11.93
Thr	19.63	12.72
Ala	6.48	5.54
Pro	3.40	3.10
Tyr	1.70	(ND)
Val	3.66	2.76
Met	2.12	0.50
Ile	16.75	26.69
Leu	2.67	4.01
Phe	8.97	12.81
Lys	3.07	2.53

^a. Cysteine and tryptophan are not reported due to their instability during acid hydrolysis.

Reaction of V-BrPO with Bromide and Stoichiometric Hydrogen Peroxide at Low pH.

As excess peroxide seemed to cause modification of multiple histidines and possibly other amino acid residues in V-BrPO, the ability of lower levels of hydrogen peroxide to cause inactivation, particularly more specific inactivation of a single residue, was examined. As shown in Table 2-4, the activity of V-BrPO was measured over time in the presence of varied amounts of H₂O₂ under conditions of 15 nM V-BrPO, 0.1 M KBr, and 0.1 M citrate pH 4.0. As shown in the table, removal of the hydrogen peroxide by ultrafiltration and reincubation with 50 μM NH₄VO₃ did not completely restore activity to any hydrogen peroxide-treated sample, including that treated with one equivalent of hydrogen peroxide (15 nM). Approximately 40% of the activity was lost.

Table 2-4. V-BrPO activities as determined by the MCD assay after incubation with varied concentrations of hydrogen peroxide for ten hours. Conditions 15 nM V-BrPO and 0.1 M KBr in 0.1 M citrate pH 4.0.

[H ₂ O ₂]	Specific Activity after turnover at pH 4	Specific Activity after addition of vanadate to the turnover sample ^a	Percent remaining activity
0.0	125 U/mg	150	100(120)
15.0 nM	44	87	58
100 nM	14	14	9
100 mM	2.5	5	1.6

^a. Samples were incubated for 3 hours with 50 mM NH₄VO₃ under conditions of 0.1 M Tris pH 8.3.

A sample of V-BrPO (1.5 nmol) partially inactivated in the presence of stoichiometric hydrogen peroxide under reaction conditions of 15 nM V-BrPO, 15 nM H₂O₂, 0.1 M KBr in 0.1 M citrate at pH 4.0 was analyzed for amino acid content by the PITC derivatization method and compared to a control sample and a sample inactivated with 100 mM hydrogen peroxide. However, no quantitative measure of histidine loss proved possible by this procedure (data not shown). In addition, HPLC-ECD of a similarly treated sample of V-BrPO did not clearly show the formation of 2-oxohistidine (data not shown). Tryptic digestion (Uchida & Kawakishi, 1994) of 2.9 nmol of V-BrPO inactivated by stoichiometric hydrogen peroxide under the conditions described above also did not clarify the modification. In fact, the tryptic traces of the inactivated enzyme were poorly resolved and inconsistent; in two runs, large broad unexplained peaks appeared (at different retention times) in the middle of the traces (Figure 2-15).

Atomic absorption of a stoichiometrically inactivated sample provided some hints regarding the modification of specific histidines. The 1.6 μmole sample of stoichiometrically inactivated V-BrPO used was determined to be ~90% inactivated even after it had been reincubated with 0.1 mM ammonium vanadate in Tris at pH 8.3 as described above. However, despite the absence of activity, atomic absorption indicated that this enzyme sample contained 0.8 μM bound

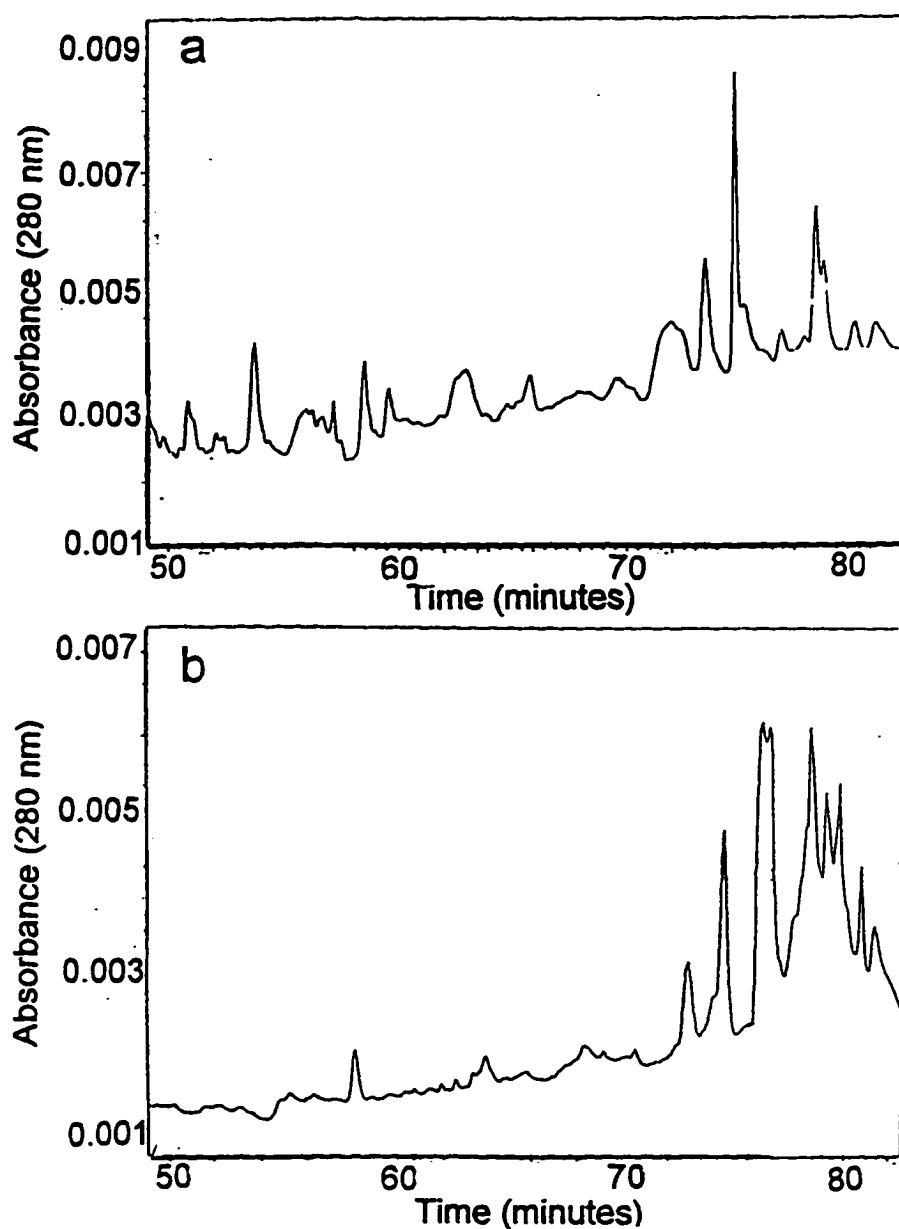


Figure 2-15. Trypsin digestion traces at 280 nM of a) 2.9 nmol native V-BrPO; b) 2.9 nM V-BrPO incubated with 0.1 M H₂O₂, 0.1 M KBr in 0.1 citrate pH 4.0 (standard inactivation conditions).

vanadium, demonstrating that the enzyme still had vanadium binding affinity unlike those samples inactivated with excess peroxide. This data suggests that if a histidine is preferentially attacked, that it is not one which is responsible for vanadium coordination.

The Effect of Peroxidative Chloride Oxidation on Activity of V-BrPO

We attempted to measure the turnover inactivation of V-BrPO and formation of 2-oxohistidine with chloride as the halide source instead of bromide. The specific *bromoperoxidase* activity of V-BrPO when it is incubated under conditions of 15 nM V-BrPO, 0.1 or 1.0 M KCl, 0.1 M H₂O₂ in 90 mM citrate, pH 4.0 for 20 minutes, was compared to that of a control in which V-BrPO was incubated in 90 mM citrate, pH 4.0 for 20 min. without chloride or hydrogen peroxide. The specific activities for the "turnover" sample (at 0.1 M KCl) and the control sample were 73 and 77 U/mg, respectively, compared with a specific activity of the starting enzyme of 115 U/mg. (The bromoperoxidase activity was measured under the standard conditions as described in the Materials and Methods section.) However, the concentration of H₂O₂ measured after 20 minutes remained at 100 mM when measured by the triiodide assay (Cotton & Dunford, 1973) showing that none of the H₂O₂ had been consumed, and further indicating that the loss in activity was not due to turnover. After one hour the specific activities for the "turnover" sample and the control sample were 53 and 58 U/mg, respectively,

and the concentration of hydrogen peroxide was still 0.1 M. The activities of both samples were restored to 90 U/mg upon addition of vanadate. Thus, under these conditions peroxidative chloride oxidation does not occur. The inactivation that was observed is due to loss of vanadium, which occurs at a higher rate in V-BrPO than the oxidation of chloride. Such inactivation is not apparent during the peroxidative bromide oxidation experiments because the bromoperoxidase activity is *much* higher than the chloroperoxidase activity and much higher than the rate of loss of vanadium. In addition, 2-oxohistidine was not formed under the conditions that result in inactivation V-BrPO (i.e., 15 nM V-BrPO, 0.1 M KCl, 0.1 M H₂O₂ in 90 mM citrate, pH 4.0 for 20 minutes).

The reaction of HOCl with N^α-benzoylhistidine was also examined for the formation of N^α-benzoyl-2-oxohistidine. Under conditions of 1.0 mM N-benzoylhistidine and 0 to 5 stoichiometric equivalents of HOCl in 0.1 M citrate pH 4.0 (approximately hour reaction time) none of the 2-oxo derivative was detected by HPLC-ECD (data not shown). HPLC UV chromatograms recorded at 230 nm show the formation of other species that are not electrochemically active under the ECD conditions used (Figure 2-16).

As will be described in subsequent chapters, other oxidative inactivation reactions of V-BrPO were performed and the resulting hydrolysates tested by HPLC-ECD for 2-oxohistidine formation. In particular, the product of the

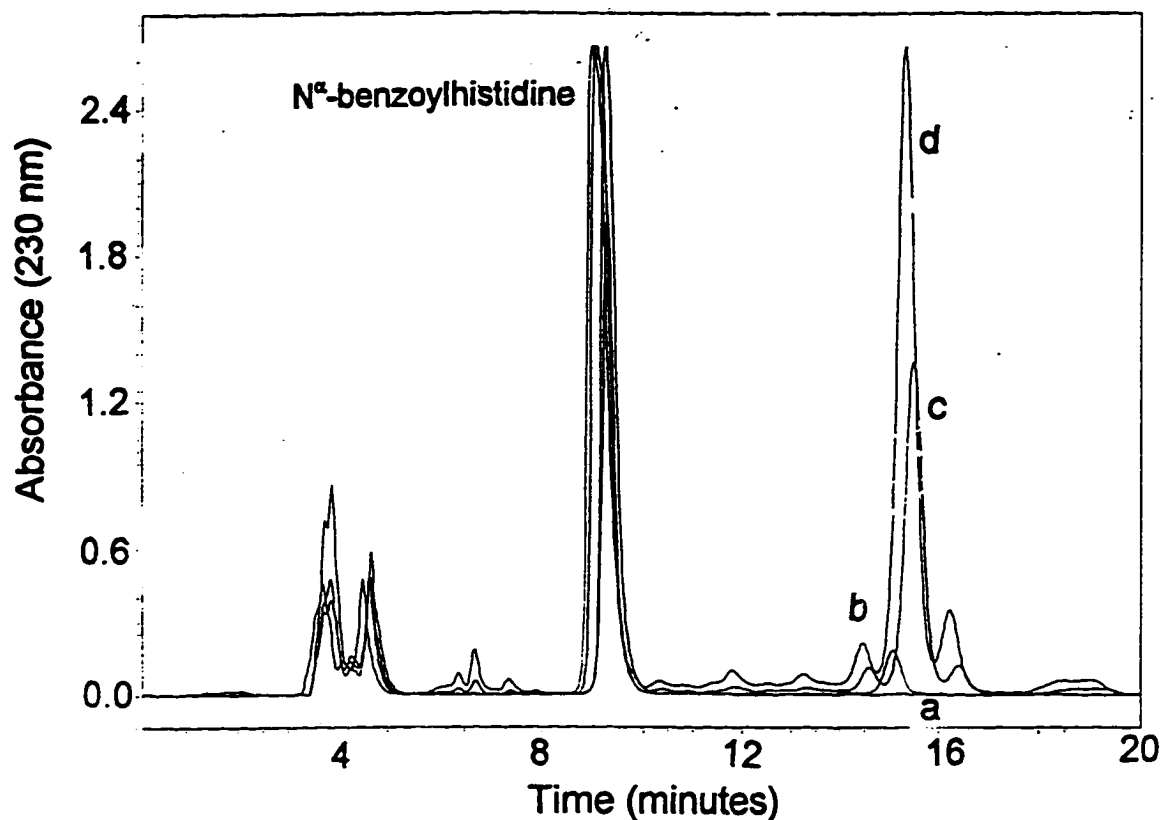


Figure 2-16. HPLC chromatograms at 230 nm of the products formed by the reaction of N^α-benzoylhistidine with varied equivalents of HOCl. Conditions: 1 mM N^α-benzoylhistidine, 0.1 M citrate pH 4.0, a) 0 equivalents HOCl added; b) 0.5 equivalents of HOCl added; c) 3 equivalents of HOCl added; d) 5 equivalents of HOCl added.

vanadium-dependent photooxidation of V-BrPO and the product of turnover with the pseudo-halide azide were examined for the formation of 2-oxohistidine. However, no 2-oxohistidine was observed in the HPLC-ECD traces, suggesting different modes of inactivation for both of these processes.

Detection of 2-Oxohistidine in Other Peroxidases.

As stated in the introduction, histidine has been shown to be an essential residue in several peroxidase enzymes. Everett et al. (1990) demonstrated that under conditions of 20 nM enzyme, 0.1 M NaBr, in 0.1 M MES pH 6.0, the turnover of 2.0 mM H₂O₂ results in total inactivation of lactoperoxidase from bovine erythrocytes (MW = 77,500 Da) and 50% inactivation of iron heme chloroperoxidase from *CaLdariomyces fumago* (MW = 44,000 Da). Thus, the possibility of 2-oxohistidine formation upon inactivation of these enzymes was explored.

Both of the peroxidases were incubated at 20 nM with 0.1 M KBr and 2.0 mM H₂O₂ in 0.1 M phosphate, pH 6.0 for one hour. They were subsequently washed, lyophilized, and hydrolyzed overnight in 6 M HCl as described in Materials and Methods for the V-BrPO samples. The resulting hydrolysates were analyzed by HPLC-ECD as described and no evidence of 2-oxohistidine was detected (data not shown). Thus the inactivation of these proteins under turnover is not due to 2-oxohistidine formation. An additional experiment was performed in which 20 nM

lactoperoxidase was incubated either in just 0.1 M citrate at pH 4.0, 0.1 M citrate pH 4.0 plus 2.0 mM H₂O₂, or 0.1 M citrate pH 4.0, plus 2.0 mM H₂O₂ and 0.1 M KBr to determine if 2-oxohistidine was formed at pH 4.0 as occurs for V-BrPO. After 1 hour of incubation, the three samples had identical activities as measured by triiodide formation under conditions of 0.1 M phosphate pH 7.2 and 10 mM KI (Figure 2-17)^{1,2}. Thus, inactivation of lactoperoxidase under bromide turnover apparently does not occur at pH 4.0, as the activity of the sample containing hydrogen peroxide and bromide was virtually the same as the native sample incubated in citrate buffer. In addition, no inactivation of lactoperoxidase occurred by incubation with just hydrogen peroxide at this pH since the native sample and H₂O₂ incubated samples had similar activity.

¹ Assay conditions: 20 μL lactoperoxidase solution were diluted into 960 μL phosphate containing KI; reaction was initiated by addition of 20 μL H₂O₂.

² The increase in starting absorbance on going from "a" to "c" in Figure 2-17 is not understood; it may have resulted from delayed measurement after the addition of H₂O₂ to the assay solution.

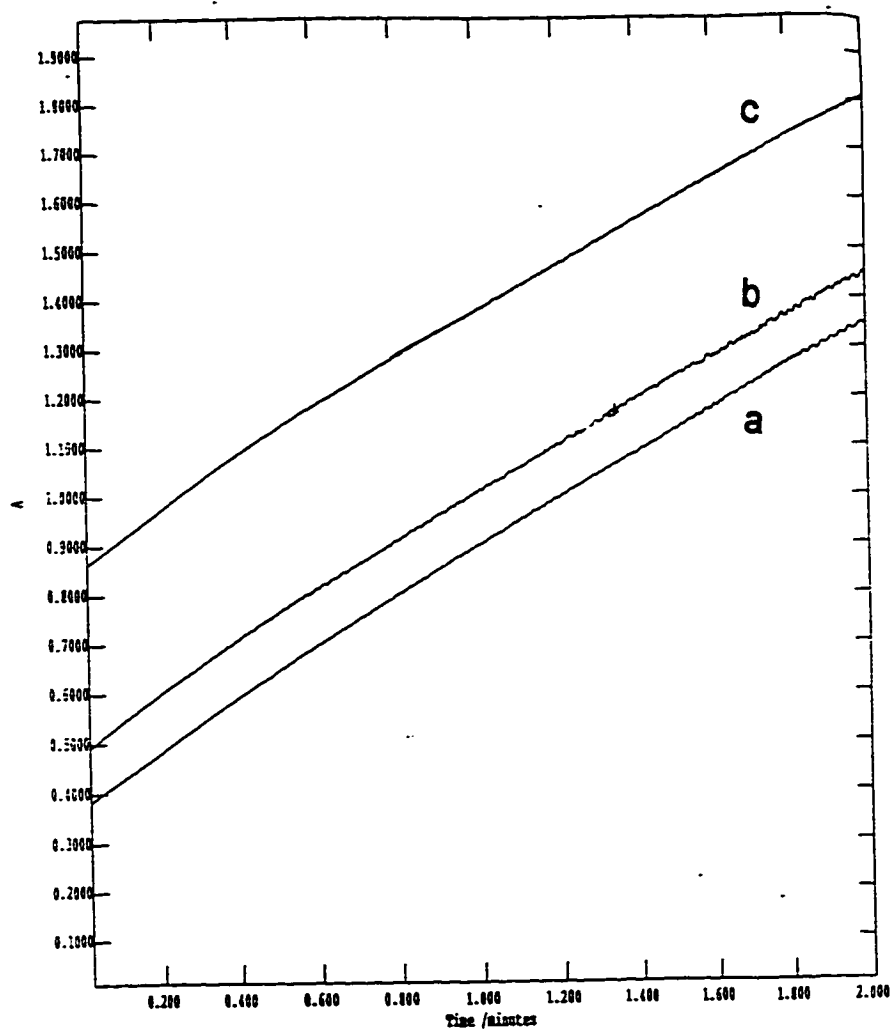


Figure 2-17. Activity of lactoperoxidase samples after incubation in citrate buffer at pH 4.0 as measured by triiodide formation at 353 nm. Conditions: 20 nM lactoperoxidase, 0.1 M citrate buffer pH 4.0, a) 1 hour incubation; b) plus 2.0 mM H_2O_2 , 1 hour incubation; c) plus 2.0 mM H_2O_2 and 0.1 M KBr, 1 hour incubation.

Discussion and Conclusions

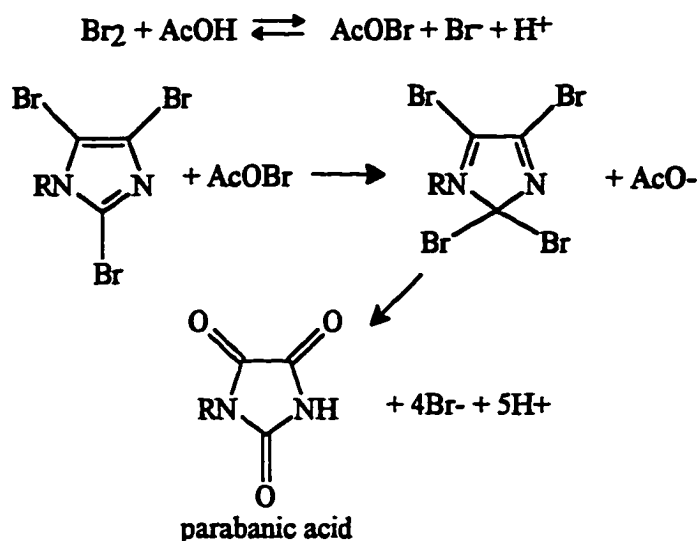
In summary, this work has demonstrated that 2-oxohistidine is formed during the irreversible inactivation of V-BrPO that occurs at low pH (i.e., < pH 5). These results indicate that histidine is the acid base group that has been proposed to be involved in the inverse relationship between reversible inactivation of the enzyme by hydrogen peroxide at high pH and the irreversible inactivation of the enzyme at low pH. The pH dependence of the inactivation of V-BrPO and the formation of 2-oxohistidine suggests that protonation of the histidine side chain is a key factor in the oxidation of this residue. Formation of 2-oxohistidine requires all of the components of turnover (i.e., bromide, hydrogen peroxide and V-BrPO) as well as low pH. 2-oxohistidine is also formed when HOBr is added to V-BrPO at low pH, thus, it is likely that histidine is oxidized by a freely diffusable bromine species versus an enzyme-bound species. The oxidation of histidine does not occur by singlet oxygen in V-BrPO, because 2-oxohistidine was not detected and inactivation did not occur under the conditions in which singlet oxygen is produced quantitatively by V-BrPO (i.e., neutral pH or above; Everett et al., 1990a). The results of the experiments with the enzyme itself are further confirmed by the parallel behavior of the reaction of N^α-benzoylhistidine with aqueous bromine under similar conditions.

While it did not prove possible to determine the effects of chloride turnover on the enzyme at low pH, the reactions with N^α-benzoylhistidine and added HOCl at pH 4.0 did not result in the formation of the 2-oxo species, despite the better oxidizing capacity of oxidized chlorine species versus bromine species. These results indicate that the formation of 2-oxohistidine is specific to bromine and likely occurs by an initial bromination process. Based on the results of imidazole oxidation in the pentamminecobalt(III) complex by aqueous bromine (Blackman et al., 1991a), further oxidation would lead to the 2-oxo product.

The pH dependences of the formation of 2-oxohistidine in V-BrPO and the formation of N^α-benzoyl-2-oxohistidine in the "model" reactions also suggest that the speciation of the oxidized bromine species is important to the formation of the oxidized residue. Under the conditions where 2-oxohistidine formation was observed, the predominant bromine species in solution are Br₂ and Br₃⁻. At the higher pH conditions, HOBr and OBr⁻ become more significant. The acid-dependent equilibria of the chlorine species in aqueous solution are shifted relative to bromine; at pH 4.0, HOCl is still the predominant species relative to Cl₂ and Cl₃⁻. Thus, if it were a general phenomenon that the X₂ and X₃⁻ oxidized halogen species are capable of halogenation and subsequent oxidation of the histidine side chain, then chlorine would not form the 2-oxo species at pH 4.0. More acidic conditions would be required.

Atomic absorption results of V-BrPO inactivated with excess peroxide under standard conditions (see above) show clearly that the enzyme loses its affinity to bind vanadium and indicate an important role for histidine in the coordination of vanadium to V-BrPO. While the bromination, oxidation and oxidative degradation of imidazoles by aqueous bromine is well known (Boulton and Coller, 1974; Schmir and Cohen, 1965; Stensio, et al, 1973), investigations of the bromination and oxidation of coordinated imidazoles are surprisingly limited. One notable exception is the thorough work on the bromination and oxidation of imidazoles coordinated to pentamminecobalt(III) (Blackman et al., 1991a,b). Reaction of excess bromine in acetate or phosphate, pH 4-6 with $RImH^+$ ($R = (NH_3)_5Co$; ImH = imidazole) results in the formation of $R(\text{parabanate})^{2+}$ (parabanate = imidazolidine-2,4,5-trione; Blackman, 1991a). The reaction was shown to proceed via the formation of $R(4,5-Br_2ImH)^{3+}$ and $R(2,4,5-Br_3ImH)^{2+}$. Addition of one equivalent of bromine to $R(2,4,5-Br_3ImH)^{2+}$ in acetate buffer produced $R(\text{parabanate})^{2+}$, quantitatively. Blackman and coworkers (1991a) propose a mechanism in which additional bromination at C-2 leads to spontaneous bromide hydrolysis as shown in Scheme 4-1. Thus in the presence of excess aqueous bromine, as in our case of enzymatic oxidation of bromide by hydrogen peroxide, oxidation of the histidyl imidazolium

moiety likely occurs first by bromination followed by subsequent bromide hydrolysis.



Scheme 2-1. Proposed mechanism for the bromination of the C-2 position of $\text{R}(2,4,5\text{-Br}_3\text{ImH})^{2+}$ and subsequent bromide hydrolysis to parabanic acid (Blackman, et. al., 1991a).

While the results on inactivation of V-BrPO by excess peroxide indicate that a ligating histidine is undergoing oxidation, the results on the stoichiometric inactivation of V-BrPO suggest that a histidine residue other than one ligated to vanadium is preferentially oxidized. In the absence of a structure/sequence of the enzyme, it will be quite a challenge to identify that histidine. This difficulty is increased by the unknown changes that cause inactivated enzyme to be resistant to the trypsin digestion procedures. In any case, the evidence is piling up in favor of an acid-base histidine in V-BrPO.

Unlike Cu,Zn-SOD, which is inactivated at neutral pH by hydrogen peroxide (Hodgson, 1975), V-BrPO requires all of the turnover components and a low pH. The oxidation of histidine in the V-BrPO system further differs from the Cu,Zn-SOD system in that the former is an electrophilic process mediated by a bromonium-like species, whereas the later is a radical process (Uchida & Kawakishi, 1989). In fact, to the best of this author's knowledge, all previous examples of 2-oxohistidine formation in proteins and peptides have been proposed to occur by radical mechanisms, typically mixed function oxidation systems involving iron or copper (Uchida & Kawakishi, 1986, 1989, 1990). Studies on these radical processes have demonstrated that asparagine and aspartic acid in particular are secondary products of the radical oxidation of histidine. Changes in the quantity of either of these amino acids in inactivated V-BrPO have not been observed; however, amino acid analysis shows a large quantity of aspartic acid/asparagine residues in the native enzyme and the addition of one or a few additional residues would not likely be clearly detected. The stoichiometry studies on N^α-benzoylhistidine and HOBr show that secondary products are formed in the inactivation of V-BrPO as well at higher quantities of oxidant, but the identities of these species have not yet been determined.

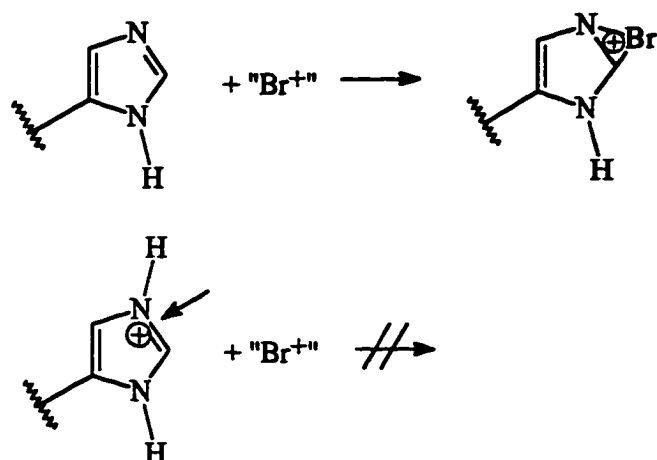
Haloperoxidases are well-established tools for the labeling of proteins with radioactive iodine (Manthey et al., 1984). Examples of radioactive bromine labeling

have also been reported. Brominations of the proteins thyroglobulin and bovine serum albumin have been effected with chloroperoxidase from *Caldariomyces fumago* (Knight et al., 1975; Knight & Welch, 1978) and lactoperoxidase (Taurog & Dorris, 1991). In addition, brominations of canine fibrinogen and human serum albumin have been achieved using myeloperoxidase (McElvany et al., 1980; Manthey et al., 1984) and the iron heme bromoperoxidase from *Penicillium capitatus* (McElvany & Welch, 1980; Manthey et al., 1984). Radioactive labeling experiments with iodine and bromine have demonstrated that tyrosine is the predominantly labeled residue both for iodination and bromination with peroxidases. However, significant bromination of histidine residues has been demonstrated for all four of the brominating peroxidases studied via radiolabeling (Knight & Welch, 1978; Taurog & Dorris, 1991; Manthey et al., 1984).

In previous studies with iodination of histidine catalyzed by lactoperoxidase, Taurog and Dorris (1991) suggested that halogenation of histidine is favored at higher pH values. They determined that iodination of histidines catalyzed by lactoperoxidase is faster at pH 7.0 than iodination at pH 5.4. The reactions performed here with lactoperoxidase turnover of bromide at pH 6.0 likely resulted in bromination instead of 2-oxohistidine formation. Furthermore, radiolabeling with chloroperoxidase in the pH range of 2.2 to 4.7 shows an increase in histidine bromination with pH (Knight and Welch, 1978). It seems possible that if the

histidyl residues in V-BrPO are accessible substrates during turnover at the higher pH values where 2-oxohistidine formation is not observed, they may in fact be brominated instead. Some of the secondary products identified in the reaction of HOBr with N^α-benzoylhistidine at pH 4.0 may be brominated products. As suggested above, the loss of a proton from the histidine residue at higher pH is likely a factor in the product distribution.

It is important to remember that at the pH values where 2-oxohistidine is observed in V-BrPO, the histidine side chain is predominantly in the protonated, or "imidazolium" form. In this form, the histidine side chain is not likely to undergo electrophilic substitution by a bromonium ion as depicted in Scheme 2-2. Thus the 2-oxohistidine detected is likely formed only by reaction of the bromonium ion with the small amount of deprotonated side chain present. The absence of the 2-oxo derivative at higher pH values where more histidines are deprotonated can be attributed to the instability of 2-oxohistidine at higher pH or, alternatively, insufficient oxidizing capability of the oxidized bromine species under these conditions. At high acid, where the amount of the imidazole form of histidine is very minimal relative to the imidazolium form, the large ECD signals that were detected for the oxidation of N^α-benzoylhistidine by HOBr can be attributed to the stability of the 2-oxoderivative under these conditions.



Scheme 2-2. Mechanism for electrophilic bromination of a histidine imidazole side illustrating why electrophilic bromination should not occur for the imidazolium form.

The amino acid data from the inactivation of V-BrPO by excess hydrogen peroxide do indicate that tyrosine is also consumed in the reaction in addition to histidine. This is not surprising considering the results of the radioactive labeling studies with peroxidases. The product of the reaction of the oxidized bromine species and tyrosine in this system has not been identified. However, Yang, et al. (1995) demonstrated through their studies of chloroperoxidase bromination with ^{82}Br that monobromotyrosine is formed by the reaction of aqueous bromine and tyrosine at pH 4.0. Thus it is likely that the free oxidized bromine species produced by V-BrPO is also brominating tyrosyl residues in the enzyme.

While consumption of tyrosine is definitely occurring in the inactivation of V-BrPO at pH 4.0, it is not likely that any of these tyrosines is a ligand to the

vanadium center. As has been referred to throughout this dissertation, the sequence similarity between the bromoperoxidase from *A. nodosum* and the chloroperoxidase from *C. inaequalis* in the vanadium binding region, including conservation of the bound histidine 496, suggests that the bromoperoxidase, like the chloroperoxidase, also coordinates vanadate through a single histidine (Vilter, 1995; Messerschmidt & Wever, 1996). In addition, earlier work by Binaries and Carrano (1986) demonstrated that when the VO^{3+} ion is complexed to phenolate ligands like tyrosine, the complex exhibits strong ligand to metal charge transfer bands in the visible region. No such spectral properties are seen for bromoperoxidase. However, while tyrosine is not a likely ligand to the vanadium center, bromination or other modification of tyrosine residues could induce conformational changes which could influence vanadium binding affinity. The existence and effects of brominated tyrosines on the activity of V-BrPO are undergoing further examination.

References

- Bhattacharyya, D.K., Bandyopadhyay, U., Banerjee, R.K. (1992) *J. Biol. Chem.*, 267: 9800-9804.
- Bhattacharyya, D.K., Bandyopadhyay, U., Banerjee, R.K. (1993) *J. Biol. Chem.*, 268, 22292-22298.
- Blackman, A.G., Buckingham, D.A., Clark, C.R., & Simpson, J. (1991a) *Inorg. Chem.*, 30, 1635-1642.
- Blackman, A.G., Buckingham, D.A., & Clark, C.R. (1991b) *J. Am. Chem. Soc.*, 113, 2656-2664.
- Blanke, S.R., Hager, L.P. (1990) *J. Biol. Chem.*, 265, 12454-12461.
- Bonadies, J.A. & Carrano, C.J. (1986) *J. Am. Chem. Soc.*, 108, 4088-4095.
- Boulton, B.E. & Coller, B.A.W., (1974) *Aust. J. Chem.*, 27, 2331-2341.
- Butler, A., & Walker, J.V. (1993) *Chem. Rev.* 93, 1937-1944.
- Carrano, C.J.; Mohan, M.; Holmes, S.M.; de La Rosa, R.; Butler, A.; Charnock, J.M.; Garner, C.D. *Inorg. Chem.* 1994, 33, 646-655.
- Clague, M.J., & Butler, A. (1995) *J. Am. Chem. Soc.* 117, 3475-3484.
- Cotton, M.L., & Dunford, H.O. (1973) *Can. J. Chem.* 51, 582-587.
- de Boer, E., Tromp, M.G.M., Plat, H., Krenn, B.E., & Wever, R. (1986) *Biochim. Biophys. Acta* 872, 104-115.
- de Boer, E., & Wever, R. (1988) *J. Biol. Chem.* 263, 12326-12332.
- de Boer, E., Boon, K., & Wever, R. (1988) *Biochemistry* 27, 1629-1635.
- De la Rosa, R.I.; Clague, M.J.; Butler, A. (1992) *Inorganic Chemistry*
- Ebert, R.F. (1986) *Anal. Biochem.*, 154, 431-435.
- Everett, R.R., & Butler, A. (1989) *Inorg. Chem.* 28, 393-395.

- Everett, R.R. (1990) Ph.D. Dissertation, UC Santa Barbara.
- Everett, R.R., Kanofsky, J.R., & Butler, A. (1990a) *J. Biol. Chem.* **265**, 4908-4914.
- Everett, R.R., Soedjak, H.S., & Butler, A., (1990b) *J. Biol. Chem.* **265**, 15671-15679.
- Faulkner, D.J., (1993) *Natural Product Reports*, **10** , 497-539 and references therein.
- Hager, L.P., Morris, D.R., Brown, F.S., Eberwein, H., (1966) *J. Biol. Chem.*, **241**, 1769-1777.
- Hecht, H.J., Sonek, H., Haag, T., Pfeifer, O., van Pee, K.-H. (1994) *Nat. Struct. Biol.*, **1**, 532-537.
- Hodgson, E.K., & Fridovich, I., (1975) *Biochemistry*, **14**, 5294-5299.
- Joanne, E.H.J.M., & van den Berg, R.H. (1991) *J. Chromatography (Biomed. Appl.)*, **566**, 461-469.
- Knight, L., Krohn, K.A., Welch, M.J., Spomer, B., Hager, L.P. (1975) in Radiopharmaceuticals (Subramanian, G., Rhodes, B.A., Cooper, J.F., Sodd, V.J., eds.) p.149.
- Knight, L.C. & Welch, M.J. (1978) *Biochim. Biophys. Acta*, **534**, 185-195.
- Krenn, B.E., Tromp, M.G.M., & Wever, R. (1989) *J. Biol. Chem.* **264**, 19287-19292.
- Manthey, J.A. & Hager, L.P. (1981) *J. Biol. Chem.*, **256**, 11232-11238.
- Manthey, J.A., Hager, L.P., McElvany, K.D. (1984) in Methods in Enzymology (Wold, F. & Moldave, K., eds.) Vol. 107, pp.439-445, Academic Press, San Diego.
- McElvany, K.D., Barnes, J.W., Welch, M.J. (1980) *Int. J. Appl. Radiat. Inst.*, **31**, 679-688.
- McElvany, K.D., Welch, M.J. (1980) *J. Nucl. Med.*, **21**, 953-960.

- Messerschmidt, A. & Wever, R. (1996) *Proc. Natl. Acad. Sci., USA*, **93**, 392-396.
- Poulos, T.L. & Kraut, J. (1980) *J. Biol. Chem.*, **255**, 8199-8205.
- Reynolds, M.S., Morandi S.J., Raebiger J.W., Melican S.P., Smith, S.P.E. (1994). *Inorg. Chem.*, **33**, 4977-4984.
- Schmir, G.L., & Cohen, L.A. (1965) *Biochemistry*, **4**, 533-538.
- Smith, P.K., Krohn, R.I., Hermanson, G.T., Mallia, A.K., Garther, F.H. & Provenzano, M.D. (1985) *Anal. Biochem.*, **150**, 76-85.
- Soedjak, H.S. (1991) PhD Dissertation, UC Santa Barbara.
- Soedjak, H.S., & Butler, A., (1991) *Inorg. Chem.*, **29**, 5015-5017.
- Soedjak, H.S., Everett, R.R., & Butler, A., (1991) *J. Ind. Microbiol.* **8**, 37-44.
- Soedjak, H.S., Walker, J.V., & Butler, A. (1995) *Biochemistry*, **34**, 12689-12696.
- Stensio, K.-E., Wahlberg, K., Wahren, R., (1973) *Acta Chem. Scand.*, **27**, 2179-2183.
- Stone, K.L., LoPresti, M.B., Williams, K.R. (1990) in Laboratory Methodology in Biochemistry: Amino Acid Analysis and Protein Sequencing, Fini, C., Floridi, A., Finelli, V.N., Wittman-Leibold, B., eds. Boca Raton: CRC Press, pp. 181-206.
- Taurog, A. & Dorris, M.L. (1991) *Arch. Biochem. Biophys.*, **287**, 288-296.
- Tien, M., & Tu, C.P.D. (1987) *Nature*, **326**, 520-523.
- Tromp, M.G.M., 'Olafsson, G., Krenn, B.E., Wever, R., (1990) *Biochim. Biophys. Acta*, **1040**, 192-198.
- Tschirret-Guth, R.A., & Butler, A. (1994) *J. Am. Chem. Soc.* **116**, 411-412.
- Uchida, K., & Kawakishi, S. (1986) *Biochem. Biophys. Res. Commun.*, **138**, 659-665.
- Uchida, K., & Kawakishi, S. (1989) *Bioorg. Chem.*, **17**, 330-343.

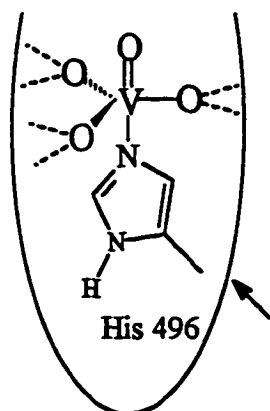
- Uchida, K., & Kawakishi, S. (1993) *FEBS Lett.* 332, 208-210.
- Uchida, K., & Kawakishi, S. (1994) *J. Biol. Chem.*, 269, 2405-2410.
- van Schijndel, J.W.P.M., Vollenbroek, E.G.M., Wever, R. (1993) *Biochim. Biophys. Acta*, 1161, 249-256.
- van Schijndel, J.W.P.M., Barnett, P., Roelse, J., Vollenbroek, E.G.M., Wever, R. (1994) *Eur. J. Biochem.*, 225, 151-157.
- Vilter, H. (1984) *Phytochemistry*, 23, 1387-1390.
- Vilter, H. (1995) *Metal Ions in Biological Systems*, 31, 325-362.
- Vilter, H., & Glombitza, K. -W. (1983) *Bot. Mar.*, XXVI, 341-4.
- Yang, Z.P.; Shelton, K.D.; Howard, J.C.; Woods, A.E. (1995) *Comp. Biochem. Physiol.*, 111B, 417-426.

Chapter 3: Molybdenum (VI)- and Tungsten (VI)-Mediated Biomimetic

Chemistry of Vanadium Bromoperoxidase

Introduction

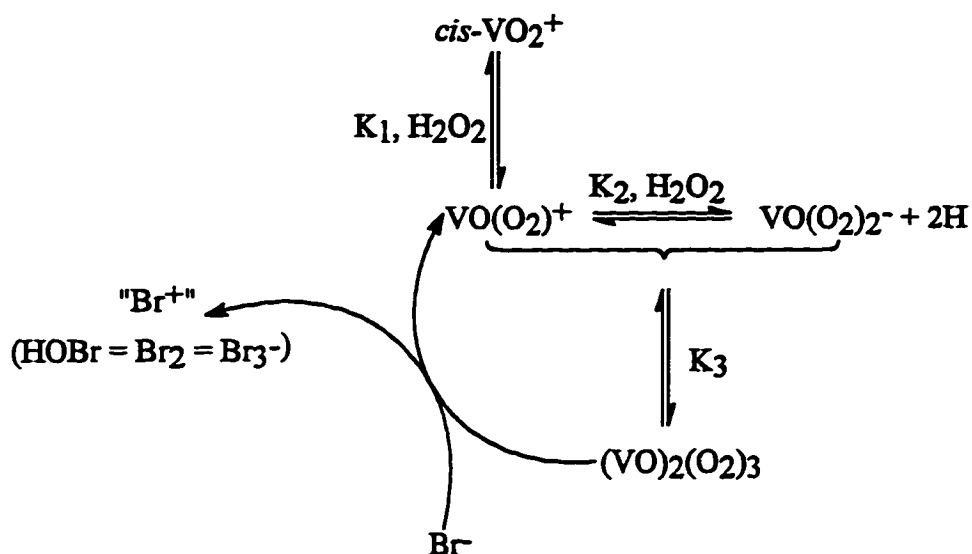
Perhaps one of the greatest obstacles to characterizing the mechanism of vanadium bromoperoxidase from *Ascophyllum nodosum* is the spectroscopic silence of the vanadium(V) ion required for catalytic activity. As described in detail in Chapter 1, it has not proven possible to characterize this d^0 metal ion by conventional spectroscopic techniques; it has no EPR signal and the ^{51}V NMR signal is very broad (Vilter & Rehder, 1987). Early EXAFS studies suggested that the vanadium had a single terminal oxo and 5 O/N ligands, including long vanadium to histidine nitrogen ligation (Arber et al., 1989). A recent bond valence sum analysis of V-BrPO (Carrano et al., 1994) is most consistent with the vanadium in a trigonal planar environment with marked similarity to the vanadium site in the crystal structure of the chloroperoxidase from *Curvularia inaequalis* (Messerschmidt & Wever, 1996).



Vanadium site in vanadium chloroperoxidase from *C. inaequalis*.

In the absence of a spectroscopic "handle" by which to monitor the reaction of V-BrPO, functional model complexes have been studied in which the vanadium(V) center can be observed (de la Rosa et al., 1992; Clague & Butler, 1995; Colpas et al., 1994; Colpas et al., 1996). The first functional mimic of V-BrPO to be reported in the literature was *cis*-dioxovanadium(V), VO_2^+ (de la Rosa et al., 1992). VO_2^+ functions in acidic solution as a biomimic of V-BrPO by catalyzing the bromination of organic substrates and the bromide-assisted disproportionation of hydrogen peroxide to form dioxygen (de la Rosa et al., 1992; Clague & Butler, 1995).

In acidic solution, VO_2^+ coordinates one or two equivalents of hydrogen peroxide to form $\text{VO}(\text{O}_2)^+$ or $\text{VO}(\text{O}_2)_2^-$, respectively, depending on the concentrations of acid and H_2O_2 . The first formation constant, K_1 , is 3.5×10^4 and the second formation constant, K_2 , is about 1, depending on ionic strength (Secco, 1980; Orhanovic & Wilkins, 1967). Thus, in acid, even in the presence of excess H_2O_2 both the monoperoxo and diperoxo species are present. Recently, Clague and Butler (1995) demonstrated that the initial rate of oxidation of bromide by micromolar concentrations of VO_2^+ in the presence of 25- to 200-fold excess H_2O_2 over vanadium and 200-fold excess NH_4Br over hydrogen peroxide in acidic solution exhibits a second order dependence on vanadium concentration (Clague & Butler, 1995). ^{51}V NMR results from Harrison and Howarth (1985) have indicated that the monoperoxo and diperoxo complexes of vanadium(V) can dimerize to form a triperoxo dimer in acid. In fact, the maximal rate of bromide oxidation in the study by Clague and Butler (1995) was achieved when the concentrations of the mono- and diperoxo complexes were equal, suggesting that in fact the triperoxo dimer is the active oxidizing species in this mimic. Clague and Butler (1995) determined a formation constant of 32 M^{-1} for the dimer:

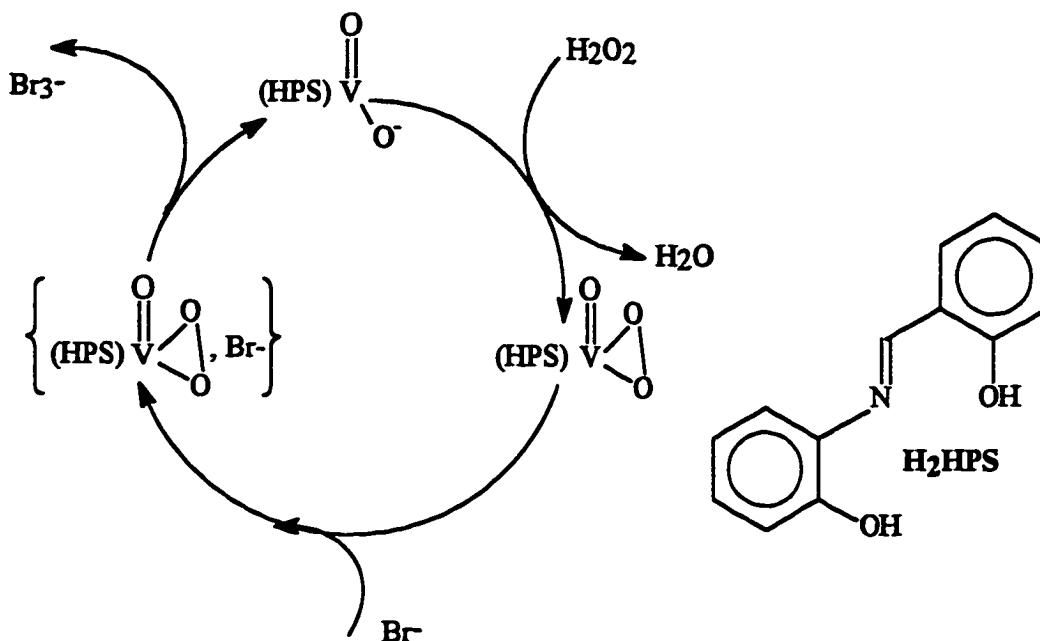


Scheme 3-1. Reaction mechanism for the oxidation of bromide by $(VO)_2(O_2)_3$.

The bimolecular rate constant for bromide oxidation by $(VO)_2(O_2)_3$ was calculated to be $4.1 \text{ M}^{-1} \text{ s}^{-1}$. This value is 10^3 to 10^5 times slower than that for the enzyme. In addition, because formation of the dimer requires both $VO(O_2)^+$ and $VO(O_2)_2^-$, this mimic functions only in acidic conditions, while the enzyme functions optimally at near neutral pH. Neither $VO(O_2)^+$ nor $VO(O_2)_2^-$ can oxidize bromide.

$(HPS)VO(OH)$, where H_2HPS is the Schiff base ligand hydroxyphenylsalicylideneimine, is also a catalyst of bromide oxidation by hydrogen peroxide in aqueous DMF solution (Clague & Butler, 1993a). ^{51}V NMR results establish that $(HPS)VO(OH)$ coordinates one equivalent of H_2O_2 forming the monoperoxo, $(HPS)VO(O_2)^-$ species and releasing one equivalent of H_3O^+ . The

monoperoxo complex $(\text{HPS})\text{VO}(\text{O}_2)^-$ then oxidizes bromide forming the dioxo species $(\text{HPS})\text{VO}_2^-$, which can then coordinate another equivalent of H_2O_2 and start through the cycle again as shown in Scheme 3-2. In the absence of added acid only one turnover is observed, however, upon the addition of stoichiometric acid with respect to H_2O_2 consumed, the reaction becomes catalytic. Thus this model system requires relatively mild acidic conditions for catalytic bromination compared to *cis*-dioxovanadium(V).



Scheme 3-2. Reaction mechanism for the oxidation of bromide by peroxide catalyzed by $(\text{HPS})\text{V}(\text{OH})$.

Similar systems were developed by Pecoraro and coworkers (Colpas et al., 1994, 1996). They prepared several functional complexes with derivatized tripodal amine chelating ligands, including $\text{VO}(\text{O}_2)(\text{Heida})^-$, where H_3eida is N-(2-hydroxyethyl)iminodiacetic acid, $\text{VO}(\text{O}_2)(\text{ada})^-$, where H_2ada is N-(2-amidomethyl)iminodiacetic acid, and $\text{VO}(\text{O}_2)(\text{Hnta})^-$, where H_3nta is nitrilotriacetic acid. Like the peroxo complex of HPS, each of these compounds requires one equivalent of acid to oxidize one equivalent of bromide or iodide in acetonitrile. In addition, these complexes also re-coordinate peroxide and proceed through catalytic oxidations provided that the necessary equivalents of acid are present.

Aside from the bromoperoxidase models described above, prior to the current work, very little had been published on transition metal catalyzed peroxidative halogenation reactions. In fact, only vanadium complexes had been examined as catalysts for the oxidation of a halide more electronegative than iodide (Clague & Butler, 1993a; Colpas et al., 1994, 1996). Vanadium(V) (Secco, 1980) and molybdenum(VI) (Smith & Kilford, 1976; Arias, 1990) have been reported to catalyze iodide oxidation by hydrogen peroxide in acidic solution. Titanium(IV), in contrast, has been reported to stabilize hydrogen peroxide against oxidation of iodide (Lydon & Thompson, 1986). Vanadium(IV) has also been reported to be a catalyst for the peroxidation of bromide (Sakurai & Tsuchiya, 1990); however, the mechanism of this reaction seems to differ from iodide peroxidation by vanadium(V) and molybdenum(VI) and bromide peroxidation by vanadium(V). Vanadium(IV) is thought to reduce hydrogen peroxide, forming a hydroxyl radical which can oxidize bromide to bromine radical (Br^\cdot). Vanadium(V), molybdenum(VI), and titanium(IV) mediated reactions are thought to proceed by two-electron oxidation of iodide, although this hypothesis has not been tested. The $(\text{HPS})\text{VO}(\text{OH})^-$ mediated reaction described above has been shown to occur by an electrophilic bromination process (Clague & Butler, 1993a).

The oxidation chemistry of peroxo complexes of molybdenum(VI) in organic systems is well-established. Mimoun and coworkers were the first to

establish the ability of complexes of the form $\text{MoO}(\text{O}_2)_2\text{L}_1\text{L}_2$ to catalyze the epoxidation of olefins in organic solvents (Mimoun et al., 1969, 1970). Molybdenum(VI) peroxy species have become widely used for organic oxygen atom transfer reactions; molybdenum is used in the Halcon process for the oxidation of cyclopropane to propylene oxide (Landau, 1979). Thompson and coworkers have studied the chemistry of mononuclear molybdenum(VI) and also tungsten(VI) peroxy complexes in acidic aqueous solution, and found them to be very effective oxygen atom transfer reagents (Lydon et al., 1987). In fact, molybdenum and tungsten species have been shown to be more effective at activation of peroxide toward oxygen atom transfer than their vanadium(V) counterparts (Ghiron & Thompson, 1990).

This chapter describes an investigation into the ability of molybdenum and tungsten peroxy species to catalyze peroxidative bromide oxidation and chloride oxidation in acidic aqueous solution. More globally, this chapter addresses the factors that govern transition metal-catalyzed peroxidative halide oxidation reactions and, furthermore, peroxidation reactions in general.

Materials and Methods

Bromination reactions. The peroxidative oxidation of bromide mediated by molybdenum(VI) was studied using $\text{Na}_2\text{MoO}_4 \cdot 2\text{H}_2\text{O}$ at concentrations less than 0.5 mM to limit oligomerization (Lydon et al., 1987). Typically, 0.15 mM $\text{Na}_2\text{MoO}_4 \cdot 2\text{H}_2\text{O}$ was used, except where noted. The ratio of Mo(VI) to H_2O_2 concentration ranged from 1:1 to 1:12. Acidity was controlled with HClO_4 in strongly acidic solutions (i.e., 0.1 M HClO_4) and 10 to 50 mM sodium acetate buffer at $\text{pH} > 3$; acetate does not coordinate to MoO_3 in acid (Ghiron & Thompson, 1989). The concentration of acid (i.e., HClO_4) and buffer (i.e., acetate) was always at least 10-fold larger than the concentration of H_2O_2 . 1,3,5-Trimethoxybenzene (TMB) was used as the primary organic substrate to monitor bromination reactions. The concentration of TMB was kept in slight excess of the H_2O_2 concentrations to prevent formation of dibromo-TMB. All reaction solutions contained 20-25% methanol to solubilize TMB (2.0 mM) and to prevent precipitation of bromo-TMB. The ionic strength was controlled with NaClO_4 in the bromide dependence and acid dependence experiments.

In the tungsten-mediated reactions, $\text{Na}_2\text{WO}_4 \cdot 2\text{H}_2\text{O}$ was used at concentrations less than 0.1 mM and typically less than 25 μM . Hydrogen peroxide was present in at least a 50-fold excess over tungsten(VI) to prevent

formation of polyoxotungstates. Otherwise the reaction conditions were the same as described above.

UV/visible and kinetic experiments. The molybdenum(VI)-mediated reactions were monitored primarily by following the disappearance of the oxodiperoxomolybdenum(VI) species at 328 nm, which is the λ_{max} for the complex $\text{MoO}(\text{O}_2)_2(\text{H}_2\text{O})_2$ and 310 nm, which is the λ_{max} for the complex $\text{MoO}(\text{O}_2)_2(\text{H}_2\text{O})(\text{OH})^-$ (see Results) (Lydon et al., 1987). Spectrophotometric data were recorded at 25.0 °C on an Hewlett Packard HP8452A diode array spectrophotometer or a Uvikon 860 spectrophotometer. The tungsten-mediated reactions were best followed by formation of brominated TMB at 266 nm as opposed to the absorbance of oxodiperoxotungsten(VI) species (sh 250 nm) because the low concentrations of $\text{WO}(\text{O}_2)_2$ required to limit polymerization (i.e., μM) do not absorb significantly. For both metal systems the dependence of the rate of bromide oxidation on metal complex concentration was monitored by the formation of tribromide (Br_3^-): 266 nm, $\epsilon = 36,100 \text{ M}^{-1} \text{ cm}^{-1}$.

GC experiments. GC data were recorded using an Hewlett Packard HP5890 Series II gas chromatograph with a flame-ionization detector using a glass capillary HP Ultra 2 column. Chromatography conditions were as follows: Equilibration time at the starting temperature of 120 °C was 0.1 minutes. Upon injection of a 3- μl sample, the temperature of the oven was held at 120 °C for two

minutes. The temperature was ramped upwards at a rate of 15 °C/min up to 250 °C. The temperature was then held at 250 °C for several minutes to clean the column. The concentrations of TMB, Br-TMB, and Cl-TMB were determined from standard curves.

Oxygen evolution experiments. Oxygen evolution was measured with a YSI Model 5331 Standard Oxygen Electrode attached to a YSI Model 5300 Biological Oxygen Monitor. Analysis was performed on 4 mL samples under conditions of 0.15 mM Na₂MoO₄, 1.5 or 5.0 mM H₂O₂, 0.1 M NH₄Br, and 0.1 M HClO₄. Reaction solutions without hydrogen peroxide were deaerated by sparging with nitrogen. Dioxygen evolution was monitored on the deaerated sample for approximately five minutes. Hydrogen peroxide was then added to the reaction mixture and dioxygen evolution was further monitored for at least five minutes.

General reagents and procedures. H₂O₂ stock solution concentrations were determined from triiodide formation according to the method of Cotton and Dunford (1973). Puratronic grade Na₂WO₄·2H₂O was purchased from Aesar. All chemicals were analytical reagent grade.

Results and Interpretation

Molybdenum(VI) Mediated Peroxidative Bromination Reactions

In acidic aqueous solution, the two primary peroxo species of molybdenum(VI) are diaquooxidiperoxomolybdenum(VI), $\text{MoO}(\text{O}_2)_2(\text{H}_2\text{O})_2$ and aquohydroxooxidiperoxomolybdenum, $[\text{MoO}(\text{O}_2)_2(\text{H}_2\text{O})(\text{OH})]^-$. The pK_a of the diaquo complex is approximately 1.85 (Lydon et al., 1987). In 0.1 M HClO_4 , $\text{MoO}(\text{O}_2)_2(\text{H}_2\text{O})_2$ (0.15 mM) oxidizes bromide (0.5 M) to produce tribromide (Br_3^-) and molybdenum(VI), formulated as MoO_3 and omitting water of coordination (Lydon et al., 1987). Because tribromide is somewhat unstable under these reaction conditions, particularly at long reaction times, the stoichiometry of the reaction was monitored by the bromination of 1,3,5-trimethoxybenzene (TMB) under conditions that favor the production of the monobromotrimethoxybenzene (Br-TMB), i.e., an excess of TMB (2.0 mM) over H_2O_2 (1.5 mM). Gas chromatographic analyses of TMB consumed and Br-TMB produced (Figure 3-1) show that one equivalent of Br-TMB is produced per equivalent of hydrogen peroxide consumed (Equation 1).



In the absence of MoO_3 , Br-TMB is not formed in the same time frame (Figure 3-1), establishing that MoO_3 is a catalyst of bromide oxidation by H_2O_2 . The turnover rate of MoO_3 is *ca.* 180 mol Br-TMB/mol Mo hr^{-1} , which is *ca.* 45 times

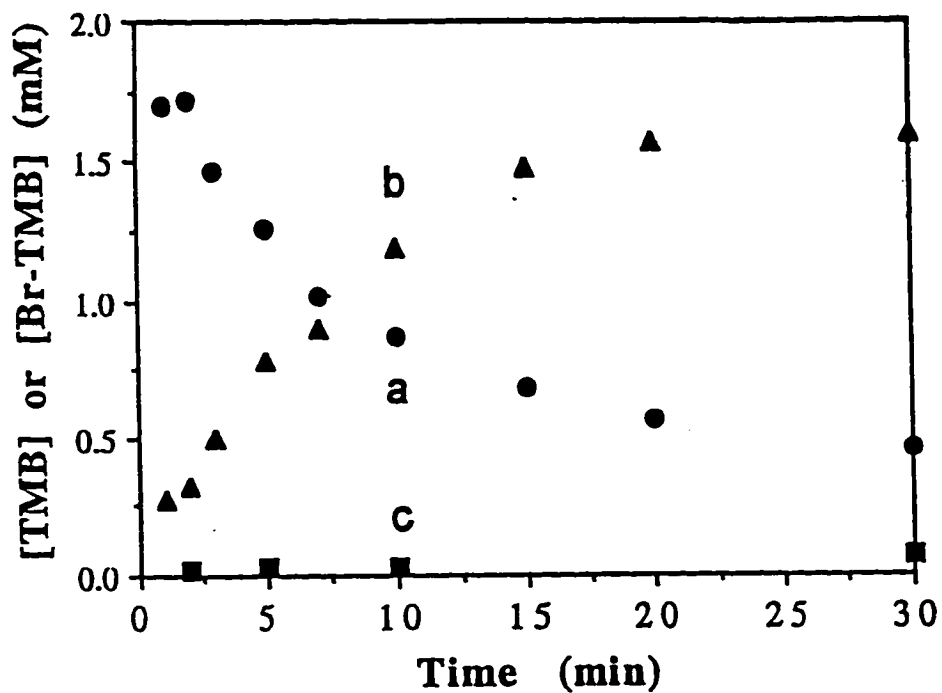


Figure 3-1. Gas chromatographic analysis of the peroxidative bromination of TMB in acid solution catalyzed by MoO_3 . a) and c) disappearance of TMB; b) appearance of Br-TMB; Conditions for a) and b): 0.15 mM Na_2MoO_4 , 1.5 mM H_2O_2 , 0.5 M NH_4Br , and 2.0 mM TMB in 0.1 M HClO_4 /25% MeOH; conditions for c): same as a) and b) but without Na_2MoO_4 . T = 25.0 °C

faster than VO_2^+ under the same conditions (i.e., 0.15 mM metallate, 1.5 mM H_2O_2 , 2.0 mM TMB, 0.5 M NH_4Br in 0.1 M HClO_4 /25% MeOH; see below).

The oxidation of bromide by $\text{MoO}(\text{O}_2)_2(\text{H}_2\text{O})_2$ and $\text{MoO}(\text{O}_2)_2(\text{H}_2\text{O})(\text{OH})^-$, the primary peroxo complexes of molybdenum(VI) in acidic aqueous solution (Lydon et al., 1987), was also monitored spectrophotometrically at 328 nm and 310 nm, which are the absorption maxima of the diaquo- and aquohydroxo-oxodiperoxomolybdenum(VI) species, respectively. Figure 3-2 shows the time course of bromide oxidation by $\text{MoO}(\text{O}_2)_2(\text{H}_2\text{O})_2$ as a function of the ratio of hydrogen peroxide to molybdenum(VI). Under conditions of 0.15 mM Na_2MoO_4 , 0.3 mM H_2O_2 , 0.5 M NH_4Br , 2.0 mM TMB in 0.1 M HClO_4 /25% MeOH, in which the molybdenum(VI) is present predominantly as $\text{MoO}(\text{O}_2)_2(\text{H}_2\text{O})_2$ (Lydon et al., 1987), the kinetic data fit well to a first-order decay (Figure 3-2) for more than 90% of the reaction. When the hydrogen peroxide concentration is increased, but under otherwise identical conditions, a lag phase in the absorbance profile occurs before the exponential decay of $\text{MoO}(\text{O}_2)_2(\text{H}_2\text{O})_2$ is observed (Figure 3-2). The duration of the lag phase in the absorbance profile is proportional to the concentration of excess H_2O_2 , as is demonstrated in the following paragraph.

MoO_3 -mediated peroxidative bromination of TMB occurs during the time-frame of the lag phase in Figure 3-1c, which is seen by comparison of Figures 3-1 and 3-2c. GC results of Br-TMB formation in Figure 3-1c performed under

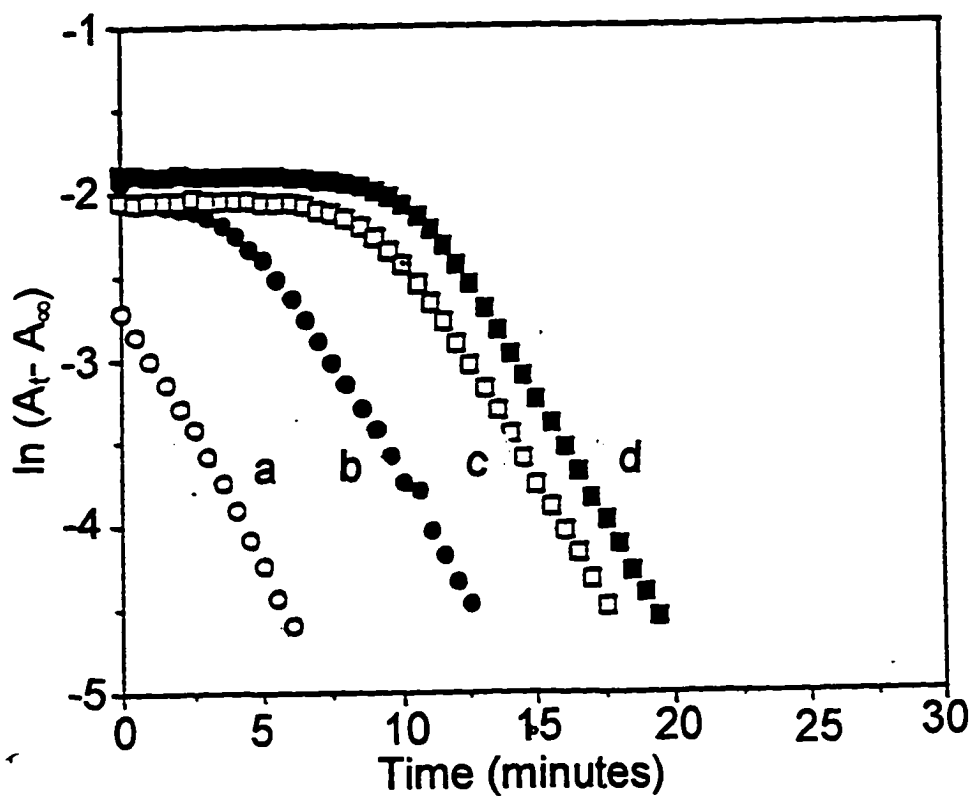


Figure 3-2. Time course for the disappearance of $\text{MoO}(\text{O}_2)_2(\text{H}_2\text{O})_2$ in the presence of Br^- and TMB as a function of H_2O_2 concentration at 25.0°C . Conditions: $0.15\text{ mM Na}_2\text{MoO}_4$, $0.5\text{ M NH}_4\text{Br}$, and 2.0 mM TMB in $0.1\text{ M HClO}_4/25\%\text{ MeOH}$ at a) $0.3\text{ mM H}_2\text{O}_2$, b) $0.9\text{ mM H}_2\text{O}_2$, c) $1.5\text{ mM H}_2\text{O}_2$ and d) $1.8\text{ mM H}_2\text{O}_2$. The reaction was monitored at 328 nm .

identical reaction conditions as Figure 3-2c show that approximately 1.2 mM Br-TMB is formed in the first 10 min which roughly corresponds to the approximate time of the lag phase in Figure 3-2c. Thus the exponential absorbance decay in Figure 3-2a is the oxidation of bromide by $\text{MoO}(\text{O}_2)_2(\text{H}_2\text{O})_2$, since approximately two equivalents of H_2O_2 per equivalent of Mo(VI) are present at the end of the apparent lag phase in Figure 3-2c. The constant absorbance value of approximately 0.175 corresponds to a total $\text{MoO}(\text{O}_2)_2(\text{H}_2\text{O})_2$ concentration of 0.15 mM ($\epsilon = 1170 \text{ M}^{-1} \text{ cm}^{-1}$), which is the initial concentration of $\text{MoO}(\text{O}_2)_2(\text{H}_2\text{O})_2$. Thus in the presence of excess hydrogen peroxide, a constant concentration of $\text{MoO}(\text{O}_2)_2(\text{H}_2\text{O})_2$ is maintained by rapid recoordination of H_2O_2 to $\text{MoO}_2(\text{O}_2)$ or MoO_3 (*vide infra*).

As established above, the oxidation of bromide by $\text{MoO}(\text{O}_2)_2(\text{H}_2\text{O})_2$ in the presence of TMB produces two equivalents of Br-TMB per equivalent of $\text{MoO}(\text{O}_2)_2(\text{H}_2\text{O})_2$ consumed; thus both equivalents of H_2O_2 are used to oxidize bromide. The disappearance of $\text{MoO}(\text{O}_2)_2(\text{H}_2\text{O})_2$, which was followed at 328 nm, proceeds in a single exponential decay (> 90% reaction). Oxidation of the first equivalent of bromide likely produces HOBr and $\text{MoO}_2(\text{O}_2)$ (Equation 2). This monoperoxo species can either oxidize a second equivalent of bromide in a faster reaction, coordinate another equivalent of H_2O_2 to reform the diperoxo species, or disproportionate producing MoO_3 and $\text{MoO}(\text{O}_2)_2(\text{H}_2\text{O})_2$ (Equation 5).

Recoordination of H_2O_2 to MoO_3 could also occur rapidly if MoO_3 is formed (Equation 6). The rate of bromination of TMB is very fast with respect to the rate of oxidation of Br^- by $\text{MoO}(\text{O}_2)_2$ (see below).



Dependence of the Peroxidation of Bromide on Acid Concentration

The rate of bromide oxidation by oxodiperoxomolybdenum(VI) was found to depend on acid concentration. A plot of k_{obs} versus $-\log[\text{H}^+]$ is sigmoidal with an inflection point at *ca.* pH 2.3 (Figure 3-3). This value is in agreement with the value we calculated spectrophotometrically at 370 nm, $\text{pK}_a = 2.2$, under the reaction conditions using the procedure described by Thompson for determination of the pK_a in aqueous solution. The small difference between Thompson's value for the pK_a of 1.85 (Schwane & Thompson, 1989) and our value of 2.2 may be due to the presence of MeOH; however the λ_{max} of the diperoxo species is the same in the presence and absence of MeOH. The observed rate constant for the

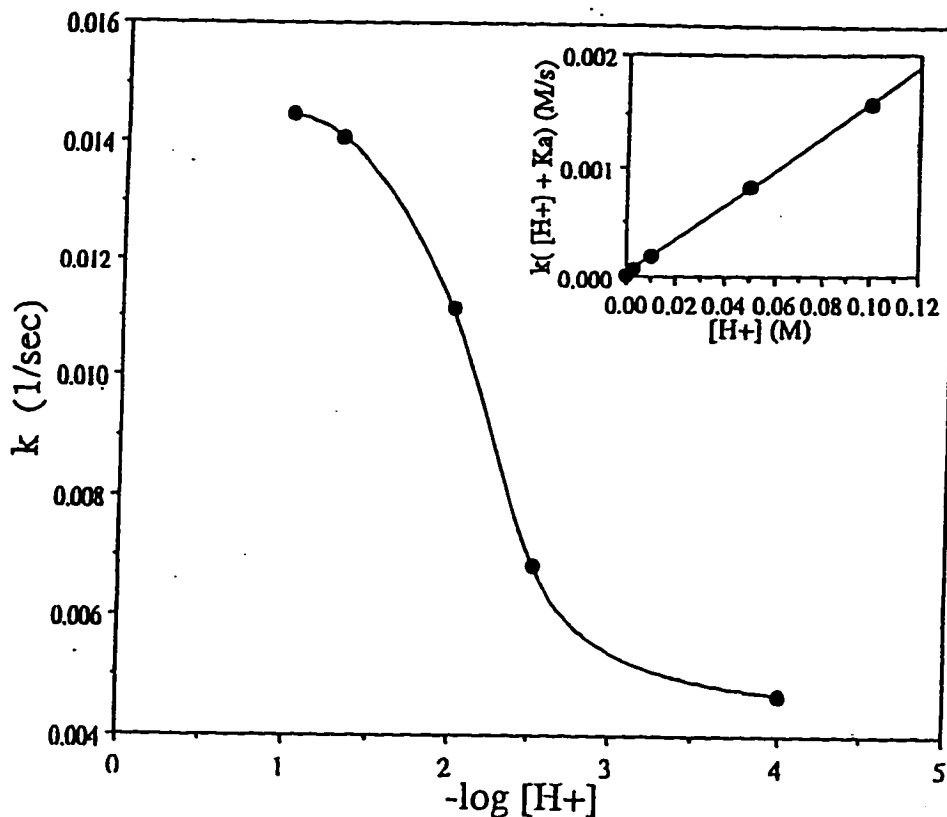


Figure 3-3. Plot of the observed rate constant for the disappearance of $\text{MoO}(\text{O}_2)_2(\text{H}_2\text{O})_2$ and $\text{MoO}(\text{O}_2)_2(\text{H}_2\text{O})(\text{OH})^-$ monitored at 328 nm during the peroxidative bromination of TMB vs. acid concentration. Conditions: 0.15 mM Na_2MoO_4 , 0.3 mM H_2O_2 , 1.0 M NH_4Br , and 2 mM TMB in 25% MeOH with varying H^+ concentration. The acid concentration was adjusted with HClO_4 below pH 3 and with 10 mM acetate buffer above pH 3. $I = 2.1$ M NaClO_4 ; Temperature = 25.0 °C. Inset: Plot of $k_{\text{obs}}(K_a + [\text{H}^+])$ vs. $[\text{H}^+]$ to determine k_A and k_{AH} .

disappearance of the oxodiperoxomolybdenum(VI) species is given by $k_{obs} = (k_{AH}[H^+] + k_{(A^-)K_a})/([H^+] + K_a)[Br^-]$. The values of k_{AH} (for $MoO(O_2)_2(H_2O)_2$) and $k_{(A^-)}$ (for $MoO(O_2)_2(H_2O)(OH)^-$) were found to be $1.51 \times 10^{-2} M^{-1} sec^{-1}$ and $2.38 \times 10^{-3} M^{-1} sec^{-1}$ using 5.0×10^{-3} as the value for K_a (Figure 3-3 inset). Thus $MoO(O_2)_2(H_2O)_2$ oxidizes bromide faster than $MoO(O_2)_2(H_2O)(OH)^-$.

The rate of oxidation of bromide by $MoO(O_2)_2(H_2O)_2$ was also found to be first-order in $MoO(O_2)_2(H_2O)_2$ concentration (Figure 3-4). These experiments were performed under turnover conditions (i.e., 0-0.8 mM $Na_2MoO_4 \cdot H_2O$, 2 mM H_2O_2 , 0.1 M NH_4Br in 0.1 M $HClO_4/25\%$ MeOH) by following the initial rate of Br_3^- formation spectrophotometrically. Under these conditions, the oxodiperoxomolybdenum(VI) species is known to be present as the monomeric oxodiperoxo species (Schwane & Thompson, 1989). The second-order rate constant calculated from this experiment is $1.88 \times 10^{-2} M^{-1} sec^{-1}$, which is in agreement with the rate constant determined from the acid dependence experiments, $1.51 \times 10^{-2} M^{-1} sec^{-1}$. If instead of using Br_3^- formation to investigate the dependence of the rate on molybdenum concentration, the disappearance of oxodiperoxo Mo(VI) complex is followed spectrophotometrically (i.e., at 328 nm and at 0.1 mM to 0.6 mM MoO_3 , 1.8 mM H_2O_2 , 1.0 M NH_4Br , and 2 mM TMB in 0.1 M $HClO_4/25\%$ methanol), the rate constant varies approximately 1.6 fold. The increase in rate constant with increase in molybdenum concentration is

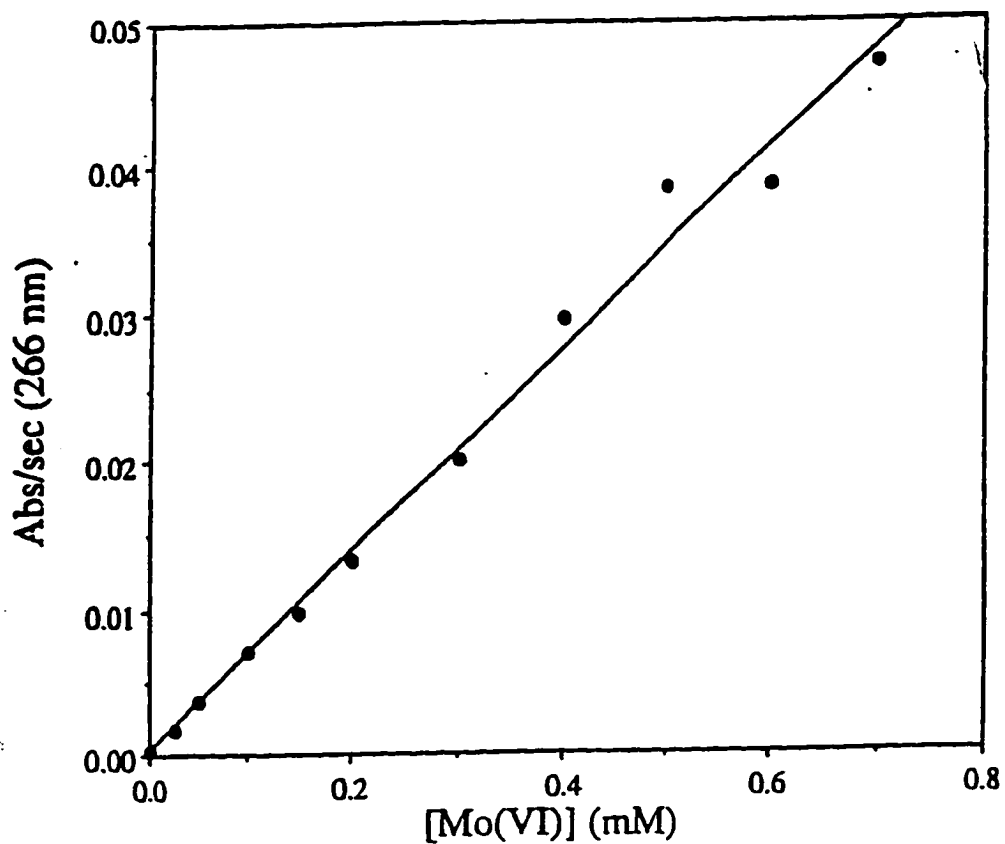


Figure 3-4. Plot of the initial rate of tribromide formation monitored at 266 nm mediated by $\text{MoO}(\text{O}_2)_2(\text{H}_2\text{O})_2$ oxidation of bromide vs. molybdenum(VI) concentration. Conditions: 0.1 M NH_4Br , 2 mM H_2O_2 and varying Na_2MoO_4 concentration in 0.1 M $\text{HClO}_4/25\%$ MeOH. Temperature = 25.0 °C

accompanied by an increase in the scatter of the value of the rate constant, for which the origin is not yet understood.

Dependence of the Rate of Bromide Peroxidation on Bromide and 1,3,5-trimethoxybenzene Concentrations

The pseudo-first order rate constant of the disappearance of $\text{MoO}(\text{O}_2)_2(\text{H}_2\text{O})_2$ monitored at 324 nm was linearly dependent on bromide concentration under conditions of 0.15 mM Na_2MoO_4 , 1.5 mM H_2O_2 , 0.1 M HClO_4 , 2.0 mM TMB, 25% methanol, and to 2.0 M KBr (Figure 3-5). Thus, the molybdenum(VI)-catalyzed peroxidation of bromide is, like the vanadium(V) reaction (de la Rosa, et al, 1992; Clague & Butler, 1995), first order in bromide concentration and does not show saturation behavior up to 2 M bromide. The rate constant for bromide oxidation by $\text{MoO}(\text{O}_2)_2(\text{H}_2\text{O})_2$ was also found to be independent of TMB concentration (i.e., 0.4-2.0 M TMB; data not shown), which is consistent with rapid TMB bromination after the rate-limiting step of Br-oxidation. These reactions were followed spectrophotometrically at 266 nm to monitor the appearance of Br-TMB. Accordingly, from the results of the acid, bromide, molybdenum complex, and TMB concentration dependence experiments, the overall rate expression for the oxidation of bromide by the oxodiperoxomolybdenum(VI) species can be expressed as shown in equation 7.

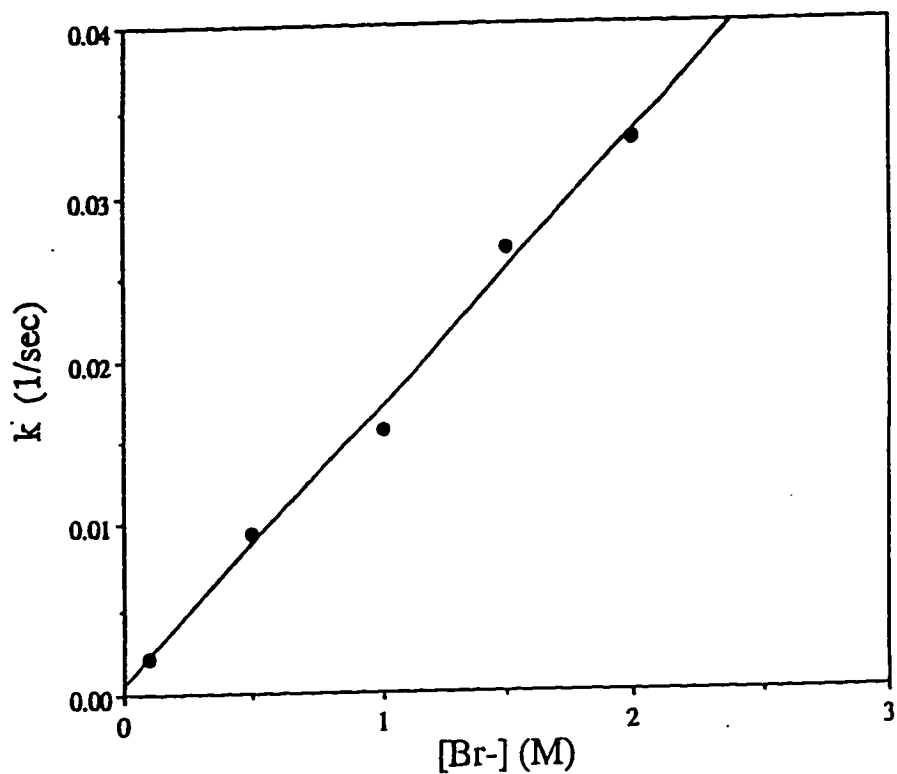


Figure 3-5. Plot of the observed rate constant for the disappearance of $\text{MoO}(\text{O}_2)_2(\text{H}_2\text{O})_2$ monitored at 328 nm during the peroxidative bromination of TMB vs. bromide concentration. Conditions: 0.15 mM $\text{Na}_2\text{MoO}_4 \cdot 2\text{H}_2\text{O}$, 1.5 mM H_2O_2 , 2.0 mM TMB and varying NH_4Br in 0.1 M $\text{HClO}_4/25\%$ MeOH. $I = 2.1\text{M}$ (NaClO_4). Temperature = 25.0 °C.

$$-d[\text{MoO}(\text{O}_2)_2(\text{H}_2\text{O})_2 + \text{MoO}(\text{O}_2)_2(\text{H}_2\text{O})(\text{OH})]/dt = \quad (7)$$

$$((k_{\text{AH}}[\text{H}^+] + k_{\text{A}} - K_{\text{a}})/([\text{H}^+] + K_{\text{a}}))[\text{Br}^-](\text{[MoO}(\text{O}_2)_2(\text{H}_2\text{O})_2] + \text{[MoO}(\text{O}_2)_2(\text{H}_2\text{O})(\text{OH})])$$

Effect of Alcohols on the Rate of Bromide Peroxidation

As stated above in the interpretation of the acid dependence results, methanol is apparently capable of shifting the speciation equilibrium between the diaquo- and the aquohydroxomolybdenum(VI) complexes. A study of the methanol dependence showed that the rate of bromide oxidation by $\text{MoO}(\text{O}_2)_2(\text{H}_2\text{O})_2$ under conditions of 0.15 mM Na_2MoO_4 , 1.5 mM H_2O_2 , 0.1 M NH_4Br , and 0.1 M HClO_4 decreases with increasing methanol concentration (Figure 3-6a). In addition, under conditions of 0.15 mM Na_2MoO_4 , 1.8 mM H_2O_2 , 0.1 M HClO_4 , and 0.1 M NH_4Br , the rate of bromide oxidation by $\text{MoO}(\text{O}_2)_2(\text{H}_2\text{O})_2$ also decreased with increasing ethanol concentration (3-6b). Both of these alcohols are likely weakly coordinating to the complex. Under conditions of 40 mM Na_2MoO_4 and 400 mM methyl- ^{13}C -alcohol to 250 mM molybdenum and 2.5 M methyl- ^{13}C -alcohol, 0.62 M HClO_4 , and two equivalents of H_2O_2 per molybdenum, ^{13}C NMR of the labeled methanol did not show a shift or broadening in the methanol peak at 48 ppm. Thus, it is likely that the complexation of methanol must be extremely weak (Figure 3-7). Interestingly, studies with the triperoxovanadium(V) dimer showed that ethanol also weakly coordinated this complex; however, this coordination resulted in an increase in the initial rate of

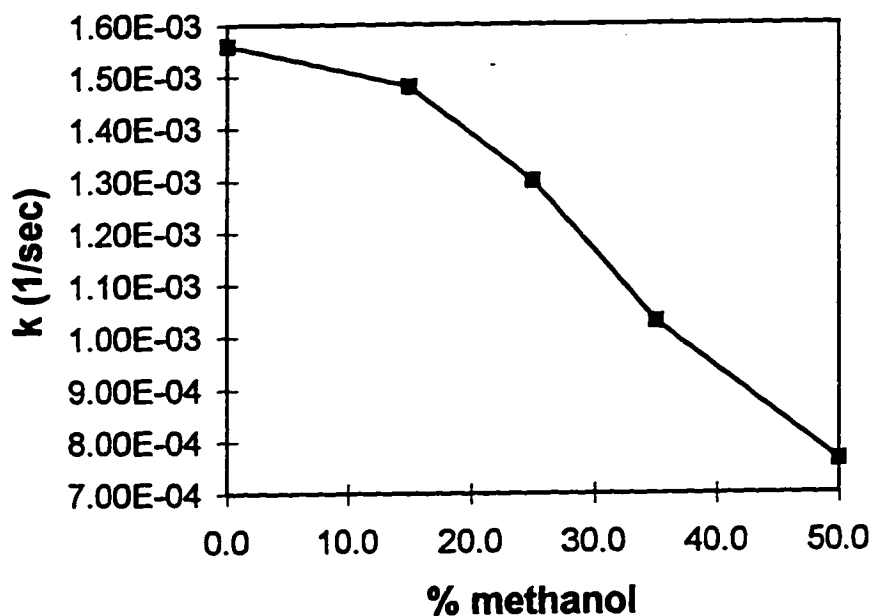


Figure 3-6a. Plot of the initial rate of tribromide formation monitored at 266 nm mediated by $\text{MoO}(\text{O}_2)_2(\text{H}_2\text{O})_2$ oxidation of bromide vs. percent methanol in solution. Conditions: 0.3 mM Na_2MoO_4 , 2.0 mM H_2O_2 , 80 mM NH_4Br , 0.1 M HClO_4 , 0 to 50% methanol. Temperature = 25.0 °C.

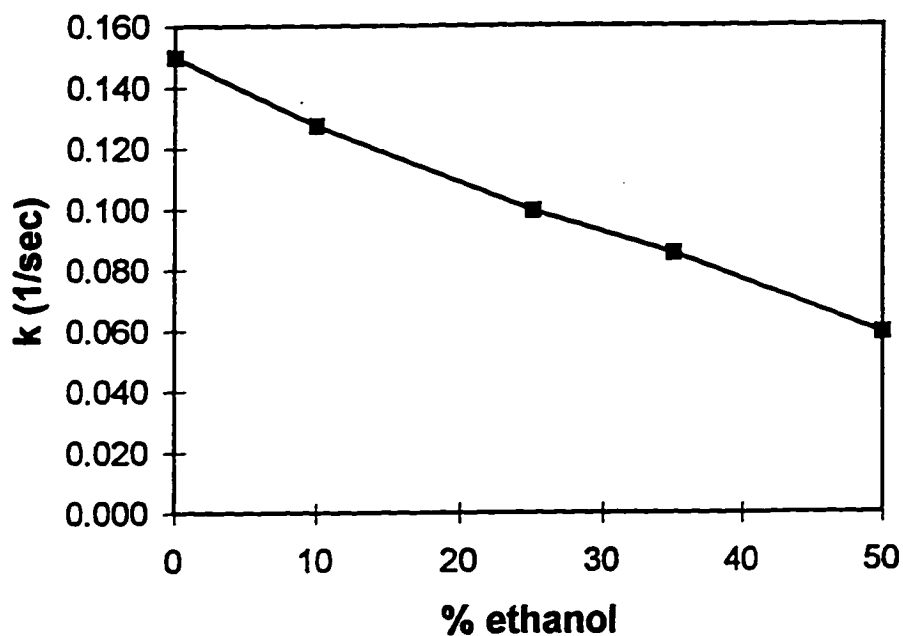


Figure 3-6b. Plot of the initial rate of tribromide formation monitored at 266 nm mediated by $\text{MoO}(\text{O}_2)_2(\text{H}_2\text{O})_2$ oxidation of bromide vs. percent ethanol in solution. Conditions: 0.15 mM Na_2MoO_4 , 2.0 mM H_2O_2 , 0.1 M NH_4Br , and 0.1 M HClO_4 in 0 to 50% ethanol. Temperature = 25.0 °C.

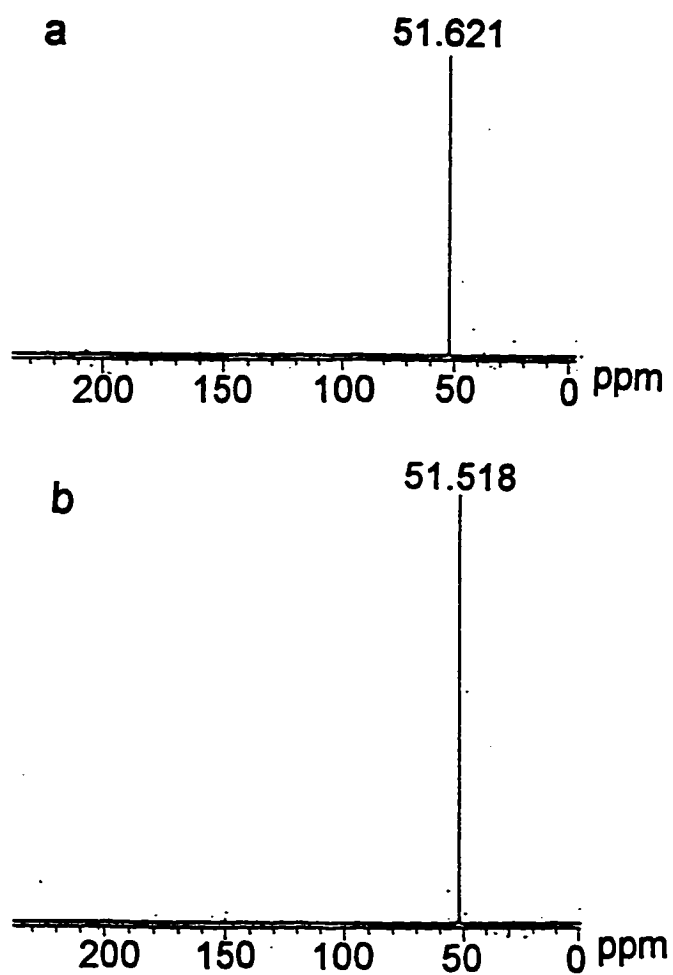


Figure 3-7. Carbon-13 NMR spectrum of ¹³C-labeled methanol in acidic aqueous solution. Conditions: a and b) 0.4 M methyl -¹³C- alcohol, 0.62 M HClO₄, and 20 % D₂O; b only) 40 mM Na₂MoO₄ and 80 mM H₂O₂. T = 23.0 °C.

bromide oxidation, presumably due to an increase in the formation of the triperoxovanadium(V) dimer (Clague & Butler, 1995).

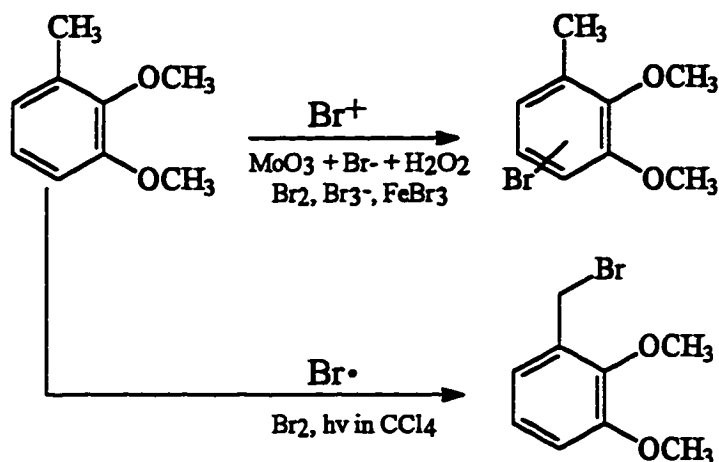
Oxygen Formation

As stated above, in the absence of an organic halogen acceptor, MoO_3 catalyzes the formation of tribromide. Based on the reactivity of oxidized bromine species with hydrogen peroxide (Kanofsky, 1989), one might expect that dioxygen would be formed when MoO_3 catalyzes the oxidation of Br^- by H_2O_2 . Under the acidic conditions of these kinetic experiments (i.e., 0.05-0.1 M HClO_4), the reduction of tribromide by hydrogen peroxide to form dioxygen is very slow. In fact experiments to monitor the possible MoO_3 -catalyzed halide-assisted disproportionation of hydrogen peroxide forming dioxygen under conditions of 0.15 mM MoO_3 , 1.5 mM H_2O_2 , 0.5 M NH_4Br in 0.05 M HClO_4 showed that the response on the oxygen probe was indistinguishable from the baseline, although tribromide was formed as detected spectrophotometrically. Thus under these conditions, the halide-assisted disproportionation of hydrogen peroxide is not observed. By contrast both VO_2^+ in acidic aqueous solution and V-BrPO at neutral pH catalyze dioxygen formation in the absence of an organic halogen acceptor (de la Rosa, et al., 1992). In the case of VO_2^+ , even though the acid concentration is 0.05 M, the concentration of hydrogen peroxide is sufficiently higher (5 mM) than in the MoO_3 (1.5 mM) experiments that the rate of H_2O_2

reduction of tribromide is observable, although this rate is still much less than the rate of VO_2^+ -catalyzed bromination of TMB. At 5 mM H_2O_2 , O_2 was formed slowly in the MoO_3 -catalyzed reaction. In the case of V-BrPO, the rate-limiting step for dioxygen formation is the oxidation of bromide because at the higher pH used in these reactions the reduction of the oxidized bromine species is fast (Everett & Butler, 1989; Everett et al., 1990, Kanofsky, 1989) On the other hand, the rate of bromide oxidation by $\text{MoO}(\text{O}_2)_2(\text{H}_2\text{O})_2$ forming tribromide is much faster than the reduction of Br_3^- by H_2O_2 .

Radical Versus Electrophilic Bromination

Experiments performed using the substrate 2,3-dimethoxytoluene (DMT) under conditions of 0.25 mM MoO_3 , 2.5 mM H_2O_2 , 1.0 M NH_4Br , 3 mM DMT in 0.1 M HClO_4 resulted in the exclusive formation of ring-substituted bromo-DMT (Scheme 3-3), establishing an electrophilic bromination mechanism. Bromo-DMT was identified by comparison of the GC retention time to that of standards of Bromo-DMT (Clague & Butler, 1993a). Thus, the absence of the methyl-substituted product, 2,3-dimethoxybenzyl bromide, shows that the oxidation of bromide by $\text{Mo}(\text{O}_2)_2(\text{H}_2\text{O})_2$ proceeds by a two-electron oxidation to form a bromonium ion equivalent and not radical bromine.



Scheme 3-3. Bromination of 2,3-dimethoxytoluene by Br^+ versus $\text{Br}\cdot$.

Effect of Chloride on Peroxidative Bromide Oxidation Catalyzed by Molybdenum(VI)

The ability of molybdenum(VI) to catalyze the oxidation of chloride was also examined. MoO_3 is capable of catalyzing the oxidation of this more electronegative halide by hydrogen peroxide; however, this reaction is much slower than the peroxidation of bromide and does not go to completion over several days. Peroxidation of chloride catalyzed by MoO_3 was investigated under conditions of 0.4 mM MoO_3 , 4 mM H_2O_2 , 2 M NaCl and 5 mM TMB in 0.1 M HClO_4 /25% MeOH. Analysis of the reaction mixture by GC showed that 59% of the TMB was converted to chloro-TMB in 15 hours.

Despite the slow rate of chloride peroxidation, the presence of chloride does affect the rate of bromide oxidation. The time period of the lag phase was found to

increase and the rate of oxidation of bromide by $\text{MoO}(\text{O}_2)_2(\text{H}_2\text{O})_2$ was found to decrease as a function of increasing chloride concentration (Figure 3-8). Moreover, saturation was observed above *ca.* 1 M chloride. GC analyses showed that chloro-TMB was not formed under these conditions. The rate constant for bromide oxidation by the $\text{MoO}(\text{O}_2)_2$ species in the presence of 1 M NaCl is $7.57 \times 10^{-3} \text{ M}^{-1} \text{ sec}^{-1}$, which is significantly reduced from the rate constant of $1.51 \times 10^{-2} \text{ M}^{-1} \text{ sec}^{-1}$ in the absence of chloride.

By contrast, chloride did not have an effect on the rate of bromide oxidation by the oxodiperoxoxalato complex of molybdenum(VI), $\text{MoO}(\text{O}_2)_2(\text{ox})^{2-}$, a complex that does not have a dissociable ligand (Dengal et al., 1987; Reynolds, et al, 1994). Bromide oxidation by this complex was monitored by following the disappearance of the complex at 324 nm. The rate constants for the oxidation of bromide by $\text{MoO}(\text{O}_2)_2(\text{ox})^{2-}$ in the absence and presence of 0.75 M NaCl (under conditions of 0.5 mM $\text{MoO}(\text{O}_2)_2(\text{ox})^{2-}$, 0.75 M NH_4Br , 1.5 mM TMB in 10 mM oxalate buffer, pH 5.1 with 20% MeOH) are $9.21 \times 10^{-3} \text{ M}^{-1} \text{ sec}^{-1}$ and $9.67 \times 10^{-3} \text{ M}^{-1} \text{ sec}^{-1}$, respectively, showing that chloride does not inhibit bromide oxidation. In fact, a slight but reproducible increase in the disappearance of the oxalato complex is observed. The cause of this increase is currently not understood.

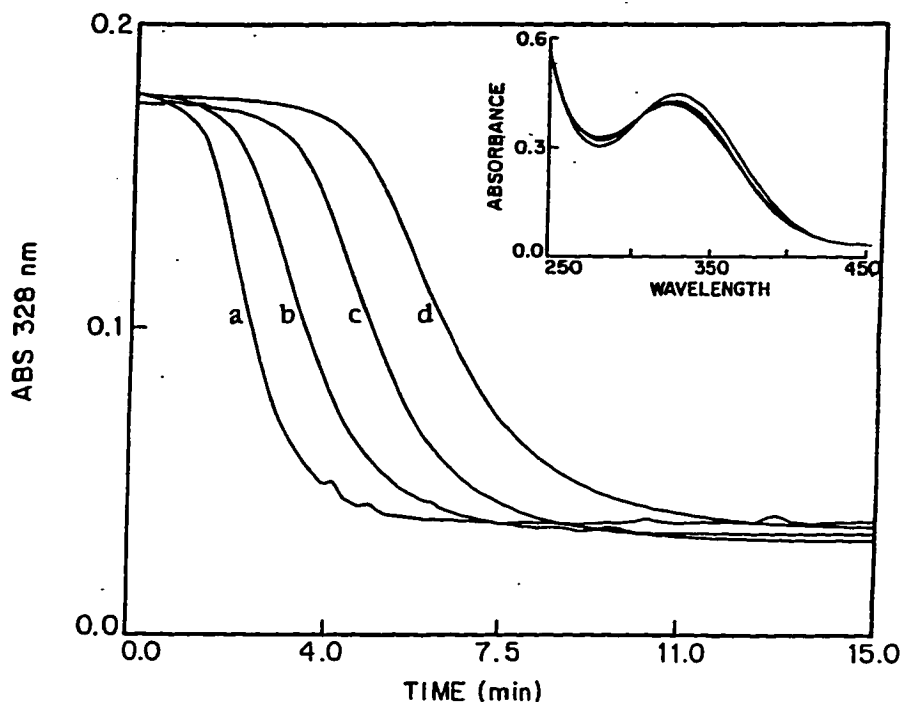


Figure 3-8. Effect of chloride on the time course of the disappearance of $\text{MoO}(\text{O}_2)_2(\text{H}_2\text{O})_2$ monitored at 328 nm during the peroxidative bromination of TMB. Conditions: 0.15 mM Na_2MoO_4 , 1.5 mM H_2O_2 , 2.0 mM TMB, and 1.0 M NH_4Br in 0.1 M HClO_4 /25% MeOH with a) no NaCl, b) 0.25 M NaCl, c) 0.5 M NaCl, and d) 1.0 M NaCl. $I = 2.1 \text{ M}$ (NaClO_4). Temperature = 25.0 °C. Inset: Effect of chloride on the uv-vis spectrum of $\text{MoO}(\text{O}_2)_2(\text{H}_2\text{O})_2$ in 0.1 M HClO_4 /2.1 M ionic strength.

Changes in the uv-vis spectrum of $\text{MoO}(\text{O}_2)_2(\text{H}_2\text{O})_2$ upon chloride addition are suggestive of chloride coordination to $\text{MoO}(\text{O}_2)_2(\text{H}_2\text{O})_2$; the λ_{max} of 324 nm for $\text{MoO}(\text{O}_2)_2(\text{H}_2\text{O})_2$ shifts to 329 nm upon addition of 0.5 M NaCl (Figure 3-8 inset). A similar shift on addition of bromide to $\text{MoO}(\text{O}_2)_2(\text{H}_2\text{O})_2$ was not observed; however, the oxidation of bromide by $\text{MoO}(\text{O}_2)_2(\text{H}_2\text{O})_2$ is sufficiently fast such that its observation may be precluded. The uv-vis spectrum of $\text{MoO}(\text{O}_2)_2(\text{H}_2\text{O})(\text{OH})^-$ at pH 5.0 in acetate or MES buffer (2-(N-morpholino)ethane-sulfonic acid) shows no effect from chloride additions up to 2.0 M (Figure 3-9). As might be expected, the addition of chloride to $\text{MoO}(\text{O}_2)_2(\text{ox})^{2-}$ also does not show an absorption maximum shift (Figure 3-10). It could be argued that for a d^0 metal ion complex with no ligand field stabilization energy, the oxalate ligand can be expected to exchange rapidly. However, the fact that neither a shift in the λ_{max} of the $\text{MoO}(\text{O}_2)_2(\text{ox})^{2-}$ complex in the presence of chloride nor a significant change in the rate of bromide oxidation in the presence of chloride occurs suggests that the $\text{MoO}(\text{O}_2)_2(\text{ox})^{2-}$ complex remains intact.

Several explanations are plausible to account for the chloride effect. The decreased rate of bromide oxidation could indicate that bromide competes with chloride coordination to the $\text{MoO}(\text{O}_2)_2$ moiety and that bromide oxidation occurs after coordination to Mo(VI). The decreased rate of Br^- oxidation could also arise from changes in the oxidation potential or the charge on the $\text{MoO}(\text{O}_2)_2(\text{H}_2\text{O})\text{Cl}^-$

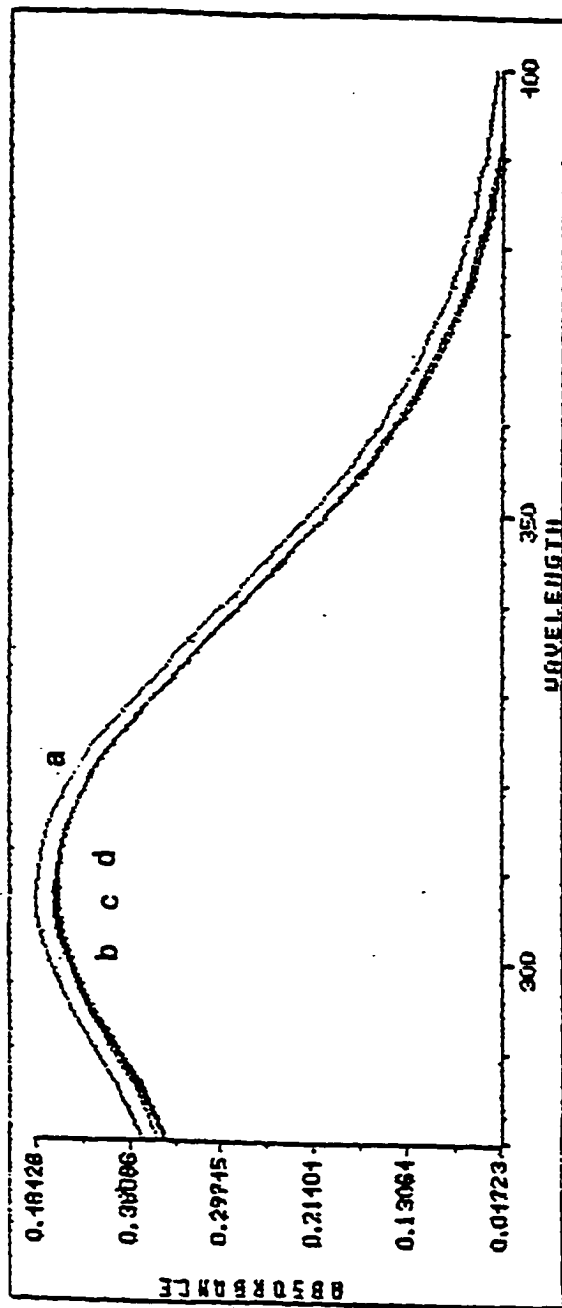


Figure 3-9. Effect of chloride on the uv-vis spectrum of $\text{MoO}(\text{O}_2)_2(\text{H}_2\text{O})(\text{OH})$. Conditions: 0.5 mM Na_2MoO_4 and 1.0 mM H_2O_2 in 10 mM acetate pH 5.1, 2.0 M ionic strength ($\text{NaCl} + \text{NaClO}_4$); a) no KCl ; b) 100 mM KCl ; c) 1.0 M KCl ; d) 2.0 M KCl .

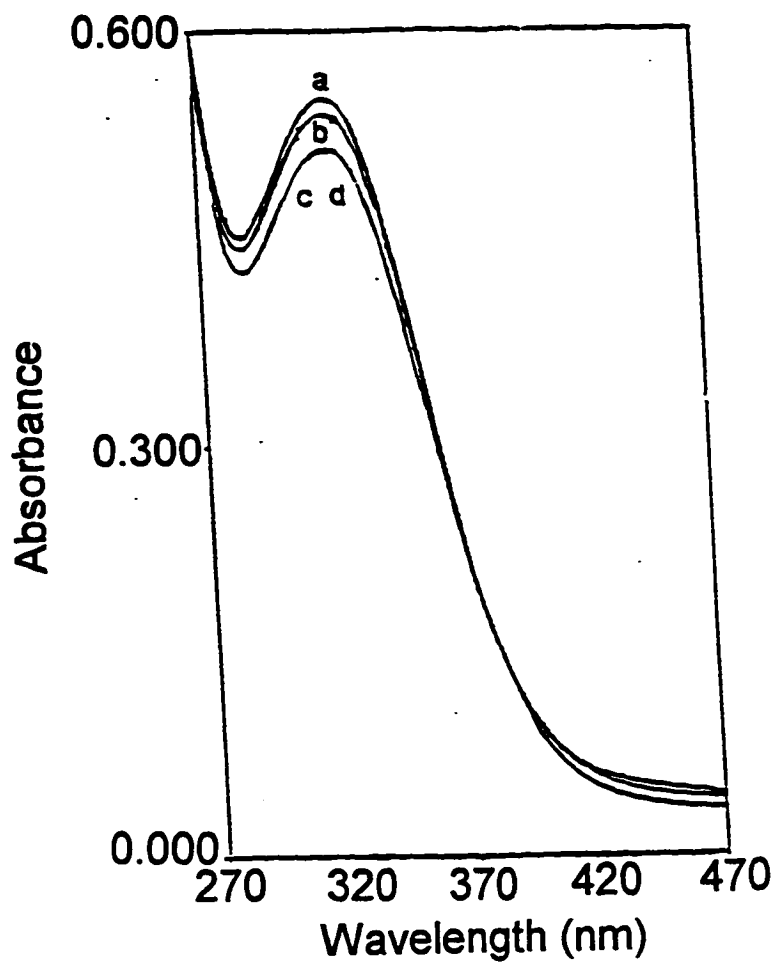


Figure 3-10. Effect of chloride on the uv-vis spectrum of $\text{MoO}(\text{O}_2)_2(\text{ox})^{2-}$.
 Conditions: 0.5 mM $\text{MoO}(\text{O}_2)_2(\text{ox})^{2-}$ and 0.5 mM H_2O_2 in 10 mM oxalate pH 5.1,
 20 % methanol ; a) no KCl; b) 10 mM KCl; c) 100 mM KCl; d) 500 mM KCl.

complex. While the chloride competition experiments do not allow us to determine whether halide oxidation occurs by halide coordination to $\text{MoO}(\text{O}_2)_2$ before oxidation or whether halide oxidation occurs by direct attack on Mo-bound peroxide, it is clear that chloride does coordinate to the $\text{MoO}(\text{O}_2)_2$ moiety in acidic aqueous solution. Other examples of oxoperoxo-chloro complexes of molybdenum(VI) are known (Chaumette et al., 1983 and see below).

The spectrum of $\text{MoO}(\text{O}_2)_2(\text{H}_2\text{O})_2$ is also effected by the presence of fluoride. Under conditions of 0.5 mM Mo(VI), 1.0 mM H_2O_2 , and 0.1 M HClO_4 , the addition of KF up to 50 mM resulted in a shift of the absorbance maximum of $\text{MoO}(\text{O}_2)_2(\text{H}_2\text{O})_2$ from 325 nm to 319 nm and a decrease in the maximum absorbance (Figure 3-11). Further increase in the KF concentration caused a shift in the absorbance to 333 nm and further decrease in the maximum absorbance. The kinetic effects of KF on bromide oxidation were not examined because KF has very limited solubility in 25% methanol. In addition, fluoride is involved in substantial hydrogen bonding at 0.1 M acid.

Spectral effects were not noted for $\text{Mo}(\text{O}_2)_2(\text{H}_2\text{O})(\text{OH})^-$ under conditions of 0.5 mM MoO_3 , 1.5 mM H_2O_2 , and 10 mM acetate buffer pH 5.0 with the addition of up to 0.5 M KF (Figure 3-12). However, under conditions of 0.5 mM $\text{MoO}(\text{O}_2)_2(\text{ox})^{2-}$, 0.5 mM H_2O_2 , and 10 mM oxalate pH 5.1, the absorbance shifts from 321 nm to 315 nm upon the addition of 0.5 M KF (Figure 3-13). It is

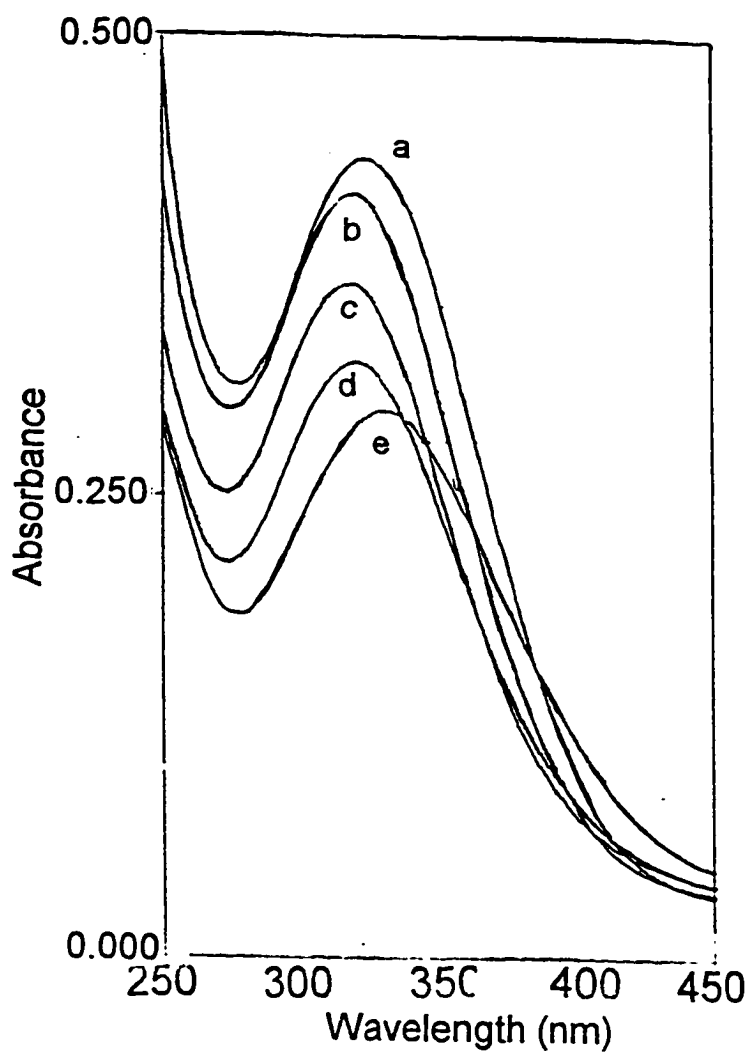


Figure 3-11. Effect of fluoride on the uv-vis spectrum of $\text{MoO}(\text{O}_2)_2(\text{H}_2\text{O})_2$. Conditions: 0.5 mM Na_2MoO_4 , 1.0 mM H_2O_2 , 0.1 M HClO_4 and a) no KF; b) 10 mM KF; c) 50 mM KF; d) 100 mM KF; e) 250 mM KF.

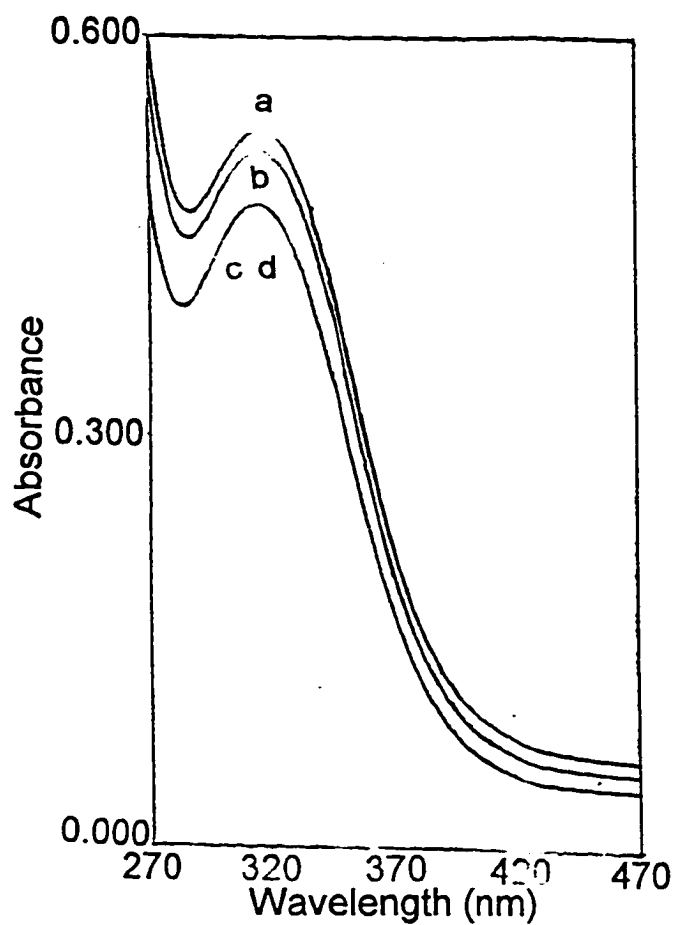


Figure 3-12. Effect of fluoride on the uv-vis spectrum of $\text{MoO}(\text{O}_2)_2(\text{H}_2\text{O})(\text{OH})^-$. Conditions: 0.5 mM Na_2MoO_4 and 1.5 mM H_2O_2 in 10 mM acetate, pH 5.1 and a) no KF; b) 10 mM KF; c) 100 mM KF; d) 500 mM KF.

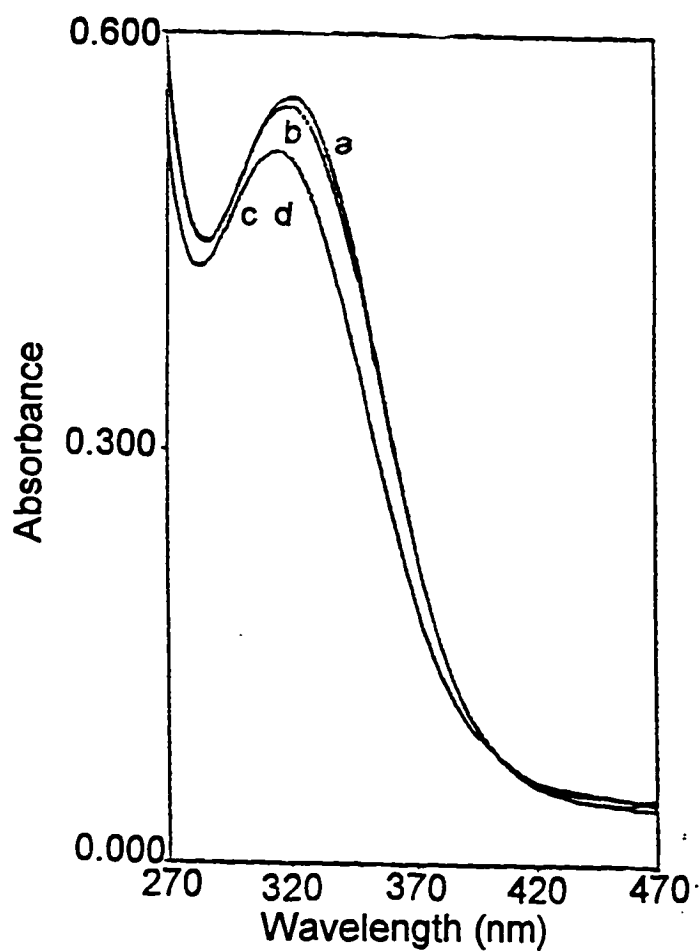


Figure 3-13. Effect of fluoride on the uv-vis spectrum of $\text{MoO}(\text{O}_2)_2(\text{ox})^{2-}$. Conditions: 0.5 mM $\text{MoO}(\text{O}_2)_2(\text{ox})^{2-}$ and 0.5 mM H_2O_2 in 10 mM oxalate pH 5.1 and a) no KF; b) 10 mM KF; c) 100 mM KF; d) 500 mM KF.

possible that fluoride, which is a much stronger ligand than chloride or bromide, may be capable of replacing one arm of the oxalate ligand, which should be in rapid exchange.

Tungsten(VI)-Mediated Peroxidative Bromination Reactions

Tungsten(VI) was also found to catalyze bromide oxidation by hydrogen peroxide, similar to the molybdenum(VI)-mediated system. The tungsten(VI)-catalyzed peroxidation of bromide forming tribromide is faster than catalysis by molybdenum(VI) and also much faster than the uncatalyzed oxidation of bromide by hydrogen peroxide (Figure 3-14). Analysis by GC using TMB as trap for the oxidized bromine species shows that one equivalent of bromide is oxidized per equivalent of hydrogen peroxide added (Equation 1) under conditions of 40 μ M tungstate, 4 mM H_2O_2 , 2 M NH_4Br , 5 mM TMB in 0.1 M $HClO_4$ /25% MeOH (Figure 3-15).

The kinetics of the tungstate-mediated reactions were best analyzed by following the bromination of TMB at 266 nm. At the low concentrations of tungsten(VI) required to limit oligomerization (Islam & Thompson, 1989), the disappearance of the peroxotungsten species could not be monitored spectrophotometrically. The absorbance data recorded at 266 nm exhibited first-order behavior for at least 70% of the reaction provided that H_2O_2 was initially present in at least 50-fold excess over tungsten. At smaller ratios of H_2O_2 to

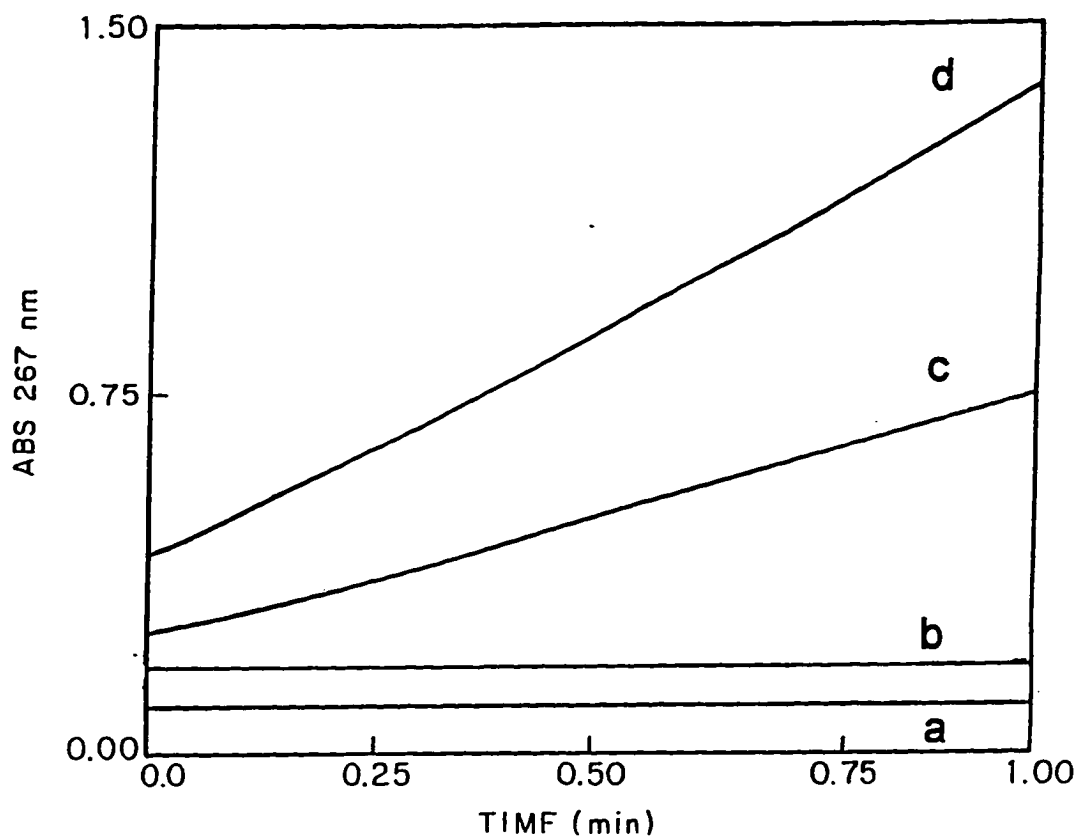


Figure 3-14. Comparison of the rates of molybdenum(VI)-, tungsten(VI)- and vanadium(V)-catalyzed formation of tribromide. Conditions: 1 mM H_2O_2 and 0.1 M NH_4Br in 0.5 M HClO_4 with a) no added metal, b) 0.1 mM NH_4VO_3 , c) 0.1 mM Na_2MoO_4 and d) 0.1 mM Na_2WO_4 .

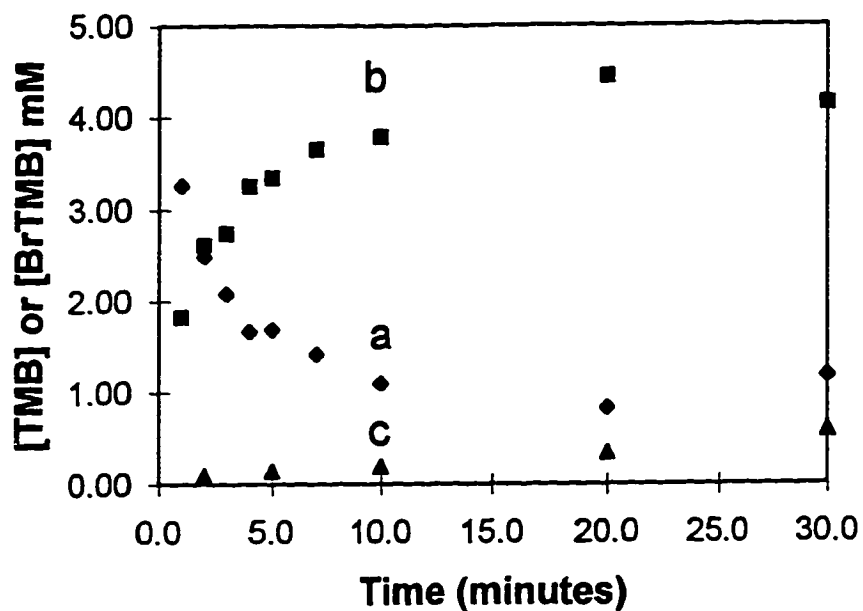


Figure 3-15. Gas chromatographic analysis of the peroxidative bromination of TMB in acid solution catalyzed by WO_3 a) disappearance of [TMB]; b) and c) appearance of [BrTMB]. Conditions: $40 \mu\text{M Na}_2\text{WO}_4$, $4.0 \text{ mM H}_2\text{O}_2$, $2\text{M NH}_4\text{Br}$, 5 mM TMB in $0.1 \text{ M HClO}_4/25\% \text{ MeOH}$. $T = 25.0 \text{ }^\circ\text{C}$; conditions for c) same as above but without added Na_2WO_4 .

W(VI), dimerization of W(VI) interferes (Islam & Thompson, 1989). In addition, k_{obs} values were independent of H_2O_2 concentration (i.e., 0.25-1.8 mM) under conditions of 5 μ M Na_2WO_4 , 2.0 M NH_4Br , 2.0 mM TMB in 0.1 M $HClO_4$ /25% MeOH.

The acid dependence on the rate of tungsten-mediated Br-TMB formation followed spectrophotometrically at 266 nm shows that bromide oxidation is faster at lower pH (Figure 3-16), similar to the molybdenum(VI)-mediated reactions. The pK_a of $WO(O_2)_2(H_2O)_2$ is 0.12 (Ghiron & Thompson, 1988); it was not possible to obtain kinetic data above 0.1 M $[H^+]$ due to complications from the increased rate of the uncatalyzed rate of oxidation of bromide by hydrogen peroxide. The rate of the tungsten-catalyzed oxidation of bromide forming tribromide was found to increase linearly with tungsten concentration between 2.5-25 μ M $Na_2WO_4 \cdot 2H_2O$ under conditions of 2 mM H_2O_2 , 0.1 M NH_4Br , in 0.1 M $HClO_4$ /25% MeOH (Figure 3-17), establishing a first-order dependence. The rate of the tungsten(VI)-catalyzed Br-TMB formation was also found to increase linearly with bromide concentration (i.e., 0-2.0 M NH_4Br) as determined under conditions of 15 μ M $Na_2WO_4 \cdot 2H_2O$, 1.8 mM H_2O_2 and 2.0 mM TMB in 0.1 M $HClO_4$ /25% MeOH (Figure 3-18). Finally, the tungsten-mediated peroxidative bromination reactions were found to occur by electrophilic bromination and not a

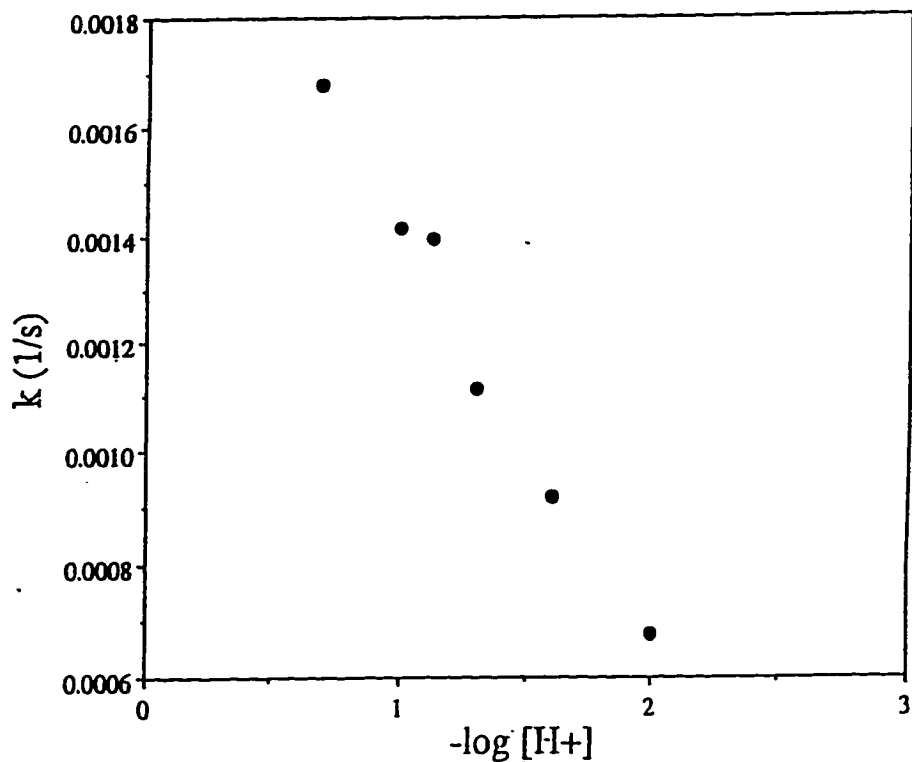


Figure 3-16. Plot of the observed rate constant of the peroxidative bromination of TMB monitored at 266 nm mediated by $WO(O_2)_2(H_2O)(OH)^-$ oxidation of bromide vs. acid concentration. Conditions: 5 μ M Na_2WO_4 , 1.0 mM H_2O_2 , 2.0 M NH_4Br , and 1.5 mM TMB in 25% MeOH with varying H^+ concentration (0.01 M to 0.1 M $HClO_4$) at 25.0 $^{\circ}C$. The ionic strength was 2.01-2.10 M.

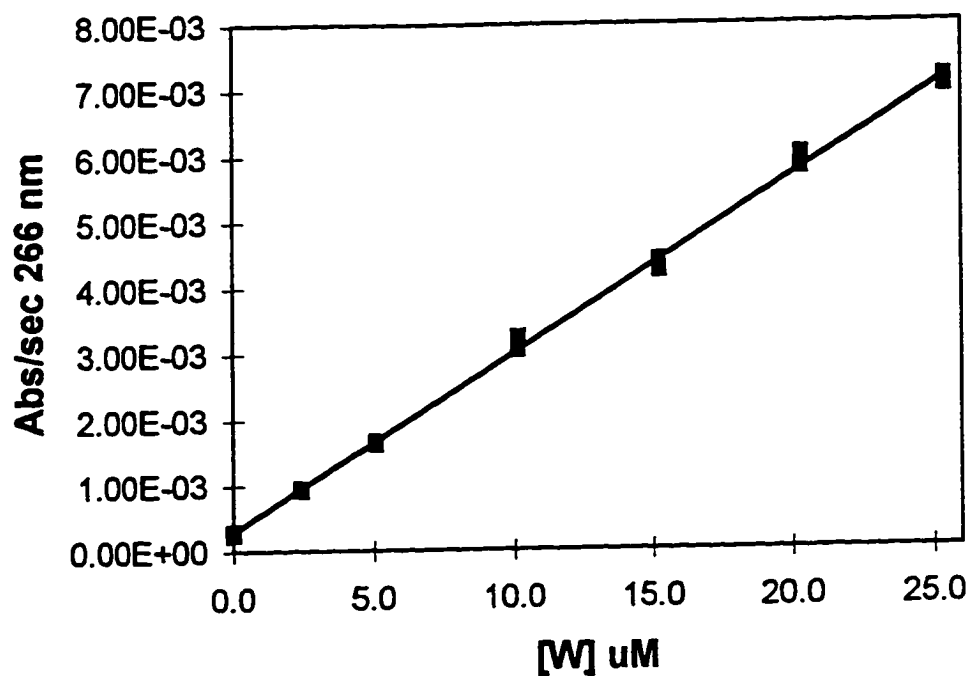


Figure 3-17. Plot of the initial rate tribromide formation monitored at 266 nm mediated by $\text{WO}(\text{O}_2)_2(\text{H}_2\text{O})(\text{OH})^-$ oxidation of bromide versus tungsten (VI) concentration. Conditions: 2.0 mM H_2O_2 and 0.1 M NH_4Br , in 0.1 M HClO_4 /25% MeOH, and 2.5-25 μM Na_2WO_4 at 25.0 °C.

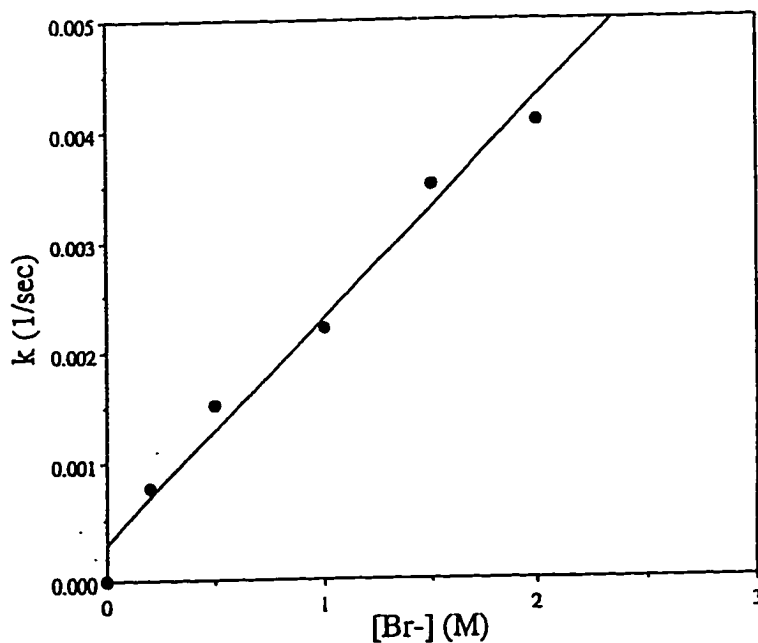


Figure 3-18. Plot of the observed rate constant of the peroxidative bromination of TMB monitored at 266 nm mediated by $\text{WO}(\text{O}_2)_2(\text{H}_2\text{O})(\text{OH})^-$ oxidation of bromide versus bromide concentration. Conditions: 15 μM Na_2WO_4 , 1.8 mM H_2O_2 , and 2.0 mM TMB in 0.1 M HClO_4 /25% MeOH and 0 to 2.0 M NH_4Br at 25.0 $^\circ\text{C}$.

radical process from the product analysis of DMT bromination, like the molybdenum(VI)-mediated reactions.

As had been done with the molybdenum(VI) reactions, the effect of alcohols on the rate of bromide oxidation was also studied for the tungsten(VI) system. Under conditions of 15 mM Na₂WO₄, 2.0 mM H₂O₂, 0.1 M NH₄Br, and 0.1 M HClO₄, the rate was slowed by increasing concentrations of methanol (Figure 3-19a). However, no rate change was observed for increasing amounts of ethanol (Figure 3-19b). ¹³C NMR of methyl-¹³C-alcohol under conditions of 20 mM Na₂WO₄, 0.2 M methanol, 0.2 M HClO₄, and 1.0 M H₂O₂ showed no evidence of broadening or shifting of the methanol peak, which would be indicative of methanol coordination (Figure 3-20).

The effect of chloride on the peroxidation of bromide catalyzed by tungsten(VI) was also examined. Like molybdenum(VI), tungsten(VI) catalyzes the oxidation of chloride by hydrogen peroxide in acidic solution at a much slower rate than the oxidation of bromide. For example, less than 1% Cl-TMB was formed in 30 min (based on TMB consumed), under conditions of 40 μM Na₂WO₄, 4 mM H₂O₂, 2.0 M NaCl, 5 mM TMB in 0.1 M HClO₄/25% MeOH, whereas under similar conditions with bromide 100% Br-TMB is formed based on the initial concentration of H₂O₂. Cl-TMB formation increases to 25% in 48 hours. However, unlike Mo(VI), up to 1.5 M NaCl did not affect the rate of bromide

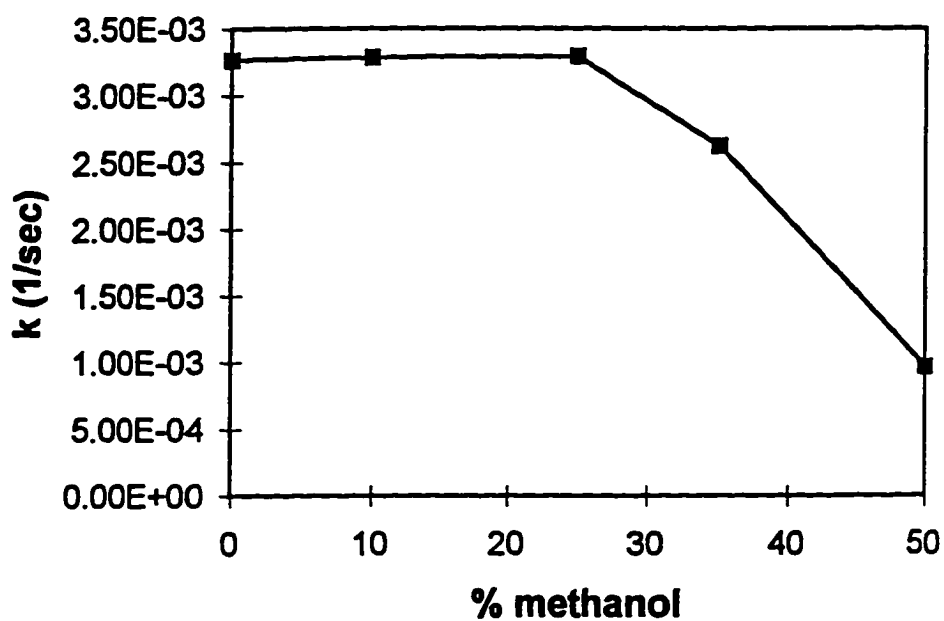


Figure 3-19a. Plot of initial rate of tribromide formation monitored at 266 nm mediated by $\text{WO}(\text{O}_2)_2(\text{H}_2\text{O})(\text{OH}^-)$ oxidation of bromide versus percent methanol or ethanol in solution. Conditions, 15 mM Na_2WO_4 , 2.0 mM H_2O_2 , and 0.1 M NH_4Br in 0.1 M HClO_4 with 0 to 50% methanol. $T = 25.0^\circ\text{C}$.

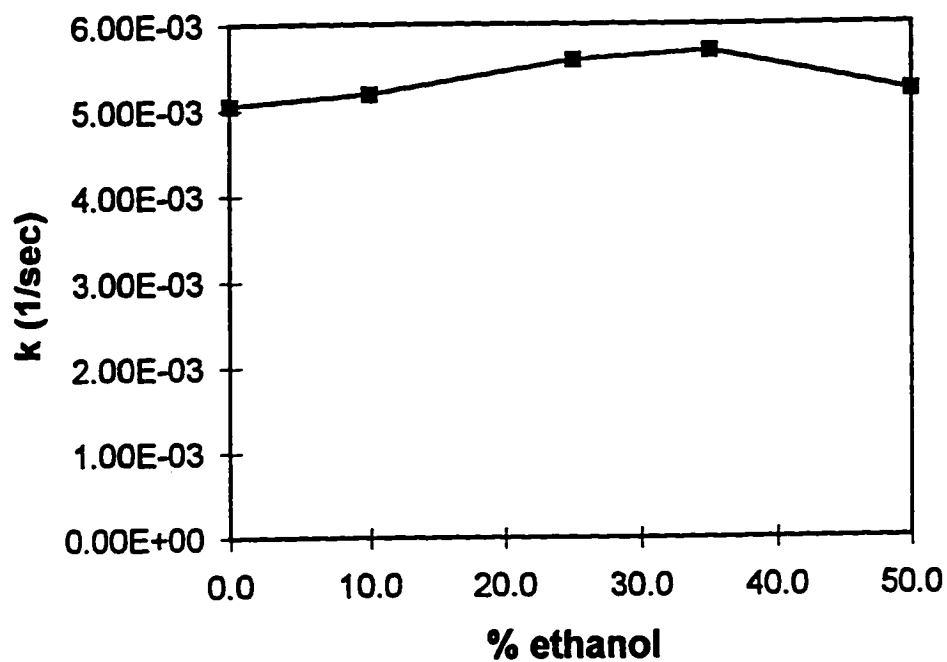


Figure 3-19b. Plot of initial rate of tribromide formation monitored at 266 nm mediated by $\text{WO}(\text{O}_2)_2(\text{H}_2\text{O})(\text{OH})$ oxidation of bromide versus percent methanol or ethanol in solution. Conditions, 15 mM Na_2WO_4 , 2.0 mM H_2O_2 , and 0.1 M NH_4Br in 0.1 M HClO_4 with 0 to 50 % ethanol. $T = 25.0^\circ\text{C}$

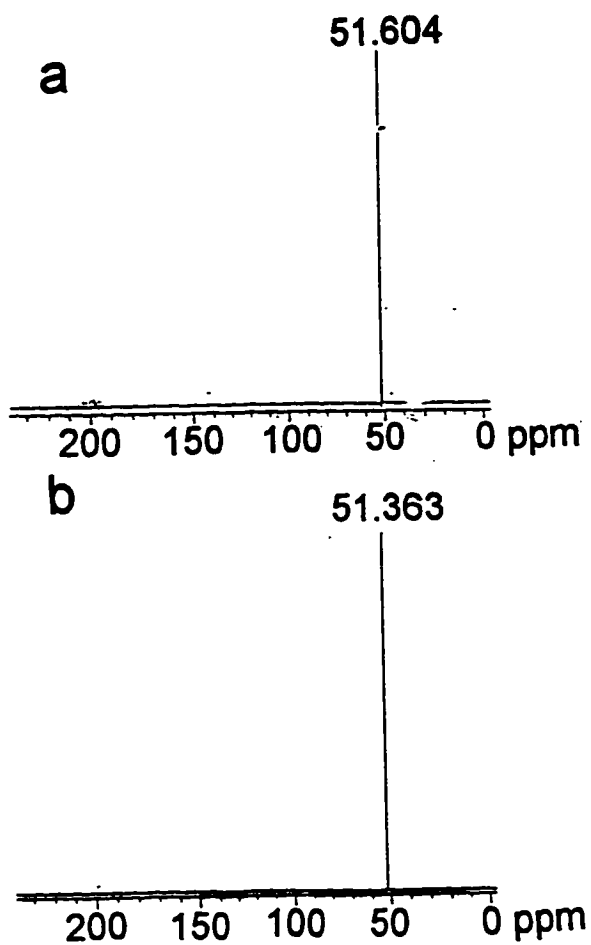


Figure 3-20. ^{13}C NMR spectrum of ^{13}C -labeled methanol in acidic aqueous solution. Conditions (a and b): 0.2 M methyl- ^{13}C -alcohol, 0.2 M HClO_4 , and 20% D_2O ; b only) 1.0 M H_2O_2 , 20 mM Na_2WO_4 . $T = 23^\circ\text{C}$.

oxidation (15 μ M W(VI), 1.8 mM H₂O₂, 2.0 mM TMB, 1.0 M KBr in 0.1 M HClO₄/25% MeOH and 2.5 M ionic strength (NaClO₄) with replacement of NaClO₄ by NaCl [i.e., 0 - 1.5 M Cl⁻] and maintaining ionic strength). The absence of a chloride effect with tungsten(VI) under these conditions is most likely because the predominant species in solution is WO(O₂)₂(H₂O)(OH)⁻, which is already negatively charged.

Further Reactions with MoO(O₂)₂(ox)²⁻ and WO(O₂)₂(ox)²⁻

Reynolds and coworkers (1994) demonstrated that MoO(O₂)₂(ox)²⁻ is quite effective at peroxidative oxidation of bromide. A second-order rate constant of 2.3 x 10⁻³ M⁻¹ sec⁻¹ for bromide oxidation by MoO(O₂)₂(ox)²⁻, which is of the same order of magnitude as the results presented here for MoO(O₂)₂(H₂O)₂ and MoO(O₂)₂(H₂O)(OH)⁻, was reported. As has been described above, the oxalato complex proved a useful tool for characterizing the mechanism of the aquated molybdenum(VI) and tungsten(VI) peroxo complexes. However, unlike that presented by Reynolds et al., (1994) our data showed clearly biphasic kinetic behavior in which the second phase most closely resembled the results reported by Reynolds, et al. (Figure 3-21) with a rate constant of 1.6 x 10⁻³ M⁻¹ sec⁻¹. The first phase exhibited a rate constant on the order of 9.2 x 10⁻³ M⁻¹ sec⁻¹.

GC results of the bromination of TMB catalyzed by MoO(O₂)₂(ox)²⁻ under conditions of 0.77 mM Mo(O₂)₂(ox)²⁻, 1.0 M NH₄Br, 2.0 mM TMB in 20 mM

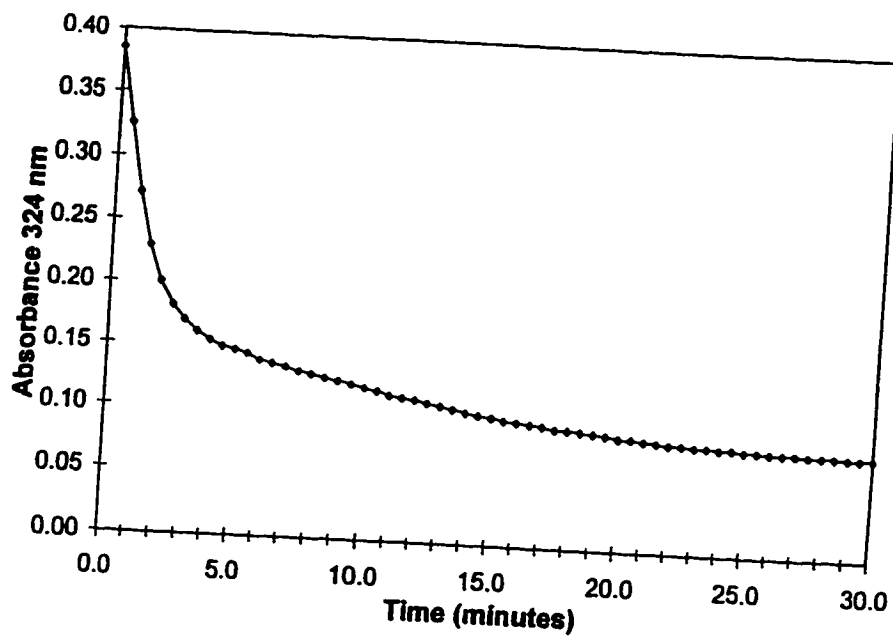


Figure 3-21. Absorbance at 324 nm vs. time for the reaction of $\text{MoO}(\text{O}_2)_2(\text{ox})^{2-}$. Conditions: 0.5 mM $\text{MoO}(\text{O}_2)_2(\text{ox})^{2-}$, 1.0 M NH_4Br , and 1.2 mM TMB in 20 mM oxalate buffer, pH 5.1/25% MeOH at 25 °C.

oxalate buffer, pH 5.14 with 25% MeOH show that 0.65 mM Br-TMB was formed in 30 minutes, at which point the concentration of Br-TMB began to level off (Figure 3-22). After 2 hours, the concentration of Br-TMB increased to 0.82 mM, approximately equivalent to the consumption of one of the two equivalents of peroxide per complex. Approximately 60% of the total Br-TMB production occurred in the first five minutes of reaction. This result is consistent with the spectrophotometric results, which show good first-order fits for the first 60-70% of the reaction (e.g., the first phase). Similar results were seen for experiments with the complex $\text{WO}(\text{O}_2)_2(\text{ox})^{2-}$. Under conditions of 0.77 mM $\text{WO}(\text{O}_2)_2(\text{ox})^{2-}$, prepared as described by Dengel et al. (1987), 20 mM oxalate pH 5.1, 2 mM TMB, 0.25 M NH_4Br , and 25% methanol, rapid conversion of 0.42 mM TMB to the brominated product was observed in the first five minutes (Figure 3-23). The formation of Br-TMB slowed markedly at this point, increasing to approximately 0.8 mM after 2 hours of reaction time.

Reynolds et al. (1994) report that for the molybdenum(VI) oxalato complex, extra equivalents of H_2O_2 are necessary at the start of the reaction to maintain the integrity of the diperoxo complex. The rapid drop noted for our kinetics in the absence of extra added peroxide can be seen in the kinetic traces by Reynolds et al. (Figure 3-24); however, the interval for data recording is large enough that this effect can appear to be a minor inconsistency in the data. In our

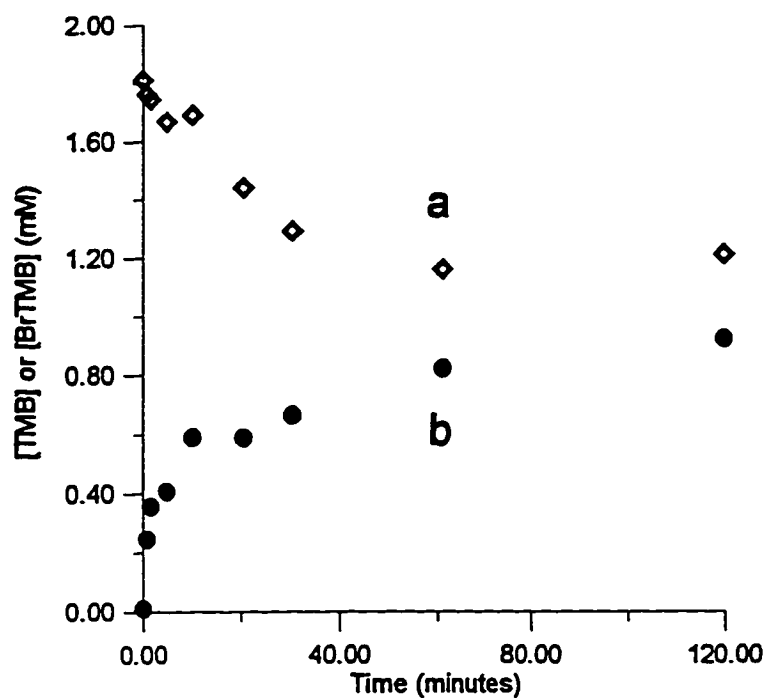


Figure 3-22. Gas chromatographic analysis of the peroxidative bromination of TMB catalyzed by $\text{MoO}(\text{O}_2)_2(\text{ox})^{2-}$. a) disappearance of TMB; b) appearance of BrTMB. Conditions: 0.77 mM $\text{Mo}(\text{O}_2)_2(\text{ox})^{2-}$, 1.0 M NH_4Br , and 2.0 mM TMB in 20 mM oxalate buffer, pH 5.1/25% MeOH. $T = 25.0^\circ\text{C}$.

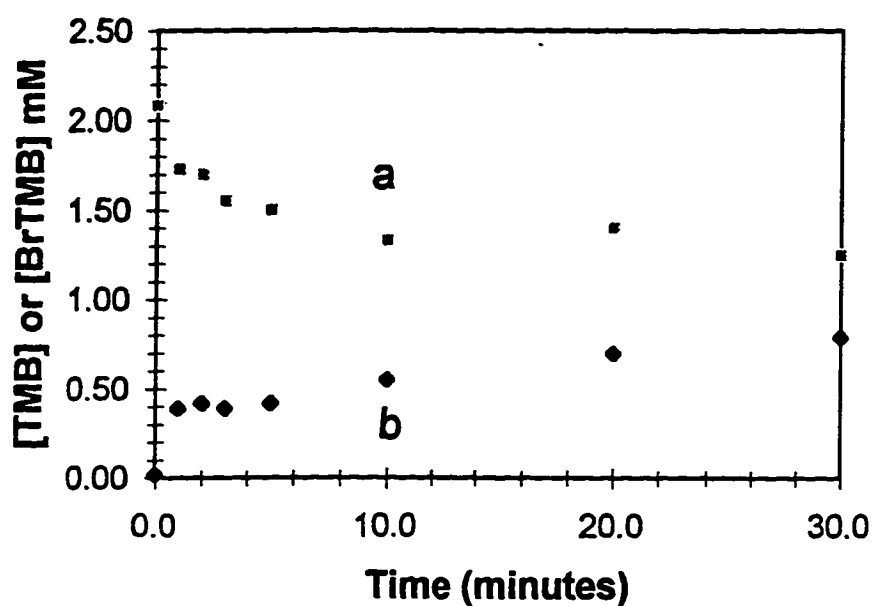


Figure 3-23. Gas chromatographic analysis of the peroxidative bromination of TMB catalyzed by $\text{WO}(\text{O}_2)_2(\text{ox})^{2-}$. a) disappearance of TMB; b) appearance of BrTMB. Conditions: 0.77 mM $\text{WO}(\text{O}_2)_2(\text{ox})^{2-}$, 2 mM TMB, and 0.25 M NH_4Br in 20 mM oxalate pH 5.1/25 % methanol at 25 °C.

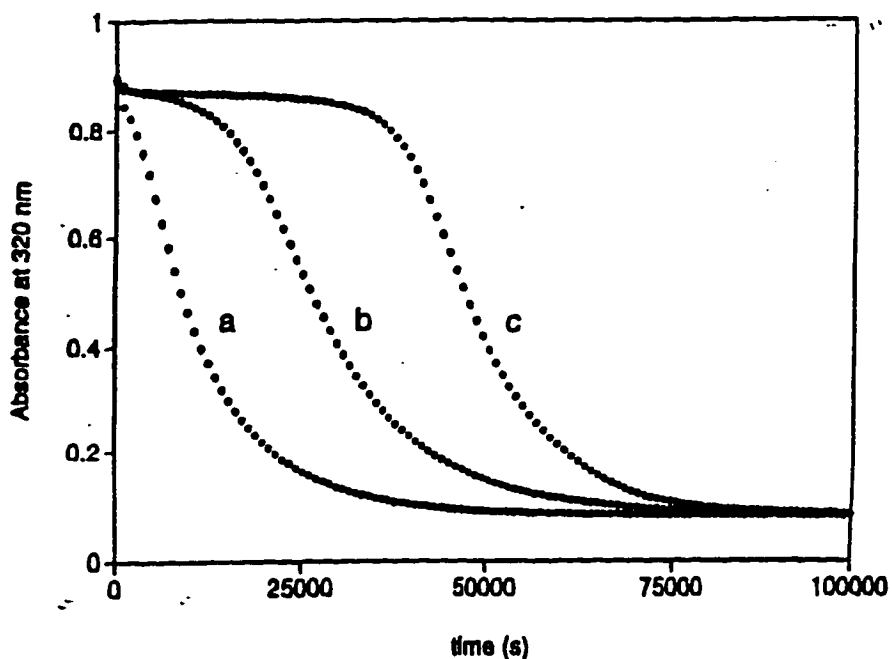


Figure 3-24. Absorbance at 320 nm versus time for the reaction of $\text{MoO}(\text{O}_2)_2(\text{ox})^{2-}$ and bromide at varied H_2O_2 concentrations. Conditions: 1.0 mM $\text{MoO}(\text{O}_2)_2(\text{ox})^{2-}$ and 25 mM LiBr at 1.0 M ionic strength and; a) 1 mM H_2O_2 , 10 mM oxalate pH 5.0; b) 5 mM H_2O_2 , 0.1 M oxalate buffer pH 5.0; c) 10 mM H_2O_2 , 0.1 M oxalate buffer pH 5.0. [Taken from Reynolds, et al., 1994].

limited studies, incubation of 1 mM concentration of the complex $\text{MoO}_2(\text{O}_2)(\text{ox})(\text{H}_2\text{O})^{2-}$, prepared as described by Dengel et al. (1987) with 1 mM H_2O_2 in 20 mM oxalate, pH 5.1 monitored at 324 nm, the λ_{max} of the diperoxo complex, shows that quantitative formation of $\text{MoO}(\text{O}_2)_2(\text{ox})^{2-}$ has not occurred even after 4 hours of incubation (Figure 3-25). Thus, while it does appear necessary to include excess peroxide in order to maintain the integrity of the oxodiperoxoalato complex, the slow rate of peroxide coordination to the dioxomonoperoxoalato complex under these conditions suggests that no peroxide coordination is occurring at least during the rapid portion of the biphasic kinetic trace observed. However, recoordination might be possible during the slow portion of the reaction, which was monitored in the study by Reynolds et al. (1994) to determine " k_{Mo} ", the rate constant determined from monitoring the change in absorbance at 320 nm.

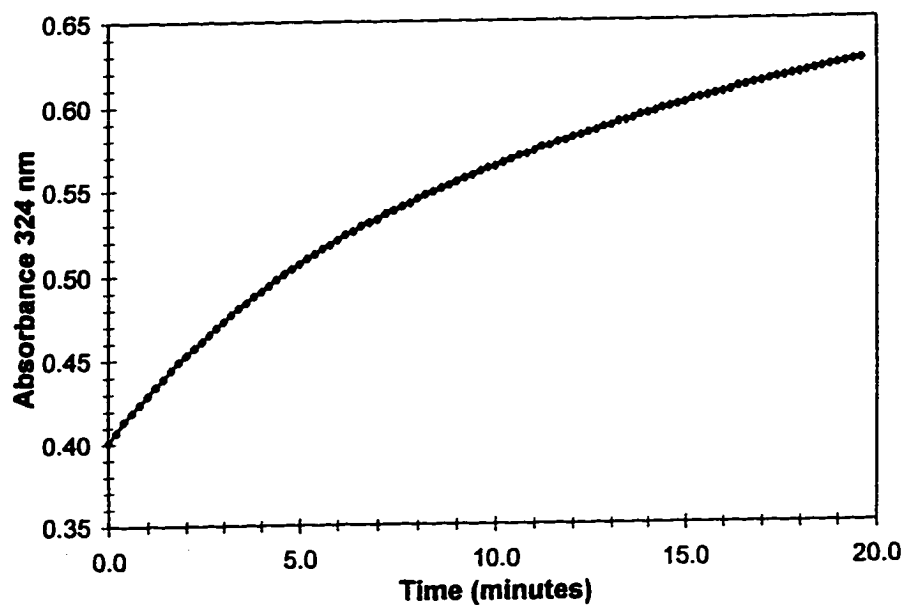
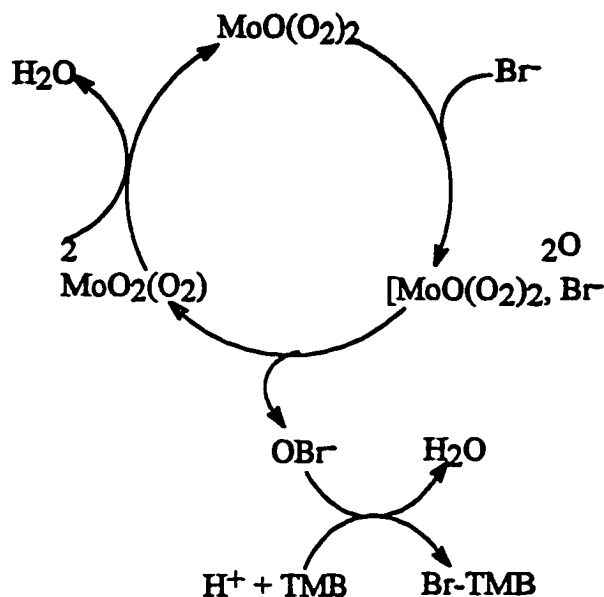


Figure 3-25. Formation of $\text{MoO}(\text{O}_2)_2(\text{ox})^{2-}$ monitored at 324 nm by incubation of $\text{MoO}_2(\text{O}_2)(\text{ox})^{2-}$ with H_2O_2 versus time. Conditions: 1.0 mM $\text{MoO}_2(\text{O}_2)(\text{ox})^{2-}$ and 1.0 mM H_2O_2 in 20 mM oxalate pH 5.1 at 25 °C.

Discussion

In this chapter it has been demonstrated that both Mo(VI) and W(VI) catalyze the oxidation of bromide by hydrogen peroxide in acidic solution. The metal-mediated reactions are fully stoichiometric, with the production of one equivalent of oxidized bromine species per equivalent of hydrogen peroxide consumed. The oxidized bromine species then brominates an appropriate substrate, which in the case of TMB is a very rapid reaction compared to the rate of oxidation of the halide. The oxodiperoxo species of Mo(VI), i.e., $\text{MO}(\text{O}_2)_2(\text{H}_2\text{O})_2$ and $\text{MO}(\text{O}_2)_2(\text{H}_2\text{O})(\text{OH})^-$, are in acid dependent equilibrium ($\text{pK}_a = 2.3$) and have somewhat different reactivities toward bromide oxidation. A consistent catalytic mechanism is shown in Scheme 3-4.



Scheme 3-4. Proposed mechanism for oxidation of bromide by oxodiperoxomolybdenum(VI)

The rate-limiting step in this scheme is the oxidation of bromide, although the detailed mechanism, such as whether nucleophilic attack occurs on Mo(VI) or bound peroxide, is still speculative. The fate of the monoperoxo species, $\text{MoO}_2(\text{O}_2)$, is not known because it cannot be observed under the experimental conditions. As shown in Scheme 3-4, this complex could re-coordinate hydrogen peroxide. Thompson's investigations show that in 0.1-1.0 M acid the rate of formation of the oxodiperoxo species is second order in H_2O_2 concentration (Lydon et al., 1987), but first order in H_2O_2 concentration at less than 0.3 mM acid (Schwane & Thompson, 1989). Thus, addition of the second peroxide is rate limiting in 0.1 M acid; nevertheless the overall rate of bromide oxidation is still

slower than the rate of formation of $\text{MoO}(\text{O}_2)_2$. $\text{MoO}_2(\text{O}_2)$ could also oxidize a second equivalent of bromide, although Thompson argues that the oxomonoperoxo species is not reactive (Lydon et al., 1987). A third possibility is that $\text{MoO}_2(\text{O}_2)$ could disproportionate to $\text{MoO}(\text{O}_2)_2$ and MoO_3 ; MoO_3 could then recoordinate two equivalents of hydrogen peroxide, reforming $\text{MoO}(\text{O}_2)_2$. All of these possibilities are consistent with the experimental results since bromide oxidation is the rate-limiting step.

Previous examination of the activation of hydrogen peroxide by molybdenum(VI) to oxidize iodide 0.05 M acid (Smith & Kilford, 1976) and 0.005 M acid (Arias et al., 1990) gave similar results to the current work. The significant differences between the iodide oxidation reaction and the current bromide oxidation reactions are: (1) the dependence of the rate of the former on hydrogen peroxide concentration due to the more comparable rates of hydrogen peroxide coordination and iodide oxidation and (2) the interference from the significant rate of the uncatalyzed oxidation of iodide by hydrogen peroxide. Smith and Kilford (1976) observed that the dependence of the rate of iodide peroxidation catalyzed by molybdate could be described by the relation in equation 8 and thus the reaction exhibited "saturation" behavior.

$$\text{rate} = \frac{I -}{x + y[I -]} \quad (8)$$

However, the rate of peroxidative oxidation of bromide catalyzed by molybdenum(VI) continued to increase up to 2.0 M NH_4Br .

The previous studies on the oxidation of iodide by peroxo complexes of molybdenum(VI), tungsten(VI), and vanadium(V) have indicated that the oxodiperoxo complexes of these metals are capable of activating hydrogen peroxide in oxidation reactions (Secco, 1980; Smith & Kilford, 1976; Arias et al., 1990). It was also shown by Ghiron and Thompson that the oxodiperoxo configuration is a much better activator of peroxide than the monoperoxo configuration for oxygen atom transfer reactions in aqueous solution (Ghiron & Thompson, 1990). Thompson has proposed that the enhanced reactivity of the diperoxo complexes may be due to a longer peroxo O-O bond and one longer M-O peroxide bond in the diperoxo form versus the monoperoxo form. Titanium(IV) forms only a monoperoxo complex, and it actually stabilizes peroxide against attack in these reactions (Lydon & Thompson, 1986).

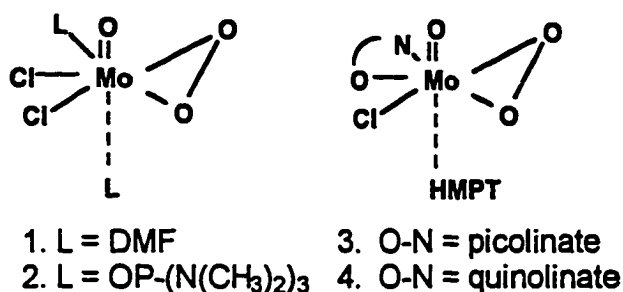
While the speciation of the peroxide complexes in acidic solution may be important in the activation of hydrogen peroxide, evidence from numerous studies on the activation of peroxide for oxygen atom transfer reactions and inner sphere one-electron oxidation reactions shows that the identity of the metal center is critical to the reactivity of the complex. Ghiron and Thompson (1990), for

example, showed that under conditions where vanadium(V), molybdenum(VI) and tungsten(VI) all in the form oxodiperoxo complexes, the relative reactivities were $10:10^4:10^5$ for oxygen atom transfer reactions in acidic aqueous solution. A similar trend can be noted within this group for the oxidation of iodide. While the behavior is not well understood, a simple correlation can be drawn between the Lewis acidity of a complex and its reactivity. The stabilization given peroxide by titanium(IV), which can be expected to have less Lewis acid character than the other complexes discussed, further extends this argument.

Recently, Espenson and coworkers (1994) reported on the ability of the organometallic complex methylrhenium trioxide, $(\text{CH}_3)\text{ReO}_3$, to catalyze oxygen transfer to bromide. This effective catalyst can coordinate one or two equivalents of hydrogen peroxide to oxidize bromide at pH 0 at a rate approximately 10^6 times faster than the uncatalyzed reaction. In contrast to what has been proposed for the group V and group VI transition metals, Espenson et al. (1994) find that the diperoxo species is less reactive than its monoperoxo counterpart. They suggest that the diperoxo complex is necessarily less electrophilic than the monoperoxo complex in this system. Thus, while the speciation dependence in Espenson's rhenium system (Espenson et al., 1994) is reversed from that proposed by Thompson for the complexes of transition metal groups (IV), (V), and (VI),

(Ghiron & Thompson, 1990), the proposed simple correlation between reactivity and acidity or electrophilicity of peroxo complexes still holds.

In addition to the issues of speciation and metal identity, this study addressed the mechanism(s) by which metal ions direct the oxidation of halides. One key question that remains to be answered is whether halide oxidation occurs by coordination to the metal or whether it proceeds by attack directly on the peroxo ligand. Espenson et al. (1994) proposed that the oxidation of bromide by the organometallic complexes $(\text{CH}_3)\text{ReO}_2(\text{O}_2)$ and $\text{CH}_3\text{ReO}(\text{O}_2)_2$ occurs by nucleophilic attack of the halide on an activated peroxide oxygen. The inhibition of the peroxidation of bromide by chloride in the molybdenum(VI) system in the absence of significant Cl-TMB production suggests that chloride coordinates to the peroxomolybdenum(VI) complex, although the reason for the inhibition could not be determined from these studies. Several examples of chloride coordination to the oxoperoxo Mo(VI) moiety in organic solvents are well known, such as 1 through 4



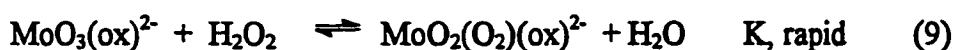
Compounds 1 and 2 are active epoxidation catalysts and 3 has been characterized by x-ray crystallography (Chaumette et al., 1983). Chloride oxidation by 1-4 was

not reported, and it may not occur if the monoperoxo moiety does not have the driving force to oxidize chloride. Moreover, these reactions were carried out in the absence of acid, which would prevent chloride oxidation (Clague & Butler, 1993b). Thus it is not known whether 1-4 could also effect chlorination. The monoperoxo species may not be capable of oxidizing chloride or, alternatively, coordination of the halide may stabilize it against oxidation by peroxide. In any case, halide coordination to the metal center is not a prerequisite for halide oxidation because $\text{MoO}(\text{O}_2)_2(\text{ox})^{2-}$, which does not have a dissociable ligand, oxidizes bromide (Meister & Butler, 1994; Reynolds et al., 1994).

Coordination of chloride to the neutral complex $\text{MoO}(\text{O}_2)_2(\text{H}_2\text{O})_2$ would necessarily require loss of one of the water ligands to form a negatively charged species, $\text{MoO}(\text{O}_2)_2(\text{H}_2\text{O})(\text{Cl})^-$. As can be seen from the acid dependence studies on the molybdenum(VI) system, the neutral diaquo species was slightly more reactive than the charged aquohydroxo complex, $\text{MoO}(\text{O}_2)_2(\text{H}_2\text{O})(\text{OH})^-$. Like the trend noted for the acid dependence, the monoanionic complex with chloride coordination may simply be less effective at catalyzing peroxidative bromination than the more electrophilic diaquo complex.

Further study of the oxalato complex of molybdenum(VI) suggests that reinterpretation of the data as presented by Reynolds et al. (1994) may be necessary. Overall, our data suggests that the $\text{MoO}(\text{O}_2)_2(\text{ox})^{2-}$ is a very effective

catalyst for the peroxidation of halides at near neutral pH. In fact, our interpretation of the data indicates that $\text{MoO}(\text{O}_2)_2(\text{ox})^{2-}$ is more effective than originally proposed. Brominated TMB is rapidly produced during the first rapid reaction of $\text{MoO}(\text{O}_2)_2(\text{ox})^{2-}$ monitored spectrophotometrically at 324 nm. The rapid decrease in the absorbance at 324 nm indicates that the oxodiperoxoxalato complex is quickly consumed. The remaining minimal absorbance at this wavelength likely results from the dioxomonoperoxoxalato complex, $\text{MoO}_2(\text{O}_2)(\text{ox})(\text{H}_2\text{O})^{2-}$. Ghiron and Thompson (1989) have suggested that the monoperoxo absorbs substantially around 324 nm. The coordination of one peroxide by $\text{MoO}_3(\text{ox})^{2-}$ has been proposed by Ghiron and Thompson to be very rapid (Equation 9). However, these same authors have proposed from their studies of oxygen atom transfer reactions that coordination of the second peroxide is rate limiting (Equation 10).



They suggest that in order to form a complex with five ligands in the equatorial plane (Jacobsen et al., 1978), substantial rearrangement is necessary (Ghiron & Thompson, 1989). The slowness of coordination of the second peroxide by $\text{MoO}_2(\text{O}_2)(\text{ox})^{2-}$ was further demonstrated by the study of peroxide binding to the monoperoxo complex presented above (Figure 3-25). In accordance with this

interpretation of the data, the lag phase observed by Reynolds et al. (1994) in the kinetic traces at 320 nm with increasing concentrations of hydrogen peroxide is potentially due to recoordination of peroxide to $\text{MoO}_3(\text{ox})^{2-}$ upon consumption of the peroxide ligand of $\text{MoO}_2(\text{O}_2)(\text{ox})^{2-}$ to oxidize bromide (Figure 3-24).

The unmatched reactivity of vanadium bromoperoxidase shows that peroxide activation could be dependent on ligation and surrounding environment in addition to or perhaps in spite of the identity of the metal center. Evidence suggests the vanadium center in the enzyme may form a monoperoxo complex that is unusually capable of peroxide activation (Tromp et al., 1990). The influence of ligation on the reactivity of peroxide complexes of vanadium(V), molybdenum(VI), tungsten(VI) and other transition metal ions is a topic of much current interest (Ghiron & Thompson, 1990). In addition, the mechanisms of halide oxidation by metal peroxo complexes, particularly vanadium peroxo complexes (i.e., Clague & Butler, 1993a; Colpas et al., 1994, 1996) is being actively pursued.

References

- Arber, J.M.; de Boer, E.; Garner, C.D.; Hasnain, S.S.; Wever, R. *Biochemistry*, **1989** *28*, 7968-7973.
- Arias, C.; Mata, F.; Perez-Benito, J. F. *Can. J. Chem.* **1990**, *68*, 1499
- Carrano, C.J.; Mohan, M.; Holmes, S.M.; de la Rosa, R.; Butler, A.; Charnock, J.M.; Garner, C.D. *Inorg. Chem.* **1994**, *33*, 646-655.
- Clague, M.J., Butler, A. *Inorg. Chem.*, **1993a**, *32*, 4754-4761
- Clague, M.J.; Butler, A., *Adv. Inorg. Biochem.*, **1993b**, *9*, 219-243, Prentice Hall Publishing, Co, New Jersey.
- Clague, M.J.; Butler, A., *J. Am. Chem. Soc.*, **1995**, *117*, 3475-84.
- Chaumette, P.; Mimoun, H.; Saussine, L. *J. Orgmet. Chem.*, **1983**, *250*, 291-310.
- Colpas, G.J.; Hamstra, B.J.; Kampf, J.W.; Pecoraro, V.L. *J. Am. Chem. Soc.*, **1994**, *116*, 3627-3628.
- Colpas, G.J.; Hamstra, B.J.; Kampf, J.W.; Pecoraro, V.L. *J. Am. Chem. Soc.*, **1996**, *118*, 3469-3478.
- Cotton, M.L. & Dunford, H.B. *Can. J. Chem.* **1973**, *51*, 582-87
- de la Rosa, R. I.; Clague, M. J.; Butler, A. *J. Am. Chem. Soc.* **1992**, *114*, 760
- Dengal , A.C.; Griffith, W.P.; Powell, R.D; Skapski, A.C. *J. Chem. Soc. Dalton Trans.*, **1987**, 991-995.
- Detty, M.R.; Zhou, F.; Friedman, A.E. *J. Am. Chem. Soc.* **1996**, *118*, 313-318.
- Espenson, J.H.; Pestovsky, O.; Huston, P.; Staudt, S. *J. Am. Chem. Soc.* **1994**, *116*, 2869-2877.
- Everett, R. R.; Butler, A. *Inorg. Chem.* **1989**, *28*, 393
- Everett, R. R; Soedjak, H. S.; Butler, A. *J. Biol. Chem.* **1990**, *265*, 15671

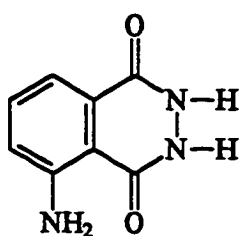
- Ghiron, A.; Thompson, R.C. *Inorg. Chem.* **1988**, *27*, 4766-4771.
- Ghiron, A. F.; Thompson, R. C. *Inorg. Chem.* **1989**, *28*, 3647.
- Ghiron, A. F.; Thompson, R. C. *Inorg. Chem.* **1990**, *29*, 4457
- Harrison, A.T; Howarth, O.W. *J. Chem. Soc. Dalton Trans.*, **1985**, 1173-7.
- Islam, M.; Thompson, R.C. *Inorg. Chem.*, **1989**, *28*, 4419-4422
- Jacobsen, S.E.; Tang, R; Mares, F. *Inorg. Chem.*, **1978**, *17*, 3055.
- Kanofsky, J.R., *Arch. Biochem. Biophys.*, **1989**, *274*, 229-23.
- Landau, R.; Sullivan, G.A.; Brown, D. *Chemtech.*, **1979**, 602.
- Lydon, J. D.; Thompson, R.C. *Inorg. Chem.* **1986**, *25*, 3694.
- Lydon, J. D.; Schwane, L. M.; Thompson, R. C.; *Inorg. Chem.* **1987**, *26*, 2606.
- Messerschmidt, A.; Wever, R. *Proc. Natl. Acad. Sci. U.S.A.*
- Mimoun, H.; Seree de Roch, I.; Sajus, I. *Bull. Soc. Chim.* **1969**, 1481.
- Mimoun, H.; Seree de Roch, I.; Sajus, I. *Tetrahedron* **1970**, *26*, 37-50.
- Orhanovic, M.; Wilkins, R. G. *J. Am. Chem. Soc.* **1967**, *89*, 278
- Reynolds, M.S.; *Inorg. Chem.* **1994**, *33*, 4977-4984.
- Sakurai, H.; Tsuchiya, K. *FEBS Lett.* **1990**, *260*, 109.
- Schwane, L.M.; Thompson, R. C. *Inorg. Chem.* **1989**, *28*, 3938-3946
- Secco, F. *Inorg. Chem.* **1980**, *19*, 2722
- Smith, R. H.; Kilford, J. *International Journal of Chemical Kinetics* **1976**, *8*, 1.
- Tromp, M.G.M.; 'Olafsson, G.; Krenn, B.E.; Wever, R. *Biochem. Biophys. Acta.* **1990**, *1040*, 192-198.

Vilter, H.: Rehder, D. *Inorg. Chim. Acta.*, 1987, 136, L7.

Chapter 4. Luminol as a Substrate for Vanadium Bromoperoxidase

Introduction

Diacyl hydrazides such as 3-aminophthalazine-2,7-dione, i.e., luminol, have useful chemiluminescent properties and have proven effective as substrates in immunoassays such as ELISA (enzyme-linked immunosorbant assay). Luminol, in particular, gives a striking emission of light when oxidized by one-electron oxidizing systems (Lind et al., 1983; Merenyi et al., 1986; Merenyi et al., 1990; Cormier & Prichard, 1968; Brestel, 1985). The oxidation of luminol by hydrogen peroxide catalyzed by horse radish peroxidase (HRP) is commonly used as a detector system in ELISAs. Detection of the emission of luminol and other diacyl hydrazides by luminometric techniques is much more sensitive than colorimetric assay detection methods commonly used for diagnostic tests.

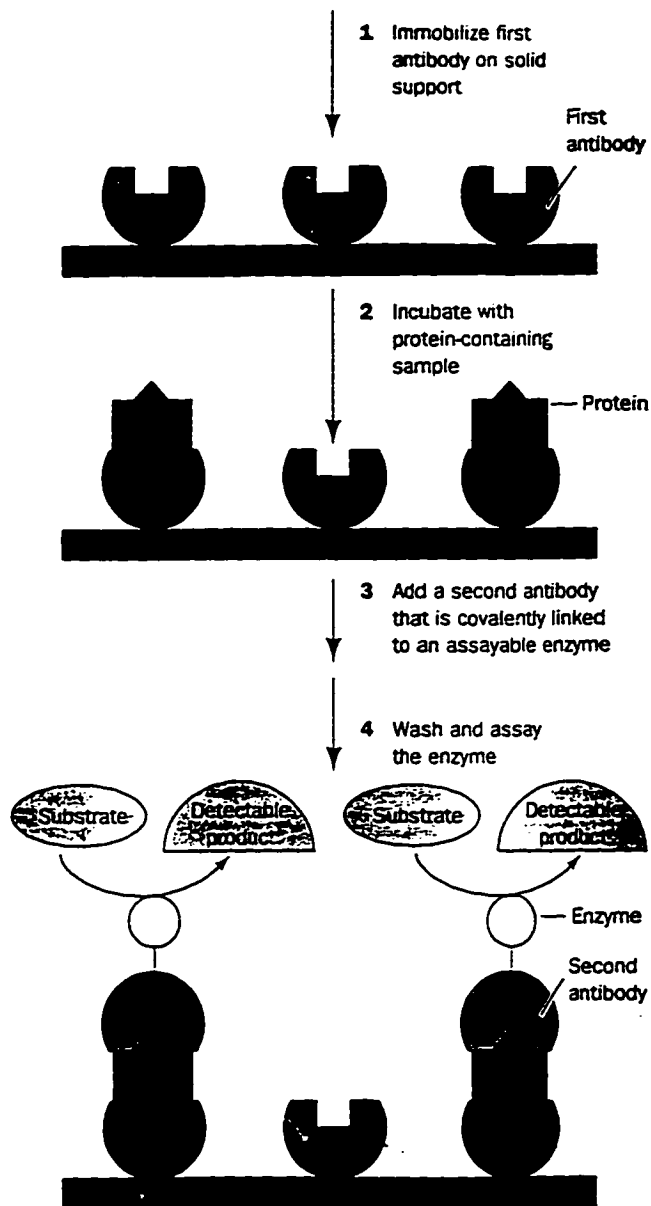


luminol: 3-aminophthalazine-2,7-dione

ELISAs are widely used to detect specific proteins and other biological substances in clinical applications. Home pregnancy tests, for example, use an ELISA to detect the placental hormone chorionic gonadotropin in the subject's

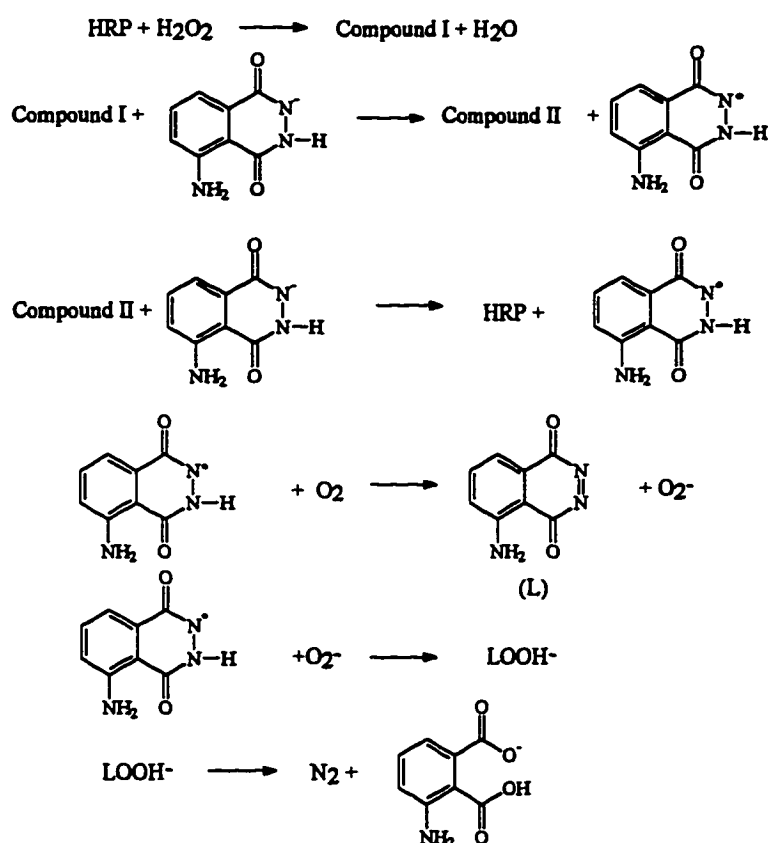
urine (Voet & Voet, 1990). In an ELISA sandwich assay, an antibody against the protein to be assayed is bound to a solid support. Next, the solution to be tested is applied, and antigen present in this solution binds to the supported antibody. The antibody-antigen complex is then reacted with a second antibody against the protein of interest that has been covalently linked to a reporter enzyme such as HRP. Unbound proteins are washed away, and the resultant complex is incubated with enzyme substrates, i.e., luminol and hydrogen peroxide in the case of HRP, under appropriate turnover conditions for the enzyme. The quantity of enzyme and, accordingly, the quantity of bound antigen can then be determined. An illustration of a typical ELISA assay is provided in Scheme 4-1.

The oxidation of luminol by hydrogen peroxide catalyzed by horse radish peroxidase proceeds as shown in Scheme 4-2. In this reaction scheme, hydrogen peroxide reacts with the ferric heme group to generate Compound I, an oxoiron(IV) pi-cation radical species, which can subsequently react with luminol to generate a luminol radical and Compound II, (Fe(IV)-heme). Compound II then can also react with luminol to produce a second equivalent of luminol radical and regenerate the ferric ground state of the enzyme. The reaction of a luminol radical with dioxygen results in a second oxidation to the luminol diazaquinone (L) and formation of superoxide. The reaction of a luminol radical with superoxide results



Scheme 4-1. Illustration of a typical ELISA sandwich assay. Taken from Voet & Voet, 1990.

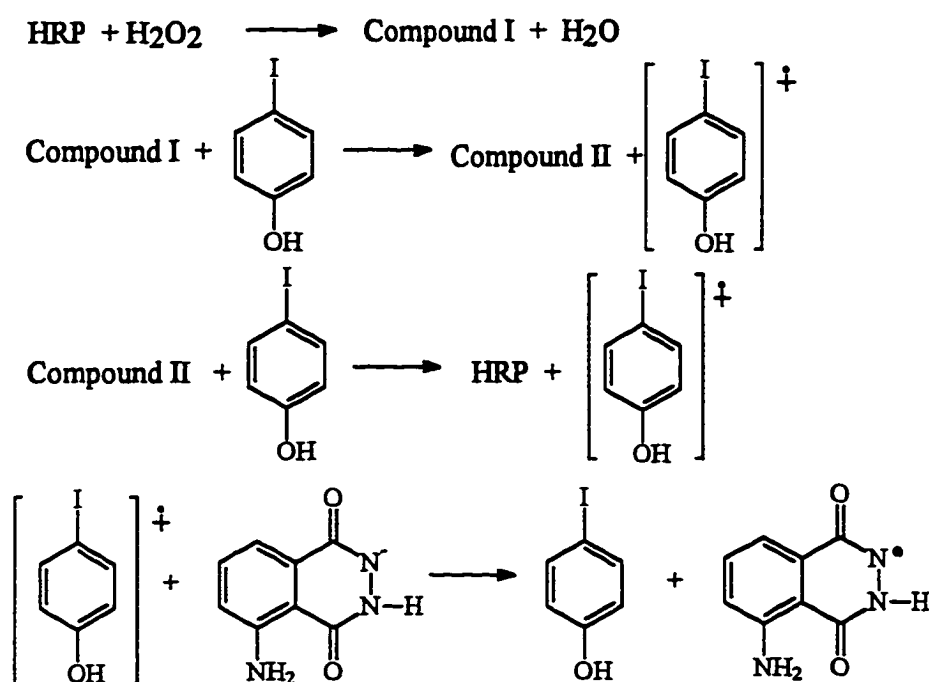
in the formation of an endoperoxide (LOOH)¹, which eliminates dinitrogen to give 3-aminophthalate. Under basic conditions, this 3-aminophthalate dianion can be in an excited state, which gives off light as it relaxes (Lind et al., 1983; Merenyi et al., 1986; Thorpe & Kricka, 1986; Merenyi et al., 1990). The profile of the emission of the excited 3-aminophthalate has an absorption maximum near 425 nm (Rosewell & White, 1973).



Scheme 4-2. Reaction sequence for the unenhanced chemiluminescent oxidation of luminol catalyzed by horse radish peroxidase. The pK_a 's of luminol are 6 (Baxendale, 1973) and 7.7 (Merenyi & Lind, 1983); thus the protonation state will depend on the pH of the reaction.

¹ The structure of this intermediate has not yet been determined.

The oxidation of luminol by HRP and other one-electron oxidants to yield chemiluminescence can be limited by the rapid decay and the low intensity of the light emission. These difficulties have been alleviated by the use of enhancers such as halophenols (Thorpe et al., 1985) and conjugated amines (Kricka et al., 1986). A typical mechanism for the production of luminol radicals in the presence of an enhancer is shown in Scheme 4-3. In this reaction scheme, Compound I of HRP reacts with the enhancer, which is a good substrate for the enzyme, to give a radical species, which proceeds to oxidize luminol to a radical species. The luminol radical then goes on to react as described in Scheme 4-2.



Scheme 4-3. Oxidation of luminol to a radical catalyzed by HRP in the presence of an enhancer.

Researchers at Johnson and Johnson Clinical Diagnostics (Rochester, NY) have recently demonstrated that vanadium bromoperoxidase (V-BrPO) from *Ascophyllum nodosum* and other marine algae functions effectively as a reporter enzyme in ELISA assays (Friedman, et al.,1995). In fact, assays using V-BrPO have been shown to be more sensitive than the standard HRP assay. The vanadium bromoperoxidase system exhibits intense, long-lived luminescence in the absence of enhancers and may prove extremely useful in diagnostic assays (Friedman et al.,1995).

As described in Chapter 1, vanadium bromoperoxidase catalyzes the oxidation of halides by hydrogen peroxide by a two-electron process (Soedjak et al.,1995). A two-electron process precludes the formation of a luminol radical as in the horse radish peroxidase reaction; thus the mechanism of oxidation and product formation of the reaction catalyzed by V-BrPO can be expected to differ from that catalyzed by HRP.

This chapter describes an analysis of the reaction of luminol with V-BrPO, hydrogen peroxide, and bromide. The products of this enzymatic reaction and the parallel chemical reaction in which HOBr is substituted for enzyme and hydrogen peroxide were characterized by mass spectrometry and nuclear magnetic resonance spectroscopy and compared to the major product of the HRP reaction, 3-aminophthalate.

Materials and Methods

Preparation of luminol products for analysis. Enzymatic reactions were performed under conditions of 30 nM V-BrPO, 0.25 to 1 mM luminol, 0 to 5 mM H₂O₂, 0.1 M KBr, and pH 5.7 to 8.1, typically in 0.1 M phosphate buffer. Non-enzymatic reactions with aqueous bromine were performed using up to 20 mM luminol and one, two, or excess equivalents of added HOBr per equivalent of luminol in 0.1 M phosphate pH 5.7 to 8.1 or in water (in which it was determined that the pH was ~6 during the course of the reaction). The solid precipitate obtained in both enzymatic and chemical reactions was removed from the reaction mixture by vacuum filtration. For some reactions, the products were extracted with ethyl acetate and a solid product was obtained by rotary evaporation.

Silica gel chromatography of the luminol products. Silica gel TLC analyses of the reaction products were obtained in 90% ethyl acetate/ 10% acetonitrile. Plates were visualized with ultraviolet light or in an iodine chamber. For some experiments, chemical reaction products were separated by a silica gel column (40 - 140 mesh) using 90% ethyl acetate/ 10% acetonitrile as the elution solvent.

HPLC analysis of luminol reaction products. Reaction conditions were 0.5 mM luminol, 0.1 M KBr, and 0, 0.5, 1.0, or 1.5 mM added HOBr (20 mM stock) or 30 nM V-BrPO, 0.5 mM luminol, 0.1 M KBr and 0, 0.5, 1.0, or 1.5 mM added H₂O₂ (20 mM stock) in 0.1 M phosphate pH 6.0. After a minimum reaction time

of 1 hour, the solutions were filtered with a 0.2 μm filter to remove precipitates in preparation for HPLC analysis. These precipitated products were collected for later spectroscopic analysis. For HPLC separation of the products still in solution, Solvent A was 0.1% TFA and Solvent B was 0.1% TFA in methanol. HPLC was carried out with Waters 510 pumps and an Alltech 0.46 x 25 cm Econosphere C-18 column. Products were detected with a Waters 996 photodiode array detector (PDA) and monitored at 230 nm using Waters Millennium Chromatography Manager software (Version 2.1). Two linear gradients proved effective for separating the reaction products: a gradient from 50% to 0% A and a gradient from 35% to 0% A. Products were identified both by retention time and PDA absorbance spectra.

Analysis of reaction products. Luminol reaction products prepared as described above were analyzed by positive electrospray and positive atmospheric pressure chemical ionization (APCI) mass spectrometry using an LC-MS equipped with a loop (no column) and a water/acetonitrile/TFA solvent system. Sodium luminol and 3-aminophthalic acid were also analyzed as controls. Products were further analyzed by ^1H NMR spectroscopy in methyl- d^3 -alcohol- d on a Varian Gemini 200 MHz NMR spectrometer or a General Electric GN 500 MHz NMR spectrometer.

Competition studies with phenol red. Kinetic binding studies with luminol were performed using phenol red as a competing substrate. The production of bromophenol blue was monitored at 596 nm on an HP8452A diode array spectrophotometer. Conditions for the enzymatic competition experiments were 25 μM phenol red, 0.5 mM H_2O_2 , 50 mM KBr, and 0 to 75 μM luminol. The experiments were performed at 4 different pH values and corresponding V-BrPO concentrations: pH 5.7, 6 nM ; pH 6.5, 3 nM; pH 7.2, 15 nM; pH 8.0, 75 nM. Similar experiments were done with aqueous bromine under conditions of 25 μM phenol red, 50 mM KBr, and 0 to 75 μM luminol. HOBr was added in small volume aliquots every 30 seconds; at pH 6.5, 20 μL of 1.9 mM HOBr was added every 30 seconds, and at pH 5.7, 7.2 and 8.1, 5 μL of 4.4 mM HOBr was added every 30 seconds.

Competition studies between substrate attack and dioxygen evolution. Competition studies between reaction of luminol and evolution of dioxygen catalyzed by V-BrPO were performed by monitoring the evolution of dioxygen with a YSI Model 5331 Standard Oxygen Electrode attached to a YSI Model 5300 Biological Oxygen Monitor. The experiments were executed under conditions of nanomolar concentrations of V-BrPO, 0.1 M KBr, 0 to 1 mM luminol where possible (solubility decreases at lower pH), 10 mM H_2O_2 , and 0.1 M phosphate buffer at pH 5.7, 6.5, 7.2, or 8.1. V-BrPO concentration was increased with pH to

maintain similar rates of dioxygen evolution in the absence of luminol: pH 5.7, 6 nM; pH 6.5, 7 nM; pH 7.2, 15 nM; and pH 8.1, 37 nM. Dioxygen evolution was measured by first monitoring the dioxygen level in the reaction solution in the absence of H_2O_2 for at least five minutes prior to initiation of the reaction with hydrogen peroxide. The reaction was monitored for at least five minutes after the introduction of H_2O_2 . Parallel non-enzymatic experiments were performed with HOBr at pH 6.5 again by first monitoring the dioxygen level of the blank of buffer and luminol without HOBr for at least five minutes and then introducing the HOBr at a consistent flow rate of 50 $\mu\text{M}/\text{min}$ using a syringe pump. The non-enzymatic dioxygen evolution was monitored over the same time period as the V-BrPO experiments.

Fluorescence quenching. Fluorescence data were recorded on a Perkin-Elmer LS50B fluorometer set at 2.5 nm excitation and emission slit widths, an excitation wavelength of 355 nm, and an emission wavelength of 425 nm. Multiple aliquots of 2 mg/mL V-BrPO (i.e., 20 μM) or bovine serum albumin (BSA) were added to a 2 mL solution of 2 μM or 3 μM luminol in 0.1 M Hepes buffer at pH 6.4. The fluorescence data were plotted in a Stern-Volmer plot format of F_0/F versus Q where F_0 is the initial fluorescence emission, F is the fluorescence data upon addition of protein quencher, and $[Q]$ is the concentration of V-BrPO (i.e., the quencher). The data were fit to the Stern-Volmer equation:

$$F_0/F = K_{app}[Q] + 1 \quad (1)$$

Linear fitting of the Stern-Volmer plot then results in determination of the K_{app} quenching constant for V-BrPO and luminol.

Luminescence emission spectra. Luminescence from the V-BrPO/luminol/H₂O₂/NaBr system was measured on the Perkin-Elmer LS50B luminescence spectrophotometer. Reaction conditions for monitoring luminescence were 6 or 30 nM V-BrPO, 0.6 mM luminol, 1.8 mM H₂O₂, and 0.1 M photograde NaBr (Eastman Kodak, Inc; gift from Alan Friedman, Johnson and Johnson Clinical Diagnostics) in 0.1 M phosphate pH 8.0. For measurement of luminescence spectra, the excitation slit was closed (0 nm slit width) and the emission slit was set at 5 or 10 nm. The luminescence spectrum was measured every 4 minutes (6 nM V-BrPO) or 1 minute (30 nM V-BrPO) until the reaction reached completion.

Results and Interpretation

Reports from Johnson and Johnson Clinical Diagnostics (Rochester, NY) that V-BrPO is an effective reporter enzyme in luminol-based immunoassays (Friedman et al.,1995), generating more intense, longer-lived signal compared to horse radish peroxidase systems, prompted an investigation into the mechanism of the V-BrPO-catalyzed reaction with luminol. In order to observe directly the reported emission properties of luminol as a substrate for V-BrPO, luminol was included in reactions of the enzyme-catalyzed peroxidation of bromide. Under conditions of 2 nM V-BrPO, 2 mM H₂O₂, 50 mM KBr, 0.2 mM luminol in 0.1 M phosphate pH 7.0 or 8.0 and in the absence of room light, greenish luminescence was observed from the enzymatic reaction. This luminescence persisted for several minutes.

Identification of the Products of Luminol in the V-BrPO-Catalyzed Reaction.

TLC analyses. The products of luminol in the enzymatic reaction were examined by thin-layer chromatography (TLC). Effective separation was achieved using 90% ethyl acetate/ 10% acetonitrile as the elution solvent. TLC analysis of reaction mixtures run at pH 5.7 and 8.1 under conditions of 30 nM V-BrPO, 0.5 mM luminol, 0.5 mM H₂O₂, and 0.1 M KBr indicated two species when visualized by near ultraviolet light. The low *R_f* compound matched well with luminol itself and fluoresced purple similarly to a control sample of luminol. The high *R_f* spot

fluoresced green under ultraviolet light. These compounds were also detected from the reaction of 0.5 mM luminol with 0.5 mM HOBr in 0.1 M phosphate pH 5.7 or pH 8.1. In addition, the same compounds were observed under the conditions of 5.0 mM luminol, 5.0 mM HOBr or up to 20 mM HOBr just in water. The pH of the reaction mixture in water was approximately 6 both prior to and after the addition of HOBr. Comparison by TLC of the V-BrPO and the HOBr reaction mixtures to a standard of 3-aminophthalate clearly indicated that the HRP product did not match the compounds detected in these reaction mixtures. While the compositions of the V-BrPO and the HOBr reactions were the same regardless of pH according to the TLC analysis, precipitation was observed at lower pH values. Dissolution of the precipitate in methanol followed by TLC revealed that this solid contained both of the compounds previously observed by TLC.

In order to examine the stoichiometry of the luminol reaction, the amount of oxidant was increased in both the enzymatic and chemical reactions. When the concentration of H₂O₂ in the V-BrPO reaction was increased from 0.65 to 6.5 mM under conditions of 0.65 mM luminol and 0.1 M KBr, in 0.1 M phosphate pH 6.5 or 8.1, TLC analysis showed that the low *R_f* species, most likely luminol itself, disappeared when the hydrogen peroxide concentration was increased, leaving only the higher *R_f* spot which fluoresces green under ultraviolet light. Similar results were seen for the reaction of 1.0 mM luminol with either 1.0 mM or 10.0 mM

HOBr in 0.1 M phosphate pH 5.7 or 8.1 or in water. Overall, the TLC analysis suggested that approximately 2.5 (\pm 0.5) equivalents of oxidant are required to completely convert luminol to other compounds.

Mass spectral analyses. To further characterize the products of the reaction of H₂O₂, KBr, and luminol catalyzed by V-BrPO, mass spectrometry was performed on the solid precipitate that can be isolated at lower pH values. The solid was prepared by reacting 18 mM luminol and 42 mM HOBr (i.e., 2.3 equivalents) in water for 10 to 15 minutes and filtering off the solid product. Analysis of the sample by positive APCI (atmospheric pressure chemical ionization), as shown in Figure 4-1, revealed two M+1 peaks of essentially equal intensity at 256 and 258 m/z. These peaks have the appropriate masses and isotopic distribution for brominated luminol. A peak cluster corresponding to a doubly brominated species was also observed at M+1 values of 334, 336, and 338 m/z, which match the expected mass for doubly brominated luminol. In addition, the starting material, luminol, C₈H₇N₃O₂, was also detected in this sample at M + 1 = 178 m/z. Overall, the mass spectral data suggest that the luminol simply undergoes bromination; the N-N bond remains intact in these products. The different brominated products identified by mass spectrometry appeared as a single spot in the TLC analyses.

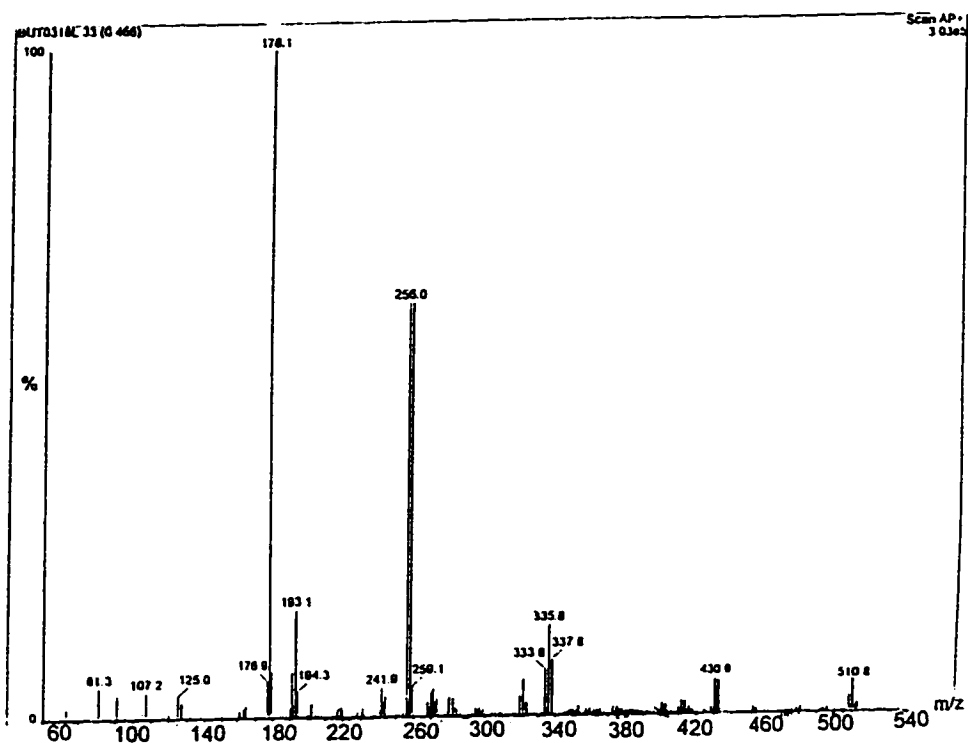
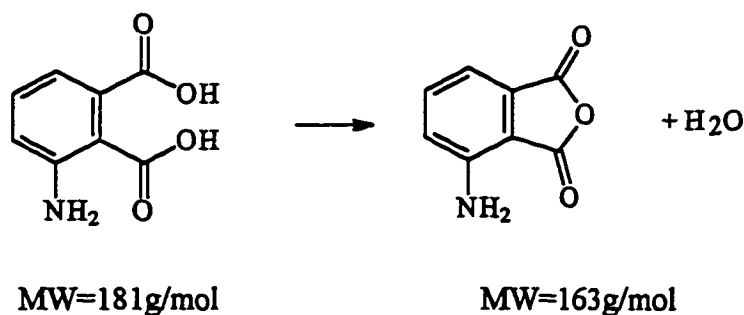


Figure 4-1. Positive APCI mass spectrum of the solids from the reaction of luminol and HOBr. Preparation conditions: 18 mM luminol, 54 mM HOBr in water. Precipitated solids were filtered from solution.

Minor peaks were also detected in the mass spectrum of the luminol products at $M + 1 = 430.9$ m/z and $M + 1 = 510.8$ m/z. The isotopic distribution of these peaks indicated that they represented a monobrominated and a dibrominated species, respectively. In addition, they were each 175 mass units higher than the singly and doubly brominated luminol products. The species associated with these minor peaks have not been identified, but the mass difference between these compounds and the bromoluminol suggests that an unknown "di-luminol" species may be formed.

As was suggested by TLC, all of the luminol was not consumed in the mass spectrometry sample even though 2.3 equivalents of oxidant were added. However, the mass spectral data indicate that luminol can be effectively brominated a second time; thus monobromoluminol and luminol compete for the HOBr still present in solution.

A positive APCI mass spectrum of 3-aminophthalic acid has an $M+1$ peak at 164 m/z (Figure 4-2), which corresponds to elimination of H_2O from this compound:



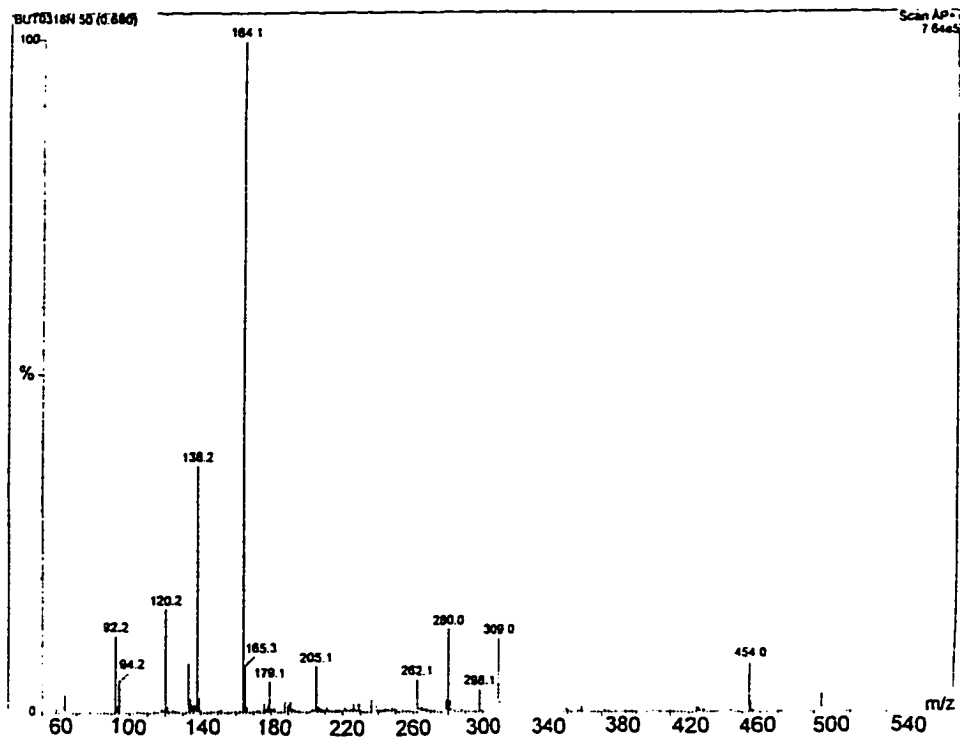
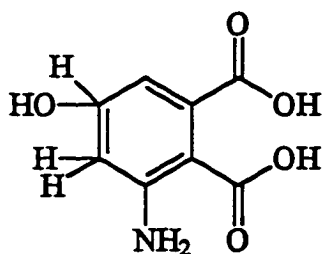


Figure 4-2. Positive APCI mass spectrum of 3-aminophthalic acid

A peak is not observed at 164 m/z in the mass spectrum of the V-BrPO/HOBr reaction products as shown in Figure 4-1. This result further confirms that the products from the V-BrPO/H₂O₂/KBr/luminol system at near-neutral pH differ from the products of the oxidation of luminol by one-electron oxidants such as the HRP system.

After the primary product of the reaction of 18 mM luminol and 42 mM HOBr was filtered and collected, the remaining filtrate possessed a bright yellow color. This solution changed to a brownish color over several minutes, possibly due to hydrolysis. Extraction of this solution with ethyl acetate and rotary evaporation produced a small amount of a tan solid. This solid gave a weak spectrum by positive APCI with M + 1 peaks at 200 and 214 (Figure 4-3). The peak at 200 may correspond to a hydroxylated aminophthalate species such as:



Regardless, this species is not observed by TLC and is likely not a major component of the product mixture. Other spectroscopic methods did not help to clarify the identity of this compound.

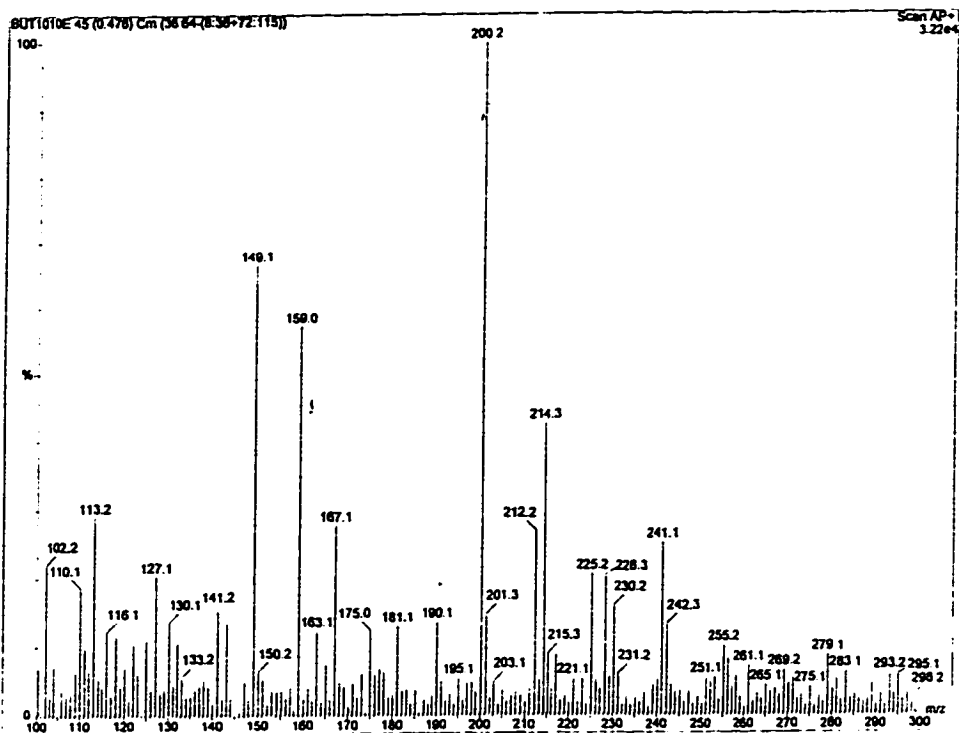
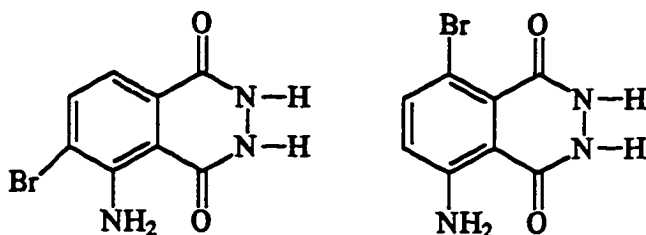


Figure 4-3. Positive APCI mass spectrum of the yellow filtrate from the reaction of luminol and HOBr. Preparation Conditions: same as figure 4-1.

NMR analyses. ^1H NMR analysis in deuterated methanol of the luminol product prepared by the reaction of 18 mM luminol and 42 mM HOBr as described in the section on mass spectrometry showed that two singly brominated species with different bromination sites were present in this product (Figure 4-4). Both species displayed two doublets in the aromatic region which were matched according to splitting and integration. The doublets at 7.8 and 7.1 ppm correspond to one species, and the doublets at 7.65 and 6.8 ppm correspond to the other species. The presence of two coupled doublets for each species suggests that two aromatic protons are coupled exclusively to one another in both species. Two structures are reasonable for the monobrominated products.



In addition, a singlet was observed at 8.08 ppm, which likely corresponds to the doubly brominated species seen by mass spectrometry. Because the amino group is ortho- and para-directing for electrophilic substitution, the doubly brominated luminol is most likely brominated at those positions.

:

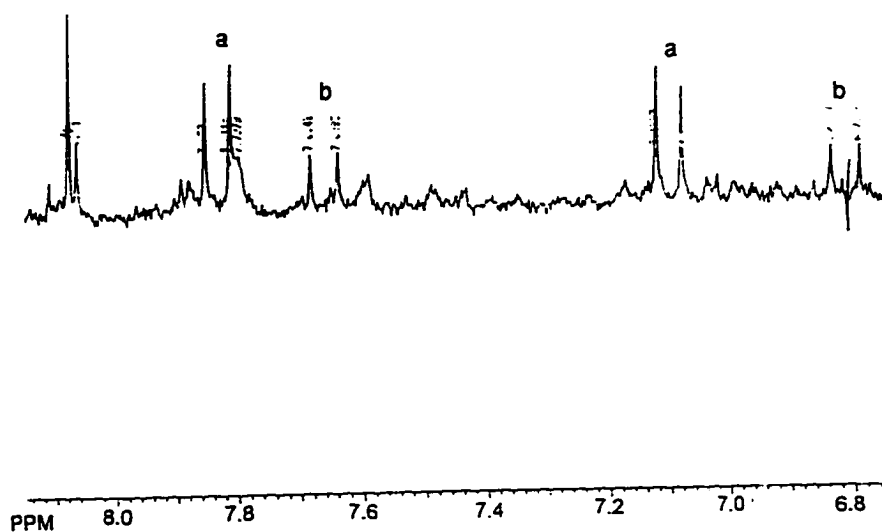
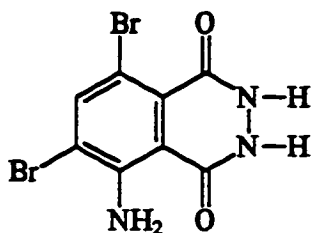


Figure 4-4. ^1H NMR spectrum in deuterated methanol of the solid products from the reaction of luminol and HOBr. "a" and "b" label the matched peaks for each monobrominated species; "c" labels the singlet for the dibrominated species. Preparation conditions same as Figure 4-1.



Thus the unique major products of the reaction of V-BrPO under turnover of luminol have been identified. As predicted, the reaction of V-BrPO with luminol is strikingly different than the previously studied reactions with HRP (Cormier & Prichard, 1968), hypochlorite (Brestel, 1985), and other one-electron oxidizing species (Lind et al., 1983; Merenyi et al., 1986; Merenyi et al., 1990).

HPLC analysis of the luminol product mixtures. Comparative analyses by HPLC of the products produced in the reaction of luminol with the V-BrPO system or with HOBr using a gradient of 50% methanol/ 50% H₂O/ 0.1% TFA to H₂O/ 0.1% TFA show more clearly the products formed by the V-BrPO/luminol/H₂O₂/bromide system. HPLC traces of reactions run at 30 nM V-BrPO, 0.7 mM luminol, 0.1 M KBr, and 0.7 or 2.1 mM H₂O₂ in 0.1 M phosphate pH 5.7 show that the major products of these reactions appear at approximately 18 minutes and are the brominated luminols initially observed from the reaction of luminol with HOBr (Figure 4-5). It did not prove feasible to clearly separate the different brominated species. The spectrum of the primary component

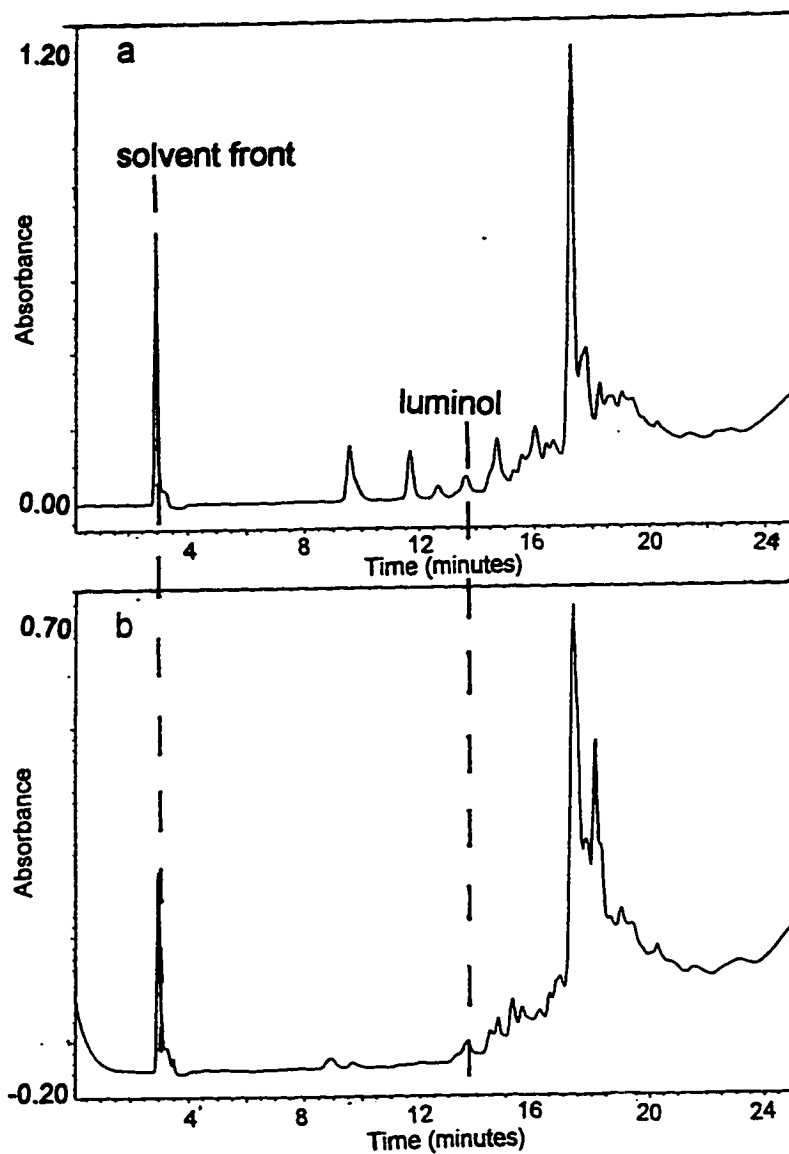


Figure 4-5. HPLC chromatograms at 230 nm of the reaction mixture of luminol, V-BrPO, H_2O_2 , and KBr at pH 5.7. Conditions: 30 nM V-BrPO, 0.7 mM luminol, 0.1 M KBr in 0.1 M phosphate pH 5.7, a) 0.7 mM H_2O_2 ; b) 2.1 mM H_2O_2 .

of the 1:1 reaction is shown in Figure 4-6a and matches well with a UV/vis spectrum recorded of the precipitate from the HOBr preparation (Figure 4-6b). The HPLC traces of the parallel HOBr reactions run at 0.7 mM luminol, 0.1 M KBr, and 0.7 mM or 2.1 mM HOBr in 0.1 M phosphate pH 5.7 show similar products, as confirmed by PDA spectra, but the specificity appears to be lower (Figure 4-7). Several other compounds are detected at retention times of 9.5, 12, and 13 minutes. Some of these products may be brominated or hydroxylated aminophthalate species.² The compound at ~13.5 minutes is unreacted luminol.

The products of the V-BrPO/luminol/H₂O₂/KBr system at pH 8.0 were also analysed in order to investigate the pH dependence of the reaction. HPLC chromatograms of enzymatic reactions performed under conditions of 30 nM V-BrPO, 1.4 mM luminol, 1.4 to 4.2 mM H₂O₂, and 0.1 M KBr in 0.1 M phosphate pH 8.0 indicate less specificity than their pH 5.7 counterparts (Figure 4-8). Several other peaks appeared between 14 and 16 minutes. However, the major peaks of the HPLC chromatograms from the reactions run under these conditions match those of the reactions at pH 5.7 and also the peaks of the HPLC chromatograms of the parallel reactions performed under conditions of 1.4 mM luminol, 0.1 M KBr, and 1.4 to 4.2 mM HOBr in phosphate pH 8.0 (Figure 4-9). As at pH 5.7, the

² For some of these peaks, the UV spectrum recorded by the PDA detector resembled that of 3-aminophthalate (but was not identical).

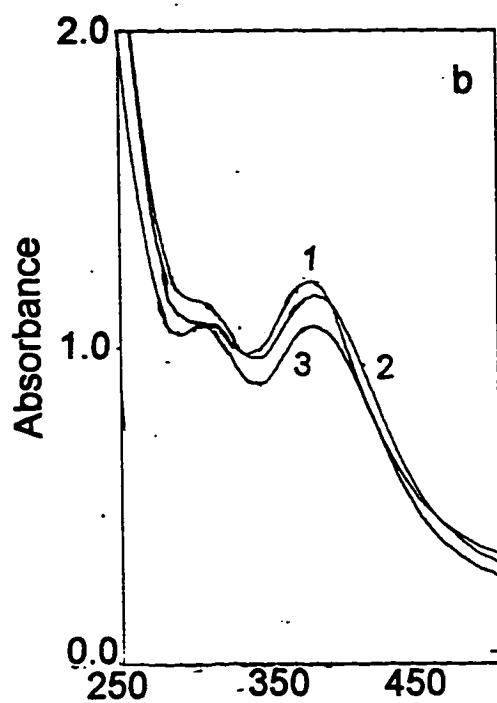
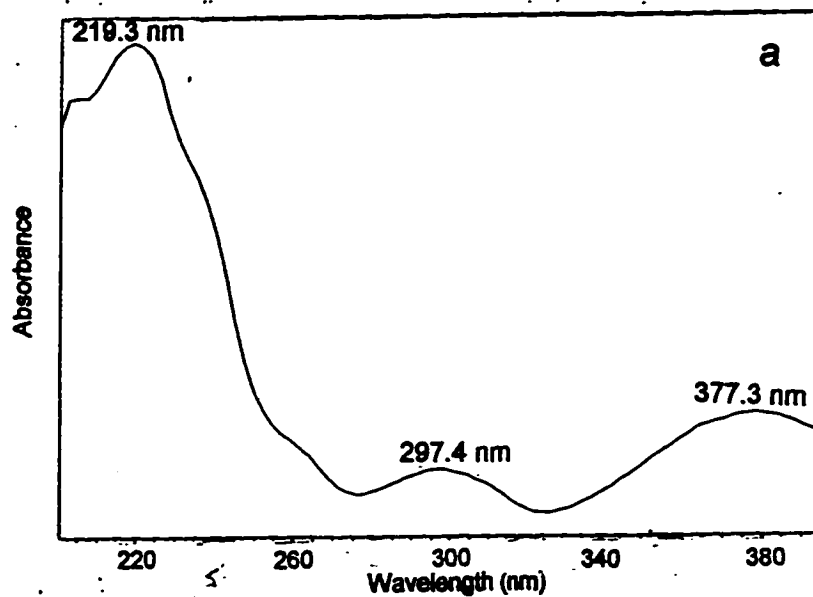


Figure 4-6. a) UV/vis spectrum of the major product in the chromatogram in Figure 4-5. b) UV/vis spectrum of the precipitate of the reaction of luminol and HOBr in water. 1) 1:1 luminol:HOBr; 2) 1:2 luminol:HOBr; 3) 1:10 luminol:HOBr.

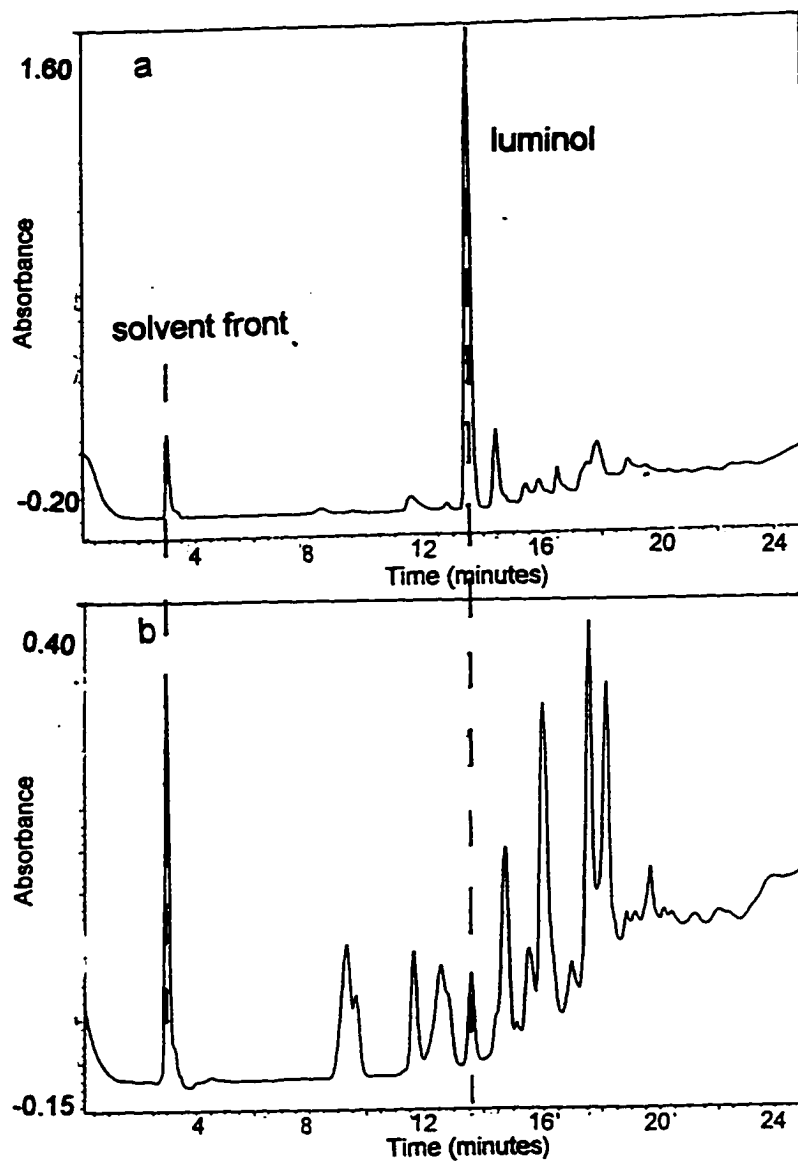


Figure 4-7. HPLC chromatograms at 230 nm of the products of the reaction of luminol plus HOBr at pH 5.7. Reaction conditions: 0.7 mM luminol, 0.1 M KBr in 0.1 M phosphate pH 5.7 a) 0.7 mM HOBr; b) 2.1 mM HOBr.

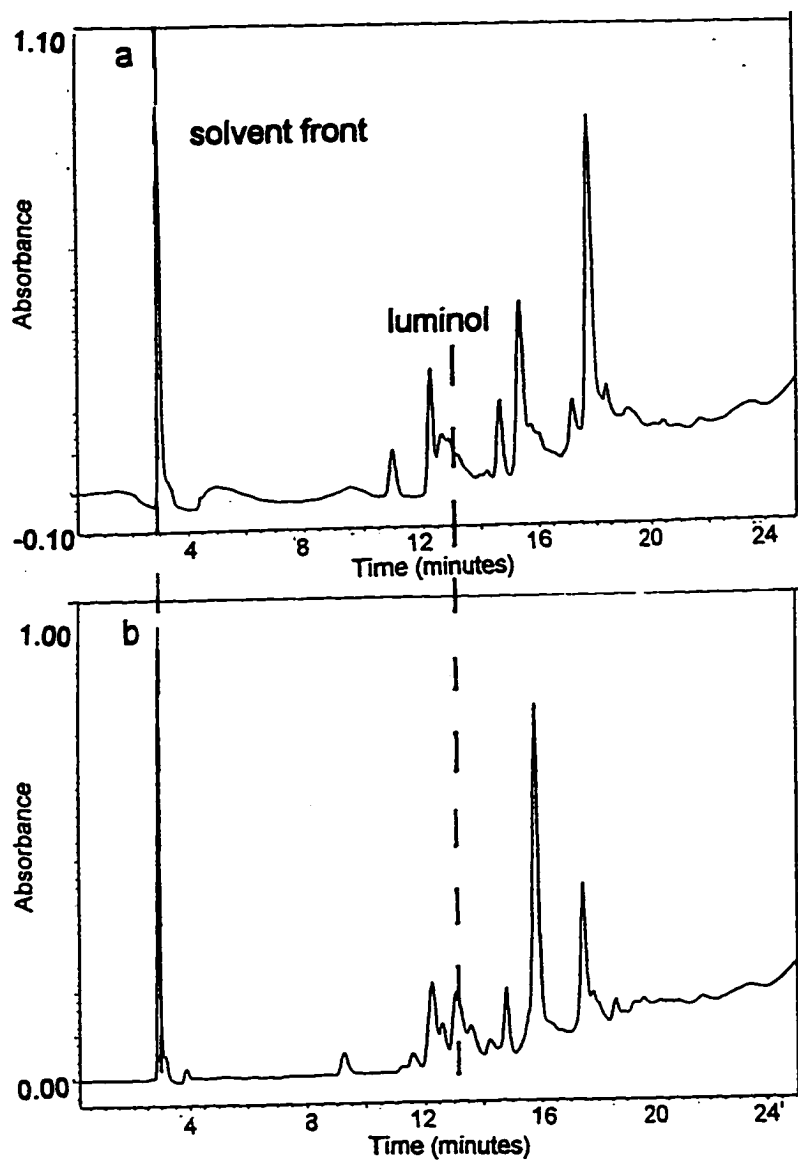


Figure 4-8. HPLC chromatograms at 230 nm of the reaction mixture of luminol, V-BrPO, H_2O_2 , and KBr at pH 8.0. Conditions: 30 mM V-BrPO, 1.4 mM luminol, 0.1 M KBr, in 0.1 M phosphate pH 8.0, a) 1.4 mM H_2O_2 ; b) 4.2 mM H_2O_2 .

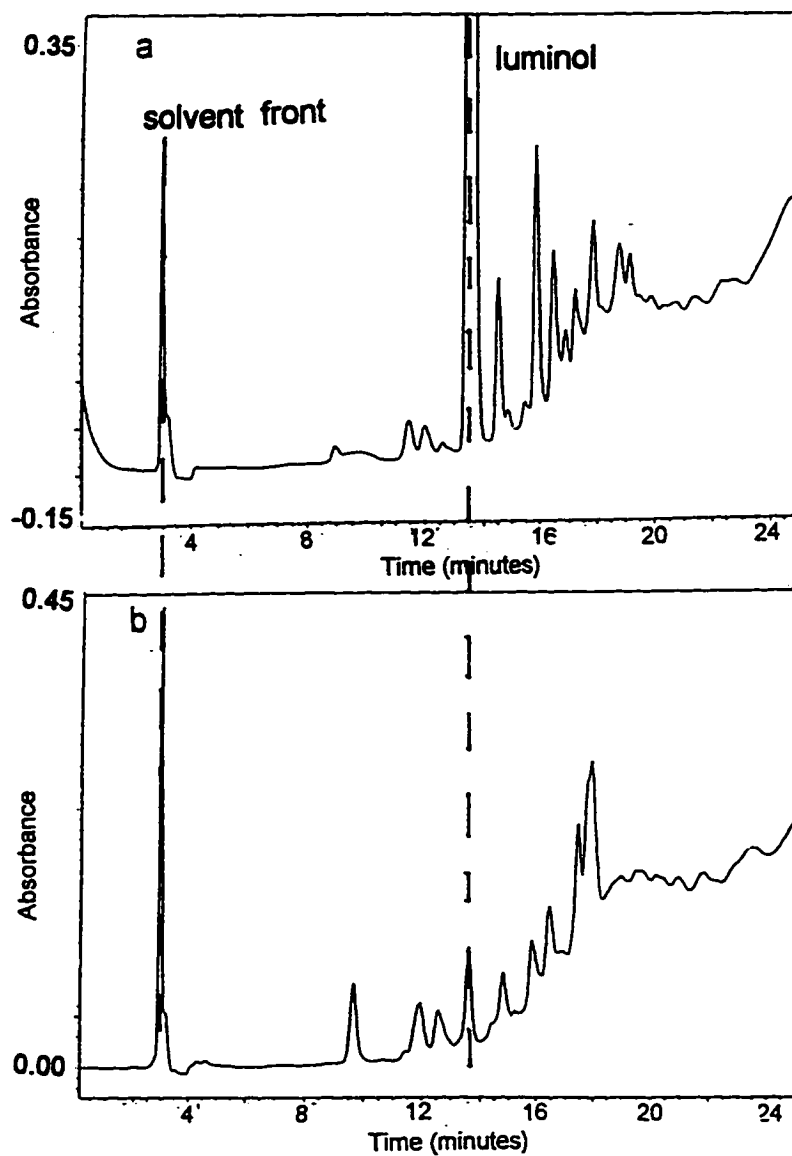


Figure 4-9. HPLC chromatograms at 230 nm of the products of the reaction of luminol plus HOBr at pH 8.0. Reaction Conditions: 1.4 mM luminol, 0.1 M KBr in 0.1 M phosphate pH 8.0 a) 1.4 mM HOBr; b) 4.2 mM HOBr.

large peak at 13.5 minutes in the 1:1 luminol:HOB_r reaction corresponds to unreacted luminol.

A standard of 3-aminophthalic acid had a retention time of 10 minutes when run on the 50% A to 0% A gradient (Figure 4-10). This compound appeared as a minor product in the HPLC traces of both the enzymatic and chemical reactions at both pH values tested. However, at pH 8.0, where the enzyme reaction with luminol produces the most luminescence, the 3-aminophthalate peak is minor compared to the brominated luminols at 18 minutes and the unidentified products between 14 and 16 minutes (Figure 4-8). The HPLC data presented here suggest that a species other than the 3-aminophthalate dianion should be considered as a possible source of the luminescence of the V-BrPO/H₂O₂/bromide/luminol reaction system.

Reaction of Brominated Luminols with Hypochlorite

It was of interest to determine if the brominated luminol products were capable of undergoing luminescence/oxidation chemistry like that of luminol itself. When excess HOCl was added to the brominated luminols in ethanol, no visible luminescence occurred. The addition of HOCl to luminol, in contrast, causes a rapid burst of blue light. The absence of visible luminescence from the reaction of HOCl and the brominated compounds is most likely due to the so-called "heavy atom effect" in which the presence of a heavy atom, in this case bromine,

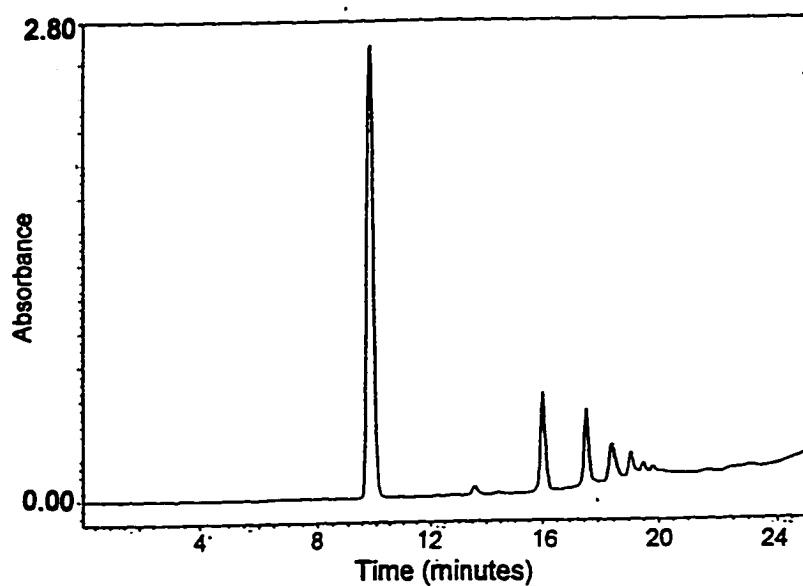


Figure 4-10. HPLC chromatogram at 230 nm of 3-aminophthalic acid.

results in a decrease in the fluorescence quantum yield and a concurrent increase in the phosphorescence quantum yield (Turro, 1978).

Mass spectrometric analysis of the products of HOCl plus the brominated luminols revealed three major products, including a peak at $M+1 = 383$ m/z, two peaks corresponding to a singly brominated species at 461 and 463 m/z, and three m/z (Figure 4-11). Each of these products has masses that are 205 mass units higher than luminol, monobromoluminols, and dibromoluminol, respectively.³

While the reaction of HOCl with bromoluminols did not have the striking emission of light seen with luminol, the reaction likely followed a pathway known for luminol. As described in the Introduction to this chapter and in Scheme 4-2, two one-electron oxidations of luminol can result in the formation of 'L', a diazaquinone, which can then react with a nucleophile such as H_2O_2 to generate an adduct, i.e., LOOH. Other nucleophiles, such as hydroxy anion or even luminol itself can react with 'L' (Merenyi et al., 1986, 1990). The product of the reaction of the diazaquinone with luminol has not been identified. In the reaction described here between HOCl and the luminol products, luminol was most likely oxidized, and luminol, monobromoluminol(s) and dibromoluminol were the resident nucleophiles.

³ The added mass likely corresponds to the addition of both a diazaquinone and two oxygens to the three species. Possible reactions are described in the following paragraph. However, to date no structure has been determined that matches the mass spectral data.

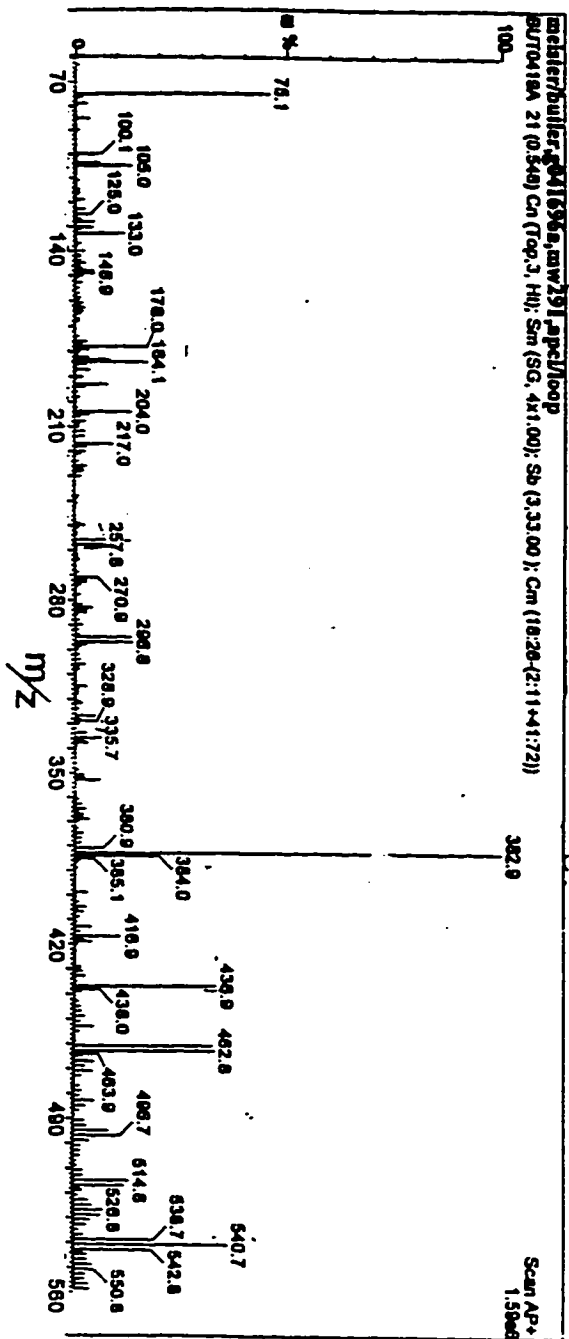


Figure 4-11. Positive APCI mass spectrum of the product of the reaction of
 "bromoluminol"--luminol, monobromoluminol, and dibromoluminol--with excess
 HOCl.

The absence of tri- and tetrabrominated species suggests that the brominated luminols were not themselves oxidized to diazaquinones, which could then react with nucleophiles. Thus, while the brominated luminols are effective nucleophiles, they undergo oxidation more slowly than luminol itself.

Kinetic Competition Experiments

Substrate competition experiments between luminol and phenol red at pH 6.5. As referred to in the Introduction to this chapter, recent studies by Tschirret-Guth and Butler (1994) comparing the bromination of 2-phenylindole and phenol red catalyzed by V-BrPO demonstrated that 2-phenylindole essentially halted phenol red bromination until the indole had been completely consumed. Upon consumption of the indole, the rate of phenol red bromination was identical to that in the absence of the indole. However, in a control experiment, the rate of bromination of phenol red by added HOBr decreased with added 2-phenylindole. This data suggests that V-BrPO is not simply releasing free HOBr *into solution* in the presence of 2-phenylindole; it is evidence that 2-phenylindole is interacting with the enzyme and accordingly being preferentially brominated over phenol red. .

To examine if luminol also interacts with V-BrPO, a substrate competition experiment was undertaken with luminol and phenol red. Under conditions of 3 nM V-BrPO, 0.5 mM H₂O₂, 50 mM KBr, and 25 μM phenol red in 0.1 M phosphate buffer pH 6.5, the introduction of luminol in net 25 μM aliquots showed

an increasing lag phase in the bromination of phenol red at 596 nm. After the lag phase, the rate of bromination (i.e., the slope of absorbance versus time at 596 nm) was very similar to that in the absence of luminol (Figure 4-12a). The results of this experiment were compared to the reaction of aqueous bromine with phenol red and luminol. Under conditions of 50 mM KBr, 25 μ M phenol red, 0.1 M phosphate pH 6.5 and 20 μ L additions of 1.9 mM HOBr to the 3 mL reaction volume every thirty seconds, the inclusion of luminol in net 25 μ M amounts only changed the slope of phenol red bromination at 596 nm (Figure 4-12b). Phenol red bromination was not preceded by the lag phase corresponding to luminol bromination. Thus luminol is interacting with V-BrPO and is preferentially brominated over phenol red, which does not interact with the enzyme.

Competition between luminol bromination and dioxygen evolution at pH 6.5. The substrate behavior of luminol was also studied by oxygen evolution measurements. As shown in Scheme 4-4 above, after the rate limiting step of 'Br[•]' formation in the V-BrPO-mediated catalysis of the reaction of hydrogen peroxide and bromide, the 'Br[•]' intermediate can proceed through one of two competitive pathways: either interaction with a substrate or reaction with a second equivalent of H₂O₂ to generate singlet oxygen. If luminol interacts with the enzyme and essentially prevents the diffusion of HOBr into solution, one would expect that the dioxygen evolution pathway would be blocked. Under conditions of 7.5 nM V-

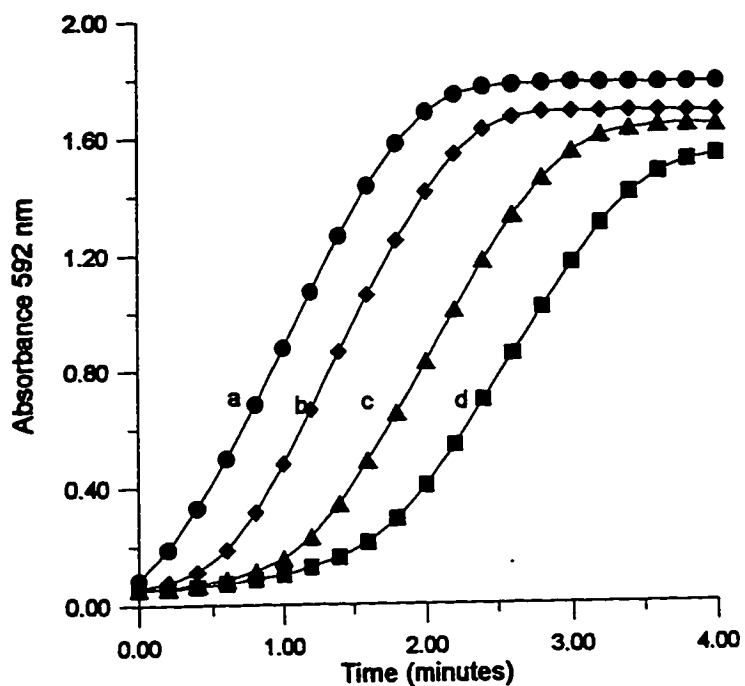


Figure 4-12a. Bromination of phenol red catalyzed by V-BrPO at pH 6.5 at varied luminol concentration. Conditions: 8.0 nM V-BrPO, 0.5 mM H₂O₂, 50 mM KBr, 25 μM phenol red, a) 0 μM luminol; b) 25 μM luminol; c) 50 μM luminol; d) 75 μM luminol in 0.1 M phosphate pH 6.5.

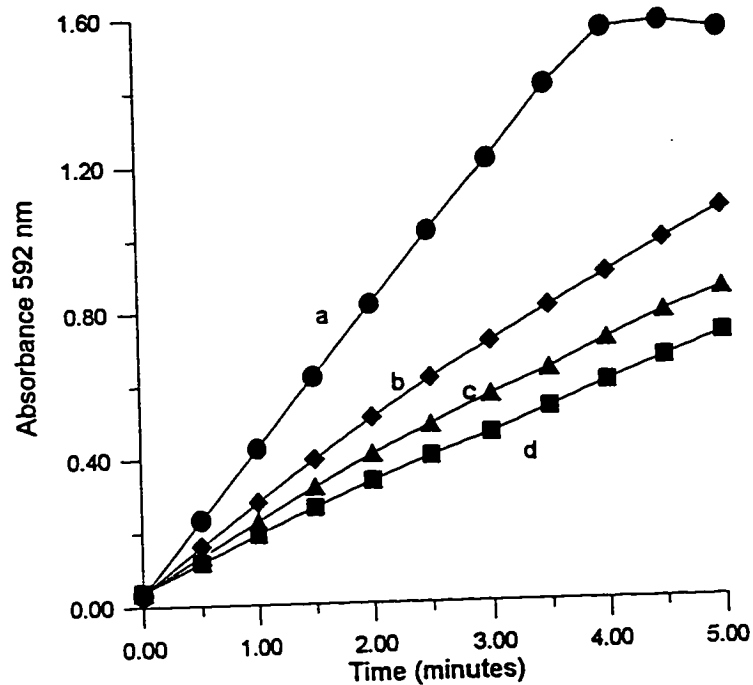


Figure 4-12b. Bromination of phenol red by HOBr at pH 6.5 at varied luminol concentration. Conditions: 50 mM KBr, 25 μM phenol red, a) 0 μM luminol; b) 25 μM luminol; c) 50 μM luminol; d) 75 μM luminol in 0.1 M phosphate pH 6.5. 20 μl of 1.9 mM HOBr was added every 30 seconds prior to spectrophotometric measurement. Absorbance values were corrected for the volume increase.

BrPO, 9.7 mM H₂O₂, and 0.1 M KBr in 0.1 M phosphate buffer pH 6.5, increasing the luminol concentration from 0 to 400 μM resulted in a decrease in the rate of oxygen evolution to approximately 10% of the original value (Figure 4-13).

However, if the dioxygen evolution of the parallel reaction with HOBr was monitored, the effect of increasing luminol concentration was minimal. Under conditions of 0.1 M KBr, 9.7 mM H₂O₂, 0.1 M phosphate buffer pH 6.5, the addition of a stock solution of 3.3 mM HOBr by syringe pump at an approximate rate of 50 μM/min produced a rate of dioxygen evolution similar to the V-BrPO reaction in the absence of luminol but was only slightly decreased by the addition of up to 400 μM luminol. The minor decrease was most likely due to the reaction of HOBr plus luminol. These results of the chemical and enzymatic oxygen evolution experiments are both displayed in Figure 4-13.

pH dependence of the kinetic competition between luminol and phenol red.

While the results above indicate that luminol interacts with V-BrPO at pH 6.5, V-BrPO was most effective as a reporter enzyme in immunoassays with luminol as the substrate at pH ~8 (Friedman et al., 1995). This *apparent* discrepancy prompted an investigation into the pH dependence of the substrate specificity of V-BrPO for luminol. Accordingly, the phenol red competition experiments originally executed at pH 6.5 were carried out at pH values of 5.7, 7.2, and 8.1. Under conditions of 50 mM KBr, 25 μM phenol red, 0.1 M phosphate buffer pH 5.7, and either 5.0 nM

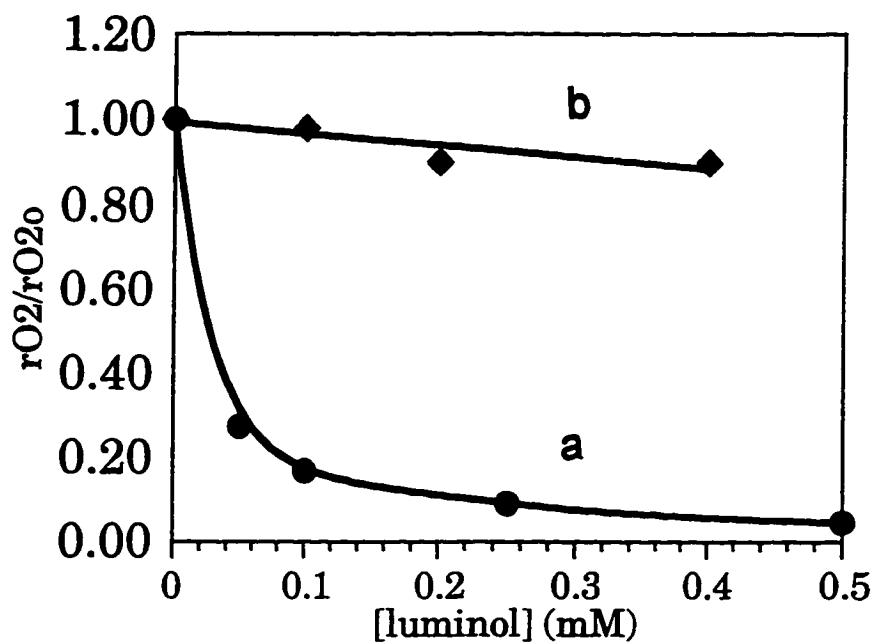


Figure 4-13. Dioxygen formation from the disproportionation of hydrogen peroxide at pH 6.5 a) catalyzed by V-BrPO and b) by reaction with added HOBr at varied luminol concentration. Conditions: 0.1 M KBr, 10 mM H_2O_2 , 0 to 0.4 mM luminol, 0.1 M phosphate pH 6.5, a) 7.5 nM V-BrPO or b) addition of 3.3 mM HOBr by syringe pump at a rate of $\sim 50 \mu M/min$.

V-BrPO and 0.5 mM H₂O₂ or 5 μL additions of 4.4 mM HOBr to a 1 mL reaction every 30 seconds, the phenol red bromination traces were qualitatively similar to that seen at pH 6.5 for both reactions given that different concentrations of V-BrPO were used (Figure 4-14). In fact, the lag phase of phenol red bromination in the enzymatic reaction in the presence of increasing luminol was perhaps more distinct at pH 5.7. However, as the pH was increased to 7.2 (Figure 4-15) and 8.1 (Figure 4-16), the substrate behavior of luminol became less specific. In particular, under conditions of 50 mM KBr, 25 μM phenol red, 0.5 mM H₂O₂, and 15 nM V-BrPO in phosphate buffer at pH 8.1,⁴ the lag phase in the phenol red bromination with increasing luminol is not flat; it is more of a concave upward slope (Figure 4-16). However, the slopes of the phenol red bromination at different luminol concentrations are still very similar after the initial lag phase. Additionally, regardless of pH the traces from the enzymatic reaction are different from the HOBr reactions. As was observed at pH 6.5, the inclusion of luminol in the reaction changed the slope of the phenol red bromination by HOBr at the other pH values tested and did not cause a lag phase as was observed in the enzymatic reactions. The drop in the absorbance at 596 nm with increasing number of HOBr additions is

⁴ Recent evidence from Johnson and Johnson Clinical Diagnostics (Rochester, NY) indicates that H₂O₂ may be inhibiting at higher pH at micromolar levels (Friedman et al., 1995). This behavior is currently under investigation. Previous experiments in our laboratory by Soedjak (1991) indicated that H₂O₂ was only inhibiting at high pH at *millimolar* levels. The experiments presented in this chapter were all performed at non-inhibiting hydrogen peroxide concentrations according to the results of Soedjak.

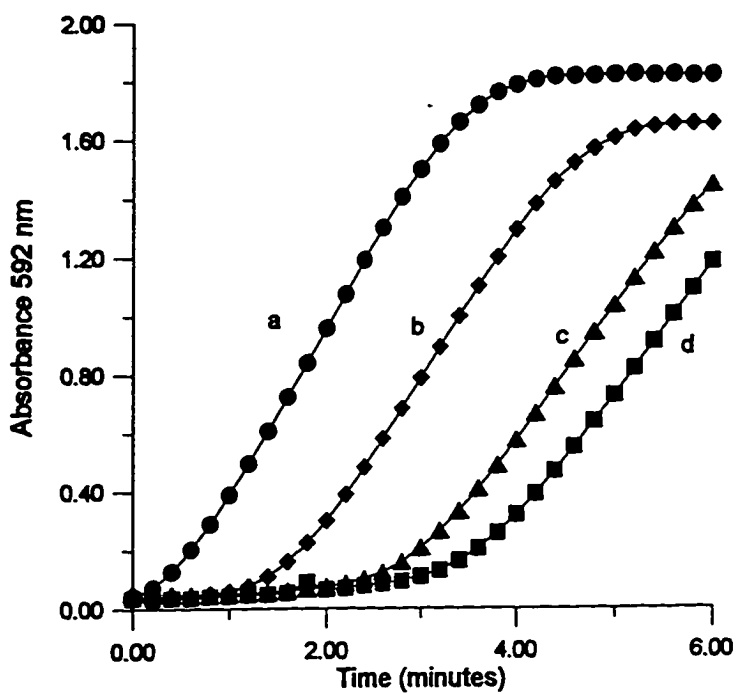


Figure 4-14a. Bromination of phenol red catalyzed by V-BrPO at pH 5.7 at varied luminol concentration. Conditions: 5.0 nM V-BrPO, 0.5 mM H₂O₂, 50 mM KBr, 25 μ M phenol red, a) 0 μ M luminol; b) 25 μ M luminol; c) 50 μ M luminol; d) 75 μ M luminol in 0.1 M phosphate pH 5.7.

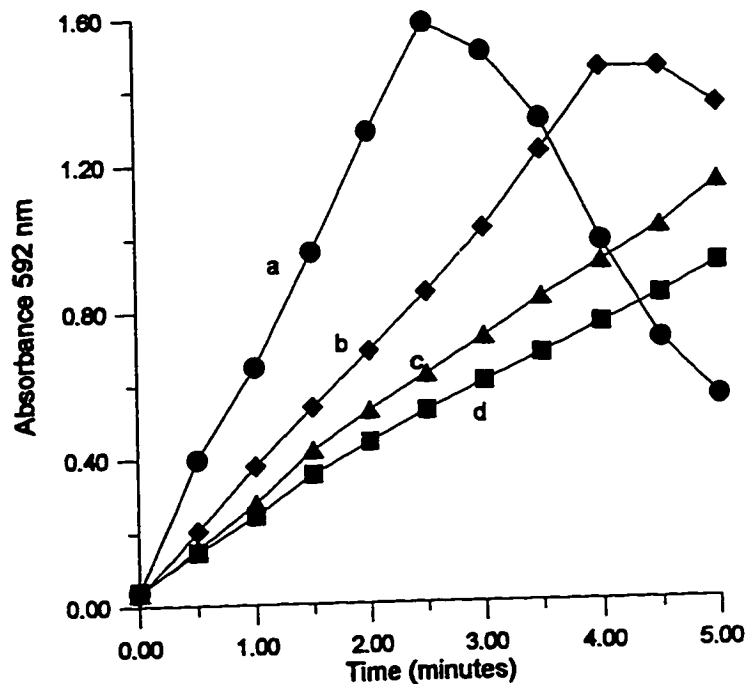


Figure 4-14b. Bromination of phenol red by HOBr at pH 5.7 at varied luminol concentration. Conditions: 50 mM KBr, 25 μ M phenol red, a) 0 μ M luminol; b) 25 μ M luminol; c) 50 μ M luminol; d) 75 μ M luminol in 0.1 M phosphate pH 5.7. 5 μ l of 4.4 mM HOBr was added every 30 seconds prior to spectrophotometric measurement. Absorbance values were corrected for volume increase.

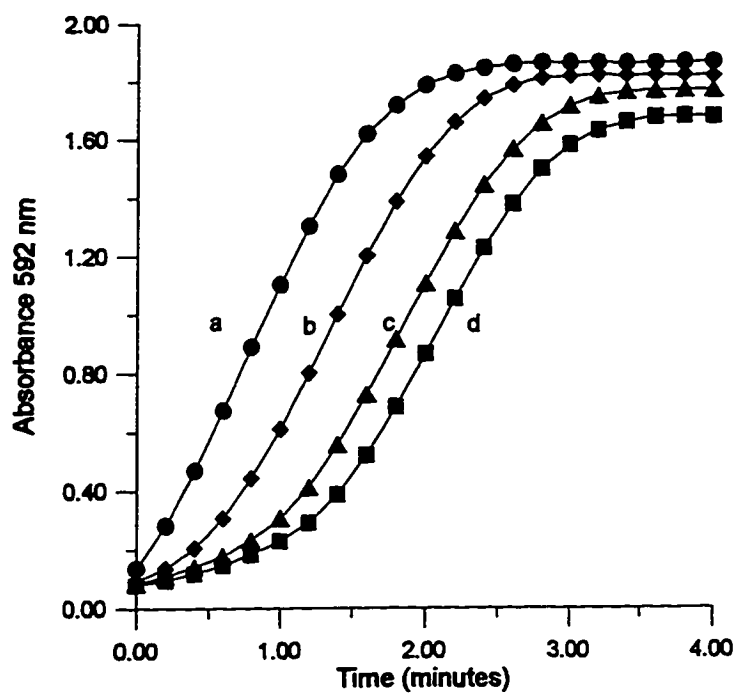


Figure 4-15a. Bromination of phenol red catalyzed by V-BrPO at pH 7.2 at varied luminol concentration. Conditions: 10.0 nM V-BrPO, 0.5 mM H₂O₂, 50 mM KBr, 25 μM phenol red, a) 0 μM luminol; b) 25 μM luminol; c) 50 μM luminol; d) 75 μM luminol in 0.1 M phosphate pH 7.2.

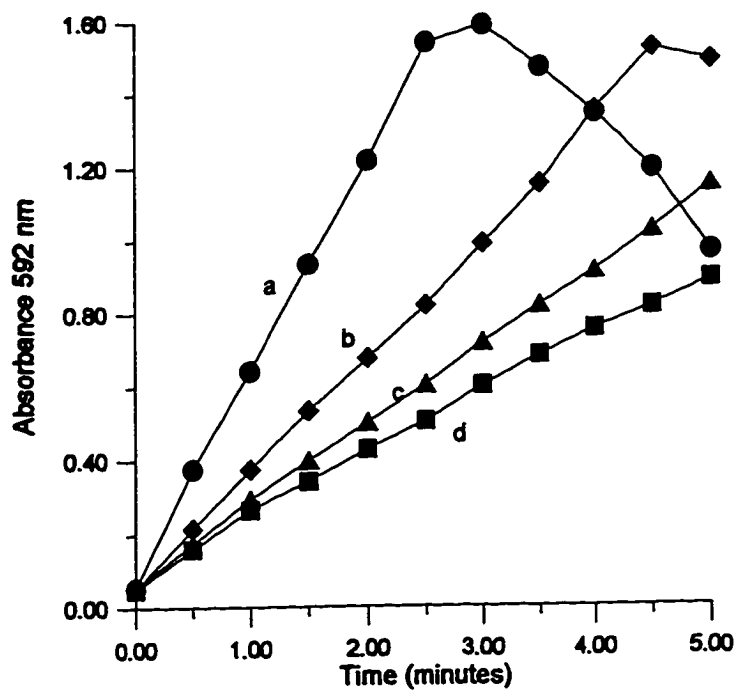


Figure 4-15b. Bromination of phenol red by HOBr at pH 7.2 at varied luminol concentration. Conditions: 50 mM KBr, 25 μM phenol red, a) 0 μM luminol; b) 25 μM luminol; c) 50 μM luminol; d) 75 μM luminol in 0.1 M phosphate pH 7.2. 5 μl of 4.4 mM HOBr was added every 30 seconds prior to spectrophotometric measurement. Absorbance values were corrected for volume increase.

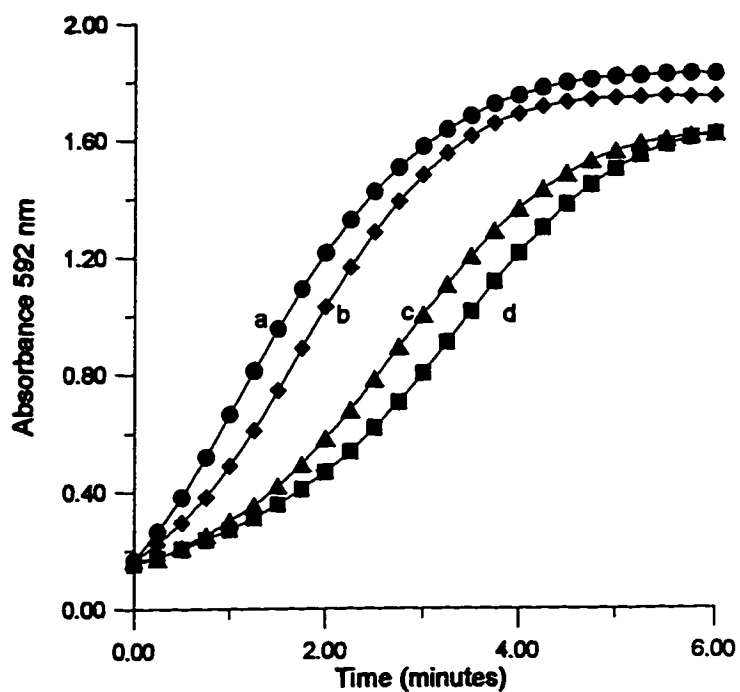


Figure 4-16a. Bromination of phenol red catalyzed by V-BrPO at pH 8.1 at varied luminol concentration. Conditions: 15.0 nM V-BrPO, 0.5 mM H_2O_2 , 50 mM KBr, 25 μM phenol red, a) 0 μM luminol; b) 25 μM luminol; c) 50 μM luminol; d) 75 μM luminol in 0.1 M phosphate pH 8.1.

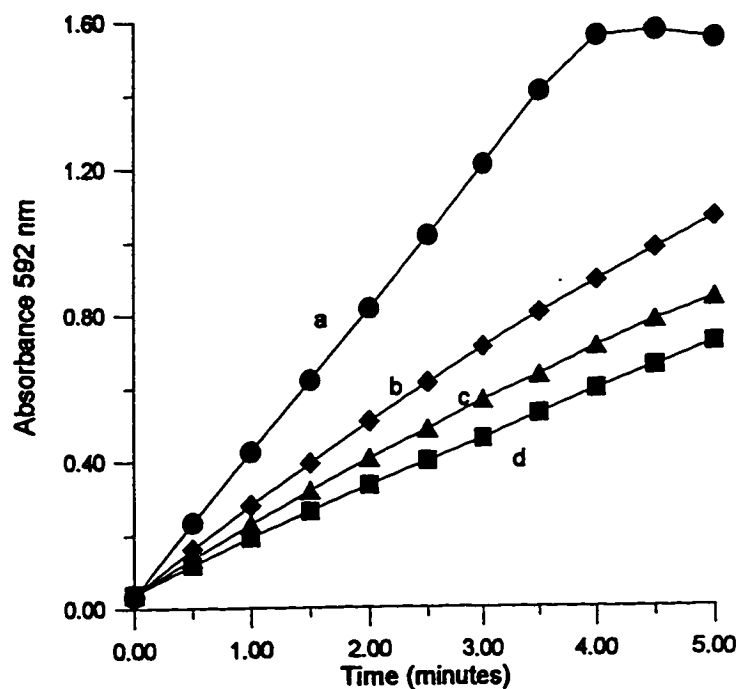


Figure 4-16b. Bromination of phenol red by HOBr at pH 8.1 at varied luminol concentration. Conditions: 50 mM KBr, 25 μ M phenol red, a) 0 μ M luminol; b) 25 μ M luminol; c) 50 μ M luminol; d) 75 μ M luminol in 0.1 M phosphate pH 8.1. 5 μ l of 4.4 mM HOBr was added every 30 seconds prior to spectrophotometric measurement. Absorbance values were corrected for volume increase.

not yet understood. Regardless, these experiments demonstrate that while luminol is interacting with V-BrPO over the range of pH values utilized, the interaction appears to be weaker at higher pH.

Although the rates of phenol red bromination were very similar after the lag phase in the enzymatic reaction, careful examination of Figures 4-12a, 4-14a, 4-15a, and 4-16a reveals that the rates did decrease slightly relative to the rate without added luminol with increasing luminol concentration at all pH values studied. On going from 0 to 75 μM luminol, the rate of phenol red bromination at pH 6.5 decreased by 18%, the rate at pH 5.7 decreased by 21%, the rate at pH 7.2 decreased by 30%, and the rate at pH 8.1 decreased by 27%. To test if the products of the luminol reaction were inhibiting the bromination of phenol red, previously prepared "bromoluminols" were included in the phenol red reaction. Under conditions of 6 nM V-BrPO, 25 μM phenol red, 0.5 mM H_2O_2 , and 50 mM KBr in 0.1 M phosphate pH 5.7, the slope corresponding to phenol red bromination measured from 1.0 minute to 2.2 minutes was 0.631 Abs/min at 596 nm. However, if approximately 25 μM bromoluminols was also included with all other conditions identical, the slope, measured in this case from 1.2 minutes to 2.4 minutes, was reduced to 0.587 Abs/min, a decrease of 7% (Figure 4-17). The interference in phenol red bromination is most likely due to the bromination of monobromoluminols to form dibromoluminol. Because this second bromination of

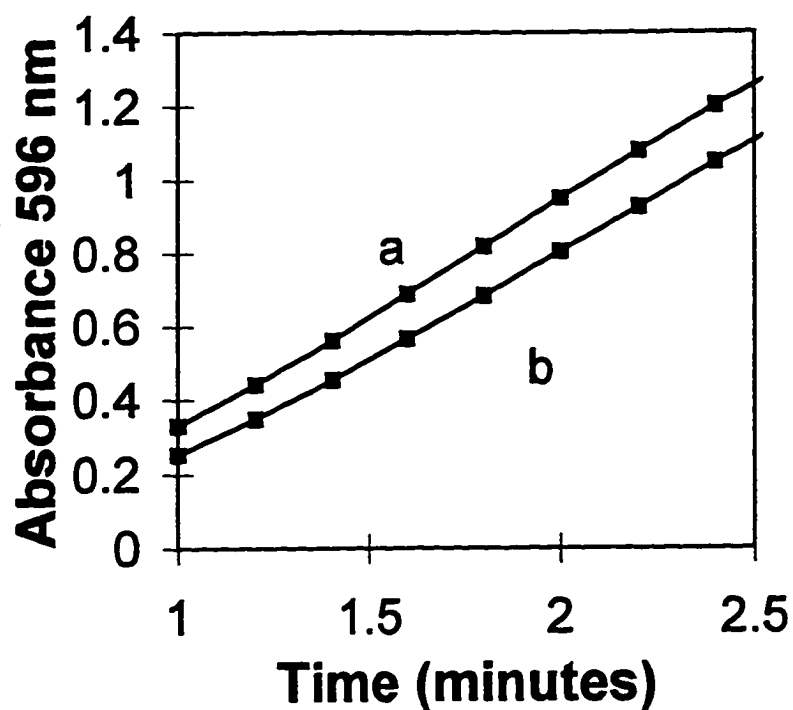


Figure 4-17. Change in the rate of phenol red bromination in the presence of bromoluminols. Conditions: 6 nM V-BrPO, 25 μM phenol red, 0.5 mM H_2O_2 , 50 mM KBr, in 0.1 M phosphate pH 5.7 a) 0 μM bromoluminols; b) $\sim 25 \mu\text{M}$ bromoluminols.

luminol results in a slope change like that seen for the substrate competition studies with aqueous bromine, monobromoluminol likely do not interact strongly with vanadium bromoperoxidase.

pH dependence of the kinetic competition between luminol bromination and dioxygen evolution. The pH dependence of the substrate specificity of V-BrPO and luminol was also investigated by monitoring dioxygen evolution at different pH values. Under conditions of 0.1 M KBr, 10 mM H₂O₂, 6.0 nM V-BrPO, 0.1 M phosphate pH 5.7, and 200 μM luminol, the rate of dioxygen evolution decreased to only 10% of the value in the absence of luminol (Figure 4-18a). When the pH was increased to a value of 8.1, under conditions of 0.1 M KBr, 10 mM H₂O₂, and 37 nM V-BrPO in 0.1 M phosphate, the rate of oxygen evolution only decreased to ~75% of the rate in the absence of luminol (Figure 4-18d). Thus, as seen for the phenol red competition experiments, the preference of V-BrPO for luminol is strongest at lower pH under the conditions used for the oxygen evolution experiments. It should be noted for Figure 4-18 that the concentration of V-BrPO was increased with increasing pH so that the initial rate of dioxygen evolution in the absence of luminol was similar at each pH value studied.

Calculation of K_{app}

A plot of $r_{O_2}/r_{O_2_0}$, where $r_{O_2_0}$ is the rate of dioxygen evolution in the absence of luminol and r_{O_2} is the rate of dioxygen evolution in the presence of

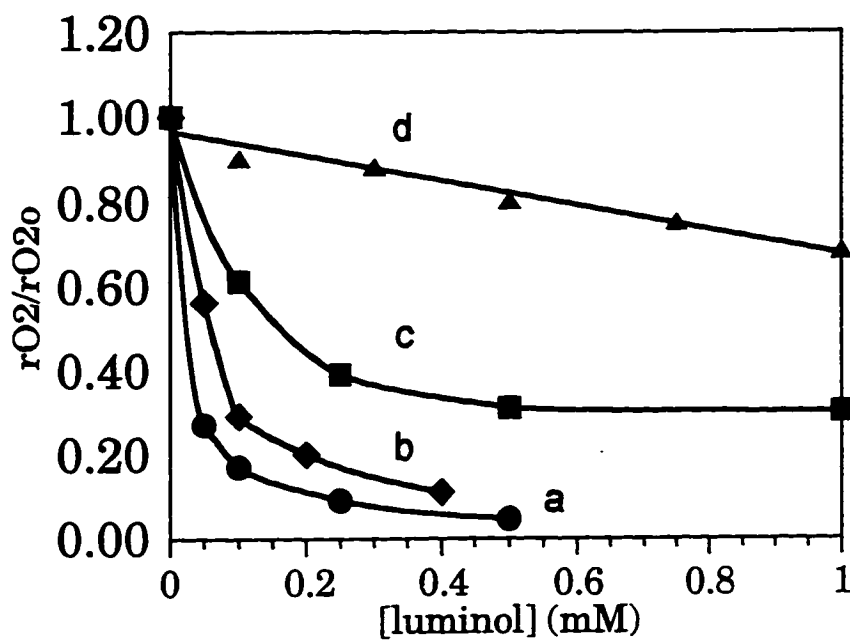


Figure 4-18. Formation of dioxygen catalyzed by V-BrPO at varied luminol concentration and varied pH. Conditions: 0.1 M KBr, 10 mM H₂O₂, a) 6.0 nM V-BrPO, 0.1 M phosphate pH 5.7; b) 7.5 nM V-BrPO, 0.1 M phosphate pH 6.5; c) 15.0 nM V-BrPO, 0.1 M phosphate pH 7.2; d) 37.0 nM V-BrPO, 0.1 M phosphate pH 8.1.

luminol, versus the concentration of luminol is linear at all pH values studied and can be expressed by the relation in equation 4:

$$\frac{rO_{2o}}{rO_2} = 1 + K_{app}[S] \quad (4)$$

If the enzyme mechanism presented in Scheme 4-4 is accurate, K_{app} is equal to K_s , the binding constant for luminol to V-BrPO. Plots of rO_{2o}/rO_2 versus luminol concentration for all four pH values studied (Figure 4-19) yielded K_{app} values, which decrease with increasing pH, in agreement with the decrease in selectivity at higher pH (Figure 4-19 inset).

Table 4-1. Binding and dissociation constants for luminol and V-BrPO at different pH values calculated from dioxygen evolution data.

pH	K_{app} (K_s)	K_d ($= 1/K_s$)
5.7	$4.05 \times 10^4 M^{-1}$	24.7 μM
6.5	$2.02 \times 10^4 M^{-1}$	49.5 μM
7.2	$2.19 \times 10^3 M^{-1}$	456 μM
8.1	$4.35 \times 10^2 M^{-1}$	2299 μM

Fluorescence Quenching of Luminol by V-BrPO

In order to determine whether the specificity of V-BrPO for luminol is due to the binding of luminol to the enzyme, the quenching of luminol fluorescence by V-BrPO was investigated. The fluorescence spectrum of luminol has a maximum emission at 425 nm when excited at 355 nm. Monitoring the fluorescence of the

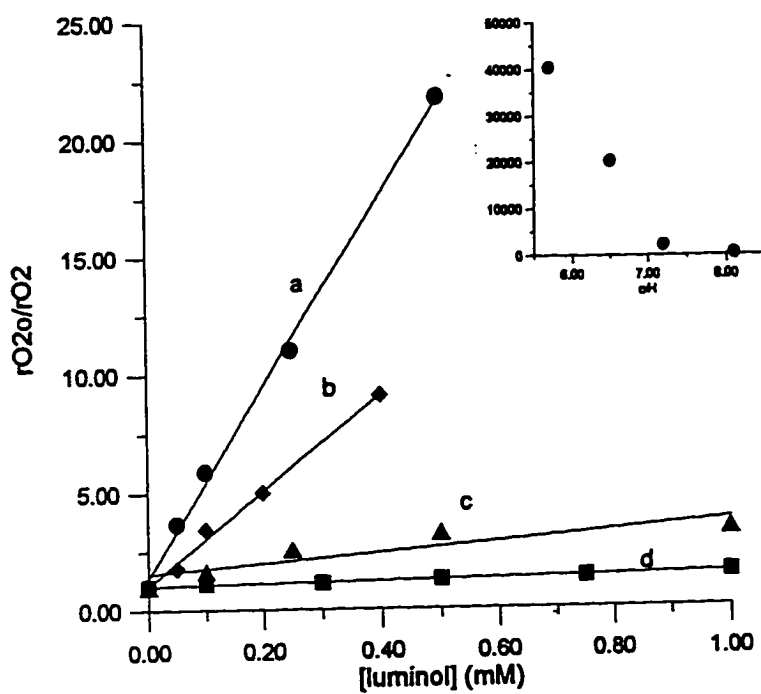


Figure 4-19. Plots of rO_{2o}/rO_2 versus luminol concentration at varied pH. Conditions for a,b,c, and d same as Figure 4-18. Inset: Plot of slopes of a,b,c, and d (K_{app}) versus pH.

luminol at 425 nm under conditions of 3.0 μM luminol in 2 mL phosphate pH 6.4 while introducing 20 μL aliquots of 2 mg/mL V-BrPO (29 μM) showed a marked decrease in the luminol fluorescence with increasing V-BrPO concentration (Figure 4-20). A parallel experiment performed with bovine serum albumin, which is of similar size and molecular weight to V-BrPO, showed less of a decrease in the fluorescence of luminol (Figure 4-21). Changes in fluorescence for both proteins are shown as F/F_0 versus protein concentration in Figure 4-20 where F_0 is the fluorescence in the absence of added protein and F is the fluorescence at the specific protein concentration. This plot demonstrates that V-BrPO is more effective at quenching the luminol fluorescence than the "inert" protein BSA.

A plot F_0/F versus $[E]$ for the experiment with luminol and V-BrPO is nearly linear with a correlation coefficient (R^2) of 0.996 (Figure 4-21a). This line had a slope of $2.62 \times 10^5 \text{ M}^{-1}$, which can approximate the value of the binding constant K_{app} , and a y-intercept of 0.976, which agrees with the expected intercept value of 1 according to equation 1. The dissociation constant K_d for luminol to V-BrPO is described by equation 2:

$$K_d = \frac{[E][S]}{[ES]} = 1/K_{app} \quad (2)$$

where $[E]$ is the enzyme concentration, $[S]$ is the luminol equation, $[ES]$ is the concentration of the enzyme-substrate complex, and K_{app} is the slope of the Stern-

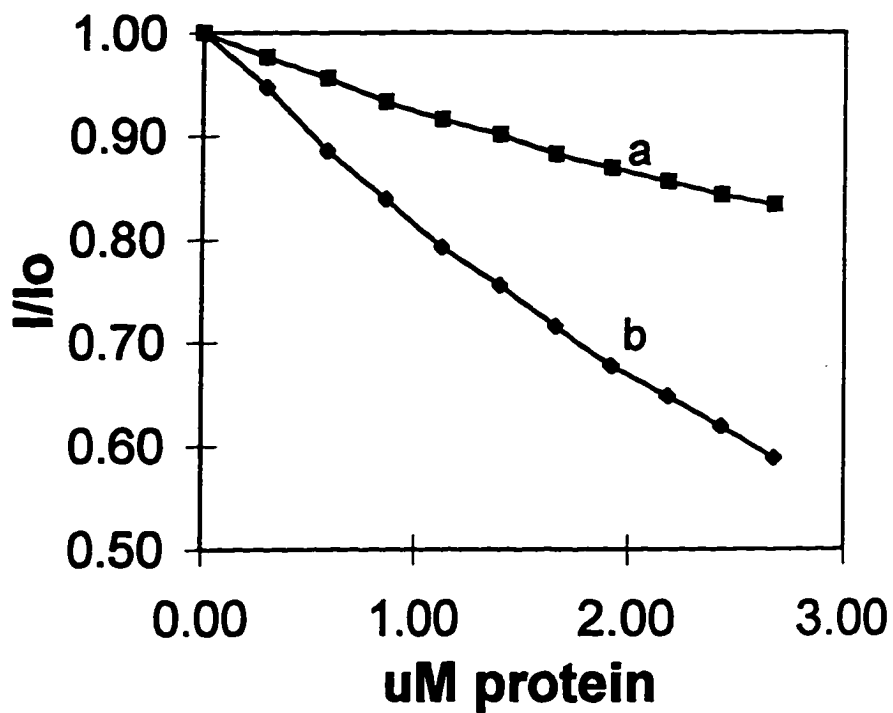


Figure 4-20. Quenching of luminol fluorescence at 425 nm by BSA and V-BrPO at pH 6.5 . Conditions: 2.0 μ M luminol in 3.0 ml 0.1 M HEPES pH 6.5, 20 μ L additions of 30 μ M BSA (a) or V-BrPO (b). Excitation Wavelength 355 nm, Ex. Slit 2.5 nm, Em. Slit 2.5 nm.

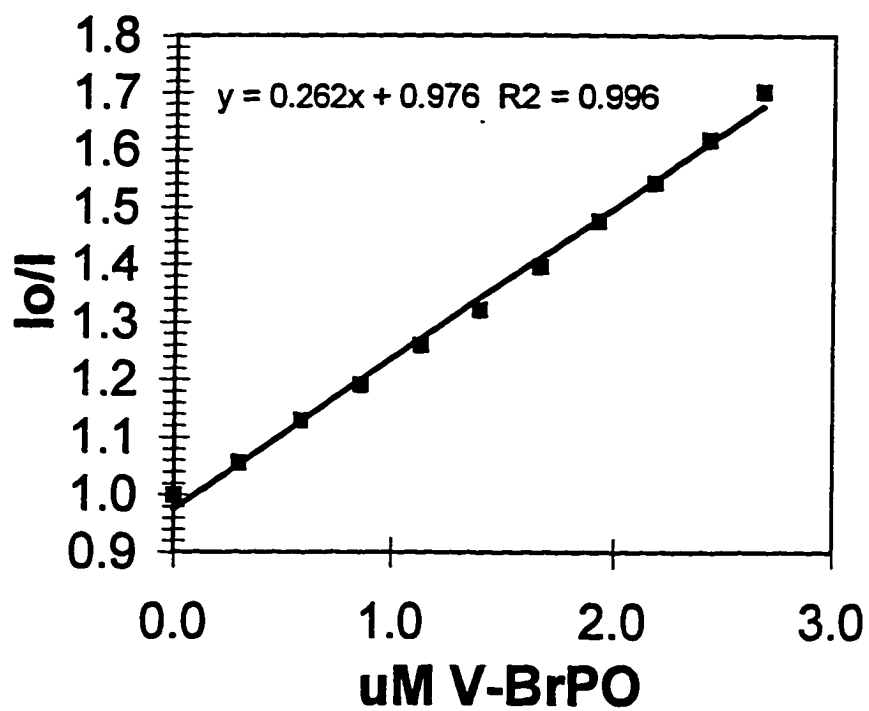


Figure 4-21. Modified Stern-Volmer plot of the quenching of luminol fluorescence at 425 nm by V-BrPO at pH 6.5. Conditions same as Figure 4-19.

Volmer plot. The dissociation constant of luminol to V-BrPO was determined to be 3.8 μM at pH 6.4⁵.

As was achieved above in the substrate competition experiments between phenol red and luminol, the pH dependence of the binding of luminol was of interest, as the immunoassay with V-BrPO functions best at higher pH. However, while fluorescence quenching experiments were attempted at pH 8.1, the fluorescence of luminol is greatly decreased at this pH, particularly as the concentration of luminol is increased. The cause of this decrease is not understood but may involve a self-quenching mechanism. Alternatively, it did not prove possible to design conditions at pH 8.1 under which luminol fluorescence quenching by V-BrPO could be effectively observed. In any case, the confirmation of binding at the lower pH certainly suggests that binding is the mechanism by which luminol is a preferred substrate of V-BrPO.

Luminescence Emission Produced by the V-BrPO/H₂O₂/NaBr/luminol System

Upon identification of the major products of the V-BrPO/H₂O₂/NaBr/luminol system, one question that remained was how the different compounds generated by this system give rise to the luminescence emission of this system versus that of the standard HRP system. Luminescence

⁵ Calculations on the data for BSA and luminol give a value of $7.50 \times 10^4 \text{M}^{-1}$ for K_{app} and a value of 13.3 μM for the dissociation constant.

emission spectra were recorded every minute under conditions of 30.0 nM V-BrPO, 0.6 mM luminol, 1.8 mM H₂O₂, and 0.1 M KBr in 0.1 M phosphate pH 8.0 throughout the course of the reaction after initiation with hydrogen peroxide. The emission spectrum at the beginning of the reaction has a λ_{max} value of 423 nm, which is similar to the spectrum observed for 3-aminophthalate chemiluminescence (Roswell & White, 1973). However, with successive measurements, the λ_{max} value shifts out to 441 nm within approximately 5 minutes and remains there until virtually no more signal is observed at approximately 9 minutes (Figure 4-22). The emission of the HRP-catalyzed oxidation of luminol at 425 nm does not shift (Roswell & White, 1973). One possible explanation for this shift is that luminol is binding slowly to the enzyme and at the beginning of the reaction, much of it is unbound and producing the standard 3-aminophthalate ion (Baxendale, 1973), while later in the reaction, bound luminol is exclusively transformed to a product that luminesces at 441 nm. However, if luminol and V-BrPO incubated for at least 15 minutes prior to initiation of the reaction by addition of hydrogen peroxide, the same luminescence pattern appeared, demonstrating that the shift in the emission spectrum is not due to slow substrate binding.

Another possible cause for the shift in the luminescence profile of the enzyme reaction is contamination of either the luminol or the bromide source. Although high purity photograde NaBr (Eastman Kodak, Inc.) was used, even high

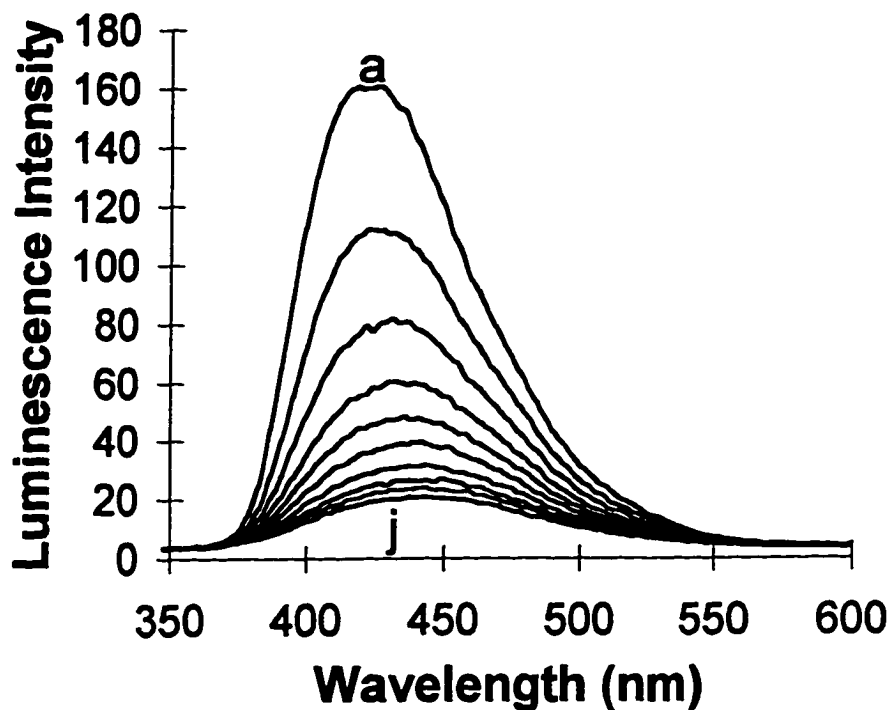


Figure 4-22. Luminescence spectra of the reaction mixture of luminol, V-BrPO, H_2O_2 , and NaBr at pH 8.0. Spectra were recorded every four minutes after initiation with H_2O_2 . Conditions: 6.0 nM V-BrPO, 0.6 mM luminol, 1.8 mM H_2O_2 , 0.1 M photograde NaBr in 0.1 M phosphate pH 8.0. "a" recorded at 0 minutes, "j" recorded at 36 minutes.

purity bromide salts are frequently contaminated with iodide. To test this possibility, luminescence spectra were recorded for the enzymatic reaction with iodide in the presence of luminol under conditions of 0.6 nM V-BrPO, 0.6 mM luminol, 1.8 mM H₂O₂, and 50 mM KI in phosphate pH 8.0. For this reaction, the luminescence emission spectrum at the start of the reaction was extremely weak and had a λ_{max} value of 419 nm. This spectrum did not shift appreciably over time (Figure 4-23). Thus, while it is possible that the more rapid turnover of iodide by V-BrPO causes an initial luminescence burst at lower wavelengths in the bromide turnover reaction, the poor intensity of the iodide reaction suggests that iodide is not a major contributor. Thus the cause of the shift in the luminescence spectrum of the V-BrPO-catalyzed bromination of luminol is not dependent on iodide contamination.

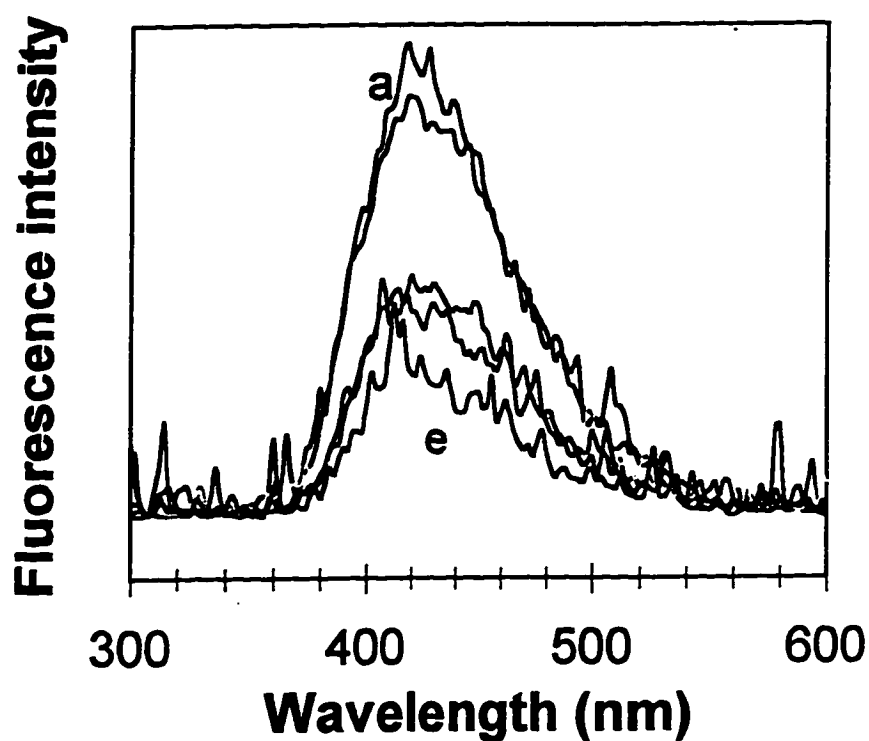


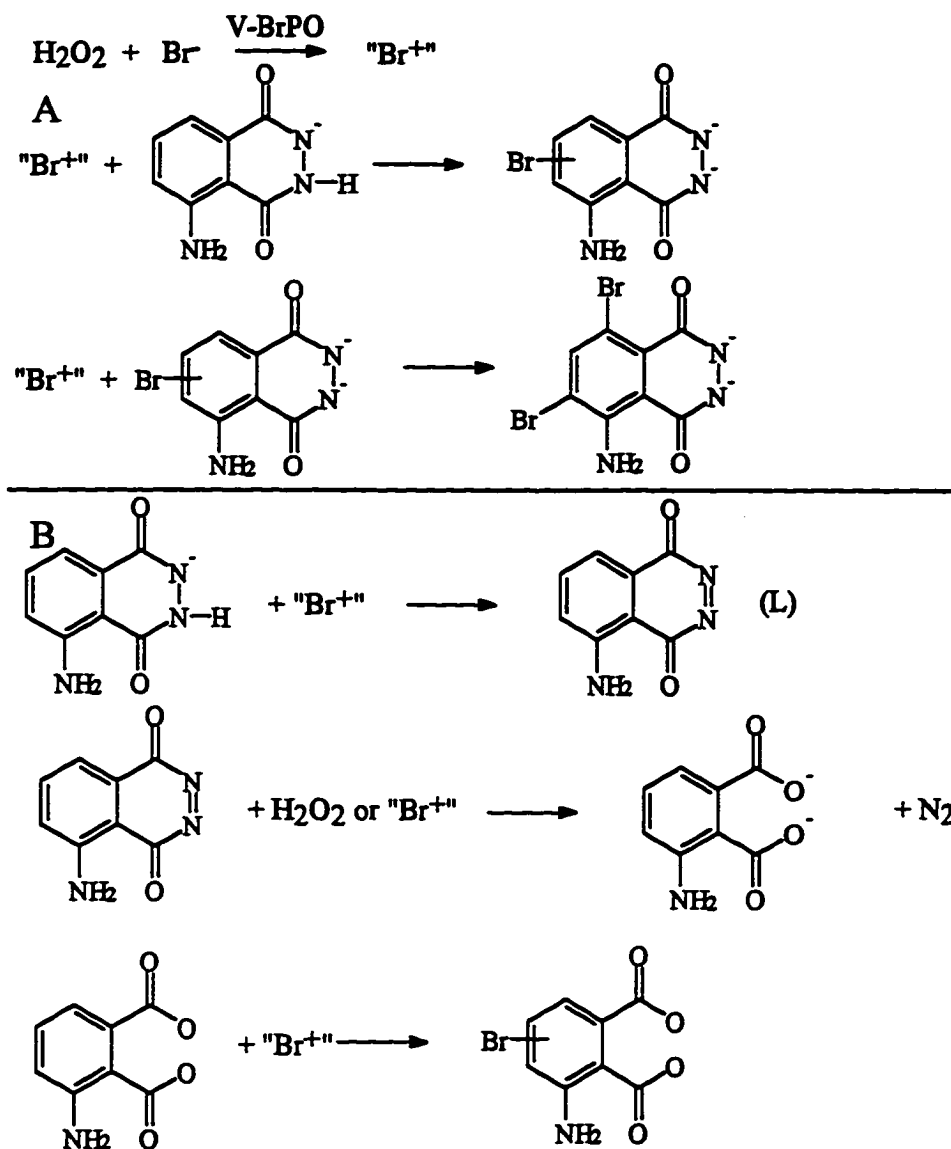
Figure 4-23. Luminescence spectra of the reaction mixture of luminol, V-BrPO, H_2O_2 , and KI at pH 8.0. Spectra were recorded every five minutes after initiation with H_2O_2 . Conditions: 0.6 nM V-BrPO, 0.6 mM luminol, 1.8 mM H_2O_2 , 50 mM KI in 0.1 M phosphate pH 8.0. "a" recorded at 0 minutes, "e" recorded at 20 minutes.

Discussion

In this chapter, an investigation of the luminescent reaction of the V-BrPO/luminol/H₂O₂/bromide system has been described. TLC and HPLC data have shown that, unlike the luminescent reaction of the HRP ELISA system, 3-aminophthalic acid is not a major product of the V-BrPO reaction. The major products of the V-BrPO reaction, which have been identified by mass spectrometry, are mono- and dibrominated luminols. Several unidentified products were present in the HPLC traces in addition to the brominated luminols; these other compounds may be 3-aminophthalate species that are *brominated* or *hydroxylated*.

Possible steps in the V-BrPO-catalyzed luminescent reaction with luminol, hydrogen peroxide, and bromide are proposed in Scheme 4-5. As stated in the Introduction to this chapter, a potentially important difference between the V-BrPO reaction with luminol and the previously studied systems is that V-BrPO functions by two-electron steps while HRP and HOCl, for example, function by one-electron steps (Cormier & Prichard, 1968; Brestel, 1985). In part A of Scheme 4-5, the oxidized bromine species generated by the V-BrPO-catalyzed peroxidation of bromide brominates luminol and monobromoluminol, forming the products observed by NMR and mass spectrometry. However, these products may not be the source of the emission of the V-BrPO catalyzed reaction. Therefore, other reactions which may produce the luminescent excited state species have been

considered, and possible reactions are presented in part B of Scheme 4-5. As shown in part B, "Br[•]" could oxidize luminol to yield the "diazaquinone" that has been referred to as "L" in this text. The unstable diazaquinone could then be converted to 3-aminophthalate with concomitant release of dinitrogen, as occurs in the HRP system (Lind et al., 1983). This 3-aminophthalate species could then be brominated by the oxidized bromine species generated by the enzymatic reaction. The UV spectra of some of the unidentified products in the HPLC traces of the enzymatic reactions do resemble the spectrum of 3-aminophthalate. However, thus far, no brominated aminophthalate species have been conclusively identified.



Scheme 4-5. Proposed mechanism for the V-BrPO catalyzed bromination of luminol. A) Bromination of luminol and monobrominated luminol.; B) Oxidation of luminol to the diazaquinone and conversion to 3-aminophthalate and brominated 3-aminophthalate.⁶

⁶ The pK_a 's for brominated luminols are likely lower than the corresponding pK_a 's for luminol itself due to the electron withdrawing bromines on the ring.

The luminescence emission profile of the V-BrPO-catalyzed bromination of luminol at pH 8.0 initially has a λ_{max} at 423 nm and is very similar to the emission spectrum of the HRP reaction. However, as the V-BrPO catalyzed reaction continues, the peak shifts to 441 nm. This shift can be interpreted based on the reactions proposed in part B of Scheme 4-5. In this scheme, luminol is oxidized to the diazaquinone "L" and then is further converted to 3-aminophthalate. If 3-aminophthalate is formed in its excited state, it emits at approximately 425 nm as it relaxes, just as occurs in the HRP reaction (Rosewell & White, 1973). In the V-BrPO reaction, the 3-aminophthalate can then be brominated, and production of monobrominated 3-aminophthalate in the excited state would likely lead to an emission profile that is shifted from the 3-aminophthalate spectrum. Alternatively, the 3-aminophthalate formed in the previous reaction of the diazaquinone could interact with other products as the reaction continues, resulting in the formation of an exciplex, and this species could then have a red-shifted emission spectrum.

The substrate specificity of V-BrPO for luminol was also examined. Kinetic competition studies with phenol red showed that luminol is preferentially brominated by V-BrPO over phenol red. In addition, competition studies between reaction with luminol and production of dioxygen show that luminol is capable of blocking the dioxygen evolution pathway as shown in Scheme 4-4. The preferential bromination of luminol catalyzed by V-BrPO likely involves binding of the substrate

to the enzyme as demonstrated by Stern-Volmer fluorescence quenching studies. V-BrPO was able to quench the inherent fluorescence of luminol quite effectively; an appreciable K_d of $3.8 \mu\text{M}$ ($K_s = 2.62 \times 10^5 \text{ M}^{-1}$) was calculated for the enzyme-substrate interaction at pH 5.7. This is the second reported example of binding of an organic substrate to V-BrPO; the first example was the indole study by Tschirret-Guth and Butler (1994), where a value of $9 \mu\text{M}$ was obtained for the K_d at pH 8.0. The K_d value at pH 5.7 calculated from the dioxygen evolution experiments (i.e., under turnover experiments) was $24 \mu\text{M}$, approximately four times higher than that calculated by fluorescence quenching but still in good agreement.

The binding of luminol to the enzyme is most likely influenced by the hydrophobicity of this substrate under the conditions used. Furthermore, the weakening of the interaction of luminol and V-BrPO as pH is increased is consistent with the expected changes in the hydrophobicity of this substrate. [This weakening effect was perhaps best illustrated by the dependence of the K_d calculated from the dioxygen evolution experiments on pH: K_d increased from $24 \mu\text{M}$ at pH 5.7, which is indicative of strong binding, to 2.30 mM at pH 8.0 (Table 4-1).] The $\text{p}K_s$ values of the protons bound to the azo nitrogens on luminol are approximately 6 (Baxendale, 1973) and 7.7 (Merenyi & Lind, 1983). Accordingly, in the experiments at pH 5.7 and 6.4, luminol was primarily a monoanion, while at

the higher pH values, luminol was predominantly a dianion. The monoanion is much more hydrophobic than the dianion and, accordingly, much more likely to interact with the enzyme, while the dianion remains in the aqueous solution. Furthermore, as was demonstrated by the inclusion of brominated luminols in a competition experiment between luminol and phenol red, *brominated* luminols are expected to be more hydrophilic than luminol itself and thus would not interact with the enzyme. Electron-withdrawing groups such as bromines are expected to decrease the pK_a values of the protons on the azo nitrogens; accordingly, bromoluminol is most likely predominantly hydrophilic dianion at all pH values studied.

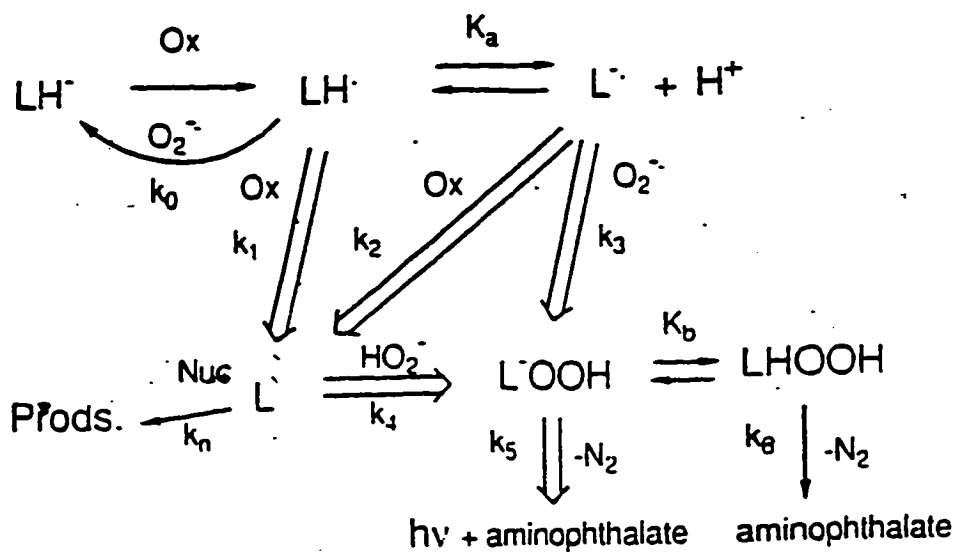
Interestingly, the luminescence of the V-BrPO/luminol/H₂O₂/bromide system is stronger at the higher pH values investigated (Friedman et al., 1995). In the current study, while appreciable luminescence was observed at pH 8.0, virtually none was observed at pH 5.7. Thus, an inverse relationship exists between the magnitude of the luminescence and the strength of the binding of luminol to V-BrPO. As demonstrated by the Stern-Volmer fluorescence quenching studies with V-BrPO and luminol, the interaction of a luminescent species with the enzyme is most likely going to quench the luminescence. The pH dependence data from both the luminescence experiments and the kinetic competition experiments suggest that if the luminescent compound or compounds in this reaction have hydrophobicity

similar to luminol, then luminescence will only be observed at the higher pH values where the species are freely diffusable in solution.

The pKa values of as yet unidentified intermediates in the V-BrPO-catalyzed reaction also are likely to effect the luminescence. Merenyi and coworkers (1990) proposed a mechanism for luminol luminescence generated by one-electron oxidants in which pH played a key role in the intensity of luminescence. These workers demonstrated in an earlier paper (Merenyi et al., 1986) that formation of the mono-anionic hydroperoxide of luminol, L-OOH, leads to chemiexcitation of the aminophthalate, but formation of the neutral hydroperoxide of luminol, LHOOH, does not, as shown in Scheme 4-6. The pKa for LHOOH was determined to be approximately 8.1.

The role of the oxidized bromine species may be critical to the ability of the V-BrPO/luminol/H₂O₂/bromide system to luminesce. As the pH is increased from 5.7 to 8.1, the equilibrium between Br₂ /Br₃⁻ and HOBr shifts so that substantially more HOBr is present at the higher pH values. Because HOBr is a better oxidant than bromine or tribromide, it is more likely to react with luminol to produce a diazaquinone as shown in Scheme 4-5B than to brominate luminol as shown in Scheme 4-5A. The diazaquinone formed in Scheme 4-5B is subsequently converted to 3-aminophthalate and brominated 3-aminophthalate, and, as suggested above, the phthalate compounds are likely the luminescent species in the V-BrPO-

catalyzed reaction. Thus according to this mechanism increasing the pH of the reaction mixture favors the formation of luminescent species. However, the *exact* identity of the luminescent species remain to be elucidated.



Ox = One-electron acceptor

Scheme 4-6. Detailed scheme of luminol oxidation pathways. Taken from Merenyi et al., 1990.

References

- Baxendale, J.H. (1973) *J. Chem. Soc. Faraday Trans. I* 69, 1665-1677.
- Brestel, E.P. (1985) *Biochem. Biophys. Res. Commun.* 126, 482-488.
- Cormier, M.J. & Prichard, P.M. (1968) *J. Biol. Chem.* 243, 4706.
- Friedman, A.E., Groulx, S.F., Butler, A. (1995) U.S. Patent Application 08/522.604 filed September 1, 1995.
- Jansen, E.H.J.M. & Van Den Berg, R.H. (1991) *J. Chromatography* 566, 461-469.
- Kricka, L.J., O'Toole, A.M., Thorpe, G.H.G., Whitehead, T.P. (1986) *UK Patent Pub.* 2162946A.
- Lind, J., Merenyi, G., Eriksen, T.E. (1983) *J. Am. Chem. Soc.* 105, 7655-7661.
- Merenyi, G. & Lind, J. (1983) in 5th Symposium on Radiation Chemistry, Dobo, J., Schiller, R., Hedvig, P., eds., Akademiai Kiado, Budapest, pp.103-108.
- Merenyi, G., Lind, J., Eriksen, T.E. (1986) *J. Am. Chem. Soc.* 108, 7716-7726.
- Merenyi, G., Lind, J., Eriksen, T.E. (1990) *J. Biolumin. Chemilumin.* 5, 53-56.
- Rosewell, D.F. & White, E.G. (1973) *Methods Enzymol.* 57, 409-423.
- Soedjak, H.S., Walker, J.V., Butler, A. (1995) *Biochemistry*, 34, 12689-12696
- Thorpe, G.H.G., Kricka, L.J., Mosely, S.B., Whitehead, T.P. (1985) *Clin. Chem.* 29, 1474.
- Thorpe, G.H.G. & Kricka, L.J. (1987) in 'Bioluminescence and Chemiluminescence: New Perspectives' Scholmerich, J., ed. Wiley & Sons, New York, pp. 199-208.
- Tschirret-Guth, R.A., & Butler, A. (1994) *J. Am. Chem. Soc.* 116, 411-412.
- Turro, N.J. (1978) in 'Modern Molecular Photochemistry' Benjamin/Cummings, Menlo Park, pp.125-127.

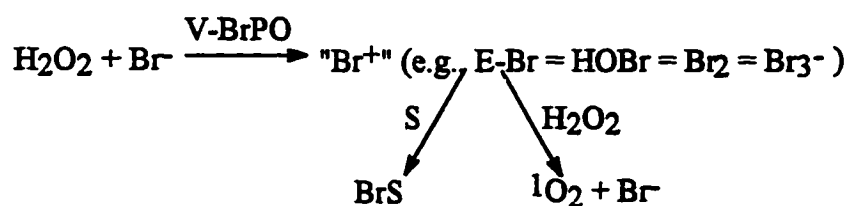
Voet, D. & Voet, J.G. (1990) "Biochemistry" Wiley & Sons, New York, p.78.

Chapter 5. Indoles as Preferred Substrates of Vanadium Bromoperoxidase:

Product Analyses and Photoaffinity Labeling

Introduction

The abundance of chiral halogenated products isolated from marine algae suggests that V-BrPO is capable of regio- and stereoselectivity. The V-BrPO-catalyzed oxidation of bromide by hydrogen peroxide, shown in Scheme 5-1, results in the formation of a "bromonium ion equivalent", the nature of which has been the subject of much investigation:

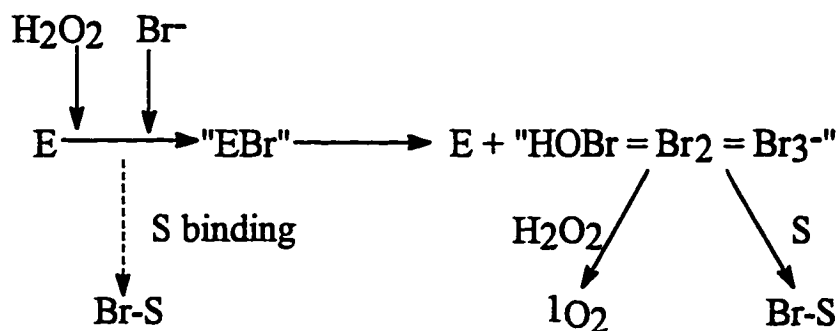


Scheme 5-1. Basic reaction scheme for the V-BrPO catalyzed bromination/bromoperoxidative oxidation of substrates and halide-assisted disproportionation of hydrogen peroxide.

De Boer and Wever (1988) attempted to characterize the oxidized bromine intermediate by examining the dependence of bromination or bromoperoxidative oxidation of organic substrates on the concentration of these substrates. The absence of any apparent dependence led to the unsatisfying conclusion that the enzyme was simply generating an aqueous bromine species. Early studies by Itoh and coworkers on the reactivity of V-BrPO from *Corallina pilulifera* with

monochlorodimedone, phenol, and cytosine did not demonstrate any selectivity (Itoh et al., 1987, 1988).

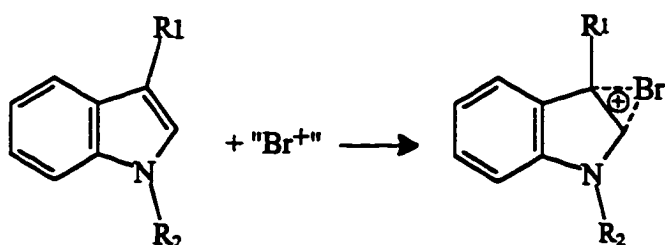
More recently, kinetic studies on the bromination and bromoperoxidative oxidation of several 2- and 3-substituted indoles have demonstrated that the reactions of these substrates catalyzed by V-BrPO differed from those of freely diffusable aqueous bromine species. Furthermore, strong evidence for binding of these indoles to V-BrPO was obtained from Stern-Volmer fluorescence quenching studies (Tschirret-Guth & Butler, 1994); V-BrPO was able to effectively quench the fluorescence of 2-phenylindole. A binding constant K_s of $1.1 \times 10^5 \text{ M}^{-1}$ for V-BrPO and 2-phenylindole at pH 8.0 was calculated from these experiments (Tschirret-Guth, 1996). These results suggested a revised scheme for the enzymatic reaction (Scheme 5-2):



Scheme 5-2. Updated reaction scheme for the V-BrPO catalyzed bromination/bromoperoxidative oxidation of substrates and halide-assisted disproportionation of hydrogen peroxide including the potential substrate binding step.

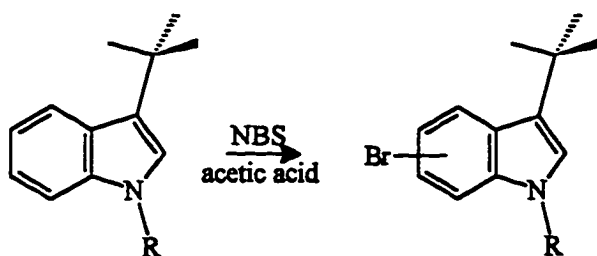
This demonstration that substituted indoles bind to V-BrPO created renewed interest in examining the possible regio- and stereoselectivity of V-BrPO-catalyzed bromination and bromoperoxidative oxidation reactions.

It has been proposed previously that the mechanism of electrophilic bromination of indoles by a bromonium ion involves first attack at the double bond of the pyrrole ring (DeFrabizio, 1968):



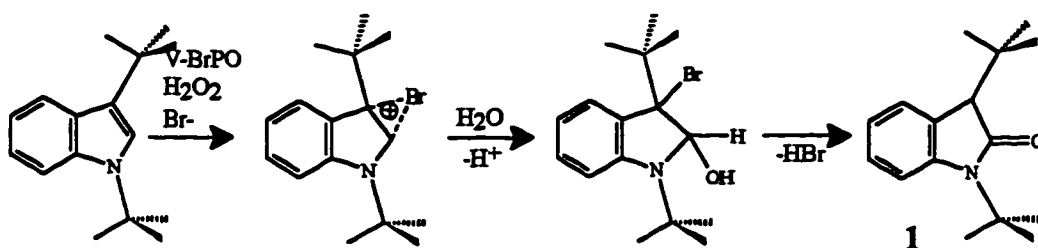
Scheme 5-3. Attack of a bromonium ion equivalent on the double bond of the indole pyrrole ring to form a bromoindolinium cation.

However, in studies of the bromination of 3-*tert*-butylindoles by NBS in acetic acid solution, the bulky 3-substituent prevented attack at that position, and instead the indole was brominated on the benzene ring (Hino et al., 1977):



Scheme 5-4. Bromination of a sterically hindered 3-*tert*-butyl substituted indole on the benzene ring of the indole.

Preliminary studies by Tschirret-Guth (1996) suggested that regardless of this possible steric hindrance at the 3 position, the bromination of 1,3-di-*tert*-butylindole by V-BrPO at pH 6.5 resulted in almost exclusive formation of the “2-oxo” indole product, 1,3-di-*tert*-butyl-2*H*-indol-2-one (1), which requires bromohydrin formation at the 2 and 3 positions:

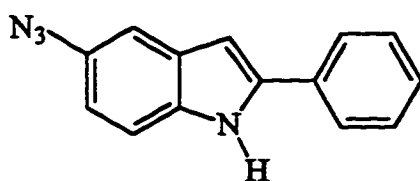


Scheme 5-5. Formation of 1,3-di-*tert*-butyl-2*H*-indol-2-one catalyzed by V-BrPO (Tschirret-Guth, 1996).

Thus, work was undertaken to determine if the products of the reaction of 1,3-di-*tert*-butylindole with HOBr under similar conditions as the enzymatic reaction resulted in the formation of different products. In particular, the question was whether binding of the indole substrate to V-BrPO somehow prevents access to the benzene ring, thus resulting in the formation of the oxygenated product. Described in this chapter is the first example of regioselective bromoperoxidative oxidation of an organic substrate by V-BrPO.

Consequent to the demonstration of substrate binding in V-BrPO, it also became of interest to identify the site at which organic substrates can bind to the enzyme. Photoaffinity labeling has proved, in some instances, a useful technique for the identification of substrate binding sites in proteins (Kotzya-Hibert, et al, 1995). To this end, Tschirret-Guth (1996) photolabeled V-BrPO with several azido-substituted indoles, including tritium-labeled 5-azido-1,2-dimethylindole. A new peptide identified in the tryptic digest of the enzyme photolabeled with this indole compound contained the majority of the tritium counts, indicating that the label had crosslinked with the enzyme at a specific site (Tschirret-Guth, 1996).

While an indole-bound peptide was identified and isolated from V-BrPO, it remained to be characterized (Tschirret-Guth, 1996). In this chapter, the photoaffinity labeling of V-BrPO is carried out again in an attempt to characterize the indole binding site in V-BrPO. In this case the substrate 5-azido-2-phenylindole was used as the photolabel:



5-azido-2-phenylindole

Materials and Methods

Synthesis of 1,3-di-*tert*-butylindole. Indole (1.71 g; 13 mmol) was dissolved with stirring in 5 mL dry THF at room temperature in a 25 mL 3-necked round bottom flask equipped with a reflux condenser and an addition flask. Methylmagnesium chloride (3 M, 5 mL) was added at room temperature dropwise by syringe, which resulted in bubbling and a temperature increase of the reaction solution. After 10 to 15 minutes, 1.5 mL *tert*-butyl chloride was added. The mixture was refluxed using a heating mantle with stirring for approximately 2 hours. Small aliquots (several μL) were removed periodically, extracted with ethyl acetate, and analyzed by TLC in 90% hexanes/10% ethyl acetate to determine reaction progress. After two hours, the reaction mixture was allowed to cool to room temperature, whereupon another 5 mL of methylmagnesium chloride was added dropwise. After 15 minutes, another 1.5 mL *tert*-butyl chloride was added. The reaction mixture was then refluxed gently for another 2 hours. After 2 hours, the reaction was quenched by hydrolysis with 10 mL of H_2O . The resulting viscous brown reaction mixture was extracted 3 times with ~25 mL volumes of CH_2Cl_2 . The dichloromethane extracts were combined and dried overnight over anhydrous MgSO_4 .

After vacuum filtration, the dichloromethane was evaporated on a Buchi RE011 Rotovapor rotary evaporator. The viscous, oily product mixture was then

separated on a silica gel column (2 x 100 cm) prepared in hexanes. The column was eluted with successive 100 mL volumes of 99%/1% hexanes/ethyl acetate, 98%/2% hexanes/ethyl acetate, 97%/3% hexanes/ethyl acetate, 96%/4% hexanes/ethyl acetate, 95%/5% hexanes/ethyl acetate, and finally 90%/10% hexanes/ethyl acetate. The 1,3-di-*tert*-butylindole, which was the fastest eluting compound (Tschirret-Guth, 1996), was mixed with a second orange product in most fractions according to TLC analyses.

The fractions containing the 1,3-di-*tert*-butylindole were combined and concentrated. They were run on a second silica gel column (2 x 30 cm) with 100% hexanes as the eluant. The collected fractions were run repeatedly on this column until TLC analyses showed that the desired products were pure.

Reactions with 1,3-di-*tert*-butylindole. Enzymatic reactions were performed under conditions of 0.5 mM or 1.0 mM 1,3-di-*tert*-butylindole, 0.1 M KBr, 30 nM V-BrPO, and 1 or 2 equivalents of H₂O₂ (i.e., 0.5 or 1.0 mM H₂O₂ for 0.5 mM indole and 1.0 or 2.0 mM H₂O₂ for 1.0 mM indole) in 0.1 M phosphate pH 6.0/ 30–40% ethanol. Enzymatic reactions were initiated with H₂O₂. Chemical reactions were prepared under conditions of 0.5 mM or 1.0 mM 1,3-di-*tert*-butylindole, 0.1 M KBr, and 1 or 2 equivalents of HOBr (i.e., 0.5 or 1.0 mM HOBr for 0.5 mM indole and 1.0 or 2.0 mM HOBr for 1.0 mM indole) in 0.1 M

phosphate pH 6.0/ 25% ethanol. Chemical reactions were initiated by the addition of HOBr. HOBr stock solutions were between 80 and 200 mM.

HPLC analysis of 1,3-di-*tert*-butylindole reaction products. The reaction mixture was analyzed by HPLC after a minimum of one hour of reaction time. Products were separated in 80% acetonitrile/ 20% water on a YMC-ODS AQ C-18 column (4.5 x 250 mm) at 0.7 mL/min on a Waters HPLC system equipped with Waters 510 pumps and a Waters 996 photodiode array detector, and running Millennium Chromatography Manager software version 2.1. Data acquisition was monitored over 200 to 300 nm; chromatograms were extracted at 214, 230, 254, and 280 nm for analysis. Sample injections were 100 μ L in a 200 μ L sample loop. Peaks were collected at 0.5 minute intervals on a Gilson model FC-205 Fraction Collector.

Mass spectral analysis of reaction products. The products of the reaction of 1,3-di-*tert*-butylindole with HOBr were analyzed by positive FAB mass spectrometry on a VG 70E Magnetic Sector Double Focussing Mass Spectrometer equipped with an OPUS/SIOS data acquisition system (Micromass, Inc, Altricham, UK). The products of the HOBr reactions were extracted with 1 mL hexanes and concentrated by Speed Vac concentrator or Argon bubbling for analysis. The separated products were analyzed by positive chemical ionization mass spectrometry on the VG 70E Mass Spectrometer.

NMR analysis of reaction products. The HPLC-separated products of the reaction of 1,3-di-*tert*-butylindole with HOBr were further characterized by ¹H NMR on a Varian Gemini-200 NMR Spectrometer in deuterated chloroform and DMSO.

Synthesis of 5-azido-2-phenylindole.

a) Synthesis of 5-nitro-2-phenylindole. 5-nitro-2-phenylindole was synthesized previously by Tschirret-Guth (1996). To a solution of 3.0 g 2-phenylindole (15.5 mmol) in 100 mL conc. H₂SO₄ at 5°C was added over a five-minute period 1.4 g NaNO₂ (20.3 mmol) in 50 mL conc. H₂SO₄. After 30 minutes, the solution was poured over approximately 200 g of crushed ice, which resulted in the formation of a yellow precipitate. The precipitate was vacuum filtered, washed with water, and dried in a dessicator. Net yield was 93%. (Tschirret-Guth, 1996)

b) Synthesis of 5-amino-2-phenylindole. 5-nitro-2-phenylindole (0.23 g, 0.93 mmol) was dissolved in 80 mL ethanol and 10 mL water in a 250-mL round-bottom flask. Concentrated HCl (2 mL) and approximately 2.5 g of mossy zinc were added. The mixture was gently refluxed for approximately two hours. After cooling, 100 mL H₂O was added to the mixture. Addition of concentrated NaOH (~3 M) resulted in the formation of a flocculent white precipitate. The NaOH solution was added until the pH of the mixture was approximately 11. The mixture was then extracted twice with ethyl acetate (100 mL volumes). The ethyl acetate

extracts were combined and dried over anhydrous MgSO_4 . The solution was filtered and concentrated on a rotovap. The resulting product was grayish yellow. Yield of the amino product after drying overnight was 91% (0.18 g; 0.85 mmol)

c) Synthesis of 5-azido-2-phenylindole. 5-amino-2-phenylindole (0.17 g 0.82 mmol) was dissolved in 50 mL 80% acetic acid in an ice bath. The resulting solution had a bluish tinge. NaNO_3 (0.057 g, 0.82 mmol) and NaN_3 (0.053 g, 0.82 mmol) were separately dissolved in a minimum amount of H_2O and chilled in the ice bath, and the NaNO_2 solution was added dropwise to the 5-amino-2-phenylindole. A red-brown solution resulted. After five minutes, the chilled NaN_3 solution was added dropwise to the mixture. The mixture was left to stir for approximately 4 hours on ice. The color remained red-brown. The resulting mixture was subsequently freeze-dried on a Labconco Freezone 6 lyophilizer (Labconco, Inc). The dried product was suspended in 15 mL ethanol and activated charcoal was added. The mixture was heated just to boiling and then filtered over Celite®. Water (100 mL) was then added to the filtered ethanol solution, resulting in precipitation of the yellow-brown product. The product was collected by filtration and suspended in 20 mL H_2O . The suspension was subsequently freeze dried.

Photoaffinity labeling of vanadium bromoperoxidase. An aliquot (1.5 mL) of 15 μM V-BrPO in ~50 mM Tris pH 8.3 was added to a 3 mL plastic disposable cuvette which had a wavelength cutoff of 308 nm. An aliquot (300 μL) of 8.5 mM

5-azido-2-phenylindole in ethanol was then added. A single sample of 1.5 mL 15 μ M native V-BrPO in 50 mM Tris pH 8.3 and 300 μ L ethanol was also prepared as a control sample for trypsin digestion (see below). This sample was not photolyzed. The cuvettes containing photolabel were then irradiated for 1 hour with an Oriel Model 6047 Hg pen lamp at a distance of approximately 1 cm. (Note: the lamp was warmed up for at least 15 minutes prior to photolabeling experiments.) The control sample and the irradiated sample(s) were then washed several times in Centricon 30 filters to remove Tris buffer and non-covalently bound photoaffinity label.

Trypsin digestion. Control and photoaffinity labeled V-BrPO samples were digested with trypsin using a procedure adapted from a method by Uchida and Kawakishi (1994) for Cu,Zn-superoxide dismutase. In this procedure, V-BrPO (1.5 to 4.5 mg) was first demetallated by incubation in 2 mLs of 0.1 M citrate-phosphate buffer, pH 4.0 containing 1.2 mM EDTA for at least 10 hours. The enzyme sample was washed in a Centricon 30 and evaporated to dryness in the SpeedVac concentrator. The dried sample was then diluted to 800 μ L with water to which was added 100 μ L 10 M urea, 50 μ L neat 2-mercaptoethanol, and 25 μ L concentrated NH_4OH . This mixture was flushed with pre-purified Argon, sealed, and incubated at 37 °C for 2 to 4 hours. The protein was then precipitated by the addition of ~2 mL ethanol containing 2% HCl (v/v). The protein pellet was

collected by centrifugation in an Eppendorf Centrifuge Model 5415C at 13,000 rpm for 8 to 10 min followed by removal of the supernatant. The pellet was dissolved in 300 μ L 8 M urea; 60 μ L of 20 mg/mL iodacetamide and 30 μ L concentrated NH_4OH were then added and the solution incubated for 20 to 30 min at 37 °C. The incubated solution was then treated with 60 μ L 2-mercaptoethanol and 30 μ L concentrated NH_4OH . The carboxyamidomethylated protein was precipitated twice by the addition of approximately 2 mL ethanol; the pellet was collected each time by centrifugation at 13,000 rpm for a minimum of 8 minutes. The pellet was redissolved in 500 μ L 0.1 M Tris pH 8.3 and 20 μ L of a 1 mg/mL sequencing grade trypsin solution was added. The net V-BrPO concentration during digestion was approximately 20 μ M. The sample was digested for approximately 6 hours at 37 °C. The digestion was quenched by the addition of 10 μ L concentrated acetic acid.

The digested fragments were separated by HPLC using a two step gradient of 0.1% TFA in H_2O to 80% acetonitrile, 0.1% TFA in H_2O at a flow rate of 0.7 mL/min. The gradient procedure is listed in Table 5-1. The fragments were separated on a YMC ODS-AQ C-18 column. In some cases separation was monitored with a Waters 996 photodiode array detector at a resolution of 1.2 or 2.4 nm and a data acquisition rate of 1 or 2 spectra/sec; chromatograms were extracted at 214, 230, 254, and 280 nm for comparison. For other runs, separation

was monitored using a Waters 486 tunable absorbance detector set to either 280 or 214 nm. Fragments were collected in a Gilson FC- 80 Fraction Collector.

Table 5-1. Gradient for separation of tryptic peptides by HPLC. A: 0.1% TFA in H₂O; B: 80% CH₃CN/20% H₂O/ 0.1% TFA .

Time (minutes)	Flow (mL/min.)	Percent A	Percent B
0	0.7	100	0
5	0.7	100	0
80	0.7	50	50
120	0.7	0	100
125	0.7	0	100
135	0.7	100	0
150	0.7	100	0
160	0.7	100	0

Electrospray mass spectral analysis of tryptic fragments. Key fractions collected from the separation of the tryptic fragments were subjected to analysis by positive electrospray mass spectrometry on a VG Fisons Platform II with an ESI/APCI interface (Micromass, Inc.) with an Ultrafast Microprotein Analyzer liquid chromatography (LC) system (Micromass, Inc.). Data were analyzed with MassLynx software. The peptide samples were injected on to the LC system equipped with a peptide trap and running an isocrat of 46 b% acetonitrile/ 54% water/ 0.1% TFA at a flow rate of 20 or 50 μ L /min. Mass spectral data were analyzed over a range of 300 to 1500 m/z. Sample size was 100 to 200 μ L.

Tryptic digest mixtures were also analyzed by positive electrospray LC-MS. For these runs, the LC system was equipped with a Zorbac C-18 300 μ 1 x 150 mm microbore column. Peptides were separated on the column using a water/acetonitrile/TFA gradient as shown in Table 5-2. The peptide separation was monitored by an analog UV signal set at 214 or 280 nm and mass spectral data were extracted from the corresponding mass spectral chromatogram. Typical injection volume was 50 μ L.

Table 5-2. Gradient for separation and analysis of tryptic peptides by LC-MS. A: 2% CH₃CN/ 0.1% TFA in H₂O; B: 90% CH₃CN/10% H₂O/ 0.1% TFA in H₂O.

Time (min)	Flow (mL/min)	%A	%B
0	0.05	100	0
5	0.05	75	25
60	0.05	0	100
90	0.05	0	100
100	0.05	100	0

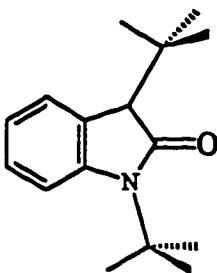
General reagents and procedures. HOBr and H₂O₂ concentrations were determined by the triiodide assay of Cotton and Dunford (1971). HOBr stock solutions (80 to 200 mM) were prepared by adding liquid bromine to 0.1 M NaOH. V-BrPO concentration was determined by the biochinconic acid assay (Pierce, Inc.). Sequencing grade trypsin was purchased from Sigma.

Results and Interpretation

I. Regioselectivity of V-BrPO with 1,3-di-*tert*-butylindole.

HPLC Analysis of the Enzymatic and Chemical Reaction Products of 1,3-di-*tert*-butylindole.

In order to compare the products of the bromination/bromoperoxidative oxidation of 1,3-di-*tert*-butylindole catalyzed by V-BrPO to the products of the reaction of 1,3-di-*tert*-butylindole with HOBr, the reaction mixtures were separated by HPLC (Figures 5-1 and 5-2). Under conditions of 1.0 mM 1,3-di-*tert*-butylindole, 30 nM V-BrPO, 0.1 M KBr, and 1 or 2 mM H₂O₂ in phosphate pH 6.0/40% ethanol, both HPLC chromatograms showed the formation of one major product at 9.2 minutes. This peak corresponds to 1,3-di-*tert*-butyl-2*H*-indol-2-one, which was previously identified by Tschirret-Guth (1996) as the major enzymatic product from its ¹H NMR spectrum.



1,3-di-*tert*-butyl-2*H*-indol-2-one

The peak at 11.4 minutes corresponds to the starting material (i.e., 1,3-di-*tert*-butylindole). Minor products were also detected at 10.2 minutes and 11.8 minutes

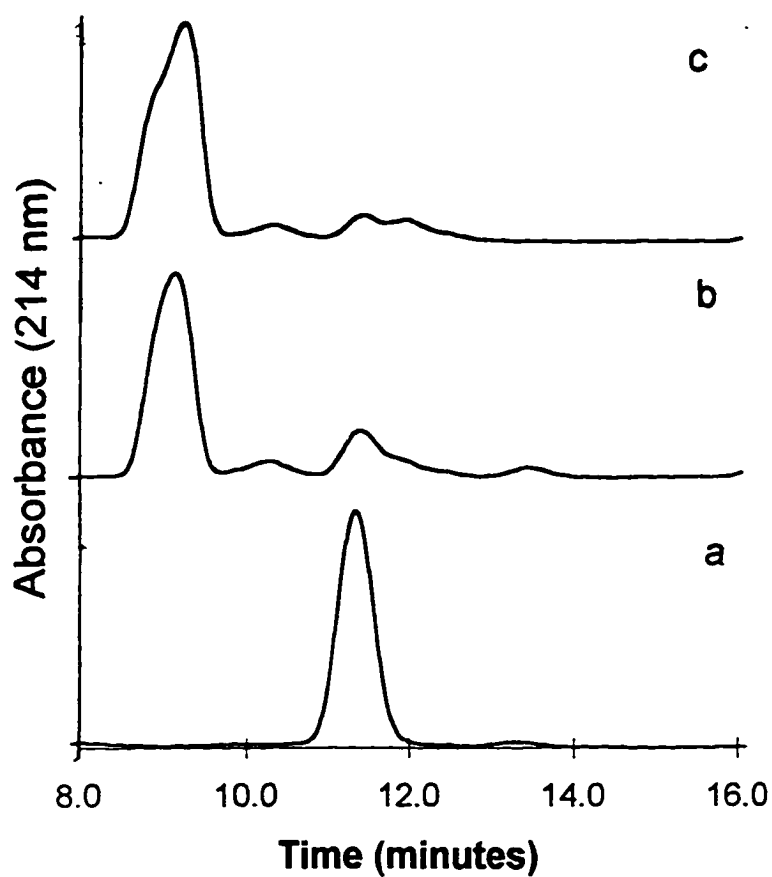


Figure 5-1. HPLC chromatograms at 214 nm of the bromoperoxidative oxidation of 1,3-di-*tert*-butylindole catalyzed by V-BrPO. Conditions: 1.0 mM 1,3-di-*tert*-butylindole, 30 nM V-BrPO, 0.1 M KBr, 0.1 M phosphate pH 5.7 and a) No H₂O₂; b) 1.0 mM H₂O₂; c) 2.0 mM H₂O₂.

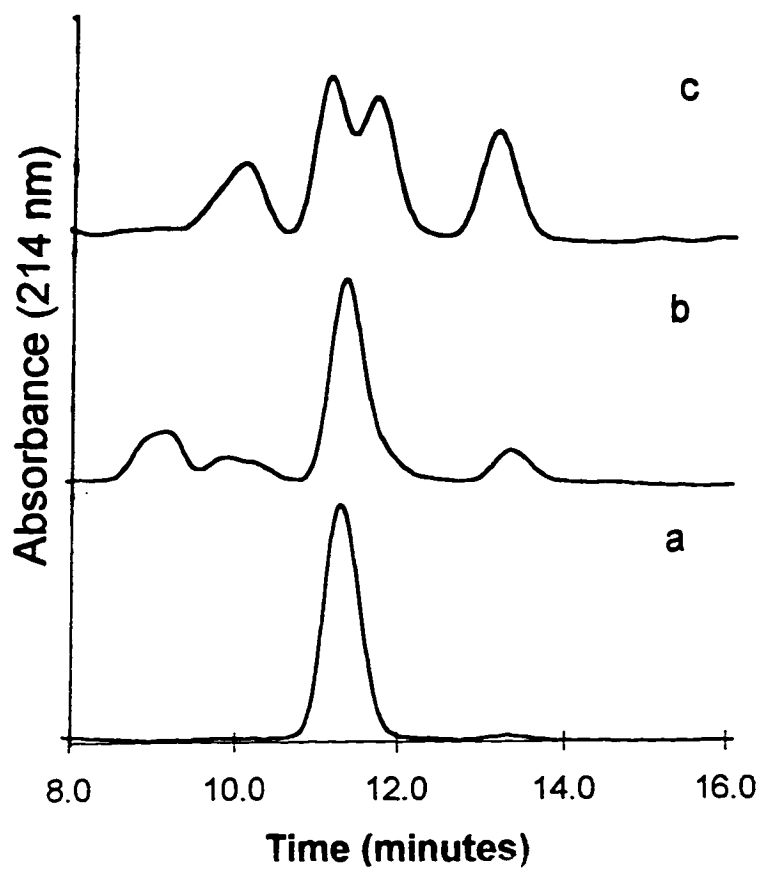


Figure 5-2. HPLC chromatograms at 214 nm of the reaction mixture of 1,3-di-*tert*-butylindole, 0.1 M KBr, 0.1 M phosphate pH 5.7 and a) No HOBr; b) 1.0 mM HOBr; c) 2.0 mM HOBr. Injection volume 100 μ L.

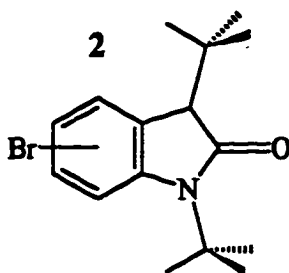
in the chromatograms of both samples (Figure 5-1). In addition, a minor peak was found at 13.4 minutes in the chromatogram of the reaction with 1.0 mM 1,3-di-*tert*-butylindole and 1.0 mM H₂O₂, which may have been present in the starting material. This peak did not appear in the sample in which 2.0 mM H₂O₂ was used.

If instead 1.0 mM 1,3-di-*tert*-butylindole was incubated with 1.0 or 2.0 mM HOBr added all at once under conditions of 0.1 M KBr and phosphate pH 6.0 with 40% ethanol, multiple significant products were detected by HPLC (Figure 5-2). For the case of 1.0 mM 1,3-di-*tert*-butylindole and 1.0 mM HOBr, major products were observed at 9.2, *ca.* 10, and 13.3 minutes. The peak at 9.2 minutes is likely the 2-oxo derivative identified in the enzymatic reaction. In addition to these products, a substantial amount of unreacted starting material was detected at 11.3 minutes. Use of 2.0 mM HOBr resulted in a decrease in the size of the starting material peak at 11.2 minutes, increases in the areas of the peaks at 10.2 and 13.2 minutes, and significant loss of the peak corresponding to the 2-oxo derivative at *ca.* 9 minutes. In addition, a new large peak was observed at 11.8 minutes. The products corresponding to the unidentified peaks in the HOBr chromatograms at 10.2 minutes, 11.8 minutes, and 13.2 minutes were collected for mass spectral analysis.

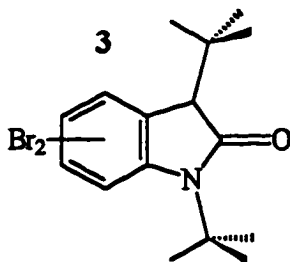
Mass Spectrometry of the Reaction Products of 1,3-di-*tert*-butylindole and HOBr.

FAB-MS analysis of the reaction mixture of one equivalent each of 1,3-di-

tert-butylindole and HOBr revealed paired peaks indicative a of single bromine with m/z values of 324 and 326 (Figure 5-3a), which are consistent with a singly brominated oxoindole (2):



FAB-MS analysis of the reaction of one equivalent of 1,3-di-*tert*-butylindole and *two* equivalents of HOBr showed both the peaks at $m/z = 324/326$ and a set of peaks at m/z values of 402, 404, and 406 (Figure 5-3b), which are consistent with a doubly brominated species, in this case a doubly brominated oxoindole (3):



Analysis of the products of the reaction of one equivalent of 1,3-di-*tert*-butylindole and two equivalents of HOBr by CI-MS (CH_4) revealed a major doublet peak 311 and 313 m/z (Figure 5-3c) which is consistent with a singly brominated product (4):

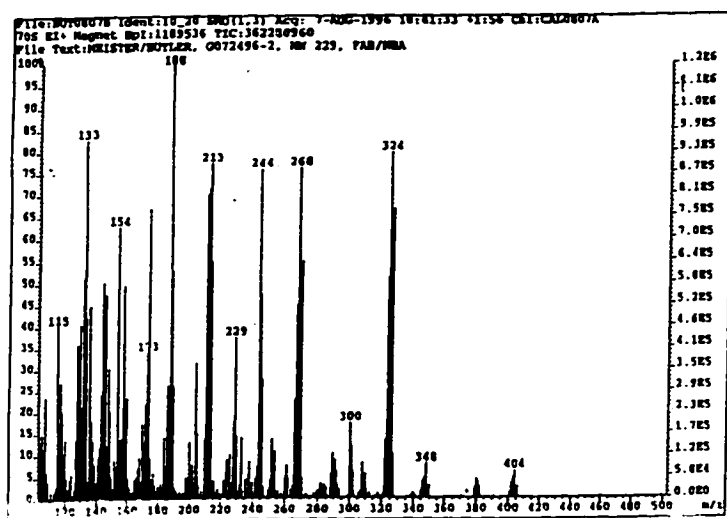
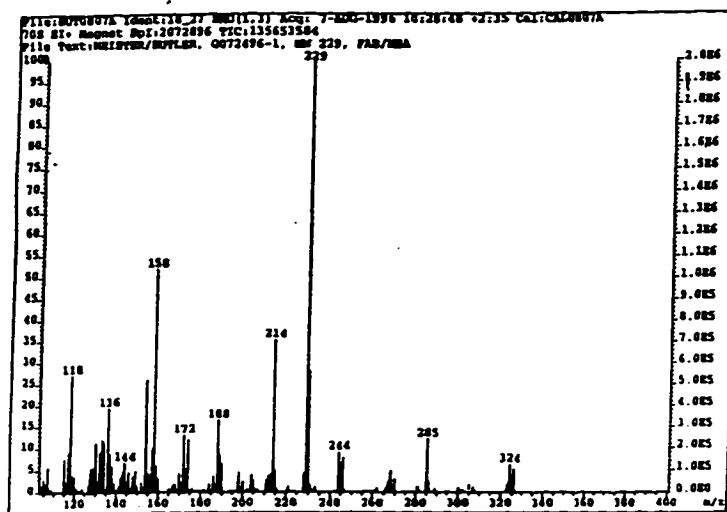


Figure 5-3. Mass spectral data for the reaction of 1,3-di-*tert*-butylindole and HOBr. a) Positive FAB mass spectrum of the 1:1 mixture; b) Positive FAB mass spectrum of the 1:1 mixture; c) Positive CI mass spectrum of the HPLC-isolated product (retention time : 10.2 minutes) from the 1:2 reaction. Reaction conditions: 1 mM 1,3-di-*tert*-butylindole and 1 or 2 mM HOBr in 0.1 M phosphate pH 6.0 containing 40 % ethanol.

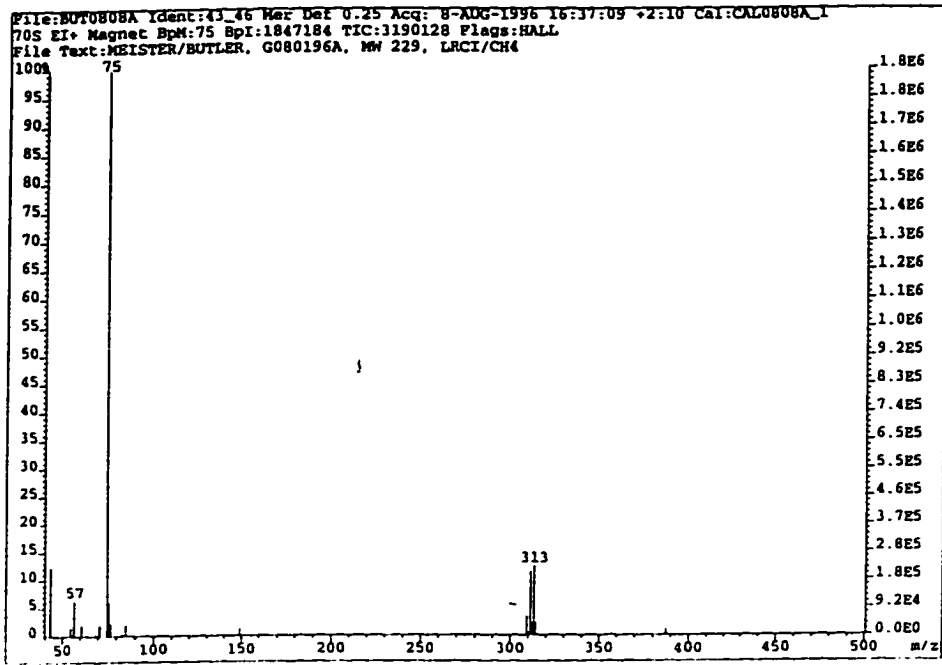
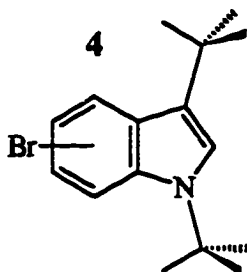
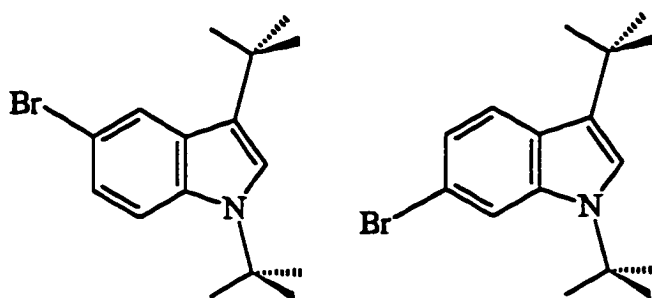


Figure 5-3 c



NMR of the Reaction Products of 1,3-di-*tert*-butylindole and HOBr.

^1H NMR spectra in deuterated chloroform of the product corresponding to a retention time of 10.2 minutes had an aromatic splitting pattern consistent with bromination at either the 5 or the 6 position of the indole compound. The spectrum had doublets at 7.38 ppm and 7.03 ppm representing two protons on the benzene ring coupled to one another, and two singlets at 7.79 ppm and 7.21 ppm, which correspond to two uncoupled aromatic protons, one on the remaining site on the benzene ring and the other proton at the 2 position on the pyrrole ring.



Scheme 5-6. Bromination of 1,3-di-*tert*-butylindole at the 5 or the 6 position

II. Photoaffinity Labelling of V-BrPO with 5-azido-2-phenylindole.

Photolabeling of V-BrPO and Analysis of Tryptic Digest by HPLC

Two samples of V-BrPO (13 μ M) and 5-azido-2-phenylindole (1.4 mM) in 0.1 M Tris buffer/20% ethanol (1.5 mL) were irradiated with an ultraviolet pen lamp for approximately one hour in plastic spectrophotometric cuvettes with 308 nm absorbance cutoff. The change in the absorption spectrum of the 5-azido-2-phenylindole agreed with the results reported previously by Tschirret-Guth (1996) (Figure 5-4). The two photoaffinity samples and a control sample of V-BrPO in 0.1 M Tris/ 20% ethanol were then prepared for trypsin digestion by demetallation, denaturation with DTT and urea, and carboxyamidomethylation as described in Materials and Methods (Uchida & Kawakishi, 1994). The samples were digested with trypsin for approximately six hours. The tryptic fragments were separated by HPLC and the resulting traces were compared for the irradiated samples of V-BrPO and the unirradiated control sample. Chromatograms for each sample extracted at 280 nm revealed that an intense peak detected at approximately 116.5 minutes for the photoaffinity sample was absent in the control sample (Figure 5-5), suggesting that a new peptide was present in the labeled sample. However, none of the original peaks in the control chromatogram clearly disappear or decrease markedly in intensity in the photoaffinity chromatogram.¹ Regardless, the

¹ Expansion of the region around 95 minutes in both chromatograms did not show clear decreases of the peaks in that region.

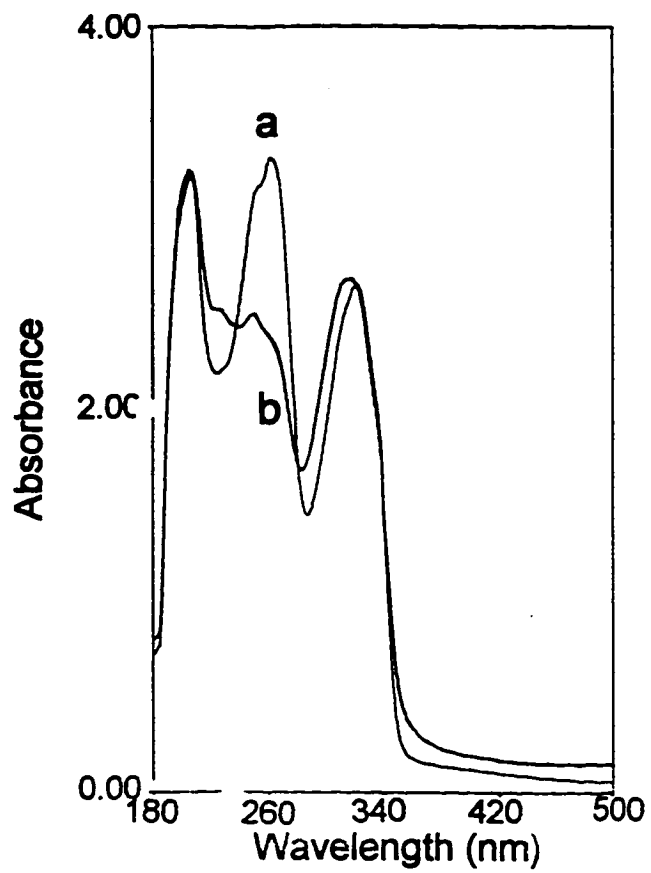


Figure 5-4. Spectrum of 5-azido-2-phenylindole in ethanol/water a) prior to irradiation; b) after one hour of irradiation at >308 nm.

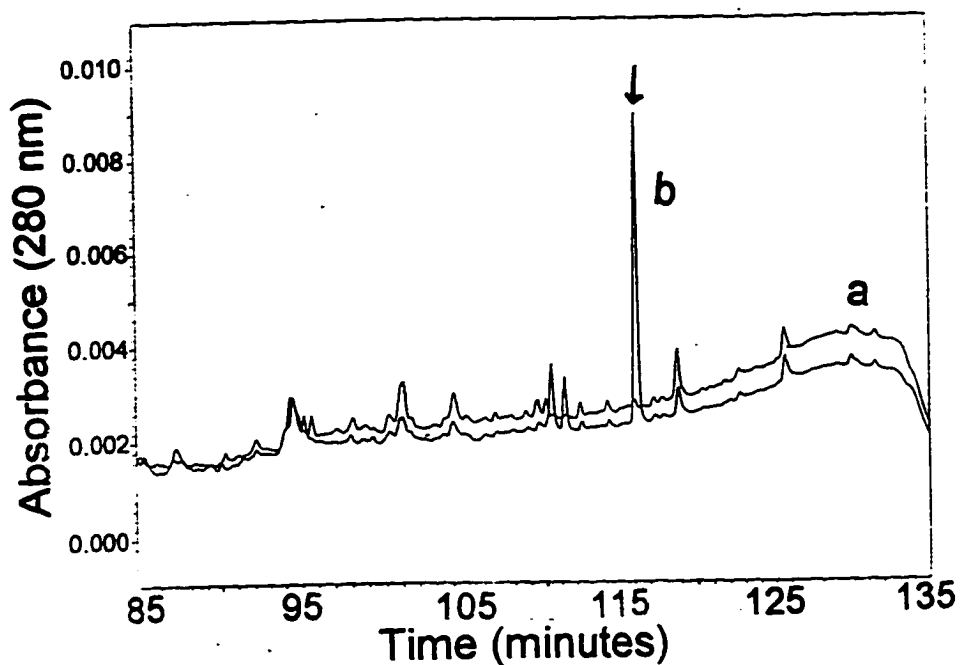


Figure 5-5. HPLC chromatograms of 6 hour tryptic peptides from a) a control sample of V-BrPO and b) V-BrPO irradiated in the presence of 5-azido-2-phenylindole for one hour. Conditions for photolabeling and digestion are as described in Materials and Methods. Injection volume 100 μ L.

new peak at at 116.5 minutes in the photoaffinity sample was collected for mass spectrometry analysis.

Mass Spectral Analysis of Modified Peptide

Analysis of the new peptide by positive electrospray mass spectrometry revealed a molecular ion cluster at $M + 1 = 956.0, 984.4, 1010.7, \text{ and } 1039.9$ (Figure 5-6). These peaks are each separated by approximately 28 mass units, suggesting that dinitrogen is released from the sample during mass spectral analysis (see Discussion).

The next intended step was to sequence this peptide by tandem MS-MS. However, because the electrospray mass signal was weak and exhibited substantial noise, further purification of the peptide was attempted by HPLC. The peptide was separated on a YMC ODS-AQ C-18 column (YMC, Inc) using a 30 min linear gradient of 0 to 80% acetonitrile in 0.1% TFA. The purified peptide was collected and re-analyzed by positive electrospray mass spectrometry using a peptide trap. However, upon the second purification step, no real signal could be detected (data not shown).

Photolabeling of V-BrPO and Analysis by LC-MS

Encouraged by the partial success of the above photoaffinity labeling experiment, another photolabeling experiment with a larger quantity of V-BrPO

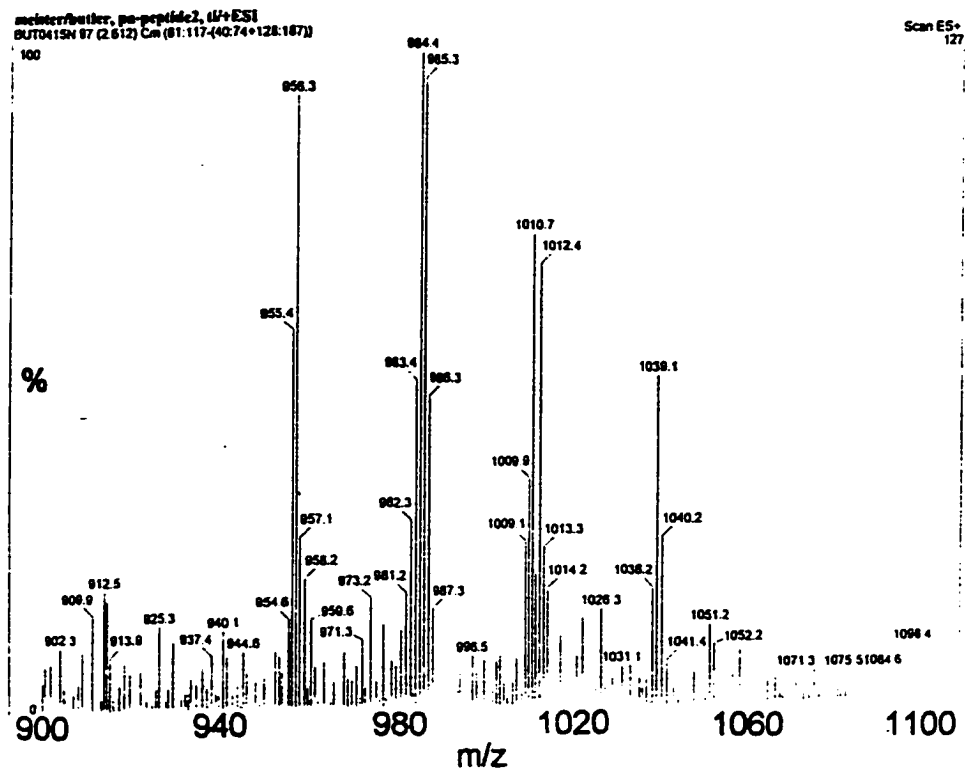


Figure 5-6. Positive electrospray mass spectrum of the peptide collected from the photolabeled sample in Figure 5-5 at 116.5 minutes retention time.

was performed to try to identify the binding site of the organic substrate. Photoaffinity labeling and trypsin digestion of V-BrPO were executed as described for the previous experiment and in the Materials and Methods section. In this case, a total of 4.5 mg of V-BrPO was subjected to photolabeling and 1.5 mg was used in the control. This time the samples were digested with trypsin for 12 hours. In order to achieve better mass signal, the tryptic fragments were separated and analyzed directly by LC-MS using the electrospray mass spectrometer. The fragments were separated on a Zorbac microbore C-18 column using the abbreviated gradient of 2% to 90% acetonitrile in 0.1% TFA described in Materials and Methods. As it did not prove possible to follow the separation at 280 nm with the LC analog detector, the peptides of the labelled and control enzyme samples were monitored at 214 nm. In this case, no new peaks could be detected in the photolabeled enzyme chromatogram (Figure 5-7). However, loss of a peak was noted in the control chromatogram at 13.03 minutes (Figure 5-7)². Examination of the mass data at this time point showed a weak signal at $m/z = 475$, which likely corresponded to a doubly charged molecular ion for the isolated peptide (Figure 5-8)³.

² The analog chromatograms from the control and photoaffinity labeled samples were shifted due to instrumental difficulties with the LC system in the UCSB Mass Spectrometry Facility. For example, the peak at 17.21 minutes in Figure 5-7a corresponds to the peak at 15.87 minutes in Figure 5-7b (A net shift of approximately -1.35 minutes was observed.)

³ Mass Lynx software permits the selection of a time point or time range in the mass chromatogram recorded concurrent to the analog UV chromatogram which can then be specifically analyzed for its mass spectral data only.

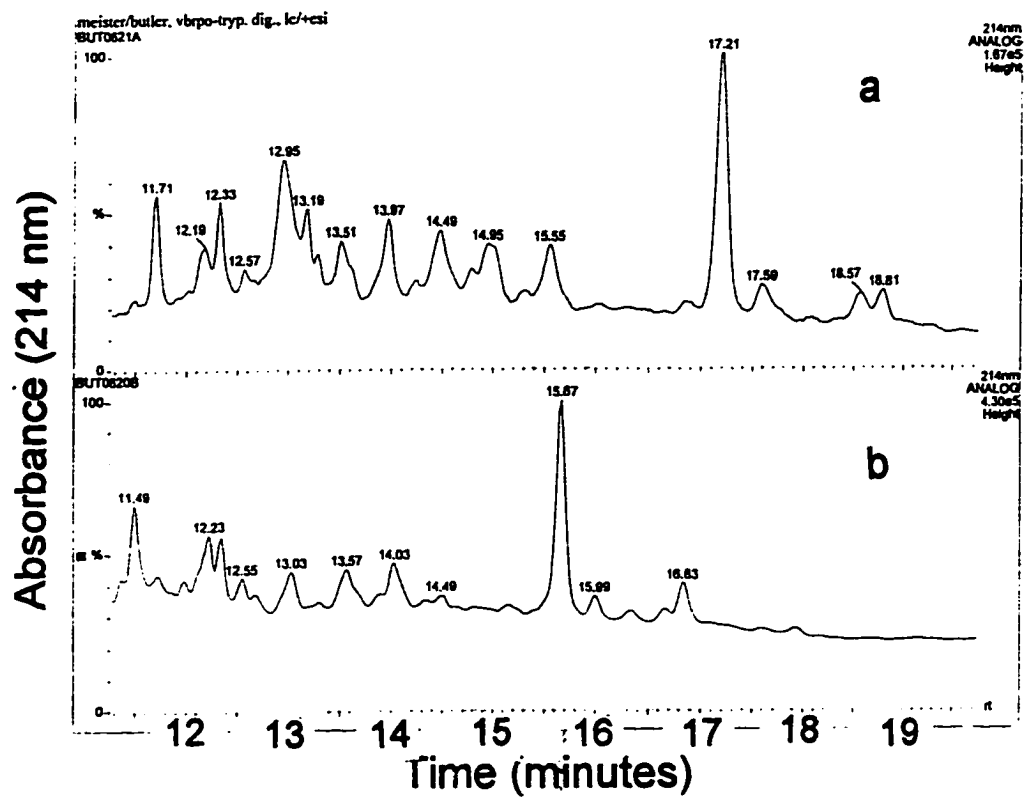


Figure 5-7. Microbore LC Chromatograms at 214 nm of the tryptic digests of a) native V-BrPO; b) photolabeled V-BrPO. Conditions for photolabeling and digestion are described in Materials and Methods. 100 μ L LC injections.

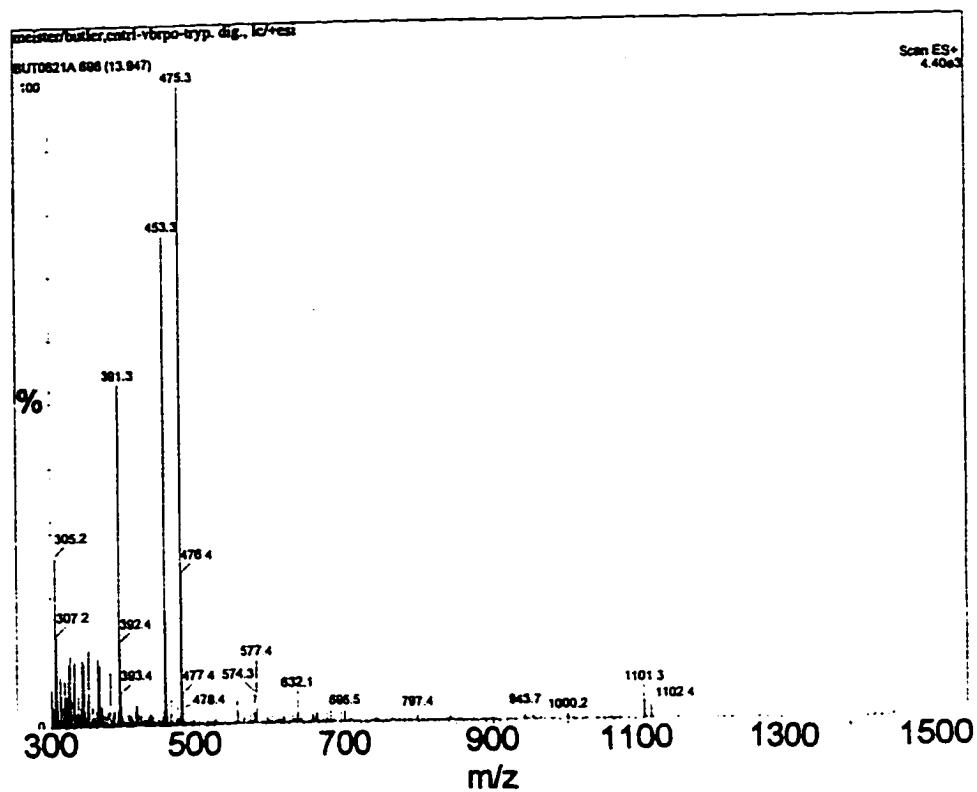


Figure 5-8. Mass spectrum of the peak at 13.03 minutes in the LC chromatogram of native V-BrPO in Figure 5-7a.

HPLC Analysis of Tryptic Digestion

Because the UV signal on the LC-MS system exhibited much lower intensity than the PDA detector used for HPLC, the remainder of the tryptic fragments for the labelled and control enzyme samples were separated prior to mass spectral analysis by HPLC using the standard stepped gradient outlined in Table 5-1 in Materials and Methods. The HPLC traces of these 12 hour digests indicated substantially more fragmentation than the previous 6 hour digest experiment. As in the first experiment, the chromatogram of the labeled V-BrPO digest had a new peak, this time at 78 minutes (Figure 5-9b). Unlike the 6 hour digest runs, this peak was not more intense than its neighbors (Figure 5-9b). In addition, a peak with a retention time of 62 minutes in the control V-BrPO tryptic digest disappeared in the chromatogram of the labeled V-BrPO, suggesting that this peptide was modified by the label to produce the peak at 78 in the chromatogram of the labeled sample (Figure 5-9a).

Mass Spectral Analysis of Collected Peptides

The peptides identified in the HPLC chromatogram were collected and analyzed by positive electrospray mass spectrometry. The peptide from the control sample collected at 62 minutes had a weak but real, Gaussian-shaped signal at 948.1 mass units (Figure 5-10a) The peptide from the labeled sample collected at 78 minutes had a similarly weak but real Gaussian-shaped signal at 616.9 mass units

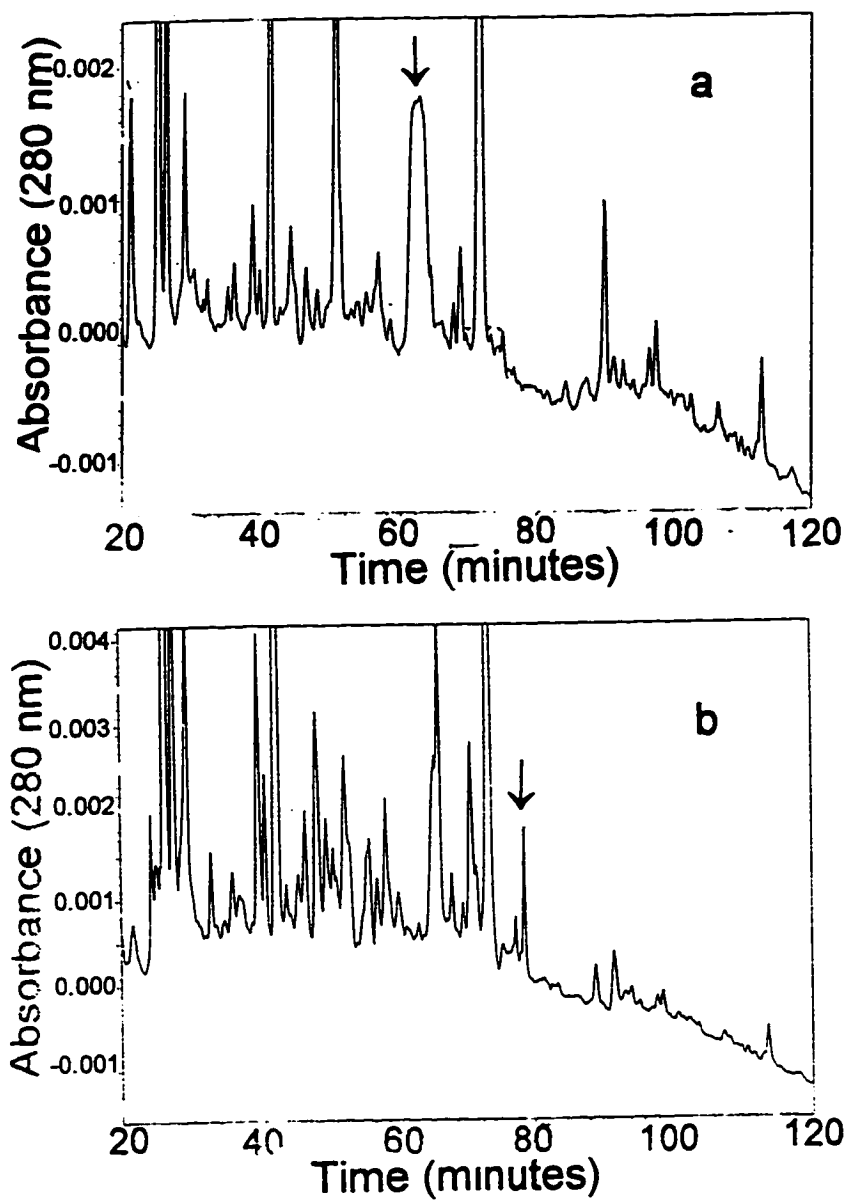


Figure 5-9. HPLC chromatograms of 12 hour tryptic peptides from a) a control sample of V-BrPO and b) V-BrPO irradiated in the presence of 5-azido-2-phenylindole for one hour. Conditions for photolabeling and digestion are as described in Materials and Methods. Injection volume 100 μ L.

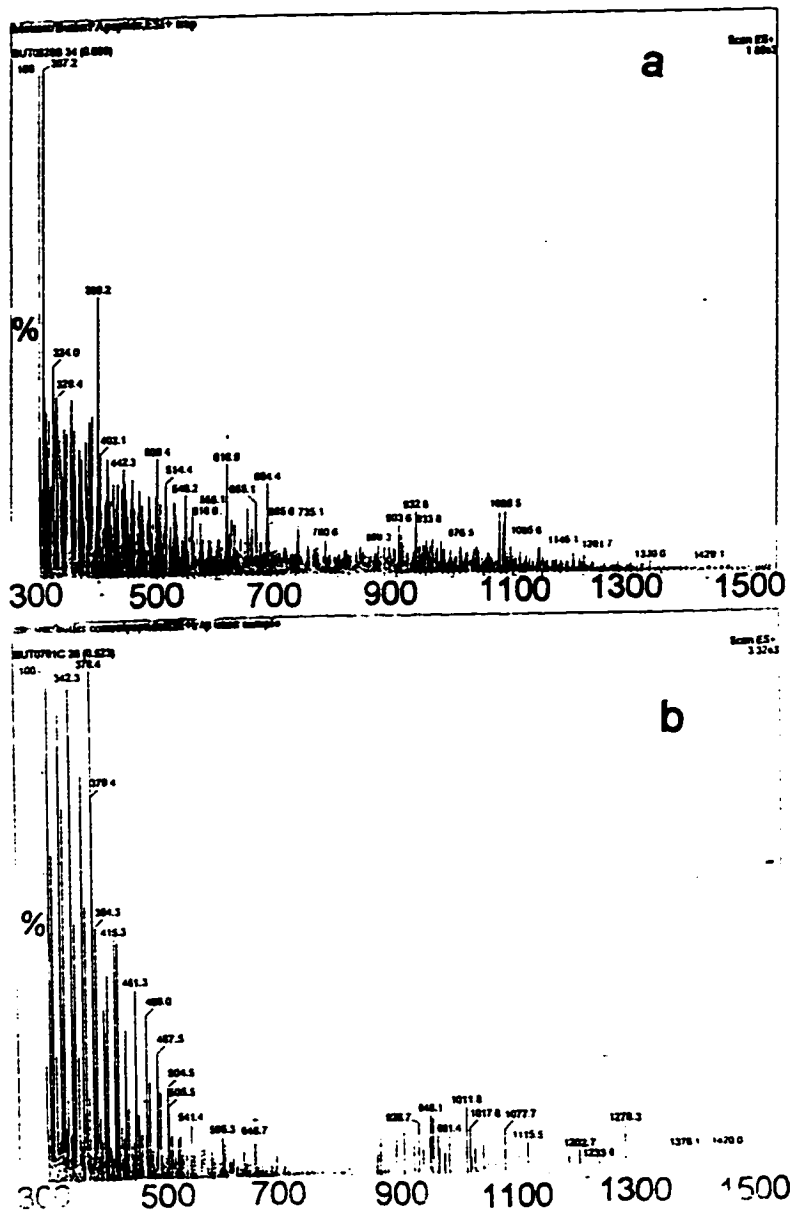


Figure 5-10. Positive electrospray mass spectra of peptides separated by HPLC in figure 5-g. a) Peptide from labeled sample, retention time 78 minutes; b) Peptide from control sample, retention time 62 minutes. Injection volume 100 μ L.

(Figure 5-10b). As can be seen in figure 5-10, the background noise in the mass spectra of these peptides is too pronounced to proceed with tandem mass spectrometry.

Micro-Amino Acid Analysis

Approximately 500 picomoles of both the control V-BrPO sample and the photoaffinity labeled sample which had been removed prior to the digestion were washed thoroughly in Centricon 30 filters (Amicon, Inc.) with water and submitted to the Caltech Protein and Peptide Mapping Facility (PPMAF) for micro-amino acid analysis on a Beckman Micro-Amino Acid Analyzer. The results of these analyses are given in Table 5-3 and in Figure 5-11.

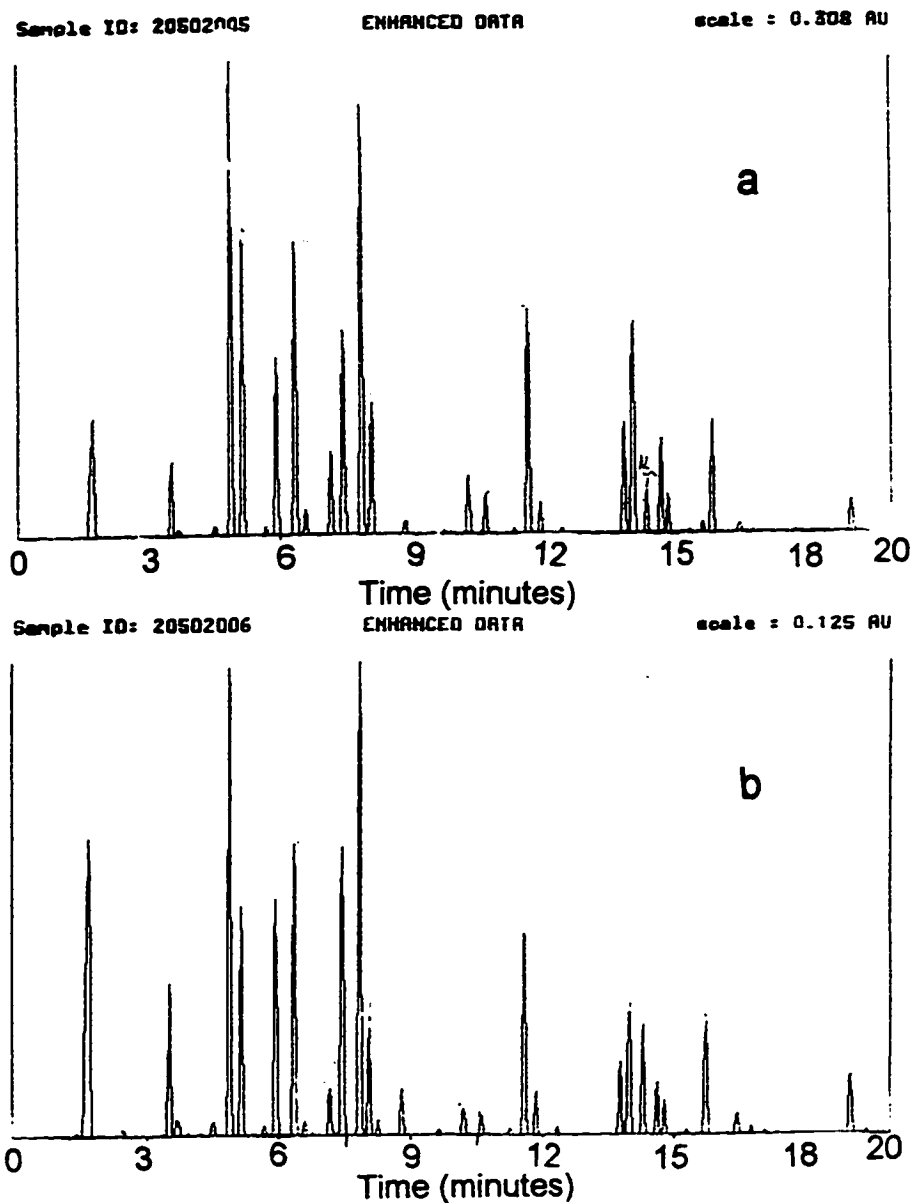


Figure 5-11. Micro- amino acid analysis chromatograms of a) native V-BrPO ; b) photolabeled V-BrPO from the Caltech Peptide/Protein Micro-Analytical Facility. Conditions for photolabeling are as described in Materials and Methods. Injection: approximately 100 pmol enzyme.

Table 5-3. Amino acid analyses of control V-BrPO and V-BrPO photoaffinity labeled with 5-azido-2-phenylindole (from the Caltech Peptide/Protein Micro-Analytical Facility).

Amino Acid	Pmol in Control V-BrPO	Pmol in Labeled V-BrPO	# of Residues in Control V-BrPO ^a	# of Residues in Labeled V-BrPO ^a
Asp	2559.43	989.51	92.068	99.346
Glu	1837.42	548.02	66.096	55.020
Ser	1221.31	642.77	43.933	64.533
Gly	1905.64	705.42	68.550	70.824
His	254.41	59.04	9.152	5.928
Arg	586.99	128.84	21.115	12.935
Thr	1566.63	878.66	56.355	88.216
Ala	3005.58	1304.96	108.117	131.017
Pro	1045.75	338.80	37.618	34.015
Tyr	179.74	12.90	6.486	1.295
Val	1245.49	445.11	44.803	44.689
Met	192.11	99.66	6.911	10.006
Ile	616.13	154.17	22.164	15.479
Leu	1278.4	303.32	45.988	30.453
(Norleucine-std)	250.00	250.00	Internal Std.	Internal Std.
Phe	566.38	116.22	20.374	11.669
Lys	525.24	198.66	18.894	19.945

^a. A molecular weight of 68 kDa was used for V-BrPO to assign the number of each residue.

The amino acid analysis chromatograms and the quantitation of the data by height provided by the Caltech facility offered clues regarding the nature of the substrate site. Substantial losses were recorded for the amino acids leucine, isoleucine, and also phenylalanine upon labeling of the enzyme. A significant loss of tyrosine was also observed for the photolabeled sample relative to the control; however, this appears to be an artifact of the data refinement procedure used at the

Caltech facility (Figure 5-11)⁴. While this data does not convincingly characterize the details of the indole binding site, it suggests that several hydrophobic residues are located in the vicinity of the binding site, as would be expected for indoles.

⁴ The procedure for correcting the baseline in the amino acid data may have an effect on the peak height and shape, particularly of smaller peaks. In addition, the quantities of each amino acid are determined by peak height as opposed to peak area.

Discussion

Regioselectivity of V-BrPO.

Comparison by HPLC of the products of the bromination of 1,3-di-*tert*-butylindole by HOBr versus catalysis by V-BrPO show that while the enzymatic reaction results in the formation of one major compound, which has been identified as 1,3-di-*tert*-butyl-2H-indol-2-one (Tschirret-Guth, 1996), the chemical reaction results in the formation of three other major products in addition to the 2-oxo-derivative. The results presented here are consistent with those reported by Hino et al. (1977) for the bromination of 1,3-di-*tert*-butylindole by NBS in acetic acid. They report the formation of a singly ring-brominated indole and a singly brominated and oxygenated indole, as shown in structures 4 and 2, respectively, from the reaction of 5 mmol 1,3-di-*tert*-butylindole and 5 mmol NBS.

Hino and coworkers (1977) did not report on the reaction of 1,3-di-*tert*-butylindole with multiple equivalents of the brominating reagent (i.e., NBS). The HPLC data from the reaction of 1,3-di-*tert*-butylindole with two equivalents of HOBr suggest that a new compound with a retention time of 11.7 minutes results when two equivalents of the brominating reagent are added (i.e., HOBr). In addition, the HPLC results show that 1,3-di-*tert*-butyl-2H-indol-2-one, the major product of the enzymatic reaction, is virtually absent when two equivalents of HOBr are used, while the peak areas of the other products detected in the reaction

with one equivalent of HOBr increase with added HOBr. The FAB mass spectrometry results from this reaction indicate that the new compound detected by HPLC is a doubly brominated oxindole as shown in structure 3. These results suggest that additional HOBr will react with 1,3-di-*tert*-butyl-2H-indol-2-one to generate singly or doubly brominated products rather than form more of the 2-oxindole.

¹H NMR data of one of the products of the reaction of HOBr and 1,3-di-*tert*-butylindole support the assertion made by Hino et al. (1977) and by Tschirret-Guth (1996) that bromination occurs on the benzene ring of this compound. The NMR data on the singly brominated compound that appeared at a retention time of 10.2 minutes in HPLC analysis indicates that the product is brominated at either the 5 or the 6 position on the benzene ring. Thus, the NMR data for this compound agree with the proposed mechanism that the two *tert*-butyl groups can hinder the approach of the bromonium ion to the pyrrole bond between the two and three positions as shown in Scheme 5-3 and instead force bromination to the less favored benzene ring.

Thus far, comparison of the products of the reaction of 1,3-di-*tert*-butylindole with HOBr versus the enzymatic reaction with V-BrPO indicates that the enzyme directly attacks at the pyrrole bond between positions 2 and 3 despite the steric hindrance from the *tert*-butyl groups. The enzyme may be blocking

attack at other bromination sites, possibly by binding interactions with the benzene ring (Tschirret-Guth, 1996). However, as is addressed in the following section, the nature of the binding of indoles to V-BrPO remains to be clarified. Regardless, the enzyme is modifying bromination selectivity.

Photoaffinity Labeling of V-BrPO.

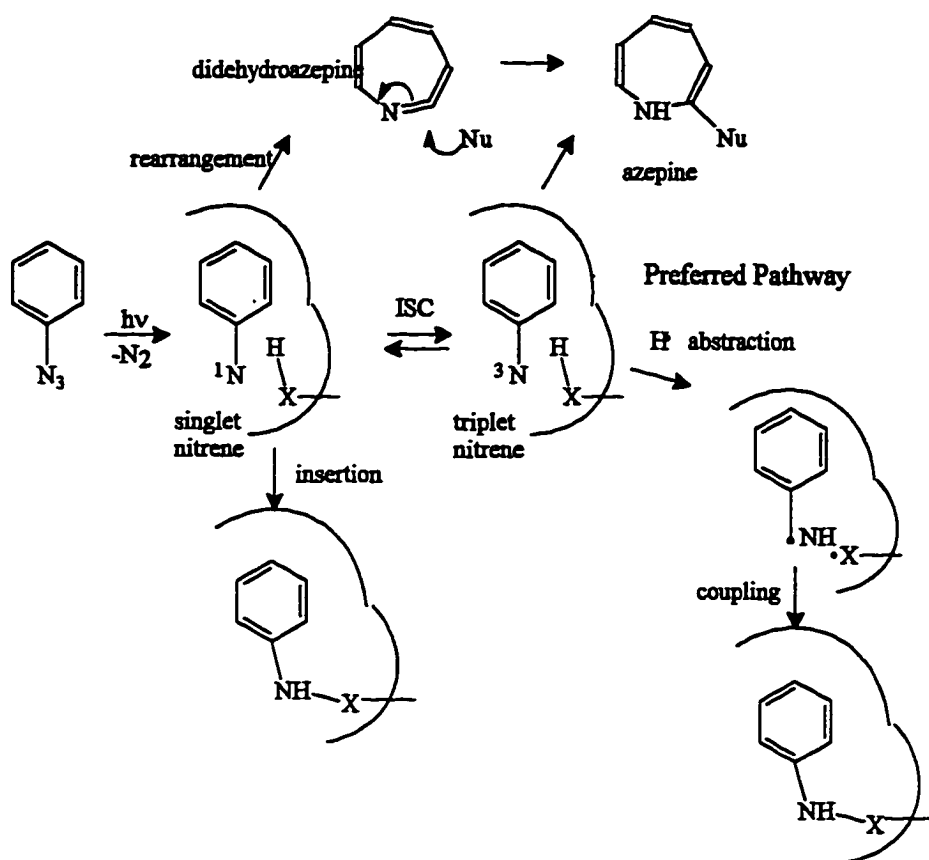
The photoaffinity experiments performed with 5-azido-2-phenylindole support the results of Tschirret-Guth (1996), which show that V-BrPO can be successfully covalently modified by an indole. Furthermore, the tryptic digests of the control and photolabeled V-BrPO in both sets of experiments presented here suggest that the crosslinking of 5-azido-2-phenylindole to V-BrPO is specific. While 5-azido-2-phenylindole did not prove to be useful as a fluorescent label (Tschirret-Guth, 1996), in the first of the photoaffinity labeling experiments presented here, the absorbance at 280 nm of the labeled peptide in the tryptic digest of modified V-BrPO was greatly enhanced over the other peptides, most likely due to the presence of the indole (Figure 5-5). Unfortunately, it did not prove possible to characterize the isolated peptide directly due to its weak mass signal.

Amino acid analysis of the control V-BrPO and photolabeled V-BrPO indicated that hydrophobic residues such as leucine, isoleucine, and phenylalanine were consumed in photolabeling reaction. It is not particularly surprising that a

hydrophobic substituted indole would bind to these residues. However, while examples exist of azido-substituted photoaffinity labels crosslinking at these residues (Garin et al., 1986; Chuan et al., 1989), they are not empirically the preferred sites for labeling; tyrosine and cysteine are the most frequently reported sites of photolabeling (Kotzya-Hibert et al., 1995). As Tschirret-Guth (1996) suggested, nucleophilic residues are frequently considered the most favorable photolabeling sites.

The actual mechanism of insertion of an azido-substituted photolabel are critical to an understanding of why certain sites are favored. Scheme 5-7 illustrates the potential pathways for azido-substituted labels, which are referred to as “nitrene precursors” (Kotzya-Hibert et al., 1995). The photoactivation of the label results in the formation of a nitrene in the singlet electronic state and the concomitant release of dinitrogen. While the singlet nitrene can theoretically insert into a carbon-hydrogen bond or a heteroatom-hydrogen bond of an amino acid residue, particularly a good nucleophile (e.g., histidine), this pathway is uncommon (Kotzya-Hibert et al., 1995). Alternatively, the singlet nitrene can rearrange to a dihydroazepine, which can react with a nucleophile such as cysteine or histidine to yield an azepine. However, azepines can be unstable to proteolysis conditions. Interestingly, empirical analysis of the residues labelled by photoaffinity techniques indicates that histidine, despite its nucleophilic character is not a common binding

site (Kotzya-Hibert et al., 1995). According to Kotzya-Hibert et al. (1995), the most promising pathway for cross-linking by a photolabel is by the intersystem crossing of the singlet nitrene to a triplet nitrene. The triplet nitrene then abstracts a hydrogen radical from an X-H bond (X = C, N, or O), which in turn results in coupling. Amino acid residues which can form particularly stable radicals for this purpose include cysteine, tyrosine, tryptophan, histidine, and phenylalanine (Kotzya-Hibert et al., 1995). However, stable radicals can also be envisaged for virtually all of the amino acid residues, with the possible exceptions of alanine, glycine, and methionine. Thus, while explanations of photoaffinity labeling have frequently favored insertion into nucleophilic residues, the formation of a stable radical may actually be frequently the key step in labeling with nitrene precursors (Kotzya-Hibert et al., 1995).



Scheme 5-7. Pathways for the coupling of aryl nitrenes to proteins.

It can be concluded that non-nucleophilic, hydrophobic residues such as leucine, isoleucine, and phenylalanine are clearly viable candidates for photoaffinity labeling sites and, as was stated previously, likely sites for the binding of a substituted indole.

The recently solved crystal structure of the vanadium chloroperoxidase from *Curvularia inaequalis* (Messerschmidt and Wever, 1996), which has been

discussed throughout this dissertation, showed that the vanadium was located at the end of a channel of helices, one side of which is hydrophobic and the other of which is hydrophilic. The hydrophobic surface is an attractive location for binding a suitable organic substrate such as an indole. Sequence similarity between the vanadium chloroperoxidase and V-BrPO from *A. nodosum* suggests that a similar structural motif may exist in the algal bromoperoxidase; for example, Phe 358, Phe 499, Ala 345, Ala 405, Ala 410, and Ala 487, from the chloroperoxidase sequence are all conserved in the bromoperoxidase.

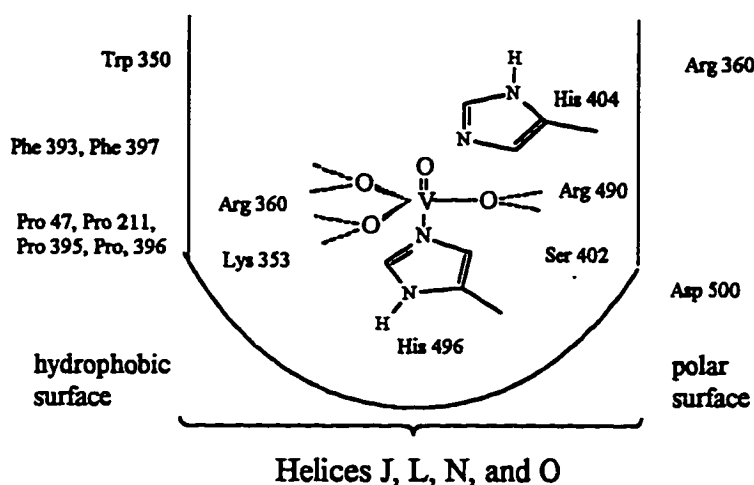


Figure 5-12. The active site of the vanadium chloroperoxidase from *Curvularia inaequalis* (adapted from Messerschmidt & Wever, 1995)

The photoaffinity experiments presented here do not further support the assertion by Tschirret-Guth (1996) that the modification of V-BrPO occurs at an arginine or lysine, which are preferred sites for trypsin cleavage, thus preventing

cleavage at that site. That explanation was based on the evidence that two peptides present in the digest of the control enzyme sample disappeared in the labeled sample and were replaced by a single peptide with a much longer retention time, a situation that was not detected in the present studies. While the experiments described in this chapter do not fully support Tschirret-Guth's assertion that the indole photolabel *reversibly* binds to a hydrophobic surface of the active site of V-BrPO and then covalently binds to arginines on a hydrophilic region of the active site, the data presented here *do* favor the binding of the indole substrate to a hydrophobic region of the protein.

In order to utilize the photoaffinity labeling technique to its full potential with V-BrPO, it will be necessary to obtain a sufficient quantity of tryptic peptide to be sequenced either by tandem mass spectrometry or by Edman's degradation procedures. It is likely that the weak signal in the electrospray mass spectrum is due to inefficient trypsin digestion. The digestion was greatly improved from previous attempts by the use of a pre-digestion preparation procedure adapted from Uchida and Kawakishi's work on superoxide dismutase, another enzyme that is resistant to proteolysis (Uchida & Kawakishi, 1994). However, despite starting with close to 5 mg (~ 70 nmol) of photolabeled enzyme, inadequate recovery was achieved for clean mass spectral analysis.

The efficiency of trypsin digestion may be greatly assisted by dilution of the target protein (i.e., V-BrPO). In both experiments described here, V-BrPO was present at μM concentrations during digestion. Unpublished observations from this laboratory indicate that V-BrPO may form oligomers at these concentrations. Accordingly, diluting the enzyme to nanomolar concentrations at which V-BrPO is primarily monomeric but maintaining the same ratio of trypsin to V-BrPO (i.e., 1:25 trypsin to V-BrPO or higher trypsin) might assist in opening up the enzyme for more complete digestion. Dilution of the trypsin would likely require increased time for digestion. Because trypsin loses its activity rapidly in solution at 37 °C, the addition of more trypsin at 3 to 6 hour intervals may also further increase the efficiency of digestion. Finally, it may prove necessary to increase the total enzyme used to 8 to 10 mgs or more in order to obtain sufficient yield of the key peptides for sequence analysis.

References

- Chuan, H., Lin, J., Wang, J.H. (1989) *J. Biol. Chem.* 264, 7981-7988.
- Cotton, M.L.. & Dunford, H.B. (1973) *Can. J. Chem.* 51, 582-587.
- DeBoer, E. & Wever, R. (1988) *J. Biol. Chem.* 263, 12326-12332.
- DeFabrizio, C.R. (1968) *Ann. Chim.* 58, 1435-1445.
- Garin, J., Boulay, F., Issartel, J.-P., Lunardi, F., Vignais, P.V. (1986) *Biochemistry* 25, 4431-4437.
- Hino, T., Tonozuka, M., Ishii, Y., Nakagawa, M. (1977) *Chem. Pharm. Bull.* 25, 354-358.
- Itoh, N., Izumi, Y., Yamada, H. (1987) *J. Biol. Chem.* 262, 11982-11987.
- Itoh, N., Hasan, A. K. M. Q., Izumi, Y., Yamada, H. (1988) *Eur. J. Biochem.* 172, 477-484.
- Kotzya-Hibert, F., Kapfer, I., Goeldner, M. (1995) *Angew. Chem. Int. Ed. Engl.* 34, 1296-1312.
- Messerschmidt, A. & Wever, R. (1996) *Proc. Natl. Acad. Sci. USA* 93, 392-396.
- Simons, B.H., Barnett, P., Vollenbroek, E.G.M., Dekker, H.L., Muijers, A.O., Wever, R. (1995) *Eur. J. Biochem.* 229, 566-574.
- Tschirret-Guth, R.A. & Butler, A. (1994) *J. Am. Chem. Soc.* 116, 411-412.
- Tschirret-Guth, R.A. (1996) Ph.D. Dissertation, University of California, Santa Barbara, 1996.
- Uchida, K., & Kawakishi, S. (1994) *J. Biol. Chem.*, 269, 2405-2410.
- Vilter, H. (1995) in "Metal Ions in Biological Systems," Sigel, H. & Sigel, A., eds. Vol 31., New York:Dekker, pp. 326-362.

Chapter 6. Vanadium Dependent Photomodification of Vanadium

Bromoperoxidase

Introduction

Inorganic vanadates, V_i ($H_2VO_4^-/ HVO_4^{2-}$), are effective analogs for phosphates in biological systems because phosphates and vanadates have similar tetrahedral structures, bond lengths and pK_a values. Vanadates have been shown to be potent inhibitors of ATPases (ATP = adenosinetriphosphate) such as dynein from sea urchin sperm flagella and myosin from rabbit skeletal muscle (Goodno, 1982). The hydrolysis of ATP by an ATPase proceeds according to equation 1:



where P_i is phosphate, $H_2PO_4^-/HPO_4^{2-}$, and ADP is adenosinediphosphate. In this reaction, ADP and P_i form a transition state complex with the ATPase. Because vanadate can bind more tightly than phosphate, inclusion of vanadate in the reaction results in the formation of a stable complex with the enzyme, ADP and vanadate. Thus ADP is trapped at the active site in a complex that mimics the transition state of the enzyme (Goodno, 1982).

The dynein ATPase from sea urchin sperm flagella is responsible for flagellar motility in the urchin sperm. Dynein is a large multisubunit protein (MW = 1,228 kDa) possessing two heavy chains (α and β), which had been estimated to weigh approximately 300 to 500 kDa each (see, for example, Huang et al., 1979)

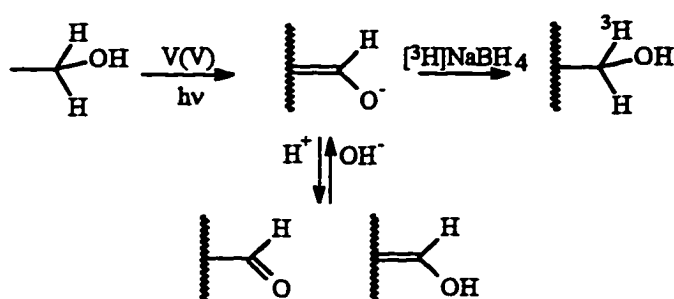
Both heavy chains have an ATPase site (Pfister et al., 1984). Gibbons and coworkers attempted to study the ATPase sites on the heavy chains of dynein by photoaffinity labeling the protein with 8-N₃ATP stabilized in the phosphate binding site by millimolar vanadate and magnesium ions (Lee-Eiford et al., 1986). They found, however, that the vanadate complex was not stable to UV irradiation at 254 or 365 nm and that the α and β heavy chains of the molecule were being cleaved at specific sites (Lee-Eiford et al., 1986; Gibbons et al., 1987), resulting in the formation of two peptides with molecular weights of 228 and 200 kDa. This cleavage was determined to be vanadate-dependent and presumably occurred at the phosphate binding site of the enzyme. Thus, in the presence of vanadium, these workers were able to map the location of the ATPase sites in dynein and determine that the exact molecular weights of the heavy chains were 428 kDa (Gibbons et al., 1987).

A subsequent study on the ATPase myosin from rabbit skeletal muscle illustrated the power of vanadium-dependent photomodification in characterizing the phosphate binding sites of proteins (Grammer et al., 1988; Cremo et al., 1988; Cremo et al., 1989). This multisubunit enzyme (MW = 460 kDa), which possesses two heavy and two light chains, is the primary motor protein in eukaryotes. Trypsin cleavage of the heavy chains gives fragments termed S1 and S2; S1, which has a molecular weight of 95 kDa, contains the ATPase site of the enzyme. As

before with dynein, attempts at photoaffinity labeling at this site in S1 with an azido-substituted nucleotide, magnesium ion and millimolar vanadate revealed that the vanadate complex was not stable to ultraviolet light. In fact, upon irradiation, while no cleavage occurred, Ca^{2+} -ATPase activity of S1 increased to 4 to 5 times that of a sample irradiated in the absence of vanadate. In addition, this activity increase was accompanied by loss of both the nucleotide and vanadate from the active site and an increased absorbance at 270 nm, particularly at higher pH values. The nucleotide complex could be reformed, and upon irradiation of the reformed complex with the photomodified S1, specific cleavage of S1 occurred, forming peptides of 21 and 74 kDa (Grammer et al., 1988).

If the photomodified S1 was subject to reduction by NaBH_4 instead of a second irradiation step, native activity could be restored. Reduction of the irradiated sample with NaB^3H_4 followed by amino acid analysis and detection of the radioactivity in the separated fractions showed that all of the tritium label was incorporated into the fraction corresponding to serine (Cremonesi et al., 1988). Thus, serine was identified as the site of photomodification. Proteolytic digestion of tritium-labeled S1 yielded peptides possessing the glycine rich consensus sequence that has been identified in several enzymes which utilize ATP or GTP as substrates. In rabbit skeletal myosin, this consensus sequence is located at residues 178 to 186. The labeled peptide included a serine at position 180, which was identified as the

site of photomodification and cleavage in the enzyme (Cremonesi et al., 1989). Based upon the pH dependence of the absorbance changes in the enzyme spectrum upon photomodification, it was proposed that the serine is oxidized to a "serine aldehyde", which is primarily a chromophoric enolate at higher pH but is in non-chromophoric enol and aldehyde forms at lower pH (Cremonesi et al., 1988); (Scheme 6-1).



Scheme 6-1. Oxidation of serine in rabbit skeletal myosin to a "serine aldehyde" and subsequent reduction with $[^3\text{H}]\text{NaBH}_4$.

Since the identification of the photomodified serine in myosin, similar modifications of active site serines have been reported in other phosphate-binding proteins, including isocitrate lyase from *E. Coli* (Ko et al., 1992) and ribulose-1,5-bisphosphate carboxylase/oxygenase from spinach (Mogel and McFadden, 1989). In addition, a proline residue has been identified as the site of photomodification and cleavage in the "phosphate-loop" (i.e., the glycine-rich consensus sequence) of adenylate kinase from chicken muscle (Cremonesi et al., 1991). This proline is located

in a position equivalent to serine 180 in rabbit skeletal myosin. In adenylate kinase, the proline was modified by photooxidation and decarboxylation to give a cyclized γ -aminobutyric acid.

While vanadate-mediated photochemistry has been shown to be a powerful tool in characterizing the active sites of several phosphate-binding proteins, of equal challenge is the characterization of the binding site for a native vanadium(V) metal center as is found in vanadium bromoperoxidase (V-BrPO). Although numerous attempts have been made to characterize the vanadium(V) site of vanadium bromoperoxidase by spectroscopic and chemical modification techniques, to date no ligating amino acid has been identified with certainty. Sequence similarity between V-BrPO and the vanadium chloroperoxidase from the fungus *Curvularia inaequalis* suggests that the vanadium may be ligated to a single histidine residue (Vilter, 1995; Meeserschmidt & Wever, 1996). The presence of a histidine has been further suggest by studies on the inhibition and inactivation of V-BrPO by hydrogen peroxide (Soedjak et al., 1995; this work, Chapter 2). Vanadate-mediated photochemistry is an attractive technique for studying the vanadium center in V-BrPO since it has been shown in several phosphate-binding proteins to involve modifications of amino acid residues ligated to vanadium. Thus, this technique seemed a viable method by which to more conclusively identify amino acid residues coordinated to the vanadium(V) center in V-BrPO. This chapter

describes the results of irradiating native vanadium bromoperoxidase with ultraviolet light.

Materials and Methods

Bromoperoxidase preparation. Vanadium bromoperoxidase was isolated from *Ascophyllum nodosum* collected at Kornwerderzand, Holland in 1990. The isolation procedure for V-BrPO described previously (Everett et al., 1990) was modified as follows: Crosslinked polyvinylpyrrolidone (1.5%) was included in the initial extraction of V-BrPO in 0.2 M Tris buffer, pH 8.3. The ammonium sulfate and ethanolic precipitation steps and the Concanavalin A column were omitted. For some experiments, V-BrPO was purified by electroelution using a BioRad Model 422 Electroeluter Module (see Appendix I).

Bromoperoxidase activity measurements. The standard assay for determining the specific bromoperoxidase activity of V-BrPO from *A. nodosum* is the bromination of 50 μM monochlorodimedone (MCD), which is monitored spectrophotometrically at 290 nm under conditions of 0.1 M KBr and 2 mM H_2O_2 in 0.1 M phosphate, pH 6.0. The change in extinction coefficient between MCD and Br-MCD is $19,900 \text{ cm}^{-1} \text{ M}^{-1}$ above pH 5. The specific activity of the enzyme samples used in this study ranged from 85 to 120 U/mg, where U is equivalent to micromoles of MCD brominated per minute.

Irradiation of vanadium bromoperoxidase. V-BrPO was irradiated at 308 nm with a Lambda Physik Model LPX 105 XeCl excimer laser in Professor Peter

Ford's laboratory at UCSB. Samples of 60 to 225 nM V-BrPO (0.5 to 1.5 ml) in 0.1 M Tris pH 8.3 in high UV quartz cuvettes were set within 2 cm of the laser aperture and photolyzed with a 10 MHz pulse in 30 second intervals for up to 4 minutes.

Preparation of apo-bromoperoxidase and re-incorporation of vanadium(V).

V-BrPO was demetallated by overnight dialysis against 0.1 M citrate-phosphate buffer at pH 4.0 containing ~ 1 mM EDTA. The buffer was changed several times to facilitate vanadium(V) removal. The demetallated bromoperoxidase, still within the dialysis membrane at pH 4.0, was then placed in 0.1 M Tris buffer pH 8.3. The apo enzyme was dialyzed against several volumes of Tris at pH 8.3 to remove remaining phosphate and vanadium(V). Reincorporation of vanadium(V) into demetallated enzyme was attempted by incubating the sample overnight with 50 to 100 μM NH_4VO_3 in 0.1 M Tris buffer at pH 8.3 or higher. After incubation, excess vanadium was removed by ultrafiltration with Centricon 10 filters (10,000 MW cutoff) or Centricon 30 filters (30,000 MW cutoff).

Anaerobic irradiation of V-BrPO. V-BrPO (150 nM) in 0.1 M Tris pH 8.3 was placed in a sealable quartz spectrophotometric cell equipped with a freezing bulb. The sample was deaerated by successive cycles of freeze-pump-thaw after which the cell was filled with nitrogen. The anaerobic sample was then irradiated

as described above. MCD assay activity of the enzyme sample was determined in air after irradiation was completed.

Atomic absorption analyses. The ability of photomodified V-BrPO to bind vanadium(V) was examined by atomic absorption spectrometry (AAS). V-BrPO (60 nM), which had been irradiated for 30 seconds as described above, was washed to remove released vanadium and concentrated to 0.9 μM . This enzyme sample was then split into two samples. One of the two samples was incubated with 50 μM NH_4VO_3 overnight. The incubated sample was then rewashed with 0.1 M Tris pH 8.3 by ultrafiltration in a Centricon 30 to remove excess vanadium and then reconcentrated to 0.9 μM . These two samples and a 1.5 μM sample of untreated V-BrPO were then tested for vanadium content by AAS. AAS was performed on a Perkin Elmer SpectrAA furnace atomic absorption spectrometer with a 250 ppb vanadium standard. The samples were tested using a standard additions procedure. In this procedure, 20 μL samples were auto-injected for analysis and compared to a standard curve.

Reduction of irradiated bromoperoxidase. 150 to 250 μL samples of irradiated V-BrPO in Tris pH 8.3 were incubated with net 50 μM to 100 mM NaBH_4 . NaBH_4 was dissolved in either 0.1 M borax buffer at pH 10.0 or in a 0.2% solution of NaOH to stabilize the borohydride against conversion to borate. After addition of the borohydride to the irradiated enzyme solution, the reduction reaction

was quenched by ultrafiltration in Centricon 10 or 30 filters or by the addition of 0.1 M citrate at pH 4.0 followed by ultrafiltration. For trials at low concentrations of NaBH_4 , free vanadium released by the enzyme upon irradiation was washed out by ultrafiltration prior to incubation with borohydride. After the attempted reduction and washing of the enzyme samples, they were brought to their original volume and incubated with 50 to 200 μM NH_4VO_3 . Reactivation was determined by the MCD assay as described above.

Trypsin digestion. Samples of native V-BrPO and V-BrPO irradiated under conditions of 225 nM enzyme in 0.1 M Tris pH 8.3 for three minutes were digested with trypsin using an in-gel procedure described by Rosenfeld and coworkers (1992). In this procedure, 200 μg V-BrPO was denatured in reducing buffer for 90 minutes at 100 °C and subsequently loaded on to a doubly thick 12.5% SDS-PAGE gel (Laemmli, 1979) in a Mini-Protean II electrophoresis cell (Pharmacia). The gel was run in Tris-glycine buffer 0.1 M pH 8.0 at 300 V. After electrophoresis, the gel was stained in 20% methanol, 0.5% acetic acid containing 0.2% Coomassie Brilliant Blue R-250 for 30 minutes and then destained in 30% methanol. Stained bands of V-BrPO excised and washed twice with 300 μL 50% acetonitrile in 0.1 M $(\text{NH}_4)_2\text{CO}_3$ at pH 8.9 for 30 minutes. After partial drying, the excised bands were rehydrated with 10 to 15 μL of 0.1 M $(\text{NH}_4)_2\text{CO}_3$ pH 8.9 containing 0.02% Tween 20. Next, 5 mL of 0.5 mg/mL bovine trypsin was added.

Once the trypsin solution had been absorbed by the gel, small aliquots (5 to 10 μL) of 0.1 M $(\text{NH}_4)_2\text{CO}_3$ were added until the gel slice was fully rehydrated. The samples were digested for approximately 4 hours at 30 °C and quenched by the addition of 2 mL glacial acetic acid. The tryptic peptides were removed in two extractions from the gel slices with enough 80% acetonitrile/0.1% TFA in H_2O to completely cover the slice. The combined extracts were analysed by HPLC using a linear gradient of water and 0.1% TFA to 80% acetonitrile and 0.1% TFA in water.

Acid hydrolysis of enzyme samples. A sample of 60 nM V-BrPO in 0.1 M Tris pH 8.3, which had been photolyzed at 308 nm for 3 minutes, was washed several times with water in a Centricon 10 filter and then evaporated to dryness in a Savant Speed Vac concentrator. Hydrolysis of the enzyme was achieved by dissolving the samples in *ca.* 200 μL 6.0 M HCl in sealable ampules and deaerating with argon for approximately two minutes. The deaerated ampules were then flame sealed and placed in an oven at 110 °C overnight. After approximately 18 hours, the ampules were broken open and the contents evaporated to dryness.

HPLC electrochemical detection. 2-Oxohistidine was analyzed by HPLC electrochemical detection (HPLC-ECD) using a Waters 464 electrochemical detector equipped with a glassy carbon electrode. Detection was run in the DC mode at a potential of 850 mV (Uchida and Kawakishi, 1993). Underivatized protein hydrolysis samples were analyzed for 2-oxohistidine on a Spherisorb ODS-2

column (Phase Separations, LTD). An isocrat of 50 mM NaCl, 0.1% TFA, and 20% methanol at 0.7 mL/min was used to separate the amino acids. The protein hydrolysate samples were dissolved in the elution solvent or water and filtered through 0.2 μ m filters prior to injection. Injections were typically 100-200 μ L. Protein samples were compared to a standard of 2-oxohistidine, which was prepared as described by Uchida and Kawakishi (1986).

Amino acid analyses. Amino acid analyses were performed by Dirk S. Krapf at the Protein/Peptide Mapping Analytical Facility at California Institute of Technology using a Beckman Amino Acid Analyzer equipped with an autosampler. Approximately 50 pmol V-BrPO were irradiated for 4 minutes as described above in 0.1 M Tris buffer pH 8.3 at a concentration of 60 nM V-BrPO. This sample and a control sample of 60 nM V-BrPO in 0.1 M Tris were each washed several times in Centricon 10 filters and evaporated to dryness on a Savant Speed Vac Concentrator.

General reagents and procedures. Protein concentration was determined using the bicinchoninic acid assay kit from Pierce, Inc. Hydrogen peroxide concentration was determined with the triiodide assay as described by Cotton and Dunford (1973). All chemicals used were reagent grade or better.

Results and Interpretation

Irradiation of 1.5 mL of 150 nM V-BrPO in 0.1 M Tris buffer pH 8.3 for three minutes with 308 nm light from an excimer laser resulted in loss of ~ 90% of the bromination activity of the sample prior to irradiation as measured by the MCD assay (Figure 6-1). This inactivation was not reversible by incubation with 100 μ M NH_4VO_3 . The loss of enzyme bromination activity was determined to be proportional to the time of irradiation (Figure 6-2). The bromination activity of the photolyzed sample continued to decrease slightly after irradiation was complete (Figure 6-3).

In order to determine if the loss of activity of V-BrPO upon irradiation was a vanadium-mediated effect, the vanadium was removed from a sample of holo-V-BrPO with a specific activity of 85 U/mg, and the resulting apo enzyme was subjected to irradiation under the same conditions as the original holo-enzyme sample: 1.5 ml of 150 nM apo BrPO in 0.1 M Tris pH 8.3, three minutes of irradiation at 308 nm. The irradiated apo enzyme sample and an unirradiated control sample of apo enzyme were then each reincubated overnight with 100 μ M NH_4VO_3 in 0.1 M Tris pH 8.3. After incubation, the samples were washed in Centricon 30 filters to remove excess vanadate and tested for MCD assay activity. The control sample had an activity of 0.392 abs/min and the irradiated sample had

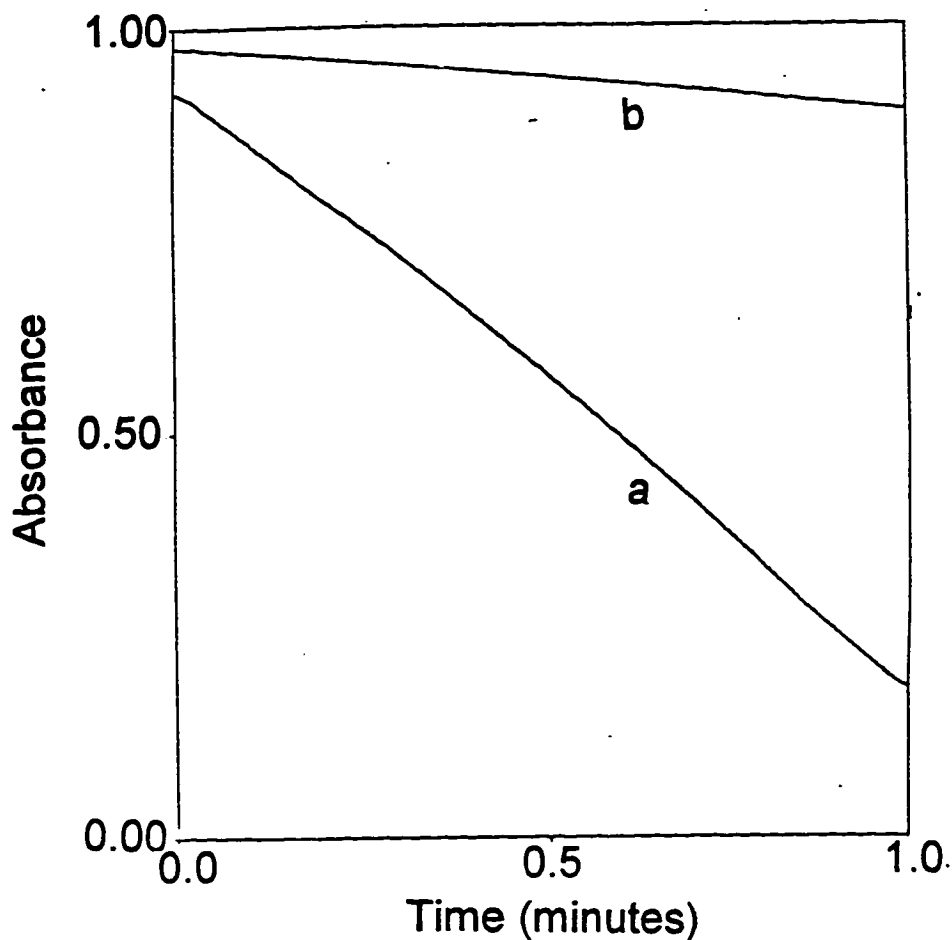


Figure 6-1. MCD assay profiles of a) native V-BrPO and b) irradiated V-BrPO. MCD assay conditions as described in Materials and Methods. Enzyme concentration: 7 nM V-BrPO. Irradiation conditions: 225 nM V-BrPO in 0.1 M Tris pH 8.3, 3 minute irradiation at 308 nM; 1.5 mL sample volume.

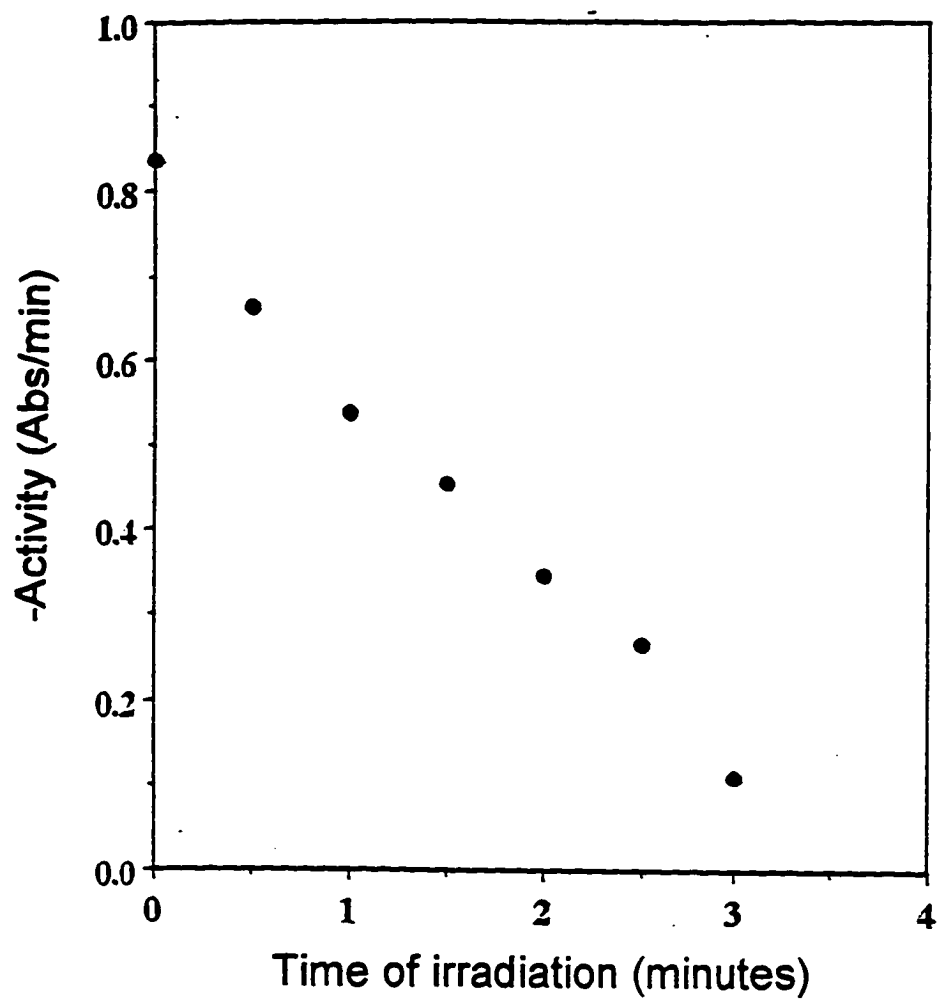


Figure 6-2. MCD bromination activity of irradiated V-BrPO versus time of irradiation. MCD assay conditions as described in Materials and Methods. Enzyme concentration: 7 nM V-BrPO. Irradiation conditions: 225 nM V-BrPO in 0.1 M Tris pH 8.3, varied duration at 308 nm; 1.5 mL sample volume.

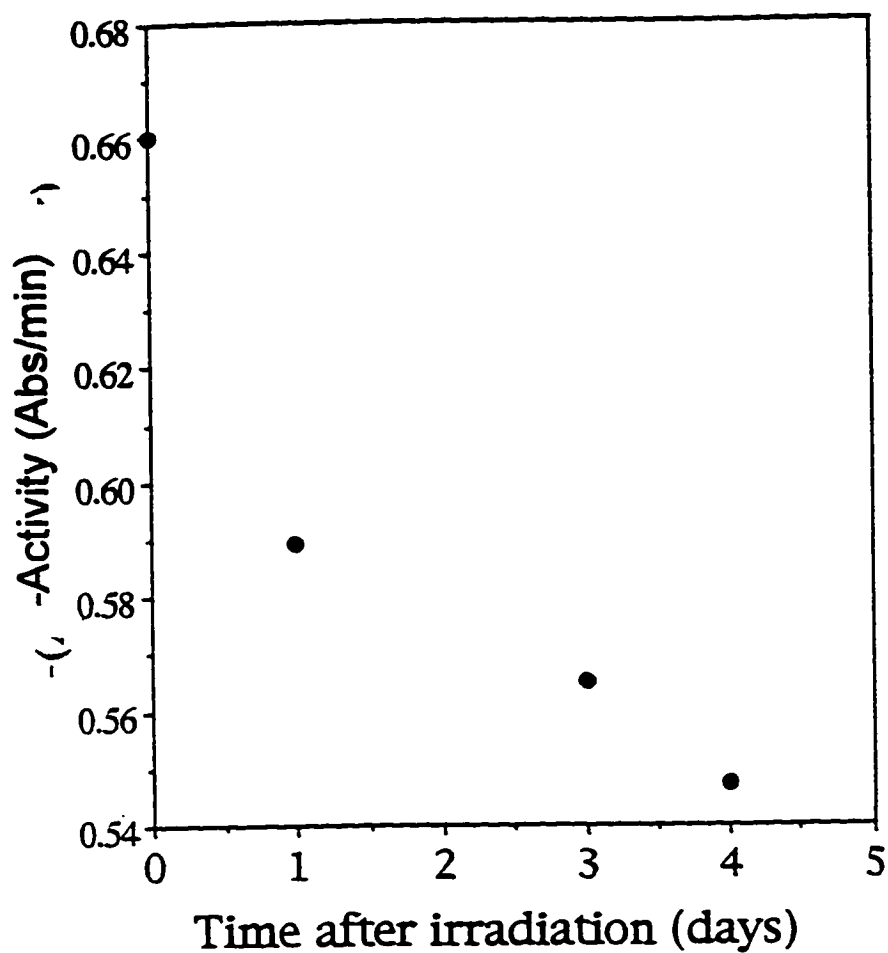


Figure 6-3. MCD bromination activity of irradiated V-BrPO versus time after irradiation. MCD assay conditions as described in Materials and Methods. Enzyme concentration: 7 nM V-BrPO. Irradiation conditions: 225 nM V-BrPO in 0.1 M Tris pH 8.3, 30 second irradiation at 308 nm; 1.5 mL sample volume.

an activity of 0.350 abs/min, which correspond to 75 U/mg and 67 U/mg, respectively. As expected, incubation of the control sample with vanadium(V) restored most of the bromination activity present in the sample prior to demetallation (i.e., 89% of 85 U/mg). Incubation of the irradiated apo enzyme sample with vanadium(V) resulted in restoration of 80% of the MCD bromination activity present prior to demetallation and 90% of the activity restored to the unirradiated apo enzyme (Figure 6-4). Thus, since irradiation of apo bromoperoxidase results in only a small amount of irreversible inactivation, the inactivation of holo-V-BrPO is a vanadium-dependent process such as the photomodifications seen with vanadate in the phosphate-binding enzymes.

Analysis by SDS-PAGE of holo-V-BrPO that had been inactivated by irradiation at 308 nm showed no evidence for cleavage of the protein backbone; both the irradiated and control samples of V-BrPO had major bands at a molecular weight of approximately 68 kDa. As described in the introduction to this chapter, cleavage also did not occur in the first irradiation of vanadate-containing rabbit skeletal myosin (Grammer et al., 1988). In the myosin studies, loss of vanadate was observed upon irradiation and photomodification. A similar loss was detected in V-BrPO after photolysis. Atomic absorption of V-BrPO irradiated for three minutes at 225 nM V-BrPO in 0.1 M Tris pH 8.3 showed a loss of 60% of the vanadium content initially present in the sample, from 0.76 equivalents of

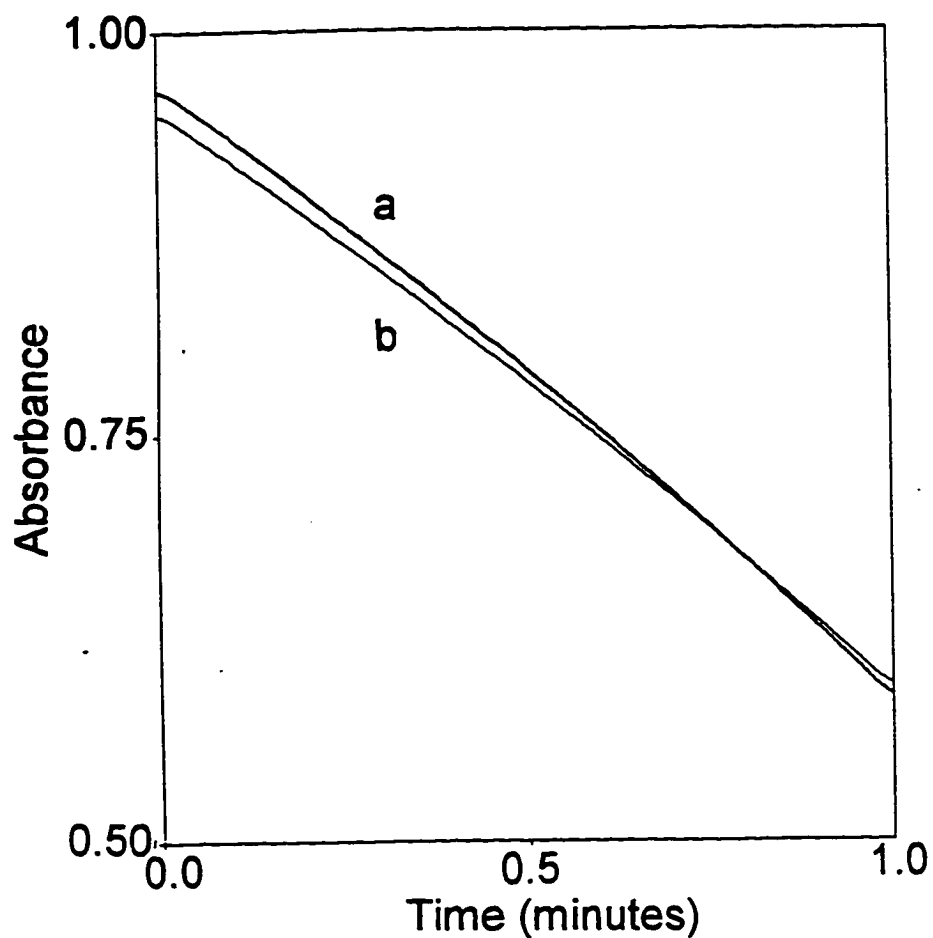


Figure 6-4. MCD activity profiles for a) apo-BrPO and b) irradiated apo-BrPO after overnight incubation with $(\text{NH}_4)_2(\text{VO}_3)$. MCD assay conditions as described in Materials and Methods Enzyme concentration: 7 nM V-BrPO. Irradiation conditions: 150 nM V-BrPO in 0.1 M Tris pH 8.3, 3 minute irradiation at 308 nm; 1.5 mL sample volume.

vanadium per protein molecule to only 0.31 equivalents of vanadium per protein molecule (Table 6-1). In addition, this loss of vanadium was proportional to the loss of bromination activity in the sample. Prior to irradiation, the enzyme sample had a specific activity of 120 U/mg; however, after 3 minutes of irradiation the specific activity was only 51 U/mg, a loss of 58% of the activity originally present in the enzyme (Table 6-1).

Table 6-1. Vanadium content and bromination activity of native and irradiated V-BrPO samples.

Sample	V/BrPO^a	Activity (U/mg)	V-normalized Activity (U/mg)
native V-BrPO	0.76	120	158
irradiated BrPO	0.31	51	165
irradiated BrPO + V(V)	0.29	52	179

^a. Vanadium content of the enzyme was determined using a molecular weight of 67,000 Da.

Attempted Reactivation of V-BrPO

In their studies on rabbit myosin, Grammer and coworkers (Grammer et al., 1988) showed that the vanadate nucleotide complex formed with myosin prior to irradiation could be reformed after the photolysis. Subsequent irradiation of the photomodified S1 /vanadate/nucleotide complex resulted in site specific cleavage of the S1 chain into 74 kDa and 21 kDa fragments. Attempts to recoordinate

vanadium to V-BrPO after the first irradiation step with the intention of performing a second photolysis step were not successful. Atomic absorption was performed on the irradiated sample described in the previous paragraph after this sample was incubated overnight with 50 μM NH_4VO_3 and washing by ultrafiltration to remove unbound vanadium. No recoordination of vanadium(V) to the photomodified enzyme was detected. As shown in Table 6-1, 0.29 vanadium centers per molecule were present in the sample reincubated with NH_4VO_3 versus 0.31 vanadium centers per molecule in the irradiated sample that was not incubated with vanadium(V). Thus, irradiated vanadium bromoperoxidase was unable to recoordinate vanadium(V), but, unlike rabbit myosin, no potential existed for performing a second irradiation in search of vanadium-dependent photocleavage.

While the similarity of the V-BrPO photochemistry to that of myosin and other phosphate-binding proteins ended after the first vanadium-mediated photomodification, it was still of interest to determine if the photomodification occurring was, like these phosphate systems, due to the oxidation of a serine to a "serine aldehyde" (Grammer et al., 1988). Accordingly, several attempts were made to reduce the protein with borohydride, as had been done in the myosin system. Incubation of photolyzed enzyme samples with borohydride was performed with NaBH_4 concentrations ranging from 50 μM to 100 mM. After removal of excess borohydride, the samples were incubated with 50 to 200 μM

NH_4VO_3 for at least two hours. However, activity was never restored to the irradiated V-BrPO samples regardless of the initial borohydride concentration used (Figure 6-5).

One possible reason that V-BrPO was not reactivated by borohydride was that borate, a hydrolysis product of borohydride, was inhibiting bromoperoxidase activity. Borates have similar configurations to phosphates and vanadates, and it has been demonstrated that phosphates can effectively inhibit the enzyme, particularly at low pH, by replacing the vanadium (Soedjak et al., 1991). The effect of borate on the bromination activity of bromoperoxidase was examined at pH 4.0 (0.1 M citrate buffer), pH 6.0 (0.1 M MES buffer), and pH 8.3 (0.1 M Tris buffer). Incubation of 60 nM V-BrPO for 12 hours in each of these buffers at borate concentrations ranging from 0.2 mM to 50 mM did not cause a decrease in activity relative to a control incubated in the absence of borate (Table 6-2). Incubation of V-BrPO at pH 4.0 resulted in activity loss regardless of the borate concentration. This decrease in activity is probably due to loss of vanadium from the enzyme at this pH. In any case, lack of reactivation of V-BrPO by NaBH_4 indicates that the vanadium-dependent photomodification of V-BrPO is not simply the photooxidation of a serine to a "serine aldehyde" as was seen in rabbit myosin (Grammer et al., 1988) and other phosphate-binding systems.

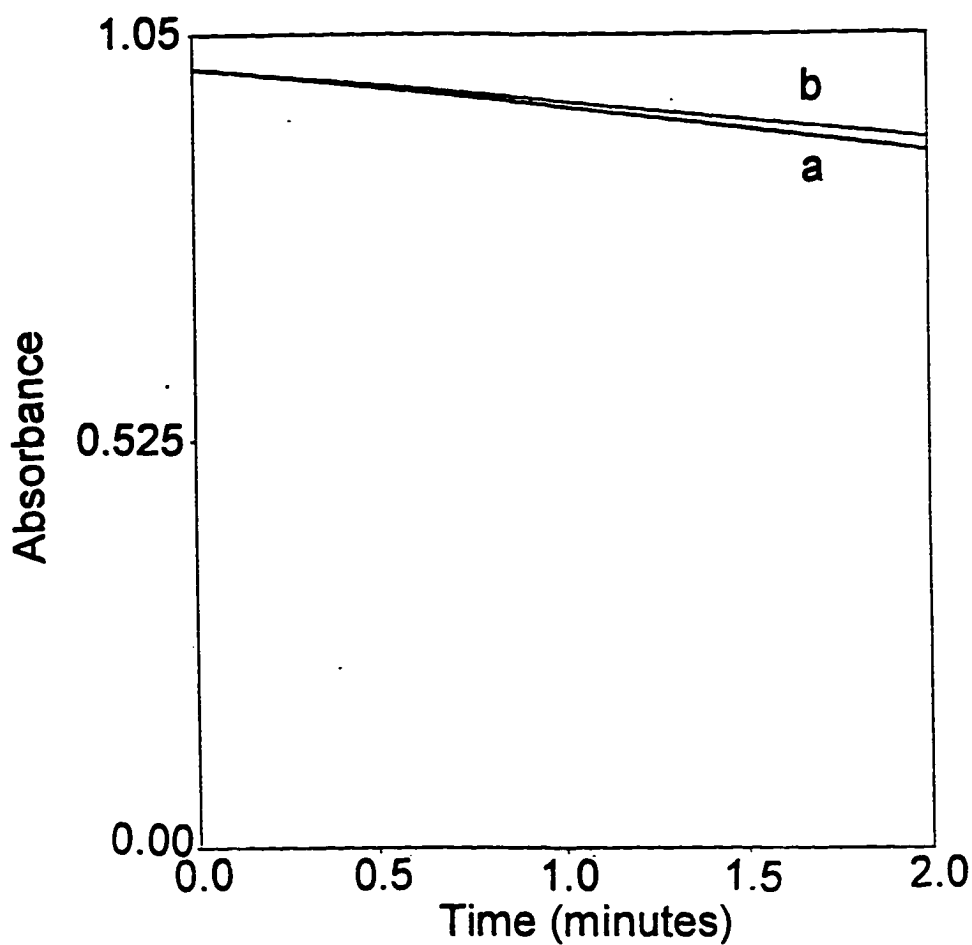


Figure 6-5. MCD activity profiles for a) irradiated V-BrPO and b) irradiated V-BrPO incubated with 50 mM NaBH₄. MCD assay conditions as described in Materials and Methods. Enzyme concentration: 7 nM V-BrPO. Irradiation conditions: 225 nM V-BrPO in 0.1 M Tris pH 8.3, 3 minute irradiation at 308 nm; 1.5 mL sample volume.

Table 6-2. Bromination activity measurements of V-BrPO samples incubated overnight with varied concentrations of borate. Incubation conditions: 75 nM V-BrPO in either 0.1 M Tris pH 8.3, 0.1 M MES pH 6.0, or 0.1 M citrate pH 4.0.

[Borate] (mM)	Activity pH 8.3	Activity pH 6.0	Activity pH 4.0
0	0.341	0.350	0.265
0.2	0.335	0.354	0.282
1	0.346	0.356	0.265
2	0.347	0.345	0.279
5	0.341	0.355	0.264
10	0.345	0.351	0.290
25	0.345	0.352	0.277
50	0.340	0.356	0.289

Anaerobic irradiation of V-BrPO.

Recent investigations of the vanadate-sensitized photochemistry of the dynein ATPase from sea urchin sperm flagella revealed that in the absence of dioxygen, irradiation of this enzyme does not result in photocleavage as it does in air (Gibbons & Mocz, 1990). To determine if the photomodification of V-BrPO was dioxygen dependent, a 150 nM sample of V-BrPO in 0.1 M Tris pH 8.3 was deaerated in vacuum-equipped spectrophotometric cell and irradiated for 3 minutes. In the absence of dioxygen, the enzyme was still inactivated to the same extent as an identical sample irradiated in the presence of air (Figure 6-6).

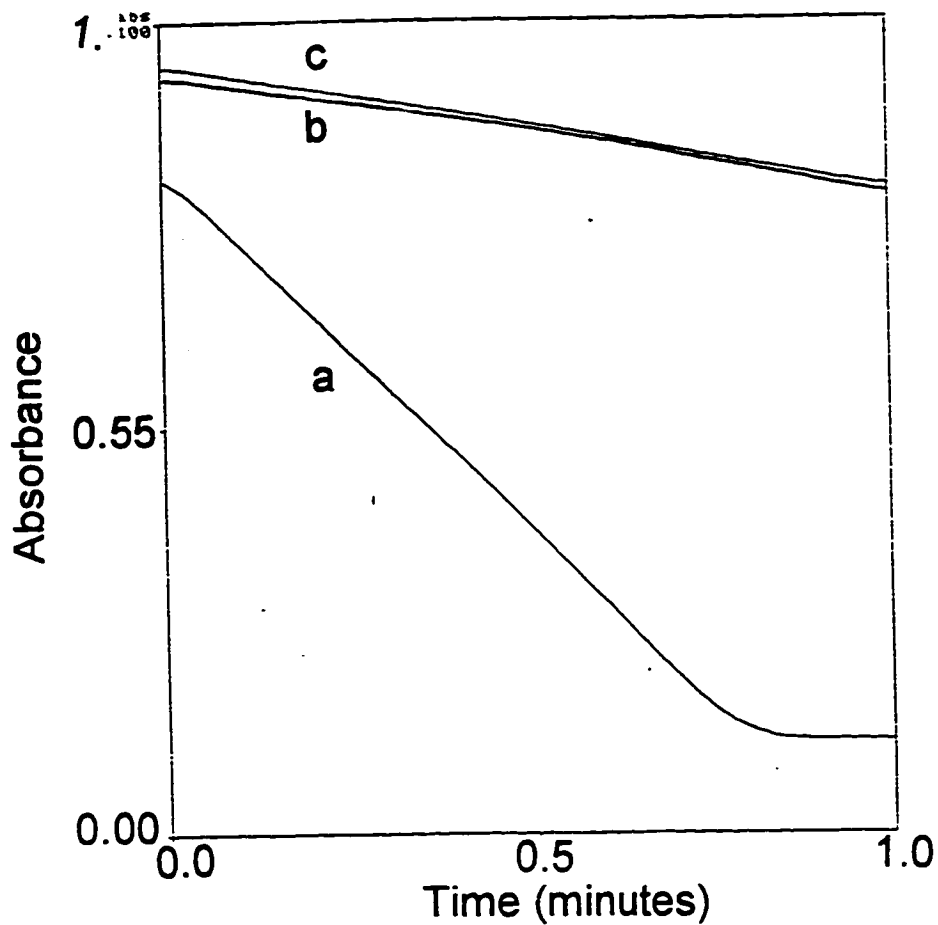


Figure 6-6. MCD activity profiles for a) native V-BrPO, b) V-BrPO irradiated in air, and c) V-BrPO irradiated anaerobically. Deaeration of V-BrPO is described in Materials and Methods. MCD assay conditions as described in Materials and Methods. Enzyme concentration: 7 nM V-BrPO. Irradiation conditions: 225 nM V-BrPO in 0.1 M Tris pH 8.3, 3 minute irradiation at 308 nm; 1.5 mL sample volume.

HPLC-ECD analysis of photomodified V-BrPO.

After this photolysis work was well underway, Messerschmidt and Wever (1996) reported the crystal structure of the vanadium chloroperoxidase from *Curvularia inaequalis*, showing that the only amino acid residue bound to the vanadium in this enzyme was a histidine. The bond valence sum analysis of the active site in V-BrPO (Butler & Clague, 1995; Carrano et al., 1994) and the sequence similarity between V-BrPO and the fungal V-CIPO (Vilter, 1995), particularly the conservation of the coordinating histidine, indicates that the binding sites in the two enzymes are quite similar. If the photomodification of V-BrPO were occurring at residues ligating to vanadium, as was suggested by the atomic absorption experiments on photomodified V-BrPO, histidine was then a logical site for this photooxidation. The possible formation of 2-oxohistidine in the photomodification of V-BrPO at 308 nm was investigated using HPLC equipped with an electrochemical detector (HPLC-ECD) as described in Chapter 2 (Uchida, and Kawakishi, 1989). For these analyses, 150 nM V-BrPO in 0.1 M Tris buffer pH 8.3 was irradiated for 3 minutes. This sample and an unirradiated control sample of V-BrPO were washed several times in Centricon 10 filters with water, concentrated, and then hydrolyzed at 110 °C in 6 M HCl for 18 hours as described in Materials and Methods. However, analysis of the hydrolysates by HPLC-ECD showed no evidence for 2-oxohistidine. Thus, this experiment showed that either

histidine is not oxidized during irradiation of V-BrPO, or the oxidized product is not 2-oxohistidine and is not electrochemically active at the 850 mV potential used for the electrochemical detection.

Amino Acid Analyses.

In a final attempt to discover the site of photomodification in V-BrPO, a sample of irradiated V-BrPO and a sample of native V-BrPO were submitted to the Protein/Peptide Mapping Analytical Facility at the California Institute of Technology. A 50 pmol sample of V-BrPO that had been irradiated for three minutes under conditions of 60 nM V-BrPO, 0.1 M Tris pH 8.3 and also a 50 pmol control sample of 60 nM V-BrPO in 0.1 M Tris pH 8.3 were washed thoroughly with water by ultrafiltration, evaporated to dryness, and redissolved in 50 μ L H₂O prior to submission for analysis. The results of the analyses obtained at Caltech are provided in Table 6-3.

Table 6-3. Micro-amino acid analysis data of 50 pmol samples of native V-BrPO and V-BrPO irradiated under conditions of 60 nM enzyme in 0.1 M Tris pH 8.3 for three minutes.

Amino Acid	Control (pmol)	Irradiated (pmol)	Control mole%	Irradiated mole%	Mole% Variation
Asx	39.40	43.86	5.11	6.70	1.59
Glx	78.18	92.37	10.14	14.10	3.97
Ser	86.16	79.93	11.17	12.20	1.03
Gly	161.13	96.61	20.89	14.75	-6.14
Thr	111.89	114.22	14.51	17.44	2.93
Ala	158.47	108.70	20.54	16.59	-3.95
Pro	56.25	35.00	7.29	5.34	-1.95
Val	35.18	34.13	4.56	5.21	0.65
Met	11.11	12.62	1.44	1.93	0.49
Leu	23.41	22.89	3.03	3.49	0.46
Lys	10.20	14.76	1.32	2.25	0.93
Totals	771.38	655.09	100.00	100.00	0.00

^a. Peaks resulting from His, Ile, Arg, and Phe were below threshold for accurate quantitation. Cys and Trp were not reported due to decomposition during acid hydrolysis.

The amino acid analysis data indicates significant changes in the quantities of several amino acid residues in V-BrPO. In particular, major losses of glycine, alanine, and proline were detected. In addition, significant increases in glutamic acid/glutamine, aspartic acid/asparagine, and threonine were reported. Thus while earlier experiments indicated that the photomodification of V-BrPO is a specific, vanadium-dependent reaction, the resultant protein modifications were nevertheless wide-ranging. The amino acids histidine, isoleucine, arginine and phenylalanine, which have been shown previously to be present in V-BrPO in small quantities

(Everett, 1990), were not effectively quantitated by the procedure used at Caltech (i.e., the quantities of these amino acids were below the detection limit of the Caltech system) and thus are not included in Table 6-3. In addition, cysteine and tryptophan are also not reported as they are subject to decomposition during hydrolysis. The extent of photomodification of those amino acids that were below the detection threshold is as yet not known but may be very important to the vanadium-mediated photochemistry of V-BrPO. Overall, however, the current amino acid analysis indicated that nonpolar amino acid residues were altered during the vanadium dependent photoreaction of V-BrPO. In addition, appreciable gains in the quantities of polar amino acid residues were detected in photolyzed V-BrPO.

Sequence comparison between the vanadium chloroperoxidase from *Curvularia inaequalis* and V-BrPO from *Ascophyllum nodosum* has shown that several non-polar and basic amino acid residues are conserved between the two systems in the vanadium binding region (Vilter, 1995; Messerschmidt & Wever, 1996). In particular, in addition to the conserved coordinating histidine, four alanines, residues 345, 405, 410, and 487 in V-CIPO, four glycines, residues 365, 403, 409, and 494 in V-CIPO, and four prolines, residues 362, 395, 398, and 401 in CIPO, are conserved in the consensus region. Other conserved amino acid residues include arginines 361 and 489, leucines 482 and 493, phenylalanines 359 and 499, and tryptophans 350 and 354. While the vanadium-mediated photooxidation of V-

BrPO is apparently less specific than the previously reported examples of phosphate binding enzymes, the residues modified by the photoreaction of vanadium in V-BrPO are quite probably within the broad "vanadium binding region" of the enzyme.

Discussion

In this investigation, the vanadium-mediated photochemistry of vanadium bromoperoxidase from *Ascophyllum nodosum* was examined. Vanadium bromoperoxidase is irreversibly inactivated in a time-dependent manner by irradiation with 308 nm light from an excimer laser. After irradiation, the enzyme is no longer capable of binding vanadium(V). In fact, bromination activity cannot be restored by the addition of ammonium vanadate. If apo enzyme is irradiated and subsequently reincubated with ammonium vanadate, bromination activity is essentially fully restored. Thus, the vanadium center in vanadium bromoperoxidase is mediating the photomodification of the protein. This work represents the first investigation of vanadium-mediated photochemistry for a naturally occurring vanadium enzyme.

Vanadate-dependent photochemistry in phosphate binding proteins has been shown to frequently result in scission of the peptide backbone. Although not well understood, the mechanism of photocleavage likely involves reduction of bound vanadate to vanadium(IV) and concurrent formation of a localized protein radical (Gibbons et al., 1987). In the case of V-BrPO, cleavage was not detected upon photolysis under the SDS-PAGE conditions employed. One possible explanation for the lack of cleavage in V-BrPO can be extracted from the studies of vanadate-mediated photolysis of myosin (Grammer et al., 1988; Cremonesi et al., 1988, 1989).

In myosin, scission of the peptide backbone requires first vanadate-mediated photooxidation of Serine 180 to a "serine aldehyde" followed by recoordination of vanadate (although to as yet an unidentified residue); (Cremo et al., 1988) and a second photolysis step, which results in cleavage at the amide bond between the oxidized serine and glycine 181 (Grammer et al., 1988; Cremo et al., 1989). In V-BrPO, after a single photolysis step the enzyme no longer has appreciable affinity for vanadium as established by atomic absorption, and thus, a second vanadium-mediated photolysis to potentially cause cleavage is not possible. Furthermore, the inability of borohydride or other reductants to reduce the photooxidized moiety to its native state, as occurs in myosin (Cremo et al., 1989), ribulose-1,5-bisphosphate carboxylase/ oxygenase (Mogel & McFadden, 1989), and isocitrate lyase (Ko et al., 1992)), indicates that a serine is at most a non-exclusive site of photomodification in V-BrPO. Irreversible oxidation of (an) amino acid residue(s) is (are) occurring during the photomodification of V-BrPO.

In fact, after numerous attempts to identify the site of irreversible vanadium-sensitized modification of V-BrPO, micro-amino acid analysis revealed that several amino acids are consumed as a result of photolysis; specifically, large decreases were seen for glycine, alanine, and proline. In addition, increases were observed for Glx, Asx, and threonine residues. The apparent lack of specificity in the vanadium-mediated photomodification of V-BrPO may be reflected in the slow loss of

remaining bromination activity observed after photolysis (Figure 6-3) which suggests that the irradiated enzyme is subject to slow hydrolysis.

As indicated by the sequence similarity between the vanadium(V) binding site regions of V-BrPO and the vanadium chloroperoxidase from *Curvularia inaequalis* (Messerschmidt & Wever, 1996; Vilter, 1995), the vanadium(V) in V-BrPO is likely located in a region of the enzyme that contains nonpolar or slightly basic amino acid residues, including glycines, alanines, and prolines. Consensus residues in the chloroperoxidase include glycines 365, 403, 409, and 494, alanines 345, 405, 410, and 487, and prolines 362, 395, 398, and 401. In the chloroperoxidase, and presumably in V-BrPO as well, these neutral or slightly basic residues are most likely responsible for stabilizing the negative charge of the vanadate ion in the binding site by hydrogen bonding (Messerschmidt & Wever, 1996) and electrostatic interactions. For example, in the crystal structure of vanadium chloroperoxidase, the vanadate center is stabilized by hydrogen bonding to the amide nitrogen of Gly-403. The alteration of these residues, particularly the conversion of these residues to more polar and acidic moieties, would conceivably eliminate the ability of this protein to support a negatively charged vanadate ion.

Although the effects of photomodification of V-BrPO can be identified and interpreted, the mechanisms of photomodification and photooxidation of glycine, alanine, and proline are not thoroughly understood. As referred to in the

introduction to this chapter, the oxidation of proline by vanadate-dependent photochemistry has been reported for the phosphate-binding enzyme adenylate kinase (Cremo et al., 1991). In this system a primary photooxidation at the proline site was followed by a cleavage step, which involved decarboxylation of the proline to produce γ -aminobutyric acid. Assuming that the cleavage of adenylate kinase requires recoordination of vanadate, this second step would not be expected to occur in V-BrPO. A proline residue in bromoperoxidase would only undergo an initial photooxidation. Potential products of this initial photooxidation as indicated by metal-mediated oxidation systems are glutamate and pyroglutamate residues (Uchida et al., 1990; Cooper et al., 1985), which would be detected as Glx residues in amino acid analysis. As reported above, a significant increase in Glx residues was detected for photolyzed V-BrPO versus the native sample (Table 6-3).

The mechanisms of modification of the glycine and alanine residues in V-BrPO remain obscure. In radiolysis oxidation experiments, α -hydrogens and methyl and methylene groups on aliphatic amino acid side chains are susceptible to attack resulting in the formation of hydroxy derivatives. (Stadtman, 1993). For example, 3-, 4-, and 5-hydroxyleucine derivatives have been identified in radiolytically oxidized peptides containing leucine (Kopoldova & Liebster, 1963). Furthermore, proline has been converted to 4-hydroxyproline by radiolysis (Uchida & Kawakishi, 1989). However, hydroxylation of an alanine side chain by this

mechanism would result in conversion to serine, and the increase in the quantity of serine after photolysis is minimal.

Glycine, alanine, and proline are definitely not the preferred targets for metal-mediated oxidations in other proteins (Stadtman, 1993). Preferred target residues include histidine, arginine, lysine, and the sulfur-containing amino acids. Oxidation of histidine, for example, has been reported in several cases to result in the formation of aspartic acid/asparagine (Farber & Levine, 1986; Creeth et al., 1983). Although histidine loss was not effectively monitored for the V-BrPO samples by the micro-amino acid analysis at Caltech (see Table 6-3), oxidation of histidine may be responsible for increases in Asx residues detected in photolyzed V-BrPO. If histidine is oxidized during photomodification of V-BrPO, the absence of 2-oxohistidine as determined by HPLC-ECD experiments is likely due to further oxidation of this compound to aspartic acid and other products, as has been demonstrated to occur at neutral and basic pH (Uchida & Kawakishi, 1994).

References

- Butler, A. & Clague, M.J. (1995) in "Mechanistic Bioinorganic Chemistry" *Advances in Chemistry Series # 246*, Thorp, H.H. & Pecoraro, V.L., eds. American Chemical Society, Washington D.C., pp 329-349.
- Carrano, C.J., Mohan, M, Holmes, S.M., de la Rosa, R., Butler, A., Charnock, J.M., Garner, C.D. (1994) *Inorg. Chem.* **33**, 646-655.
- Cooper, B., Creeth, J.M., Donald, A.S.R. (1985) *Biochem. J.* **228**, 615-626.
- Cotton, M.L., & Dunford, H.B. (1973) *Can. J. Chem.* **51**, 582-587.
- Cremo, C.R., Grammer, J.C., Yount, R.G. (1988) *Biochemistry* **27**, 8415-8420.
- Cremo, C.R., Grammer, J.C., Yount, R.G. (1989) *J. Biol. Chem.* **264**, 6608-6611.
- Cremo, C.R., Loo, J.A., Edmonds, C.G., Hatlelid, K.M. (1992) *Biochemistry* **31**, 491-497.
- Devra, V., Jain, S., Sharma, P.D. (1994) *Int. J. Chem. Kinet.* **26**, 577-585.
- Everett, R.R. (1990) Ph.D. Dissertation, University of California, Santa Barbara.
- Farber, J.M., Levine, R.L. (1986) *J. Biol. Chem.* **261**, 4574-4578.
- Gibbons, I.R., Lee-Eiford, A., Mocz, G., Phillipson, C.A., Tang, W.Y., Gibbons, B.H. (1987) *J. Biol. Chem.* **262**, 2780-2786.
- Gibbons, I.R. & Mocz, G. in *Vanadium in Biological Systems*, Chasteen, N.D., ed. Kluwer Academic Publishers pp143-152.
- Goodno, C.C. (1982) *Methods. Enzymol* **85**, 116-123.
- Grammer, J.C., Cremo. C.R., Yount, R.G. (1988) *Biochemistry* **27**, 8498-8415.
- Huang, B., Piperno, G., Luck, D.J.L. (1979) *J. Biol. Chem.*, **254**, 3091-3099.
- Ko, Y.H., Cremo, C.R., McFadden, B.A. (1992) *J. Biol. Chem.* **267**, 91-95.

- Kopoldova, J., Liebster, J. (1963) *Int. J. Appl. Radiat. Isot.* 14:493-498.
- Laemmli, U.K. (1970) *Nature* 227, 680-685.
- Lee-Eiford, A., Ow, R.A., Gibbons, I.R. (1986) *J. Biol. Chem.* 261, 2337-2342.
- Messerschmidt, A. & Wever, R. (1996) *Proc. Natl. Acad. Sci., USA* 93, 392-396.
- Mogel, S.N. & McFadden, B.A. (1989) *Biochemistry* 28, 5428-5431.
- Pfister, K.K., Haley, B.E., Witman, G.B. (1984) *J. Biol. Chem.* 259, 8499.
- Rosenfeld, J., Capdevielle, J., Guillemot, J.C., Ferrara, P. (1992) *Anal. Biochem.* 203, 173-179.
- Soedjak, H.S., Butler, A., Everett, R.R. (1991) *J. Ind. Microbiol.* 8, 37-44.
- Soedjak, H., Walker, J.V., and Butler, A. (1995) *Biochemistry*, 34, 12689-12696.
- Stadtman, E.R. (1993) *Annu. Rev. Biochem.* 62, 797-821.
- Uchida, K., Kato, Y., Kawakishi, S. (1990) *Biochem. Biophys. Res. Commun.* 169, 265-271.
- Uchida, K. & Kawakishi, S. (1989) *Bioorganic Chem.* 17, 330-343.
- Uchida, K. & Kawakishi, S. (1994) *J. Biol. Chem.*, 269, 2405-2410
- Vilter, H. (1995) *Metal Ions in Biological Systems*, 31, 325-362.

Appendix I. Optimization of Purification of Vanadium Bromoperoxidase from *Ascophyllum nodosum*.

General Isolation Procedure

The brown alga *Ascophyllum nodosum* from which V-BrPO was isolated was collected off Kornwerderzand, Holland, in 1990. The alga was stored in a -80 °C freezer. Prior to extraction, the algae (0.5 -2 kilos) was thawed in water for several hours at 4 °C. The thawed algae was then cut into small species which were homogenized in a Waring Commercial Blendor with at least an equal volume of 0.2 M Tris-sulfate, pH 8.3 containing 1.5 % crosslinked polyvinylpyrrolidone (Aldrich, Inc.); (see below). The resulting homogenate was centrifuged at 14,000 x G for 20 minutes, whereupon the supernatant containing the V-BrPO was removed and checked for enzyme activity by the MCD assay. 0.1 M Tris pH 8.3 was then added to the pellet in each centrifuge bottle, and the mixture was homogenized using an ultrasound tissue homogenizer. The mixture was centrifuged at 14,000 x G and the resulting supernatant was removed and checked for activity. Extraction of the pellet with the tissue homogenizer continued for a minimum of eight cycles, or until MCD activity had decreased significantly.

The alginic acids in the supernatant were next precipitated by the addition of 0.1 M CaCl₂. After several hours of stirring, the mixture was centrifuged at 14,000 x G for 20 minutes to remove precipitates. The resulting supernatant was then washed and concentrated on an Amicon DC 10L 20 liter concentrator equipped

with a hollow fiber filter (10,000 Da cutoff); (Amicon, Inc.). The concentrated solution was batch-loaded onto DEAE-Sephacel ion exchange resin (Pharmacia, Inc.). The resin was poured into a column, and V-BrPO was removed using a gradient of 0.1 to 0.6 M KCl in 0.1 M Tris pH 8.3. The fractions with MCD activity were pooled and concentrated. The resulting V-BrPO was then purified by a size-exclusion column of either S-200 Sephacryl or G-100 Sephadex resin¹ (Pharmacia, Inc.) using 0.1 M Tris pH 8.3 as the elution buffer. The active fractions were pooled and concentrated.

Removal of Phenols from Algal Extracts.

Brown marine algae such as *A. nodosum* have large quantities of phenolic compounds. These phenols can act as substrates for V-BrPO and accordingly can impact on kinetic studies. In addition, these phenolic compounds have high fluorescence and accordingly have limited our ability to analyze the enzyme by Resonance Raman. Thus, it was a priority to develop a procedure to reduce the background fluorescence. It has been previously reported by Loomis and coworkers (Loomis, 1974; Loomis & Battaile, 1966) that the inclusion of polyvinylpyrrolidone (PVP); (Aldrich, Inc.) in plant extracts assists in the removal of phenolic compounds from the supernatant. PVP also proved effective at

¹ An SDS-PAGE gel of G-100-purified V-BrPO is shown in Figure 2-2.

removing phenols from extracts of *A. nodosum*. Algae samples were homogenized in approximately equal volume of 0.1 M Tris pH 8.3 using a tissue homogenizer. If 1.5 % insoluble crosslinked polyvinylpyrrolidone (by weight) was added to the homogenizing buffer for the first algal extraction, the phenolic content of the extract supernatant was greatly reduced upon centrifugation at 14,000 x G relative to a sample prepared in the absence of PVP. Upon excitation of 315 nm, the fluorescence of the enzyme was reduced by as much as 70% when PVP was used in the homogenizing buffer in the first extract.

Purification of Vanadium Bromoperoxidase by Electroelution.

In order to obtain enzyme of adequate purity for amino acid analysis and similar procedures, V-BrPO that had been purified by size exclusion (either Sephacryl S-200 resin or Sephadex G-100 resin) was purified to homogeneity by electroelution of the protein from native PAGE gel bands. First, 100 to 200 µg enzyme sample was separated on a 3 mm thick gel using a Biorad Mini-Protein II electrophoresis system. In order to achieve timely removal of the protein, it proved necessary to reduce the extent of acrylamide polymerization from the standard 12.5% acrylamide to 7.5% acrylamide. In addition, for those samples which were to be subjected to amino acid analysis procedures, the running buffer was changed from the standard Tris/glycine pH 8.3 to 20 to 50 mM Tris-H₂SO₄ pH 8.3.

After completion of electrophoresis, the edges of the native gel were stained for peroxidase activity with *o*-dianisidine (Vilter & Glombitza, 1983). Upon staining, the protein becomes highly resistant to electroelution, most likely due to dye crosslinking. Accordingly, a gel band on the unstained portion of the gel which corresponded to the position of peroxidase activity was excised. This band was typically cut into six bands each of approximately 1 cm in length.

Electroelution was performed on a Biorad Model 422 Electroeluter Module. The running buffer was 20 to 50 mM Tris pH 8.3. The chambers were then fitted with 10,000 MW cut off dialysis membranes which had been filled with running buffer. One of the 1 cm gel bands was then dropped into each chamber. It proved necessary to refrigerate the entire setup prior to electroelution as the running buffer has a tendency to heat up during electrophoresis.

Electroelution was performed at a constant current of 60 mA (10 mA per chamber) for approximately 3 to 5 hours. During the course of the electroelution, the system was kept cool by ice packs. If excessive heat was noted, the entire system was disconnected from the power source and refrigerated for several minutes prior to reconnection. The electroeluted enzyme which had collected in the dialysis membrane cups was carefully removed, and the quantity of the electroeluted enzyme was determined by MCD and BCA assays. Purity was

assessed by standard SDS-PAGE analysis. Typical recovery was on the order of 10 to 20 % of the total protein loaded onto the original native gel.

Preparative Gel Electrophoresis Purification of V-BrPO.

Purification of V-BrPO to homogeneity in limited yield has also been achieved by native preparative gel electrophoresis on a BioRad 491 Prep Cell. A 6 to 8 % acrylamide separating gel of ~~minimum BioRad 491 Prep Cell~~ 4 A/6 stacking gel (approximately 2 cm) were prepared in either the 25 or 37 mm OD gel tube using dilute (i.e., 10 mM) acetate buffer at approximately pH 5.0. Gel formulations were obtained from the recipes described in the BioRad Model 491 Prep Cell manual. Dilute (mM) acetate pH 5.0 was also used as the eluting buffer. A sample of size exclusion purified V-BrPO, typically 1 to 10 mg, was loaded on to the gel in a buffer of 20 % glycerol, 0.05% bromophenol blue in a total volume less than 25 % the volume of the stacking gel. The gel was eluted at 10 W constant power and fractions were collected at a flow rate of 1.0 ml/min. Under these conditions, the purified protein eluted within approximately 2 hours. As for electroelution, purity was analyzed by SDS-PAGE, and the amount of enzyme recovered was determined by MCD and BCA assays. Retrieval ranged from less than 1 % to approximately 10 %.

Conclusions and Suggestions for Improved Purification of V-BrPO

V-BrPO purified on a G-100 column is virtually a single band on an SDS-PAGE gel (Figure 2-2) and seems adequate for most experiments. This procedure allows for reasonable purification of high quantities of enzyme with minimal loss. However, for particularly sensitive analytical applications (e.g., micro-amino acid analysis), electroelution is preferable. The most significant drawback to electroelution is that a very limited quantity of enzyme can be isolated in a single run; in many cases the quantity retrieved from a single run is inadequate for even the most sensitive of experimental techniques. A buffering system that does not include sulfate may be preferable for both the mini-gel electrophoresis and the subsequent electroelution; however, this buffer must *not* contain glycine if the sample is to be used for amino acid analysis. Techniques other than electroelution, such as nitrocellulose blotting, may prove more effective at extracting pure enzyme from gels, particularly for amino acid analysis.

References

Loomis, W.D. (1974) in "Methods in Enzymology", Fleischer, S & Packer, L., eds., vol 31. Academic Press, San Diego, pp. 528-545.

Loomis, W.D. & Battaile, J. (1966) *Phytochemistry* 5, 423.

Vilter, H. & Glombitza, K.- W. (1983) *Bot. Mar.* 26, 331-340.